2(P) mix

NASA CR-130220

TRACKING AND DATA RELAY SATELLITE SYSTEM CONFIGURATION AND TRADEOFF STUDY–PART II FINAL REPORT

Volume II
Delta 2914 Launched TDRSS – Configuration 2

HUGHES AIRCRAFT COMPANY
Space and Communications Group
El Segundo, California 90009

1 April 1973
Part II Final Report

Prepared For
GODDARD SPACE FLIGHT CENTER
Greenbelt, Maryland 20771

300

TECHNICAL REPORT STANDARD TITLE PAGE

1. Report No.	2. Government Accession No.	3. Recipient's Catalog No.
4. Title and Subtitle Tracking and Data Relay Satellite System Configuration and Tradeoff Study - Delta 2914 Launched TDRSS, Configuration 2		5. Report Date 1 April 1973 6. Performing Organization Code
7 Author(s)		8. Performing Organization Report No.
9. Performing Organization Name and Address Hughes Aircraft Company, Space and Communications Group, NASA Systems Division 1950 E. Imperial Highway El Segundo, California 90009		10. Work Unit No. 11. Contract or Grant No. NAS 5-21704
12. Sponsoring Agency Name and Address National Aeronautics and Space Administration Goddard Space Flight Center Greenbelt, Maryland 20771 G. Clark		13. Type of Report and Period Covered Final Report, Part II 22 August 1972 to 1 April 1973 14. Sponsoring Agency Code
15. Supplementary Notes		

16. Abstract

Configuration data and design information for a Delta 2914 launched configuration with greatly enhanced telecommunication service over the Part I Delta 2914 configuration is contained herein. It treats the overall system definition, operations and control, and telecommunication service system, including link budgets. A brief description of the user transceiver and ground station is presented. A final section includes a summary description of the TDR spacecraft and all the subsystems. The data presented are largely in tabular form for easy reference.

17. Key Words (Selected by Author(s))	18. Distribution Statement		
Delta 2914 Launched TDRSS with enhanced telecommunication service			
19. Security Classif. (of this report) Unclassified	20. Security Classif. (of this page) Unclassified	21. No. of Pages 302	22. Price*

*For sale by the Clearinghouse for Federal Scientific and Technical Information, Springfield, Virginia 22151.

CONTENTS

ILLUSTRATIONS

TABLES

1. SYSTEM DEFINITION

1.1 INTRODUCTION

A Delta 2914 launched TDRSS concept is described in this volume.

- Section 1, System Definition, identifies the system concept, the spacecraft configuration and the telecommunication service.

- Section 2, Operations and Control, contains an orbit insertion profile, a brief description of the spacecraft on-orbit control including a listing of auxiliary propulsion, and a description of the telecommunication service operations.

- Section 3, Telecommunication Service System, contains a summary of the telecommunication services and link budgets and presents parametric performance data. This section also discusses the general characteristics of the TDRS repeater and the requirements for the user and ground station.

- Section 4, TDR Spacecraft Baseline Configuration is comprised of three subsections.

  4.1 Configuration contains a brief discussion of the salient features of the configuration including spacecraft configuration drawings. Included is also a brief discussion of the spacecraft design objectives and the requirements and the implementation of the telecommunication service.

  4.2 Design Features and Configuration Summary contains a brief discussion of the most significant aspects of the subsystem technology and implementation. A compilation of the spacecraft parameters, electrical power budgets, mass summaries, a listing of the subsystem components and telemetry and command lists are also included.

  4.3 Subsystem Description contains descriptive material of the subsystem design and a summary of pertinent data, namely, subsystem block diagrams, requirement tables and mass summaries.

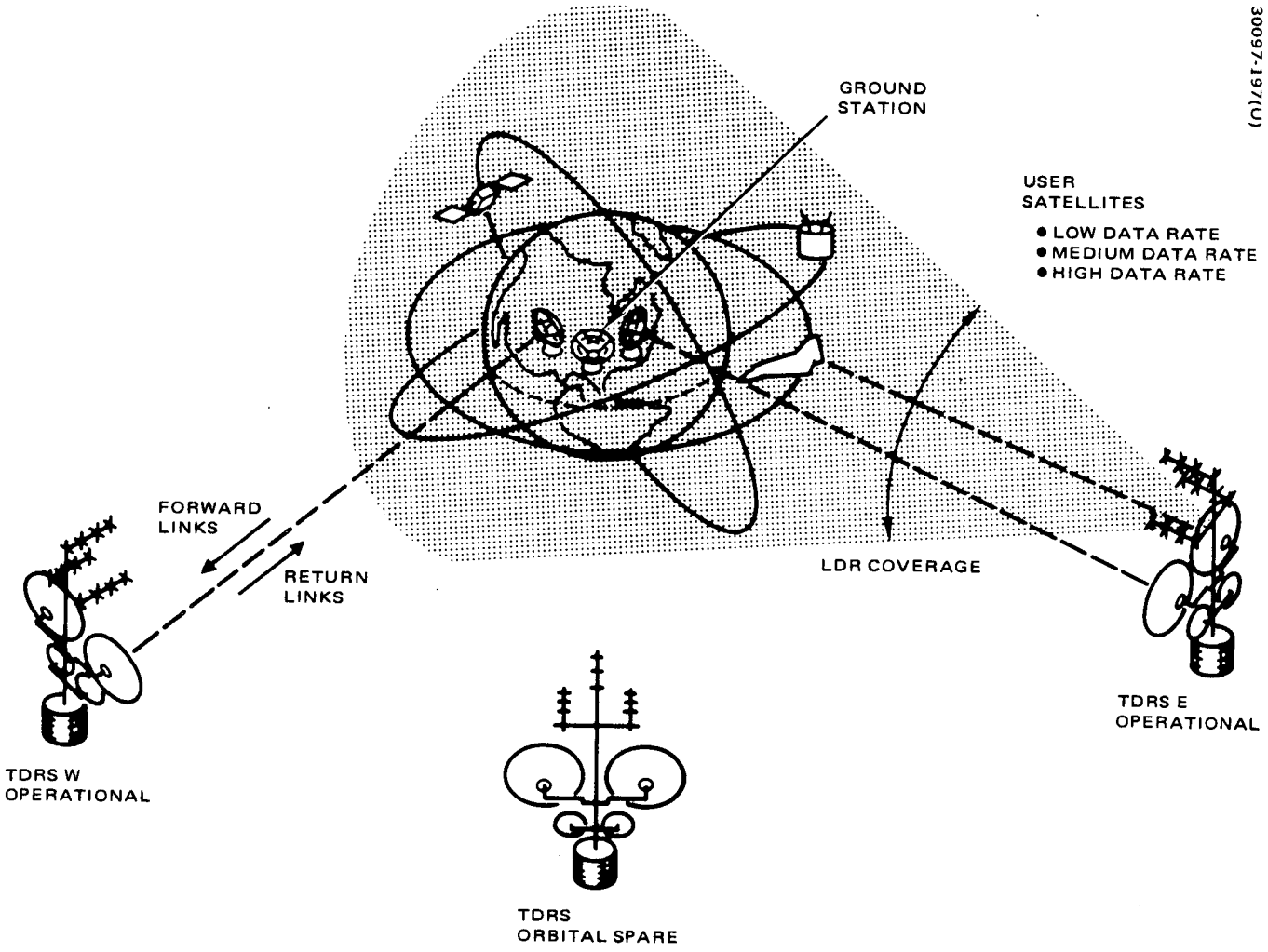

Figure 1. TDRS System Concept

1.2 SYSTEM CONCEPT

The TDRSS concept employs two operational geostationary satellites to provide relay links for telemetry, tracking, and command (TT&C) between multiple low earth-orbiting user satellites and a centrally located ground station, as shown in Figure 1, making possible continuous reception of data in real time.

The TDRSS comprises the following major elements:

- GSFC network scheduling and data processing facilities
- TDRS ground station
- TDRS control center
- Two operational TDR satellites, one in-orbit spare

The communication links from the ground station to the TDRS to the user are defined as forward links, and the links from the user spacecraft to the TDRS to the ground station are defined as return links.

The forward links contain user command, tracking signals, and voice transmissions, whereas the return links contain the user telemetry, return tracking signals, and voice.

The users are categorized as low data rate (LDR), medium data rate (MDR), and high data rate (HDR), according to their telemetry rates.

1.3 TDRS CONFIGURATION SUMMARY

A spacecraft configuration compatible with the Delta 2914 launch vehicle featuring greatly enhanced telecommunication service as compared to the Phase I configuration are presented in this volume. The configuration provides LDR service for user spacecraft up to at least 1000 km altitude, two MDR channels, and one HDR channel, which is time-shared with a MDR channel. Extensive use of low mass technology for all subsystems is required in order to achieve a communication performance compatible with the overall TDRSS program objectives.

This study has been directed to utilize a spin-stabilized spacecraft design. Recent developments in this field at Hughes have included TACSAT, Intelsat IV, Telesat, and other communication satellite programs. Both Intelsat IV and TACSAT are Hughes Gyrostat designs and all have successfully operated in orbit. TACSAT was the first of the Gyrostats and it achieved 3.7 years of useful lifetime. Its failure is attributed to the despin motor brush and commutator. Since brush type motors have not been used in subsequent Gyrostat designs, this failure mode has been eliminated. Four Intelsat IV spacecraft have been launched and no spacecraft failures have occurred. The Hughes orbital experience proves that a Gyrostat

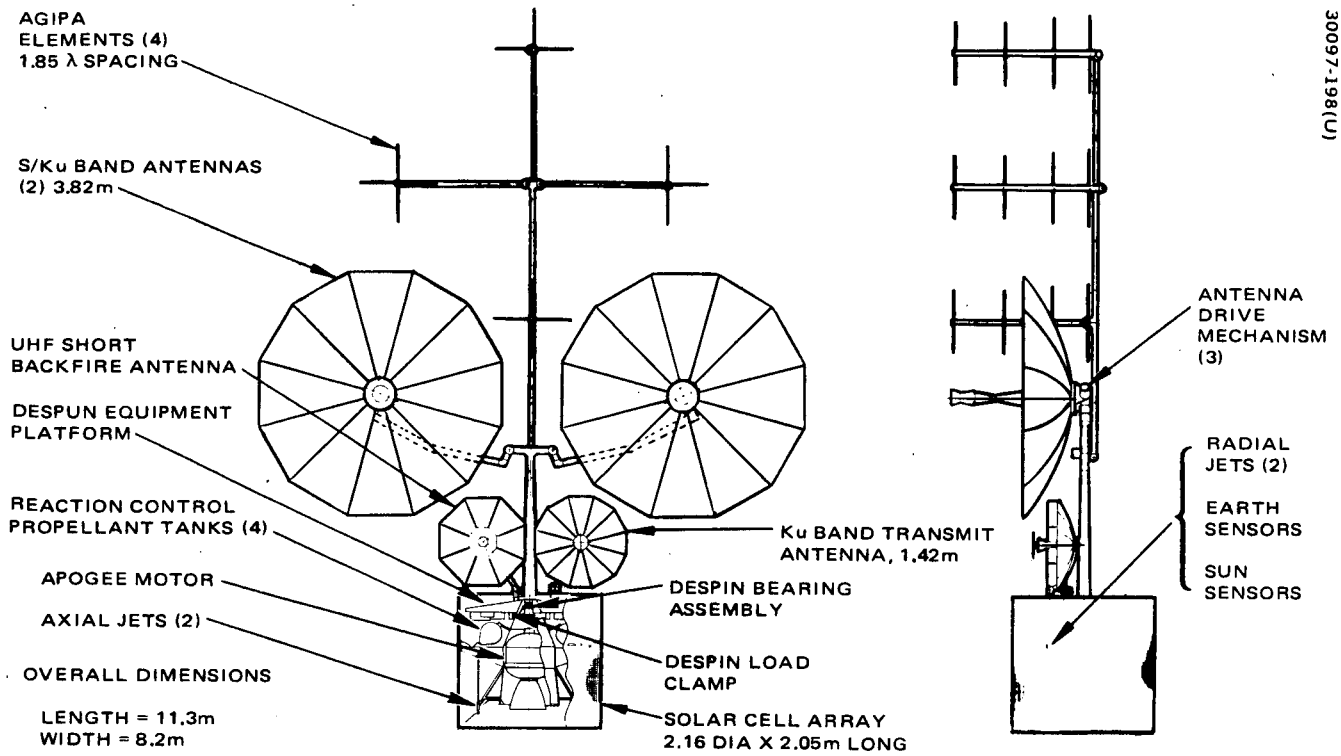

Figure 2. TDRS Baseline Orbital Configuration

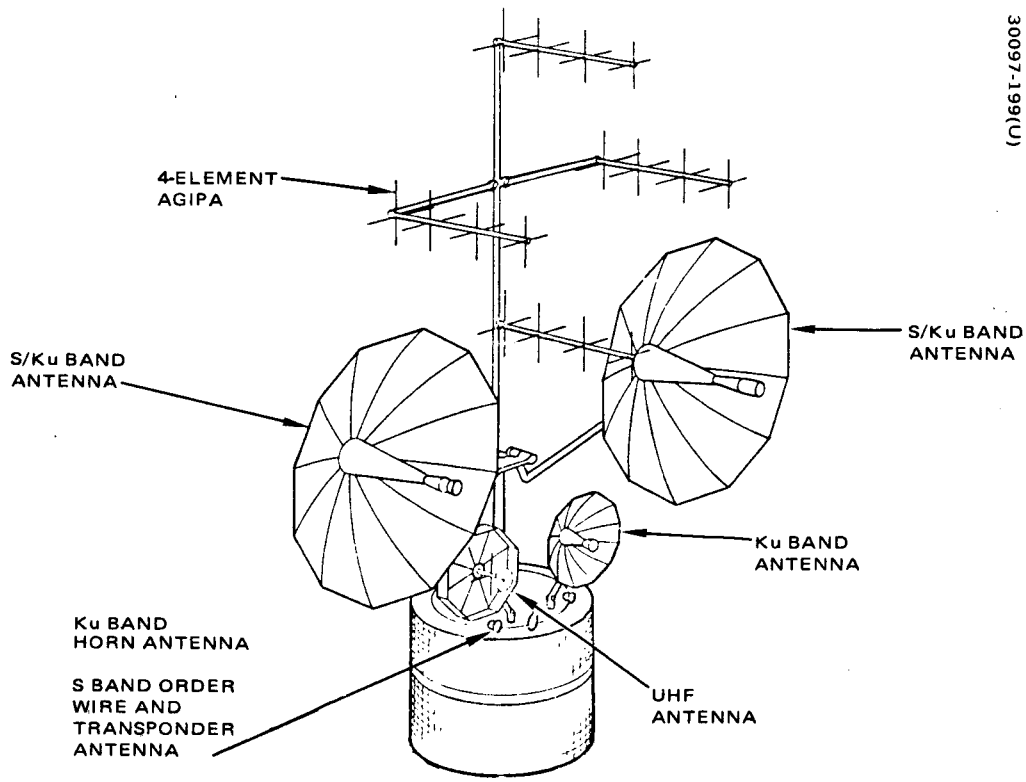

Figure 3. TDRS Orbital Configuration

configuration is a well-demonstrated design approach that has proved highly reliable. Therefore, the Gyrostat stabilization concept has been selected for the TDRS configurations. Applicable technology and components developed on the previously mentioned programs have been used in order to provide a design meeting the mission requirements that can be developed with a high level of confidence.

The Gyrostat stabilization concept provides a fully stabilized platform for the payload while exploiting the simplicity and long-life advantages associated with spinning satellites. The orbital configuration of the spacecraft is shown in Figure 2, and an artist's concept of the spacecraft is shown in Figure 3. Antennas are mounted off the despun platform on mast type support structures. The despun section also houses the communication equipment and some of the telemetry, tracking, and command equipment. Electronic equipment is mounted on thermally controlled platforms.

The spinning section of the spacecraft houses the electrical power subsystem, attitude and reaction control subsystems, and a large portion of the telemetry tracking and command subsystem. The electrical power subsystem has been sized to provide adequate voice communication service for the Space Shuttle.

1.4 TELECOMMUNICATION SERVICE

Table 1 summarizes the services provided by each TDRS. As indicated, four of the communication links have restrictions imposed by the limitations of the power subsystem. These are the LDR forward, the two MDR forward, and the HDR return links. The several combinations that are possible are discussed later in subsection 3.1.1.5. In addition, the two 3.82 meter steerable reflector antennas with S band and Ku band feeds must be shared between the two MDR links and the HDR link.

TABLE 1. TDRSS USER SERVICE

LDR Service	Forward,* UHF	Sequential to one user at a time. 30 dBw EIRP over 19.7 degrees.
	Return, VHF	Simultaneous return from up to 20 users, AGIPA for RFI suppression
MDR Service S band	Forward	Two Links: each with two EIRP levels: 47 dBw and 41 dBw
	Return	Two Links, each designed for Mbps
HDR Service Ku Band	Forward	One Link, 40 dBw EIRP
	Return	One Link designed for 100 Mbps

2. OPERATIONS AND CONTROL

The TDRS system provides telecommunication service with two geosynchronous relay satellites. The TDRSS operations and control comprise three major functions:

- TDRS launch and orbital deployment
- TDRS on-orbit control
- TDRSS telecommunication service operations

The TDRS orbital inclination of 7 degrees is selected as a compromise between spacecraft mass, inclination biasing requirements, and user coverage. This orbital inclination does not cause any operational difficulties and has a negligible effect on user visibility as compared to a zero inclination orbit. Maximum separation (compatible with ground station elevation constraints) is used between the two TDR satellites to maximize user visibility. The TRD's launch and orbit insertion is quite conventional (similar to that used for Intelsat IV). The mission profile selection of the TDRS orbital positions and coverage are discussed in detail in the Phase I final report and apply directly also for this configuration and therefore will not be included in this volume.

The TDRS on-orbit control operations are as follows:

- E-W stationkeeping
- Attitude correction maneuvers
- S/Ku and K band antenna pointing
- TDRS repeater channel settings.

All of these operations will be commanded from ground, and they are similar to the control of other synchronous satellites for which considerable orbital experience has been accumulated.

The TDRSS telecommunication service operations have been developed to stress simplicity, economy, flexibility, and ease of operations. Maximum use of existing GSFC network control and scheduling, orbit determination, and data processing capabilities has been planned.

2. 1 TDRS ON ORBIT CONTROL

There are two systems for TDRS telemetry and command; Ku band and S band. The Ku band system is prime with the S band system, which employs an omnidirectional antenna on the TDRS, for backup and initial operations.

TDRS tracking can be accomplished by using either the LDR forward link or the S band transponder. Using the former, a signal is continuously sent to each TDRS via the Ku band system. Each TDRS repeats the signal at UHF via the broad coverage antenna. A relatively low gain UHF antenna can be used to receive these signals at the ground station, where they are processed to provide range and range rate measurements for the TDRS. The S band transponder has an earth-coverage antenna and is well suited to trilateration ranging. It is also compatible with the Goddard range and rante rate system.

The on-orbit control operations for the TDRS are:

- East-west stationkeeping
- Attitude maneuvers
- S band and Ku band antenna pointing
- TDRS repeater channel settings for MDR users

The frequency of east-west stationkeeping maneuvers is approximately one maneuver every 100 days and the frequency of the attitude maneuver is one maneuver every two days. The satellite has sufficient angular momentum so that antenna pointing will not require any immediate attitude compensation maneuvers. The stationkeeping and attitude correction maneuvers do not require an interruption of the telecommunication service to the users. A summary of the requirements imposed on the auxiliary propulsion is shown in Table 2.

TABLE 2. AUXILIARY PROPULSION REQUIREMENTS

ΔV	160 m/s
Cumulative impulse predictability	
10 pulses	10 percent
50 pulses	5 percent
Burn time: Steady state pulsing	
Axial	330,000 S
Radial	700,000 S

The ground link antenna has autotrack capability and under normal conditions will require no ground control except for initial acquisition. Two dual-feed antennas (S and Ku band) are provided for MDR and HDR service. For MDR users, the antennas are pointed by commands from the TDRS Control Center. The antenna beamwidth of 2.5 degrees at S band allows relatively infrequent pointing adjustments, i.e., no more often than once every 20 seconds. For HDR service at Ku band, autotracking is implemented. The antennas have tracking Ku band feeds, but must be slewed to their acquisition position for each HDR user pass. The scan motion for link acquisition will be generated in the TDRS and will only need an activation command from the TDRS Control Center. All antenna pointing, slewing, and acquisition commands will be based on spacecraft ephemerides and a master schedule for TDRSS services.

2.2 TDRS TELECOMMUNICATIONS SERVICE OPERATIONS

The TDRS system consists of five major elements:

1) GSFC communications control and processing facility, referred to as GSFC

2) Satellite control centers for users and TDR spacecraft

3) Ground station

4) Tracking and data relay satellites

5) User spacecraft

The overall functional relationship among these elements is shown in Figure 4. Note that GSFC has the responsibility for scheduling the TDRSS communication services and providing most data processing. The TDRSS link availability will be defined by Network Scheduling and Control similar to the present NASA ground station scheduling and will be forwarded to the users on a regular schedule. Each user control center issues commands to assigned spacecraft, limited only by the predetermined schedule. During the scheduled times, the user spacecraft command data are compiled at the GSFC Control Center into a forward link data stream which is sent to the TDRS ground station for transmission to the user spacecraft.

The TDRS control center computes commands for the TDR satellites and forwards commands to the ground station for transmission to the satellites. These commands configure the repeater and point the steerable antennas as well as produce housekeeping and subsystem control functions.

The ground station is the interface between the TDRS control center, GSFC, and the TDR satellites. All modulation/demodulation, multiplexing/demultiplexing, and RF transmitting/receiving is performed at this facility.

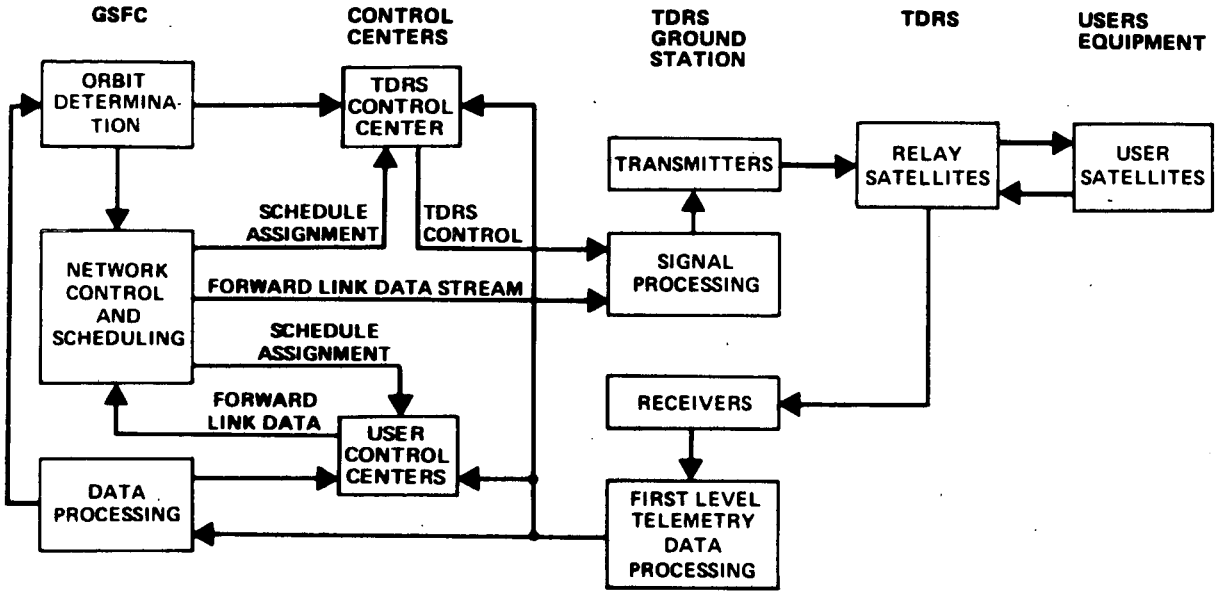

Figure 4. TDRSS Functional Operations

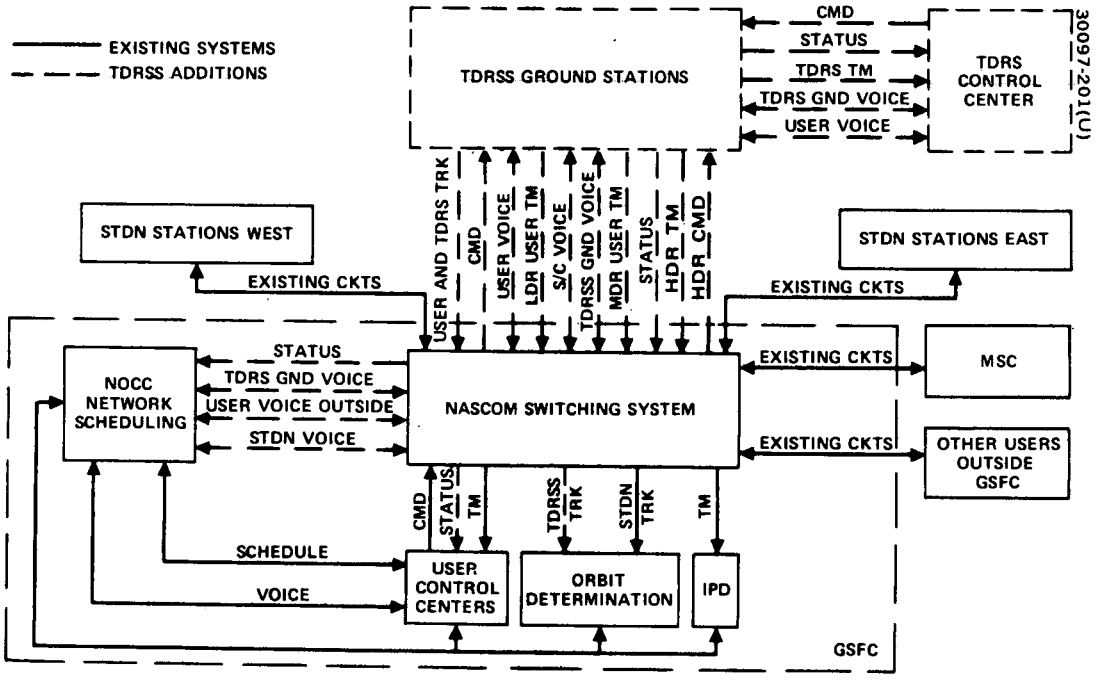

Figure 5. TDRS Ground Network

The return link data can be sent directly to the user program offices and/or to GSFC for further data processing. Orbit determination for both the TDRS and user satellites is performed at GSFC and made available to the user program offices and to the TDRS control center.

Figure 5 illustrates how the TDRSS augments the current ground network and employs much of the existing scheduling, switching, and data processing capability of GSFC. The control center operations have been briefly mentioned on the previous page. The major ground station functions include:

- Ground station antenna pointing
- Transmitting to and receiving from TDRSs
- Demultiplexing signals from GSFC into forward link channels plus additional status, scheduling, and control signals.
- Spreading spectra of forward link signals as required
- Carrier modulation
- Filtering and processing as required to separate received signals and to reduce RFI in LDR return channels
- Configuration of demodulation equipment according to schedule for all services
- Multiplexing of all return link signals, range, and range rate measurements, and status data for transmission to GSFC
- Internal forward links verification, comparing what was transmitted to the TDR satellites in each link to outputs of forward link demultiplexer

The LDR return link service is operationally the most difficult because there will be many telemetry signals simultaneously present in the eight channels from each TDRS. Should a LDR user be simultaneously visible to both TDR satellites, the choice of which TDRS shall be used is made initially at GSFC. This function may be automated based on the GSFC handover schedule. MDR and HDR functions are conceptually the same as for the LDR, but only one signal per TDRS at any time will be received per channel, and acquisition and demodulation will be simpler.

3. TELECOMMUNICATION SERVICE SYSTEM

The telecommunication service system consists of the communication equipment in the TDRS, user spacecraft, and ground station. The services and their operational aspects have been briefly discussed above and are depicted in Figure 6. The frequency plan is shown in Figure 7. The telecommunication services provided via each TDRS are summarized below in Section 3.1. Section 3.2 presents a brief treatment of some analytical aspects of the LDR, HDR, and ground links. Sections 3.3, 3.4, and 3.5 discuss respectively the TDRS repeater, user equipment, and ground station requirements.

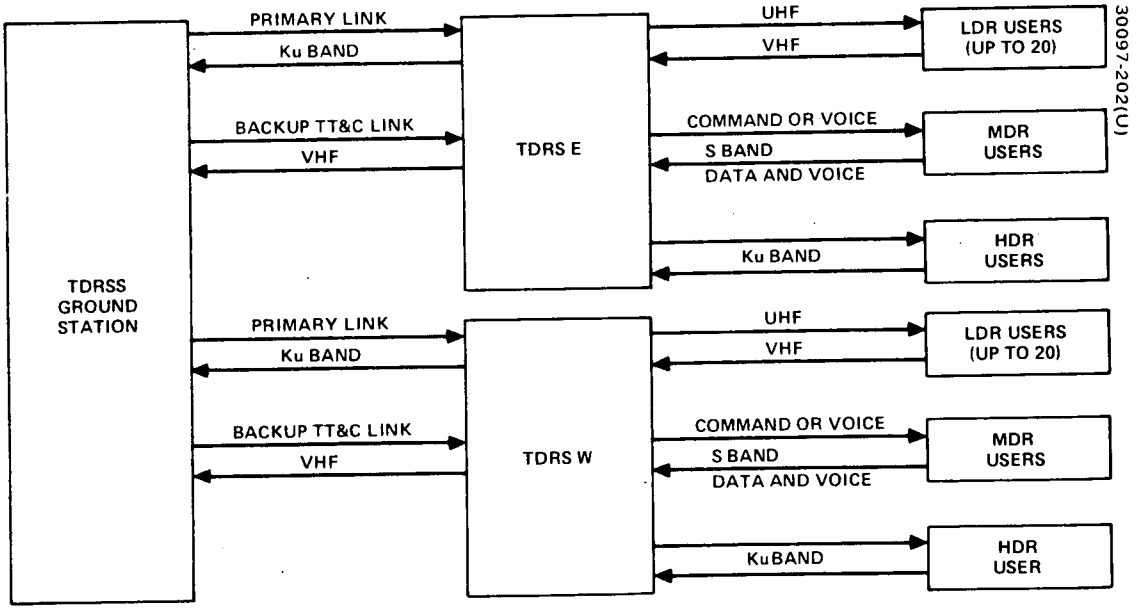

Figure 6. Telecommunications Service System

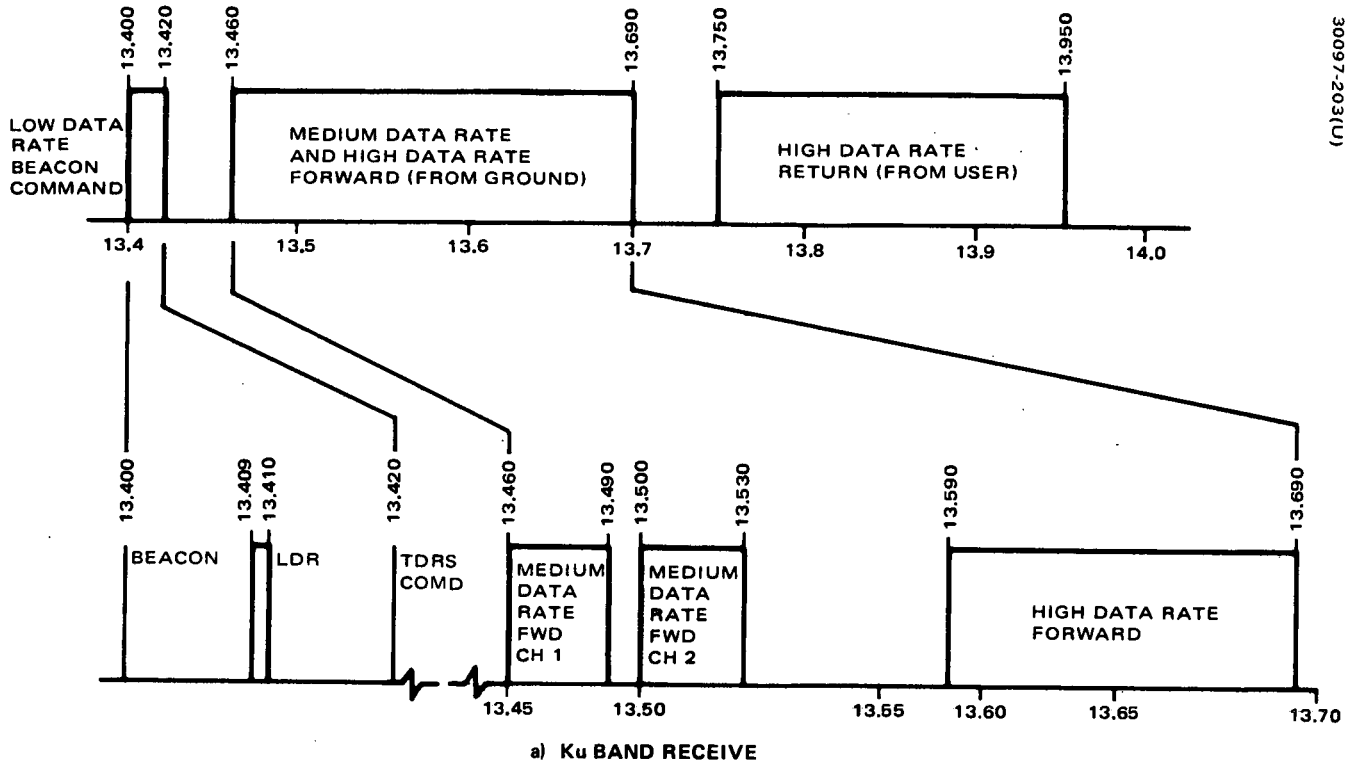

a) Ku BAND RECEIVE

Figure 7. TDRS Frequency Plan

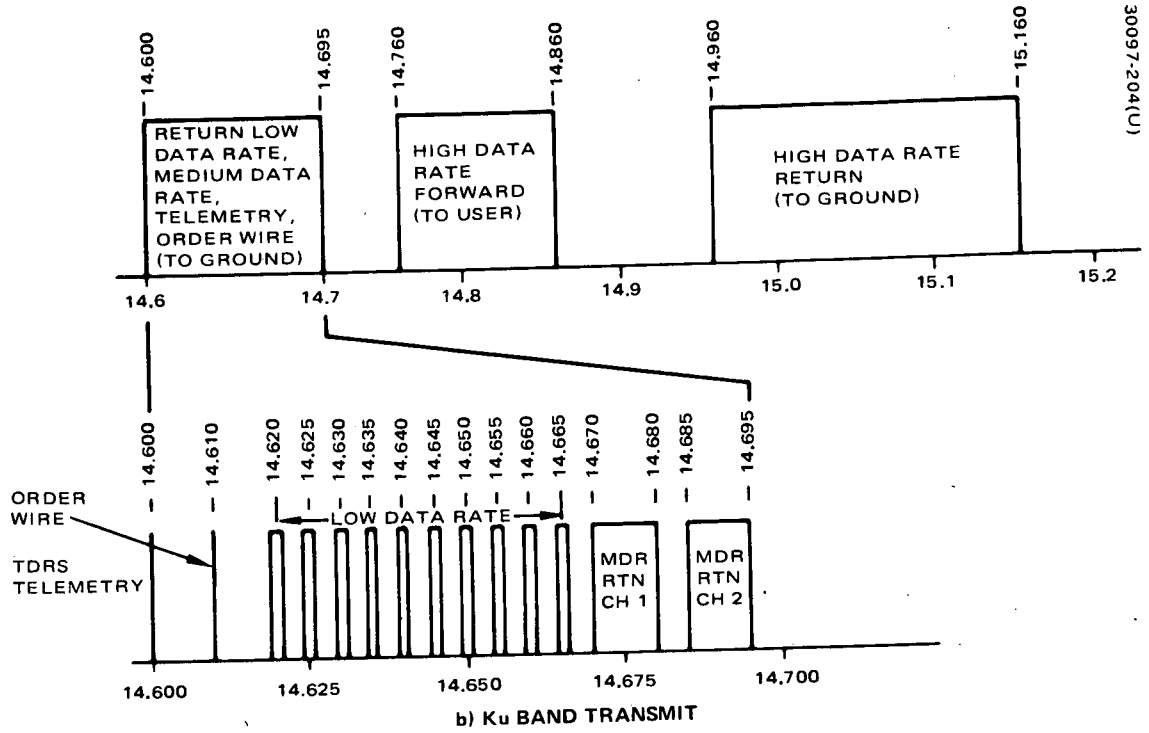

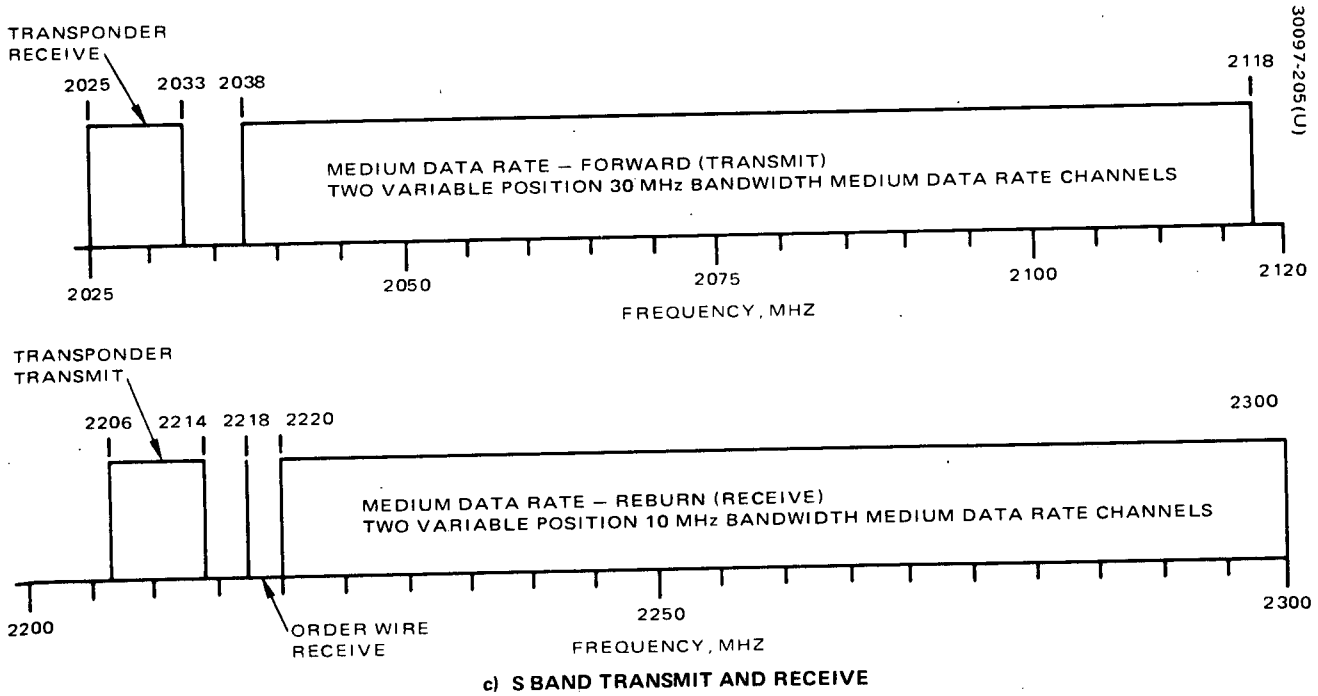

Figure 7 (continued). TDRS Frequency Plan

TABLE 3. TDRS TRANSMIT LINK BUDGETS

Parameter	LDR Command UHF	MDR Forward S Band		Ground Ku Band	HDR Forward Ku Band
		High Power	Low Power		
TDRS EIRP	30.0*	47.0	41.0	EIRP	40.0
TDRS pointing loss	–	-0.5	-0.5	-0.5	-0.5
Space loss	-177.5	-192.0	-192.0	208.4	208.9
Receive antenna gain	-3.0	G_u	G_u	63.0	G_u
Receive pointing loss	–	-0.5	-0.5	-0.5	-0.5
Receive line loss (L)	-0.5	-2.0	-2.0	-0.3	2.0
Receive ellipticity loss	-3.0	-1.0	-1.0	-0.2	-0.2
Receive power, P_r	-154.0	G_u-149	G_u-155	EIRP-146.9	G_u-172.1
Receive noise figure, dB	3.75	5.1		3.8	7.0
Receiver noise temperature, K	400.0	650.0		400.0	1160.0
Background noise temperature, K**	50.0	50.0		5.0	5.0
(1-L) 290 K - line loss noise temperature	31.0	100.0		20.0	100.0
Total system noise temperature K, at receiver input	481.0	800.0		420.0	1280.0
Noise density, η_T dBW/Hz	-201.8	-199.6		-202.3	-197.5
Pr/η_T dB-Hz	47.8	G_u +50.6	G_u +44.6	EIRP +55.4	G_u +25.4

*For 19.7 degree conical coverage, 28.4 dBW for 30 degree coverage.
**Adjusted for line loss.

3.1 SERVICES AND LINK PARAMETERS

This section consists of two major subsections. Subsection 3.1.1 presents a very brief summary of the services provided by the TDRSS. Due to power limitations, some services are restricted; the restrictions a and consequent combinations of services are then discussed. Subsection 3.1.2 contains the major assumptions, characteristics, parameters, and parametric relationships associated with each service. The order of presentation is LDR, MDR, HDR, order wire and S band transponder. Following these, the parameters of the TDRS/ground station link are listed. The link power budgets, which are the basis for all link analysis and service capability, are presented in Tables 3 and 4.

3.1.1 Services

3.1.1.1 Low Data Rate at UHF/VHF

- Command of, tracking of, and telemetry from up to 20 users; command is sequential, tracking and telemetry are simultaneous for all users.

TABLE 4. TDRS RECEIVE LINK BUDGETS

Parameter	Return LDR VHF (Minimum)	Return MDR S Band	Order Wire S Band	Forward LDR From Ground Ku Band	Forward HDR, MDR From Ground Ku Band	Return HDR Ku Band
Transmit power	7.0		20.0	P	P	
Transmit antenna gain	-3.0	EIRP	0	62.0	62.0	EIRP
Transmit line loss	–		–	-2.5	-2.5	
Transmit pointing loss	–		–	-0.5	-0.5	-0.5
Space loss	-167.5	-192.7	-192.7	-207.5	-207.5	-208.3
TDRS antenna gain	14.7*	36.2	13.2	18.5	44.0	51.9
TDRS pointing loss	–	-0.5	–	-2.0	-0.2	-0.5
TDRS line loss, L	-0.8	0.8	-1.0	-1.0	-2.3	-2.3
TDRS ellipticity loss	-0.5	-0.2	-0.2	0	-0.2	-0.2
Received power, P_r	-150.1	EIRP 158.0	-160.7	P-133	P-107.2	EIRP-159.6
Noise figure, dB	3.9	1.3	3.9	7.0	10.0	7.0
Receiver noise temperature K	840.0***	100.0	420.0	1170.0	2600.0	1170.0
Earth noise temperature, K**	600.0***	240.0	240.0	240.0	195.0	195.0
(1-L) 290 K – line loss noise temperature, K	60.0	58.0	60.0	60.0	105.0	105.0
Total system noise temperature, K	1500.0	398.0	720.0	1470.0	2900.0	1470.0
Noise density, η_T, dBW/Hz	-196.8	-202.6	-200.0	-196.9	-194.0	-196.9
P_r/η_T dB-Hz	46.7	EIRP+44.6	39.3	P+63.9	P+87.1	EIRP+37.3

*For 30 degree conical coverage.
**Adjusted for line loss.
***Total for four receivers.

3.1.1.2 Medium Data Rate at S Band

- Two simultaneous two-way links, each with the following capability:
  - Forward links: Two 24 kbps delta modulated voice signals plus 6 kbps to the Space Shuttle (a total of 54 kbps) or up to 2 kbps data continuously to a user spacecraft with a 0 dB gain antenna.
  - Return links: Up to 1 Mbps data from a user spacecraft.

3.1.1.3 High Data Rate at Ku Band

- One two-way link; must time-share the two steerable dishes with the MDR service:
  - Forward link: 40 dBW EIRP
  - Return link: Up to 100 Mbps

3.1.1.4 Order Wire at S Band

A broad coverage S band antenna has been provided for an order wire service so that a request can be made by a manned spacecraft with an omnidirectional antenna for MDR service, even if the TDRS narrow beam S band antenna is not pointed at this user.

3.1.1.5 S Band Transponder

A turnaround S band transponder has been provided to allow accurate TDRS range measurements. The bandwidth is 8 MHz centered at 2029 for receive and 2210 for transmit. The transmitted EIRP is 20 dBW. This transponder will allow the use of trilateration techniques and is compatible with the Goddard range and range rate system. This transponder is also used for backup TT&C when used in conjunction with an omnidirectional antenna.

3.1.1.6 Operational Modes

The limitations of the power subsystem (see subsection 4.3.6) restrict the use of four TDRS transmitters: the UHF transmitter for the LDR forward link from TDRS to user, the two S band transmitters for the MDR forward links from TDRS to user, and the Ku band transmitter for the HDR return link from TDRS to the ground station. The other links consisting of the LDR return, MDR return, and HDR forward require only a small amount of TDRS power and can be operated without power subsystem restrictions. Table 5 illustrates several modes that are possible with these restrictions.

The modes have been separated into two major categories corresponding to sunlight exposure and eclipse. The MDR transmitters have two power levels, selectable by ground command. The high EIRP mode is used for transmitting voice to the Space Shuttle.

TABLE 5. TELECOMMUNICATION SERVICE MODES DUE TO TDRS POWER LIMITATIONS*

Mode		LDR Forward	MDR 1 Forward, percent			MDR 2 Forward			HDR to Ground Station
			High EIRP		Low EIRP	High EIRP		Low EIRP	
Sunlight	1	■	25	or	75			■	
	2	■	25	or	75				■
	3		25	or	75	■	or	■	■
Eclipse	1							■	
	2								■
	3		25	or	75			75	

*Shaded areas indicate available service.

Sunlight Mode 1: In this mode, the LDR forward link transmitter (UHF) and the two MDR forward link transmitters (S band) may be operated simultaneously. However, the high power level of one MDR transmitter is restricted to 25 percent usage in any 24 hour period (i. e., 6 hours), and the other is restricted to the low power level only.

Sunlight Mode 2: In this mode, the power of mode 1 which was used for one of the low power level MDR transmitters is used instead of transmit the HDR signal to the ground station. This does not appear to present any limitations because the two steerable 3. 82 meter antennas must be shared between MDR and HDR services.

Sunlight Mode 3: In this mode, the power that was used in mode 2 above for the LDR forward link is used to provide an unrestricted forward MDR link in addition to the HDR return link and the other MDR link which has a 25 percent usage limitation on the high power level. In this mode, both MDR links and the HDR link are in operation, and since there are two antennas for these three links, one user spacecraft must have the capability for both MDR (S band) and HDR (Ku band) communication. This mode was included in Table 5 to show that this case can be accommodated if required by a user mission.

Eclipse Modes: In all of the eclipse modes, the LDR forward link transmitter is turned off. The available power is used either for MDR forward links or the HDR return link. In mode 1, a low power MDR link may be used continuously. In mode 2, the HDR return link may be used continuously. Mode 3 is included to show that the power may be split so that during an eclipse both MDR links may be used with approximate time restrictions as shown in Table 5.

Table 5 is an attempt to illustrate grossly the possible combinations of the restricted services. During a given 24 hour period, all of the modes shown might be used. A careful monitoring of the power subsystem would allow even more service combinations than shown in Table 5. Further, the table is based on end-of-life power and in the early years of the TDRSS considerably more service is available. For instance, at beginning of life, there is no restriction of the MDR high power mode in sunlight mode 1 of Table 5.

To reiterate, the LDR return link, capable of returning 20 user signals simultaneously, and the two MDR return links, capable of 1 Mbps each, can be operated continuously without restriction.

3. 1. 2 Link Parameters

The features, characteristics, and parameters associated with each link of each service are presented below.

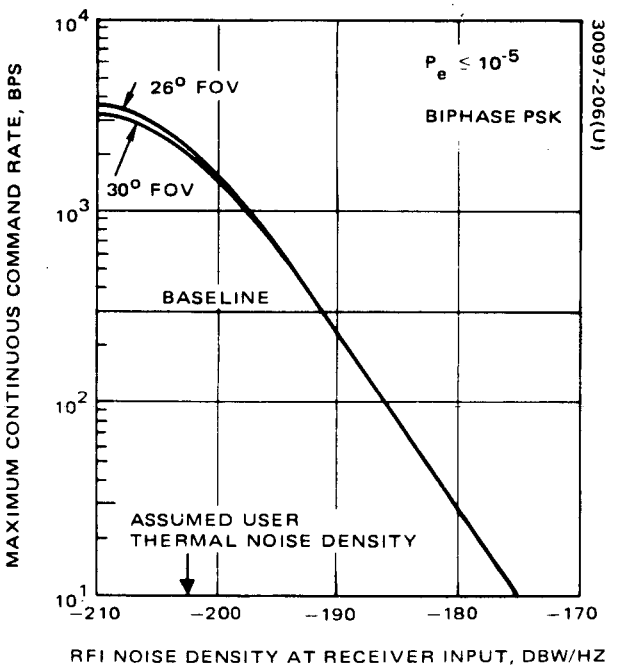

Figure 8. LDR Forward Link

3.1.2.1 Low Data Rate Service

Forward Link

The forward link, user command channel will be time-shared; that is, only one user can be commanded at a time. However, commands may be sent to many users within a period of 1 minute. All users will receive the TDRS transmitter RF signal; thus each command will have a prefix that will activate the command decoder of the intended user.

Other operational features include:

• Automatic user acquisition	User available for command shortly after becoming visible
• Time-shared link	Requires synchronized sequencing of user commands
• Fixed timing	User receivers can be standardized.
• Variable format	Number of bits and their significance in a user command can be different for every user if desired (i.e., command format flexibility).
• Baseline bit rate	300 bps
• Probability of bit error	$P_e \leq 10^{-5}$
• PN code length	2048
• One code per bit	
• Chip rate	614.4 kchips/s
• Carrier frequency	401.0 MHz
• Biphase PSK IF carrier modulation	
• EIRP	See Table 6.

Analysis of the low data rate links and a study of ground emitters have revealed that RFI is most likely the limiting factor in these links. Figure 8 shows how the bit rate is limited by RFI. The parameter chosen to quantify RFI is the average spectral density of the RFI power at the user receiver input.

TABLE 6. LDR FORWARD LINK EIRP

	19.7 Degree Field of View	26 Degree Field of View	30 Degree Field of View
Antenna gain, dB	13.4	12.5	11.8
Radiated Power, dBW	16.6	16.6	16.6
EIRP, dBW	30.0	29.1	28.4

Return Link

Up to 20 users may simultaneously return telemetry. Code division multiplexing (CDM) will be used to allow simultaneous telemetry return. The PN codes for CDM will be different for each user spacecraft's telemetry.

Convolutional encoding will be employed on user telemetry for bit error correction; link quality is improved significantly with this technique.

The baseline approach assumes that the return bit rate is standardized for all users, but this is not a system requirement. With this standardization, the baseline parameters and techniques are as follows:

- Bit rate: 1200 bps
- Probability of error $P_e \leq 10^{-5}$
- Adaptive processing of eight array antenna signals
- Rate one-half convolutional encoding
- One gold code per convolutional code symbol
- Gold code length 512
- Chip rate 1.2288 μchips/s
- Carrier frequency 136.5 MHz
- Biphase PSK carrier modulation
- User EIRP 4 dBW

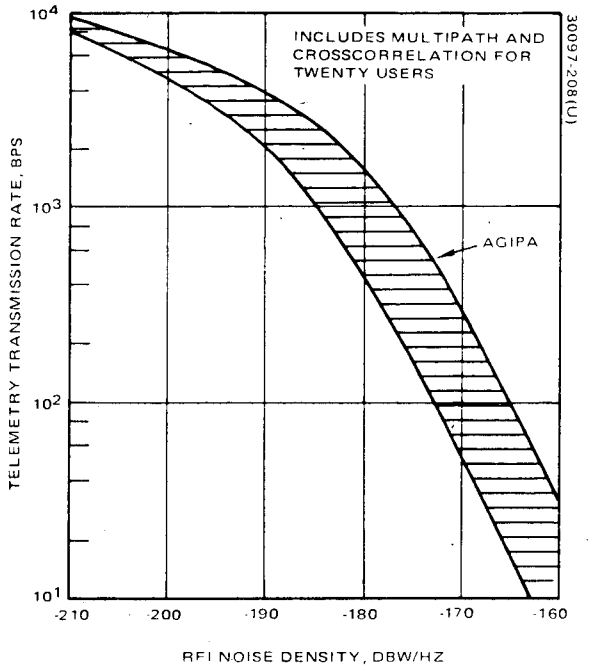

Figure 9. Telemetry Transmission Capability for 4 dBW EIRP User Satellite

- TDRS G/T per element (considering receiver generated noise only):

VHF antenna element gain (30 degree FOV)	8.7 dB
Receiver noise temperature	-26.2 K (dB)
GT (at receiver)	-17.5 dB/K

- Estimated degradation due to ground link and processing (same as for the Part I TDRS) — 3.0 dB

- Required E_b/η at decoder for $P_e = 10^{-5}$ — 4.1 dB-Hz

While the above parameters characterize the TDRS equipment capability, they do not characterize the LDR return link performance. For each user signal, there is an adaptive processor at the ground station which optimally combines the eight separate signals from the AGIPA antenna. In subsection 3.2.1, an AGIPA simulation is briefly discussed and some performance comparisons are presented. Figure 9 was the result of the simulation for the VHF array shown later in Figure 19. A performance range exists because the signal-to-interference ratio depends on the location of the user spacecraft with respect to the RFI pattern as seen by a TDRS. If the figure is correct, the baseline bit rate of 1200 bps from 20 users simultaneously is possible with an RFI noise density up to -186 dBW/Hz.

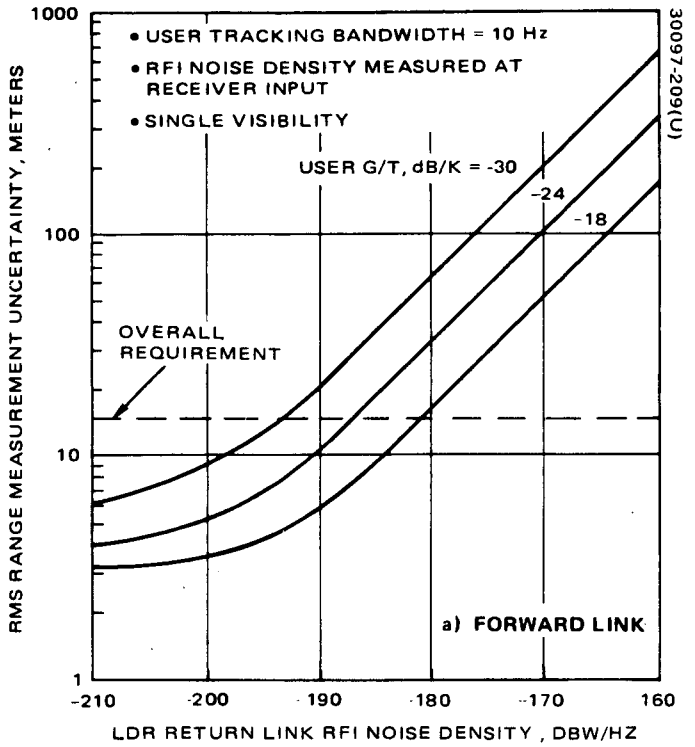

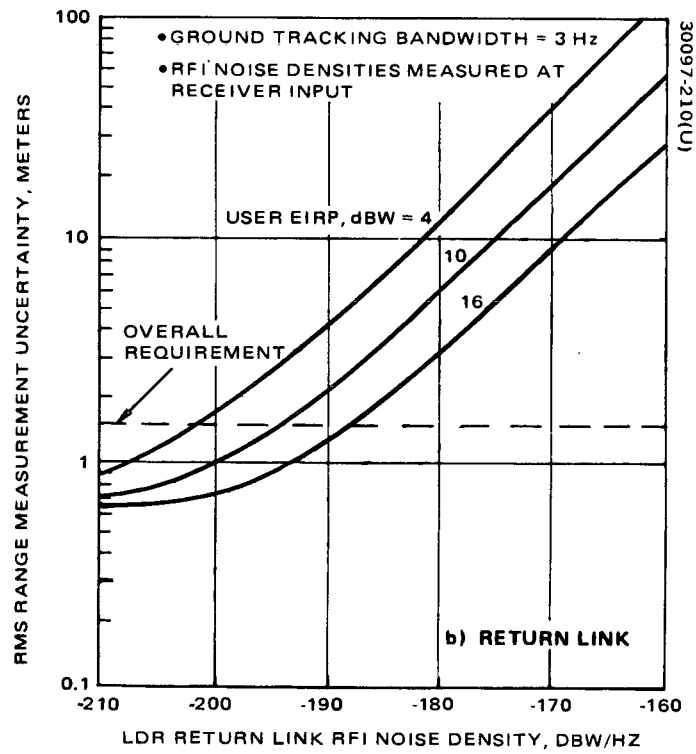

Figure 10. RMS Range Measurement Uncertainty

Tracking

Due to the PN code signaling, user spacecraft receivers automatically acquire and synchronize to the signal transmitted from a TDRS. After the brief acquisition period, range and range rate measurements can be made. However, the user's transmitter must be turned on, and the return signal acquired at the ground station. A particular operational advantage of the signaling concepts used here is that both range and range measurements can be made simultaneous with telemetry reception and no forward link commands are required.

Range measurement uncertainty is affected by system noise, of which RFI appears to be the most severe. Figure 10 shows the rms uncertainty as a function of RFI noise density for both forward and return levels. The total rms uncertainty is the sum of the two link contributions.

3.1.2.2 Medium Data Rate Service

Two independent two-way channels are provided via the two dual-feed antennas. The power subsystem and ground link transmitter have been designed to support these two links simultaneously with the required margin. Each two-way link has the following characteristics.

Forward Links

- Channel bandwidth — 30 MHz
- Channel center frequency placeable by ground command anywhere from 2038 to 2118 MHz with 1 MHz discrete steps
- High power mode
  - Antenna gain — 36 dB
  - Radiated power — 11 dBW
  - EIRP — 47 dBW
- Low power mode
  - Antenna gain — 36 dB
  - Radiated power — 5 dBW
  - EIRP — 41 dBW

Figure 11 shows the maximum possible data rate that can be sent to an unmanned user assuming no error correction encoding, a receiver system noise temperature of 800 K, and 3 dB receive losses.

The link capacity for transmitting to the Space Shuttle is shown in Figure 12. The major assumptions of the link analysis accompany the figure. Note that the requirement for 54 kbps which includes two digital voice signals plus 6 kbps data can be accommodated with the high power mode.

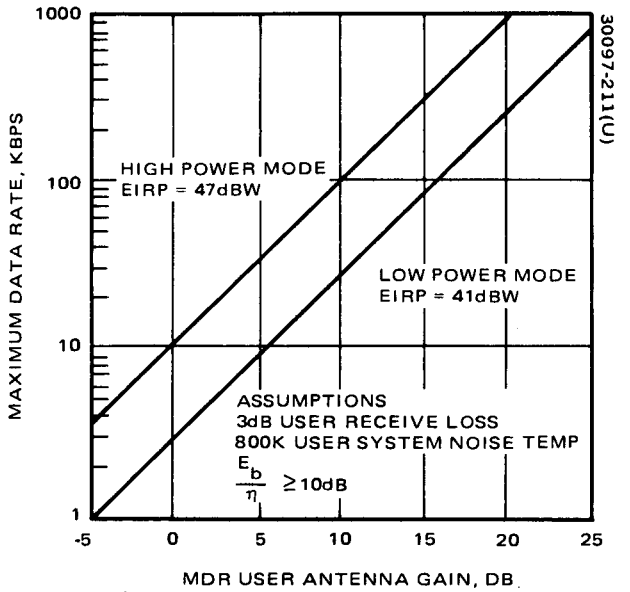

Figure 11. MDR Forward Link Capability

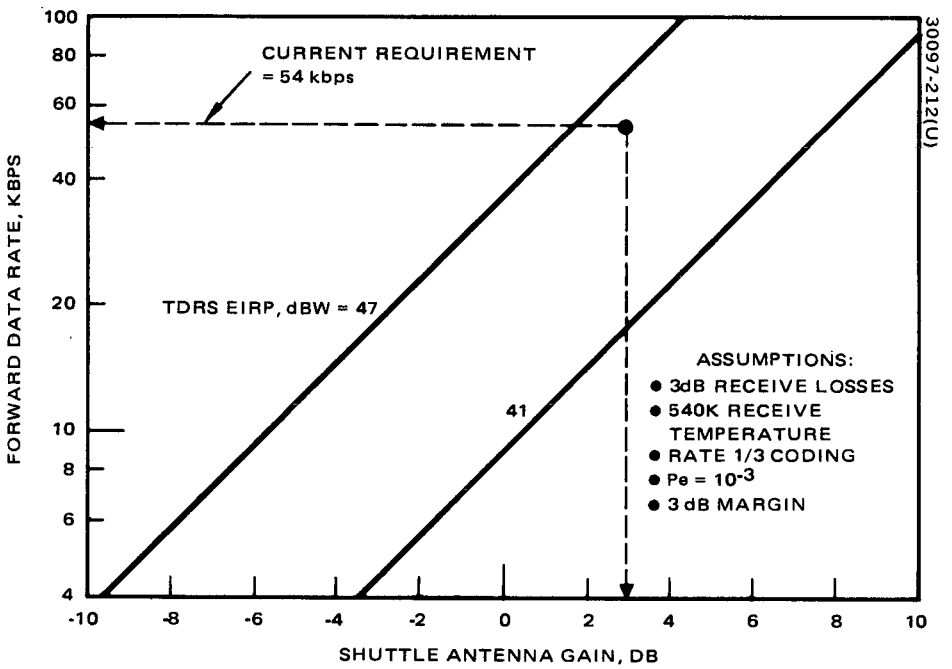

Figure 12. Space Shuttle Service Via TDRS; Forward Command Plus Voice

Return Links

- Channel bandwidth — 10 MHz
- Channel center placeable by ground command anywhere from 2220 to 2300 MHz with 1 MHz discrete steps.
- G/T at receiver input considering all noise sources. — 10.2 dB/K

The bandwidth of the return channels is smaller than that of the forward channels because the energy is radiated away from the earth most of the time. Consequently, the spectrum spreading required to reduce the earth-incident flux density to acceptable levels is less.

Figure 13 shows the relationship between the return data rate, radiated power, and antenna gain for an unmanned user. No link margin and no error correcting encoding have been assumed. Figure 14 shows the relationship between data rate, transmitter power, and antenna gain for the Space Shuttle. A number of assumptions have been made for this link as listed with the figure. The use of coding and the 10^{-4} bit error rate (BER) allow a bit energy to noise density of 5.2 dB, whereas 10 dB was used in Figure 13. The assumed line loss plus margin tends to cancel the increase in link capacity due to coding relative to Figure 13. However, note that the requirement of 192 kbps can be achieved with a 60 watt transmitter and 3 dB gain antenna on the Shuttle.

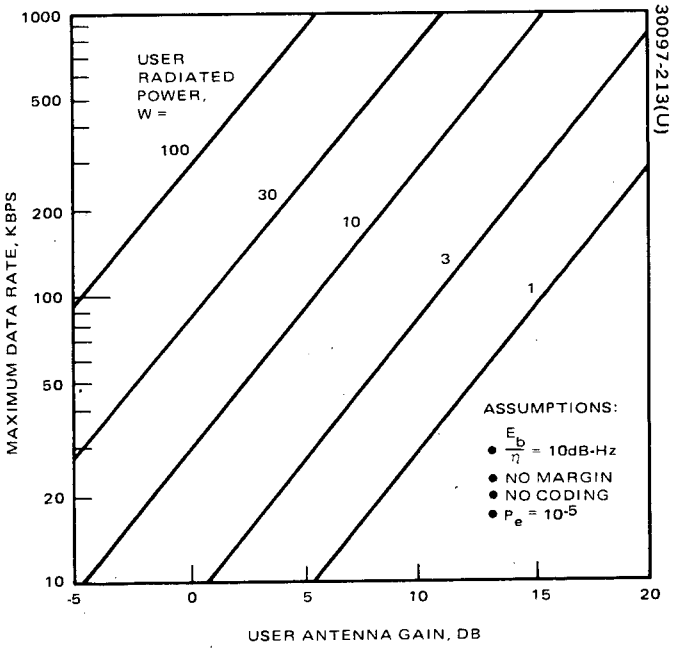

Figure 13. MDR Return Link Capability

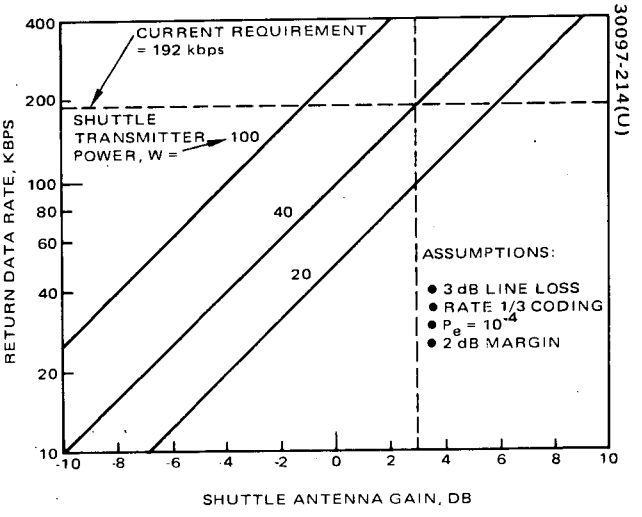

Figure 14. Space Shuttle Service Via TDRS; Return Telemetry Plus Voice

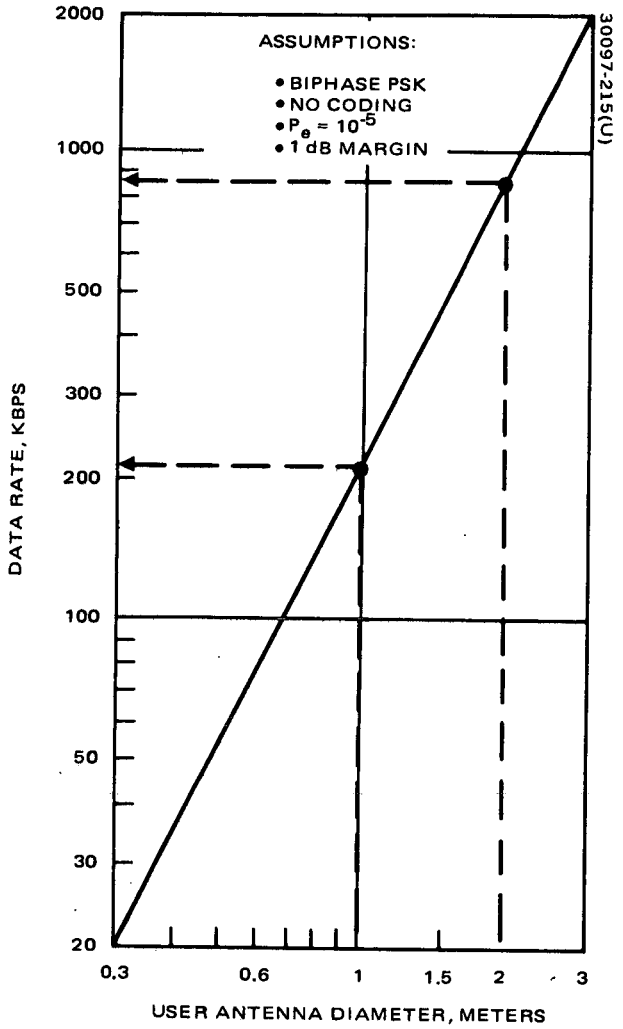

Figure 15. HDR Forward Link

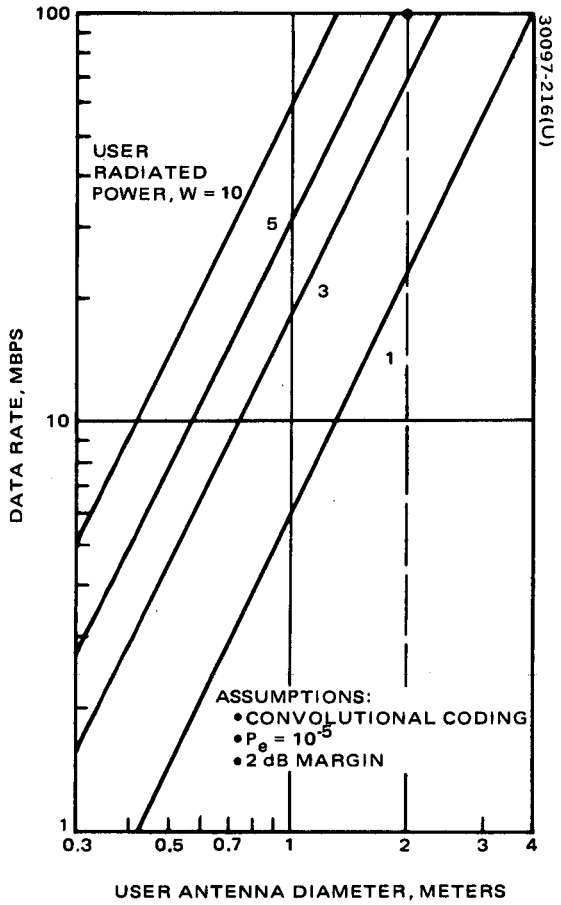

Figure 16. HDR Return Link

3.1.2.3 High Data Rate Service

Either of the two dual-feed antennas may be used for this service, but must also be shared with the MDR service. The TDRS/user link employs Ku band frequencies. If a user spacecraft has the capability, the dual feed and independence of the MDR and HDR repeater channels will allow a two-way link simultaneously at both S band and Ku band.

Forward Link

• TDRS to user frequency band	14.760 to 14.860 GHz (100 MHz)
• EIRP:	
Antenna gain	52.4 dB
Radiated power	-12.4 dBW
EIRP	40.0 dBW

Figure 15 shows the required user antenna diameter as a function of bit.

Return Link

• Variable bandwidth	200, 100, 50, 10 MHz
• Center frequency of the TDRS/ user link	13.850
• G/T	20.2 dB/K
G	51.9
T (including all sources)	1470 K (31.7 dB)

Figure 16 shows the relationship between the required user antenna size, radiated power and return data rate. Figure 17 shows the relationship between the required user antenna diameter and radiated power for a data rate of 100 Mbps with and without the use of error correcting encoding.

3.1.2.4 Order Wire Service

• Center frequency	2218 MHz
• Bandwidth	1 MHz
• G/T	-15.2 dB/K at receiver over 19.5 degree earth centered cone considering all noise sources

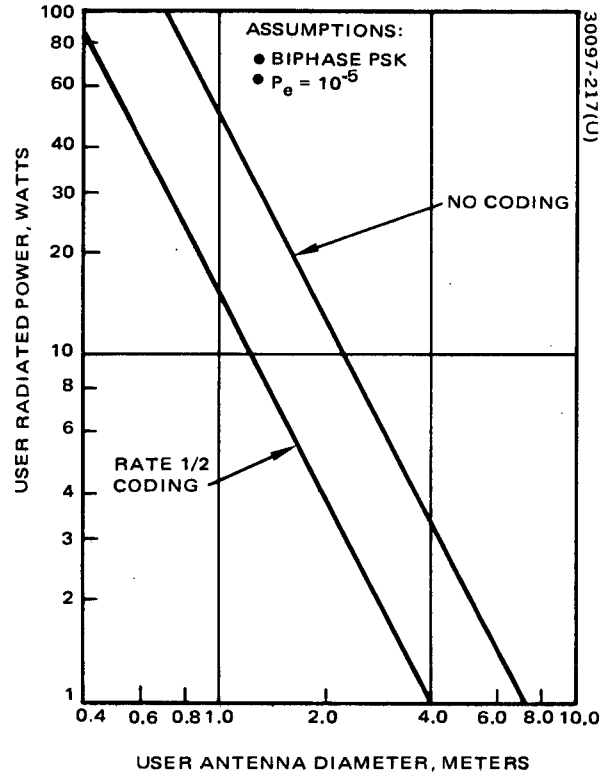

Figure 17. HDR User Requirements for 100 Mbps Telemetry

3.1.2.5 S Band Transponder

- Frequency band

Receive	2025 to 2033 MHz
Transmit	2206 to 2214 MHz

- EIRP

Antenna gain	13.5 dB
Radiated power	6.5 dBw
EIRP	20.0 dBw

3.1.2.6 Ground Links

A weather margin of 9.1 dB has been provided for all channels in both the forward and return links between the TDRS and Ground Station.

Forward Link

A northern hemisphere coverage horn is used to receive the LDR, beacon, and TDRS command channels from the ground station. A 1.43 meter reflector antenna is used to receive the two MDR and the HDR channels.

• High gain antenna (HGA) G/T	9.4 dB/K
G	44 dB
T	2900 K including all noise sources
• Low gain antenna (LGA) G/T	-13.2 dB/K
G	18.5 dB
T	1470 K including all noise sources
• The minimum carrier to noise power at the TDRS receiver in each channel	15 dB
• Frequency bands	13.400 to 13.420 GHz for LGA receiver
	13.460 to 13.690 GHz for HGA receiver

Return Link

There are two power amplifiers, the outputs of which are multiplexed and transmitted to the ground station via the 1.43 meter Ku band antenna. One of the power amplifiers contains the HDR signal and operates in a saturated mode. The other power amplifier provides linear amplification required by the multiple signals and by the LDR adaptive processing. Major link characteristics are listed in Table 7.

Note that the weather margin for the return user telemetry links is 9.8 dB which is 7.7 dB lower than the 17.5 dB margin provided by the other TDRS configurations. This lower margin was the result of decreasing the ground link antenna from that of the Atlas-Centaur launched TDRS (see Volume 3), while keeping the same transmitter. In subsection 3.2.3 it is shown that if an additional (third) ground receiving terminal is provided, the 9.8 dB margin is sufficient to limit outage to less than 0.02 percent (i.e., less than 2 hours/year).

TABLE 7. HDR RETURN LINK BIT ENERGY-TO-NOISE DENSITY

Return Service	Minimum Ground Link E_b/η, dB	Maximum Data Rate Per User, kbps	Minimum Weather Margin, dB
Low data rate telem.	14	1.2	9.1
LDR voice	14	20.0	9.1
Medium data rate	20	1,000.0	9.1
High data rate	15	100,000.0	9.1
TDRS telemetry	15	1.0	13.0
Order wire	15	1.0	13.0

However, an additional recourse has been provided, namely the use of one of the 3.82 meter S/Ku band antennas. RF switches have been provided to allow either of these antennas to be used for the ground link when desired. The margin then is approximately 17 dB; approximately 0.5 dB is lost in the switches. If one of these antennas is used for the ground link, then only one remains to provide both MDR and HDR services. Thus, it is expected that this alternative would be used infrequently during periods of extremely heavy rainfall and only when support of a single MDR or HDR user is critical.

3.2 COMMUNICATION ANALYSIS

Three subjects are treated here: 1) LDR return link employing an adaptive ground implemented phased array (AGIPA), 2) HDR link acquisition, and 3) ground link weather margin. The LDR forward link and MDR forward and return links are analyzed in Volume 4 of the Part I TDRS Final Report. The analysis of these links as well as the HDR link is straightforward and based primarily on the power budgets of Tables 3 and 4. However, the three subjects to be discussed here involve concepts that are complex but basic to the viability of the telecommunication service system.

3.2.1 LDR Return Link with AGIPA

The LDR return link service must relay signals from up to 20 user spacecraft simultaneously. User altitudes up to 5000 km must be accommodated and the VHF band 136 to 137 MHz has been selected for the user-to-TDRS link. In order to meet these requirements, the TDRS must have an antenna consisting of one or more elements each with a 3 dB beamwidth of 30 degrees or more.

The radiation received by the antenna consists of that radiated by 1) user spacecraft visible to the TDRS, 2) celestial bodies within the antenna beam, and 3) earth-based transmitters in the allocated band visible to the TDRS. It is the latter radiation that poses the greatest threat to TDRS communication in the allocated 136 to 137 MHz frequency band. More than 40 percent of the earth's surface is visible to a TDRS, and the interference in this popular portion of the VHF band has the potential for "swamping" a low power, user satellite transmission or requiring the use of undesirably low data rates.

The RFI as seen by a TDRS has been evaluated by Electromagnetic Systems Laboratories from a catalog of 45,000 emitters. The selected frequency band for the LDR return link is 136 to 137 MHz, and for a 13.9 dB gain antenna providing a 30 degree field of view, the RFI power density has been estimated as of December 1972 to be -177 and -183 dBW/Hz for TDRS East and TDRS West, respectively. If these estimates are correct and user spacecraft have omnidirectional antennas and transmitters capable of 5 watts of output power, then data rates are limited approximately to 50 and 200 bps, respectively with proposed coding and modulation techniques.

Following a NASA GSFC suggestion, an AGIPA has been used to improve the data rates in the VHF band. The AGIPA consists of 1) an array of antenna elements on the TDRS and 2) an adaptive processor at the ground station. Figure 18 shows the major functional elements of the AGIPA/TDRS system. Each array element separately receives orthogonal senses of linear polarization producing two signals. The pair of signals from each element are amplified in the TDRS and transmitted separately to the ground station. The processor at the ground station adjusts both the amplitude and phase of each signal and then adds them together. The objective of this signal weighting and combining is to enhance the user satellite signal and suppress the interference, subsequently called RFI. The processing, which employs an algorithm to determine the signal weightings, utilizes the properties inherent in the array configuration for spatial discrimination.

The AGIPA system is significantly different from the ordinary phased array where phase only is adjusted between the receiving element and the receiver. With this type of system, the spatial discrimination is primarily limited to that which can be achieved by pointing a rather broad beam in the direction which provides the best data output at the ground station. The AGIPA on the other hand allows much greater freedom in element signal weighting, i.e., amplitude and a greater range of phase shift. Because of the greater variations possible with the AGIPA, the potential performance improvement should be greater than an ordinary phased array, but cannot be easily determined by considering the ordinary properties of an array antenna.

The function of the AGIPA processor is to provide the best reconstruction of the user spacecraft's signal that has become corrupted with noise. In order to produce this estimate of the user's signal, operations

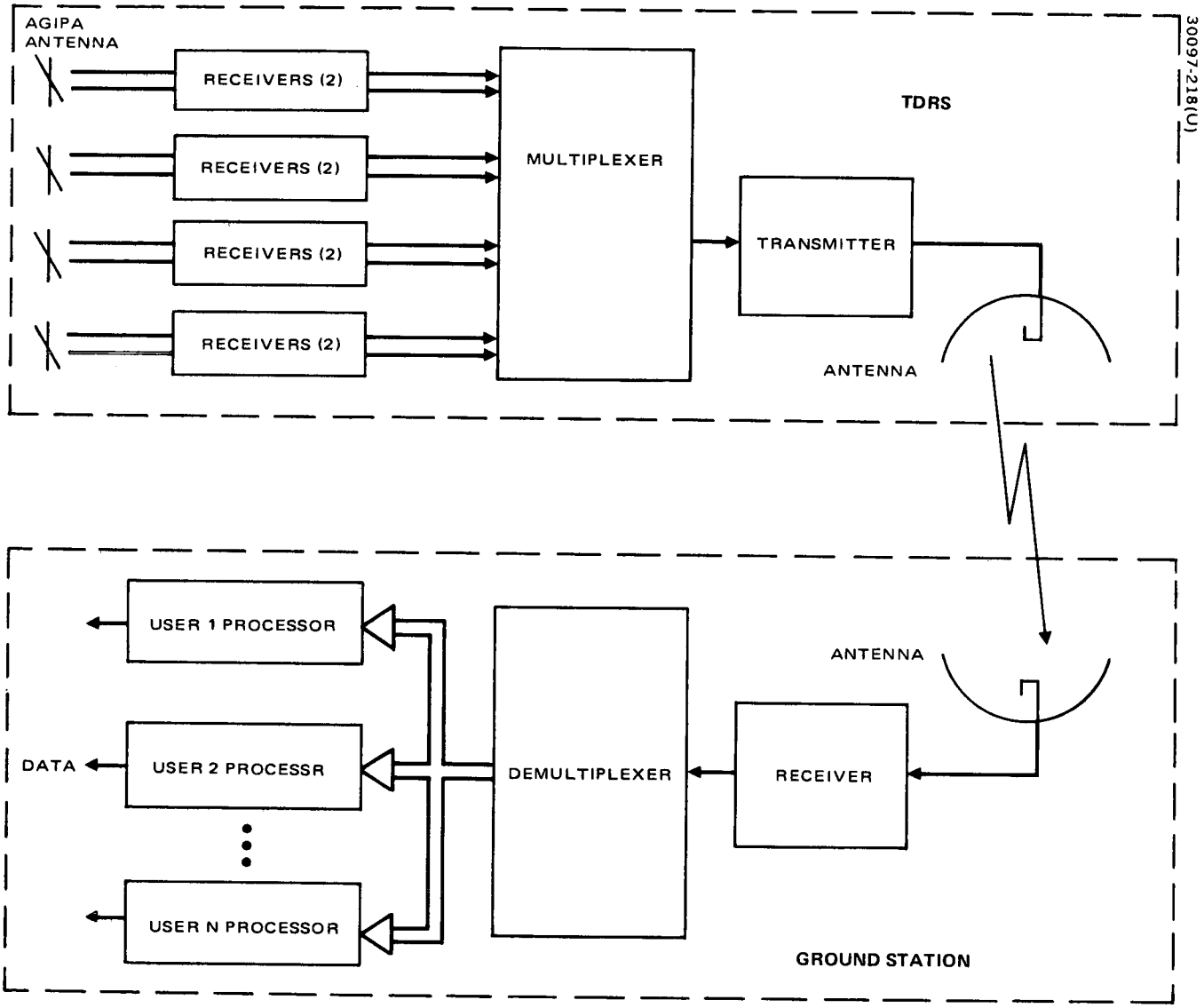

Figure 18. Major Functional Elements of AGIPA/TDRS System

on the inputs should discriminate against the noise and in favor of the signal. Much effort has been devoted in the past years to various techniques for accomplishing this with a single channel containing the desired signal plus noise. The implementation of these techniques produces a time domain smoothing and/or filtering in the frequency domain, e. g., Weiner filtering. In addition to this, AGIPA has the potential for spatial filtering, and it is this capability which is of primary interest.

In order to provide quantitative performance data and a better understanding of the AGIPA capability, a computer simulation has been developed at Hughes. This simulation allows investigation of the effects of the following major AGIPA aspects:

1) Antenna array configuration

   - Number of elements
   - Element radiation pattern
   - Array geometry

2) Processing algorithm for determining the amplitude and phase of each signal

3) RFI model: geographical distribution and signal characteristics of interfering transmitters

Referring to Figure 18, note that the functions of multiplexing, amplification and demultiplexing that occur between the antenna and the processor will not be simulated. Current TDRS requirements specify that these operations shall be linear (i. e., shall not introduce signal distortion). While this is an idealization in any real system, proper design of the equipment performing these functions will limit distortion such that the effects are second order compared to the effect of the three above listed items.

This simulation was used to estimate the performance capability of the TDRSS AGIPA system corresponding to the array antenna described later in subsection 4. 3. 3. 4.

The TDRS AGIPA antenna, illustrated in Figure 19, consists of four YAGI elements each with a peak gain of 9. 7 dB and with a spacing of 1. 8 wavelengths (4 meters). Each element separately receives orthogonal senses of linear polarization and the signals are amplified in eight separate receivers. The receiver outputs are frequency-multiplexed and amplified linearly for transmission to the ground station for adaptive processing. For the simulation a radiation pattern was used for each element which was representative of all low gain end-fire elements.

The processing algorithm results in a minimum mean square error (MMSE) estimate of the signal. The gains and phases of the incoming AGIPA signals are adjusted and added so as to minimize the average of $(s - \hat{s})^2$

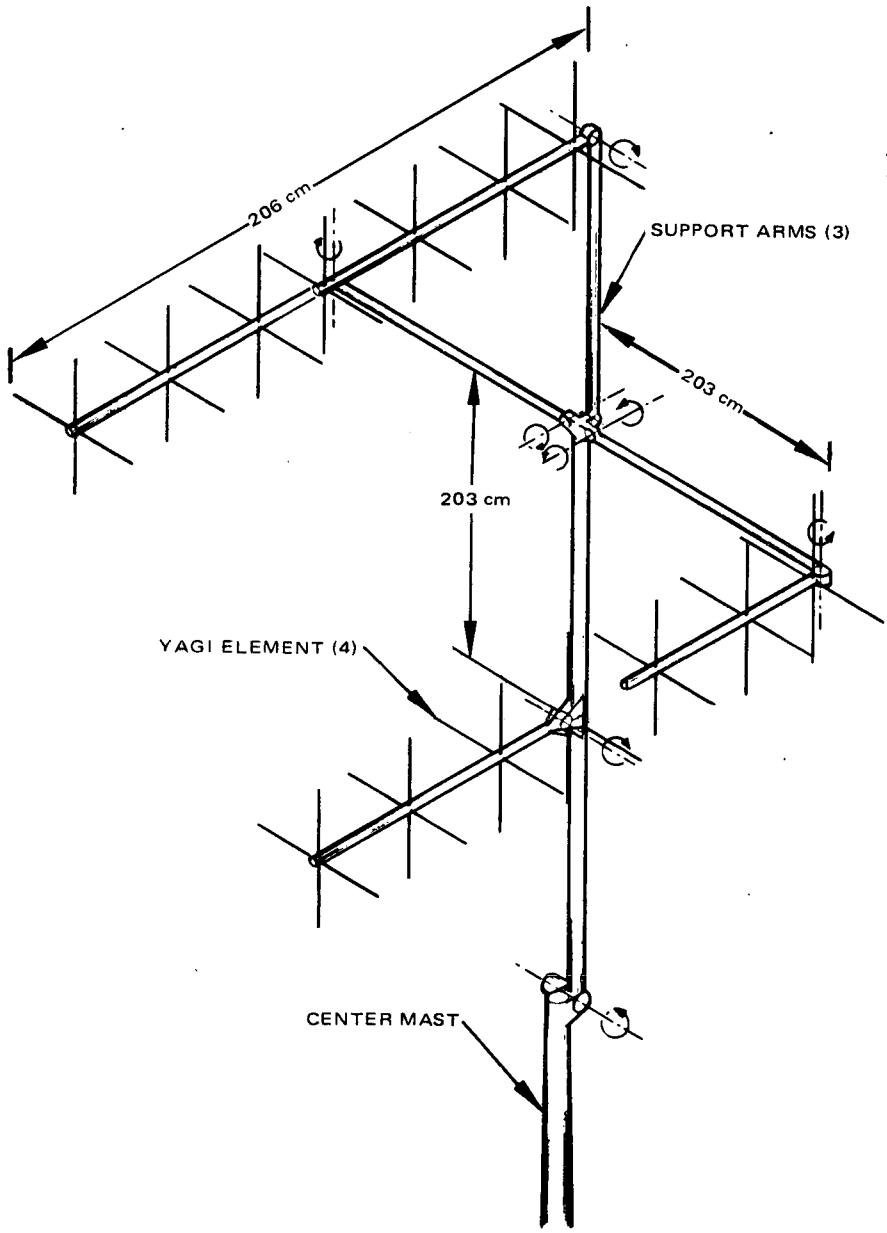

Figure 19. AGIPA Antenna Configuration

where s is the signal transmitted by the user and $\hat{s}$ is the processor's estimate. The MMSE criteria are applied to the IF signal (i.e., prior to data demodulation). The weight factors that produce the gain and phase adjustments for each signal can be written as a complex vector, W, which for the MMSE processor is of the form:

$$W = R_{xx}^{-1} P_g^*$$

R_{xx} = correlation matrix of received signal plus noise

$= R_{SS} + R_{NN} + \eta I$

R_{SS} = correlation matrix of received signal

R_{NN} = correlation matrix of received noise

η = receiver thermal noise

I = unity matrix

P_g^* = conjugate of the vector of cross-correlations between the observed signal vector and the desired signal

Where the thermal noise term, ηI, is high compared to R_{NN}, the weight factor is effectively P^*_g and the AGIPA behaves as a phased array with its beam steered toward the user. When the received RFI is large compared to the receiver thermal noise, the processor generates a pattern with nulls in the direction of the RFI.

Preliminary results show that the performance of the array design used for the current HAC Delta configuration is essentially that of the Junior AGIPA designed by Airborne Instrument Lab (AIL). The RFI distributions used in the computer analysis are listed in Table 8. These are the Atlantic and Pacific RFI distributions for TDRS E and TDRS W, respectively, given by AIL with power levels normalized in each case such that the total power is 20 dBW (100 W). These two RFI distributions are shown in Figures 20 and 21.

Figures 22 and 23 show the performance improvement achievable with the AGIPA above that possible with the same array in a fixed field-of-view (FOV) mode. The performance of the fixed FOV mode is similar to that of the Phase I Hughes design since the array's peak gain is approximately equal to that of the single-aperture antenna used in Part I. The value shown at each azimuth and elevation position is the AGIPA performance for a user at that location. Thus, each figure shows the performance difference at 441 locations. The signal-to-noise improvement shown in the figures is that which will occur with very high RFI levels — when thermal noise, multipath, and cross-correlation noise can be ignored. Multipath and cross-correlation noise will also be suppressed by AGIPA when the users are spatially separated, as will usually be the case. Receiver noise, earth noise, and galactic noise cannot be suppressed by AGIPA because to the processor they appear to have a

TABLE 8. ASSUMED RFI DISTRIBUTION

TDRS E

Number	Power, dBW	Azimuth, degrees	Elevation, degrees
1	7.0	-4.4	6.3
2	10.0	-5.6	5.8
3	12.0	-6.4	5.3
4	12.0	-6.6	4.6
5	7.0	-6.6	4.1
6	3.0	-6.8	3.3
7	5.0	-6.6	1.8
8	3.0	-7.6	-0.4
9	3.0	-2.8	-4.0
10	7.0	1.9	7.5
11	7.0	3.1	7.4
12	7.0	2.8	7.0
13	7.0	3.5	6.8
14	7.0	2.7	5.9
15	5.0	4.1	6.4
16	3.0	4.7	6.7
17	7.0	6.1	5.1
18	3.0	5.7	1.2
19	3.0	2.5	-1.5
20	3.0	5.7	-5.1

TDRS W

Number	Power, dBW	Azimuth, degrees	Elevation, degrees
1	0	-2.7	-5.9
2	3.0	-5.5	-5.6
3	0.	-8.2	-1.7
4	0.	-7.2	-0.6
5	7.0	-6.6	5.0
6	7.0	-5.8	5.8
7	12.0	-3.1	7.4
8	3.0	0.5	7.8
9	5.0	1.2	8.2
10	7.0	4.0	6.8
11	10.0	4.9	5.7
12	10.0	5.4	6.3
13	12.0	6.0	5.0
14	12.0	6.9	5.2
15	8.0	7.7	3.6
16	5.0	0.9	3.4

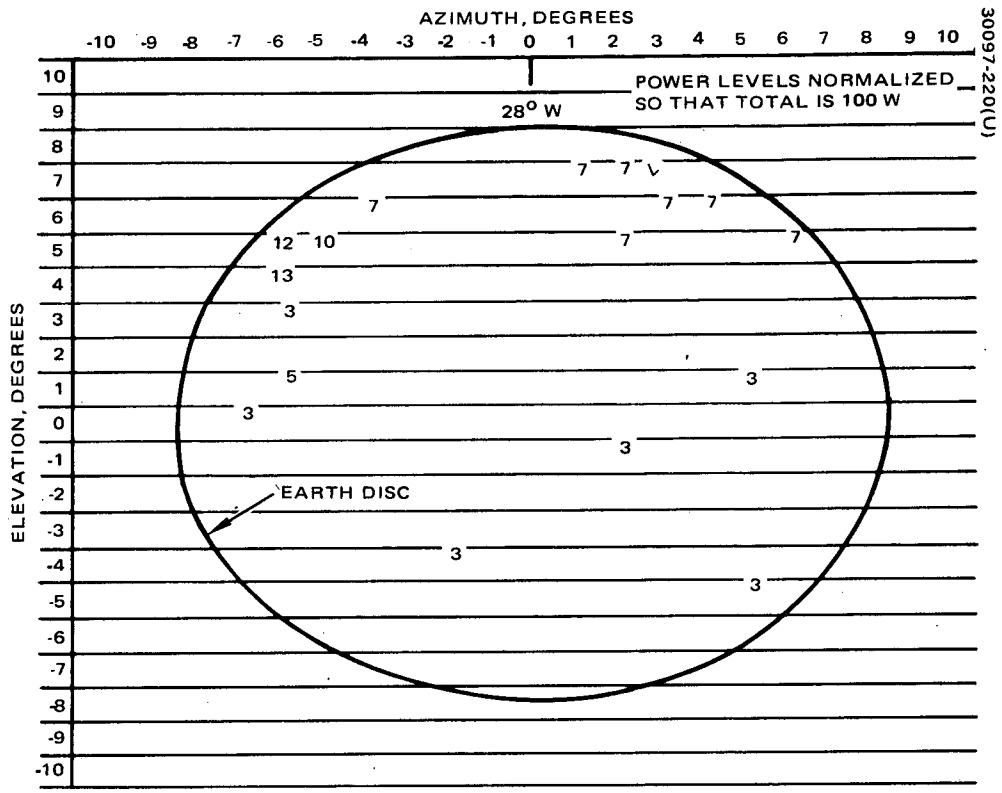

Figure 20. RFI Distribution for TDRS E, dBW

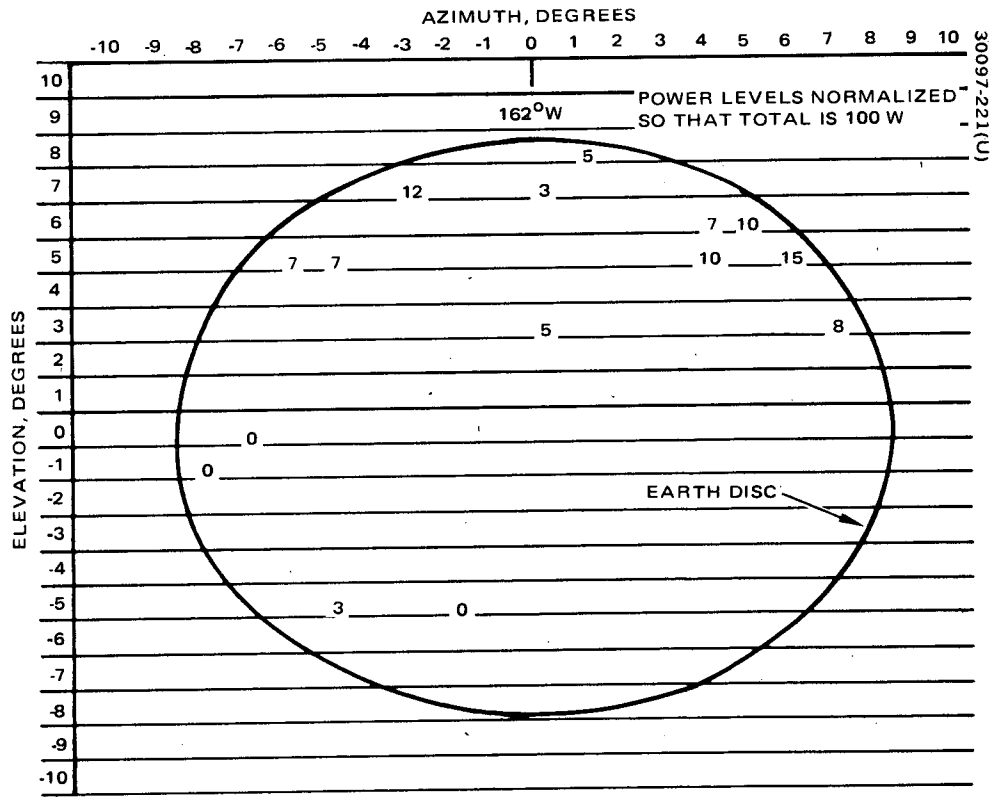

Figure 21. RFI Distribution for TDRS W, dBW

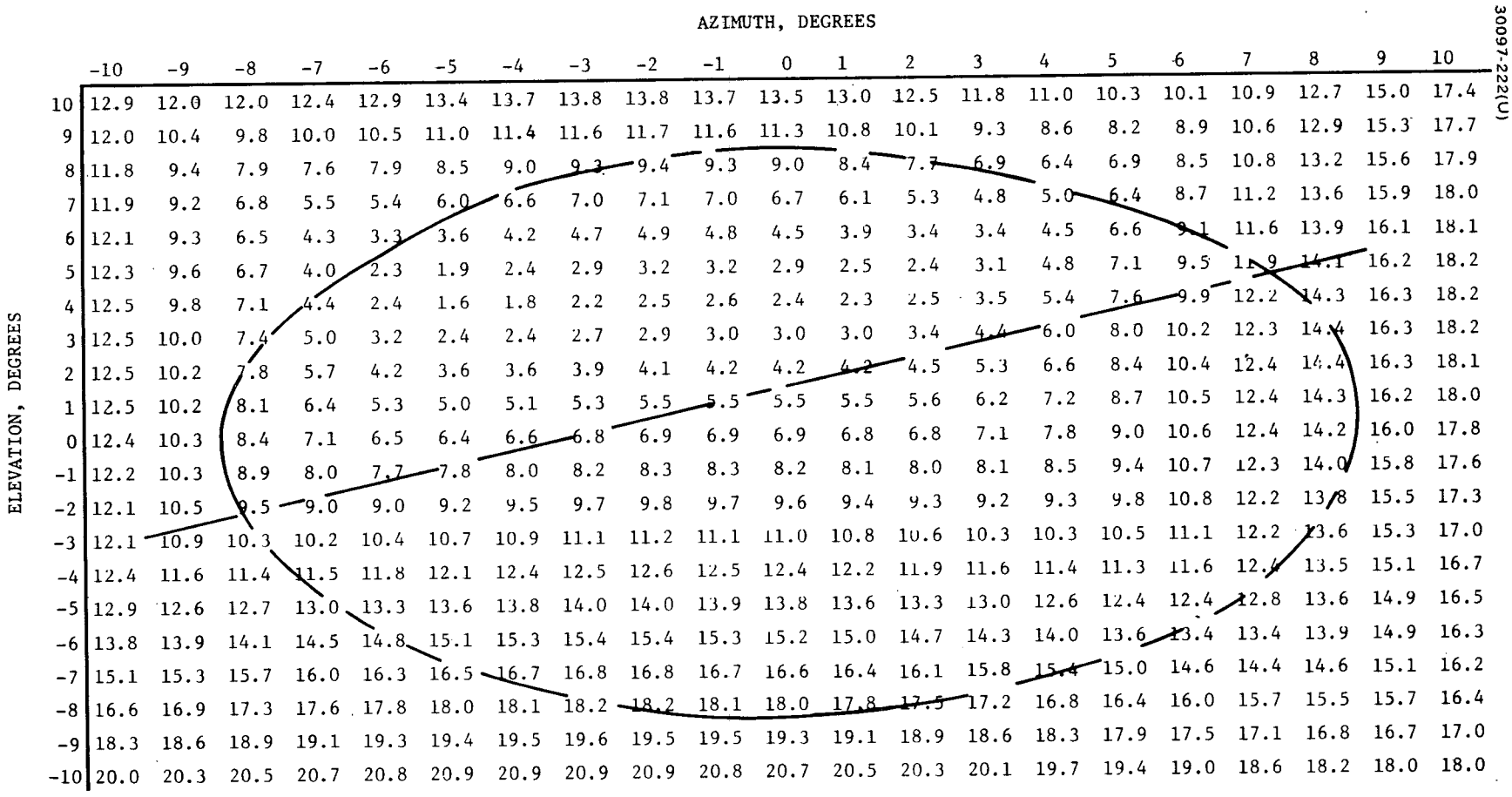

ELEV \ AZ	-10	-9	-8	-7	-6	-5	-4	-3	-2	-1	0	1	2	3	4	5	6	7	8	9	10
10	12.9	12.0	12.0	12.4	12.9	13.4	13.7	13.8	13.8	13.7	13.5	13.0	12.5	11.8	11.0	10.3	10.1	10.9	12.7	15.0	17.4
9	12.0	10.4	9.8	10.0	10.5	11.0	11.4	11.6	11.7	11.6	11.3	10.8	10.1	9.3	8.6	8.2	8.9	10.6	12.9	15.3	17.7
8	11.8	9.4	7.9	7.6	7.9	8.5	9.0	9.3	9.4	9.3	9.0	8.4	7.7	6.9	6.4	6.9	8.5	10.8	13.2	15.6	17.9
7	11.9	9.2	6.8	5.5	5.4	6.0	6.6	7.0	7.1	7.0	6.7	6.1	5.3	4.8	5.0	6.4	8.7	11.2	13.6	15.9	18.0
6	12.1	9.3	6.5	4.3	3.3	3.6	4.2	4.7	4.9	4.8	4.5	3.9	3.4	3.4	4.5	6.6	9.1	11.6	13.9	16.1	18.1
5	12.3	9.6	6.7	4.0	2.3	1.9	2.4	2.9	3.2	3.2	2.9	2.5	2.4	3.1	4.8	7.1	9.5	11.9	14.1	16.2	18.2
4	12.5	9.8	7.1	4.4	2.4	1.6	1.8	2.2	2.5	2.6	2.4	2.3	2.5	3.5	5.4	7.6	9.9	12.2	14.3	16.3	18.2
3	12.5	10.0	7.4	5.0	3.2	2.4	2.4	2.7	2.9	3.0	3.0	3.0	3.4	4.4	6.0	8.0	10.2	12.3	14.4	16.3	18.2
2	12.5	10.2	7.8	5.7	4.2	3.6	3.6	3.9	4.1	4.2	4.2	4.2	4.5	5.3	6.6	8.4	10.4	12.4	14.4	16.3	18.1
1	12.5	10.2	8.1	6.4	5.3	5.0	5.1	5.3	5.5	5.5	5.5	5.5	5.6	6.2	7.2	8.7	10.5	12.4	14.3	16.2	18.0
0	12.4	10.3	8.4	7.1	6.5	6.4	6.6	6.8	6.9	6.9	6.9	6.8	6.8	7.1	7.8	9.0	10.6	12.4	14.2	16.0	17.8
-1	12.2	10.3	8.9	8.0	7.7	7.8	8.0	8.2	8.3	8.3	8.2	8.1	8.0	8.1	8.5	9.4	10.7	12.3	14.0	15.8	17.6
-2	12.1	10.5	9.5	9.0	9.0	9.2	9.5	9.7	9.8	9.7	9.6	9.4	9.3	9.2	9.3	9.8	10.8	12.2	13.8	15.5	17.3
-3	12.1	10.9	10.3	10.2	10.4	10.7	10.9	11.1	11.2	11.1	11.0	10.8	10.6	10.3	10.3	10.5	11.1	12.2	13.6	15.3	17.0
-4	12.4	11.6	11.4	11.5	11.8	12.1	12.4	12.5	12.6	12.5	12.4	12.2	11.9	11.6	11.4	11.3	11.6	12.4	13.5	15.1	16.7
-5	12.9	12.6	12.7	13.0	13.3	13.6	13.8	14.0	14.0	13.9	13.8	13.6	13.3	13.0	12.6	12.4	12.4	12.8	13.6	14.9	16.5
-6	13.8	13.9	14.1	14.5	14.8	15.1	15.3	15.4	15.4	15.3	15.2	15.0	14.7	14.3	14.0	13.6	13.4	13.4	13.9	14.9	16.3
-7	15.1	15.3	15.7	16.0	16.3	16.5	16.7	16.8	16.8	16.7	16.6	16.4	16.1	15.8	15.4	15.0	14.6	14.4	14.6	15.1	16.2
-8	16.6	16.9	17.3	17.6	17.8	18.0	18.1	18.2	18.2	18.1	18.0	17.8	17.5	17.2	16.8	16.4	16.0	15.7	15.5	15.7	16.4
-9	18.3	18.6	18.9	19.1	19.3	19.4	19.5	19.6	19.5	19.5	19.3	19.1	18.9	18.6	18.3	17.9	17.5	17.1	16.8	16.7	17.0
-10	20.0	20.3	20.5	20.7	20.8	20.9	20.9	20.9	20.9	20.8	20.7	20.5	20.3	20.1	19.7	19.4	19.0	18.6	18.2	18.0	18.0

Figure 22. Signal-to-Noise Ratio Improvement at 441 User Spacecraft Positions Via TDRS W, dBW

uniform spatial distribution. The data in Figures 22 and 23 can be used to quickly give performance information for a typical user orbit. The lines shown in these figures correspond to the 23 degree and 63 degree inclined orbits studied by AIL. Their results for the Junior AGIPA and the Hughes results for the array of Figure 19 are shown in Figure 24 for six positions along these orbits. The curves are within 3 dB for most cases.

Figure 25 and 26 give absolute performance results for AGIPA rather than relative values. Figure 25 gives the carrier-to-noise density ratio at the output of the ground processor for a total RFI level of -180 dBW/Hz. Figure 26 shows the return link performance for various user EIRP and RFI levels. This figure is based on several computer runs of the type given in Figure 25. Figure 27 shown previously as Figure 9 summarizes the return telemetry rate performance for a 4 dBW EIRP user as a function of RFI noise density. The upper AGIPA curve corresponds approximately to performance exceeded at only 10 percent of the points on the family of figures such as Figure 25 and the lower curve corresponds roughly to performance exceeded by 60 percent of the points on the family of figures.

The RFI noise level parameter used in Figures 25, 26, and 27 is the total randomly polarized RFI power density at the input to the spacecraft receivers when a 14 dB gain antenna is used. This value of antenna gain is not that of the TDRS, but is used as the standard for defining the RFI level because this is the value used by Electromagnetic Systems Laboratories in their study of RFI. The computer model that generated the figures also includes receiver noise at a level of -200 dBW/Hz. This includes thermal noise and background noise. Both the earth and galactic background noise temperatures have a value of 300 K. These results also include the effects of multipath and correlation noise. With 20 users, the total noise due to these effects at the spacecraft receiver will be approximately -196 dBW/Hz without AGIPA processing. Since this noise is spatially distributed, several dB improvement is expected from AGIPA. A value of -200 dBW/Hz has therefore been allocated for multipath and cross-correlation. This brings the effective receiver noise level to -197 dBW/Hz.

The simulation also assumed an effective link degradation of 3 dB between the spacecraft receivers and the processor output, which is the input to the convolutional decoder. The convolutional decoder requires an E_b/η of 4.1 dB for a bit error probability of 10^{-5}. The transmission rate possible at each of the 441 angular locations in Figure 25 is therefore

$$R = P/\eta - 4.1 \text{ dB (Hz)}$$

For example, directly below the TDRS at Az = El = 0, P/η = 33.7. The transmission rate limit is therefore 33.7 - 4.1 = 29.6 dB(Hz) or 910 bps.

If the RFI noise density is between -170 and -180 dBW/Hz as has been estimated, then note from Figure 26 that even an unsophisticated user can transmit between 50 and 300 bps nearly continuously, and relatively long periods of transmission at rates between 250 and 1500 bps should also be possible. A more advanced user with a YAGI antenna and 30 watts of power can transmit between 3000 and 20,000 bps nearly continuously.

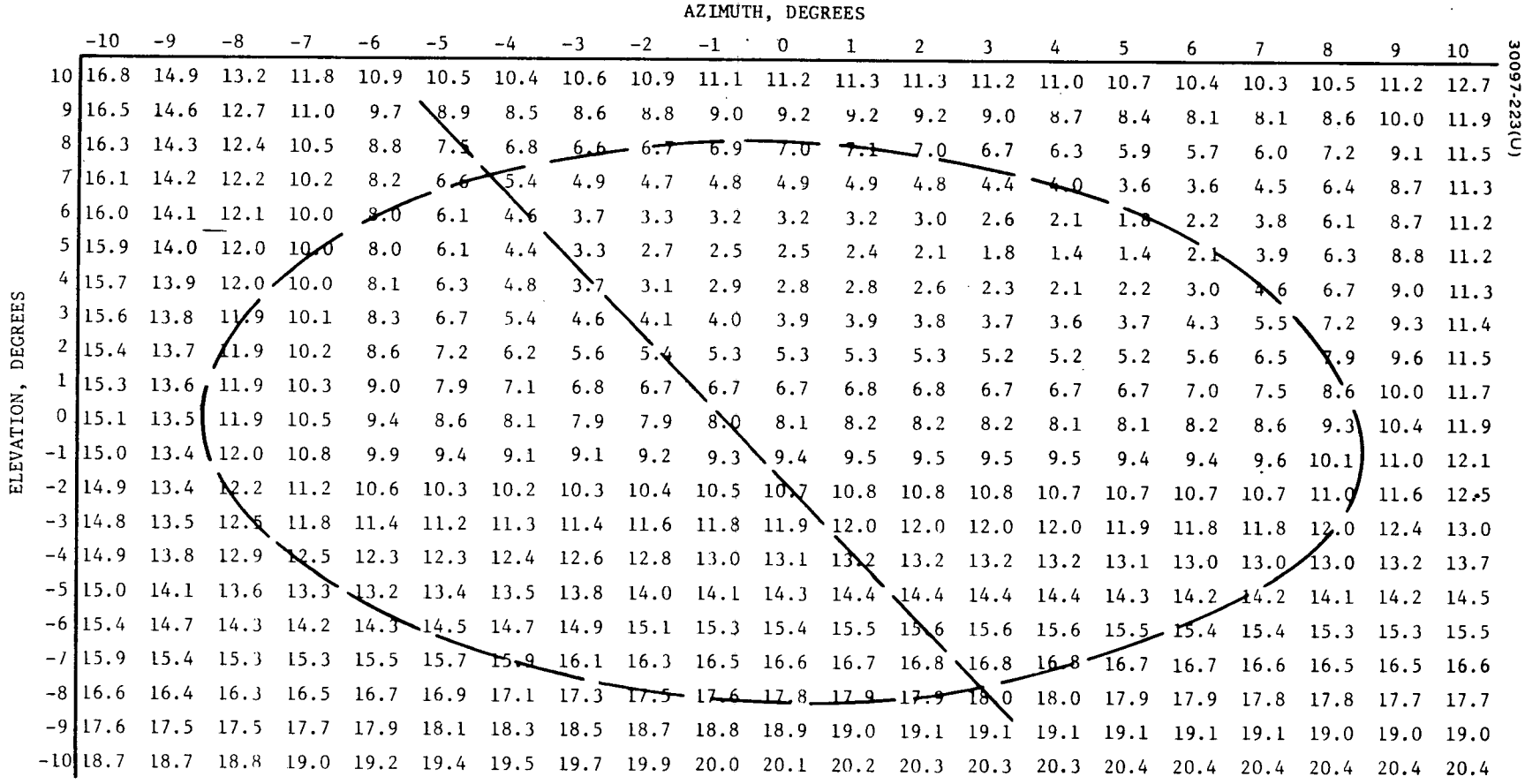

EL \ AZ	-10	-9	-8	-7	-6	-5	-4	-3	-2	-1	0	1	2	3	4	5	6	7	8	9	10
10	16.8	14.9	13.2	11.8	10.9	10.5	10.4	10.6	10.9	11.1	11.2	11.3	11.3	11.2	11.0	10.7	10.4	10.3	10.5	11.2	12.7
9	16.5	14.6	12.7	11.0	9.7	8.9	8.5	8.6	8.8	9.0	9.2	9.2	9.2	9.0	8.7	8.4	8.1	8.1	8.6	10.0	11.9
8	16.3	14.3	12.4	10.5	8.8	7.5	6.8	6.6	6.7	6.9	7.0	7.1	7.0	6.7	6.3	5.9	5.7	6.0	7.2	9.1	11.5
7	16.1	14.2	12.2	10.2	8.2	6.6	5.4	4.9	4.7	4.8	4.9	4.9	4.8	4.4	4.0	3.6	3.6	4.5	6.4	8.7	11.3
6	16.0	14.1	12.1	10.0	8.0	6.1	4.6	3.7	3.3	3.2	3.2	3.2	3.0	2.6	2.1	1.8	2.2	3.8	6.1	8.7	11.2
5	15.9	14.0	12.0	10.0	8.0	6.1	4.4	3.3	2.7	2.5	2.5	2.4	2.1	1.8	1.4	1.4	2.1	3.9	6.3	8.8	11.2
4	15.7	13.9	12.0	10.0	8.1	6.3	4.8	3.7	3.1	2.9	2.8	2.8	2.6	2.3	2.1	2.2	3.0	4.6	6.7	9.0	11.3
3	15.6	13.8	11.9	10.1	8.3	6.7	5.4	4.6	4.1	4.0	3.9	3.9	3.8	3.7	3.6	3.7	4.3	5.5	7.2	9.3	11.4
2	15.4	13.7	11.9	10.2	8.6	7.2	6.2	5.6	5.4	5.3	5.3	5.3	5.3	5.2	5.2	5.2	5.6	6.5	7.9	9.6	11.5
1	15.3	13.6	11.9	10.3	9.0	7.9	7.1	6.8	6.7	6.7	6.7	6.8	6.8	6.7	6.7	6.7	7.0	7.5	8.6	10.0	11.7
0	15.1	13.5	11.9	10.5	9.4	8.6	8.1	7.9	7.9	8.0	8.1	8.2	8.2	8.2	8.1	8.1	8.2	8.6	9.3	10.4	11.9
-1	15.0	13.4	12.0	10.8	9.9	9.4	9.1	9.1	9.2	9.3	9.4	9.5	9.5	9.5	9.5	9.4	9.4	9.6	10.1	11.0	12.1
-2	14.9	13.4	12.2	11.2	10.6	10.3	10.2	10.3	10.4	10.5	10.7	10.8	10.8	10.8	10.7	10.7	10.7	10.7	11.0	11.6	12.5
-3	14.8	13.5	12.5	11.8	11.4	11.2	11.3	11.4	11.6	11.8	11.9	12.0	12.0	12.0	12.0	11.9	11.8	11.8	12.0	12.4	13.0
-4	14.9	13.8	12.9	12.5	12.3	12.3	12.4	12.6	12.8	13.0	13.1	13.2	13.2	13.2	13.2	13.1	13.0	13.0	13.0	13.2	13.7
-5	15.0	14.1	13.6	13.3	13.2	13.4	13.5	13.8	14.0	14.1	14.3	14.4	14.4	14.4	14.4	14.3	14.2	14.2	14.1	14.2	14.5
-6	15.4	14.7	14.3	14.2	14.3	14.5	14.7	14.9	15.1	15.3	15.4	15.5	15.6	15.6	15.6	15.5	15.4	15.4	15.3	15.3	15.5
-7	15.9	15.4	15.3	15.3	15.5	15.7	15.9	16.1	16.3	16.5	16.6	16.7	16.8	16.8	16.8	16.7	16.7	16.6	16.5	16.5	16.6
-8	16.6	16.4	16.3	16.5	16.7	16.9	17.1	17.3	17.5	17.6	17.8	17.9	17.9	18.0	18.0	17.9	17.9	17.8	17.8	17.7	17.7
-9	17.6	17.5	17.5	17.7	17.9	18.1	18.3	18.5	18.7	18.8	18.9	19.0	19.1	19.1	19.1	19.1	19.1	19.1	19.0	19.0	19.0
-10	18.7	18.7	18.8	19.0	19.2	19.4	19.5	19.7	19.9	20.0	20.1	20.2	20.3	20.3	20.3	20.4	20.4	20.4	20.4	20.4	20.4

Figure 23. Signal-to-Noise Ratio Improvement at 441 User Spacecraft Positions Via TDRS E, dBW

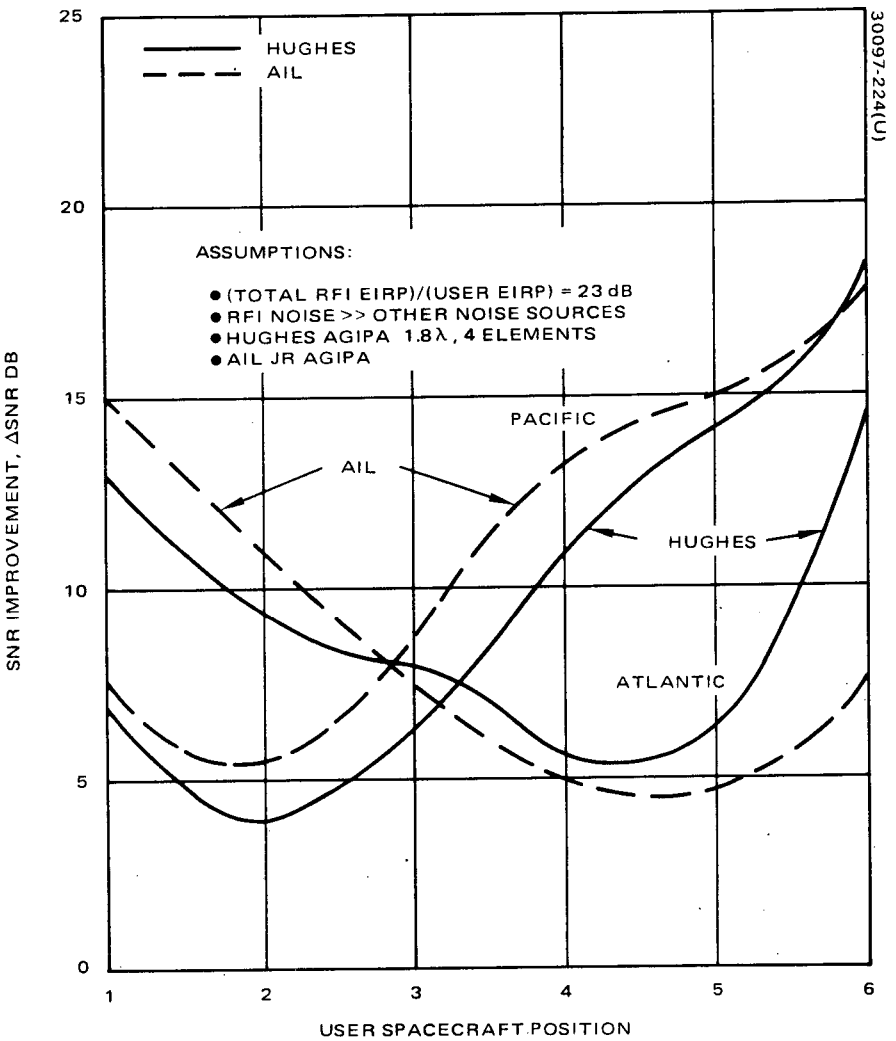

Figure 24. SNR Improvement with AGIPA Over Fixed Field of View Array

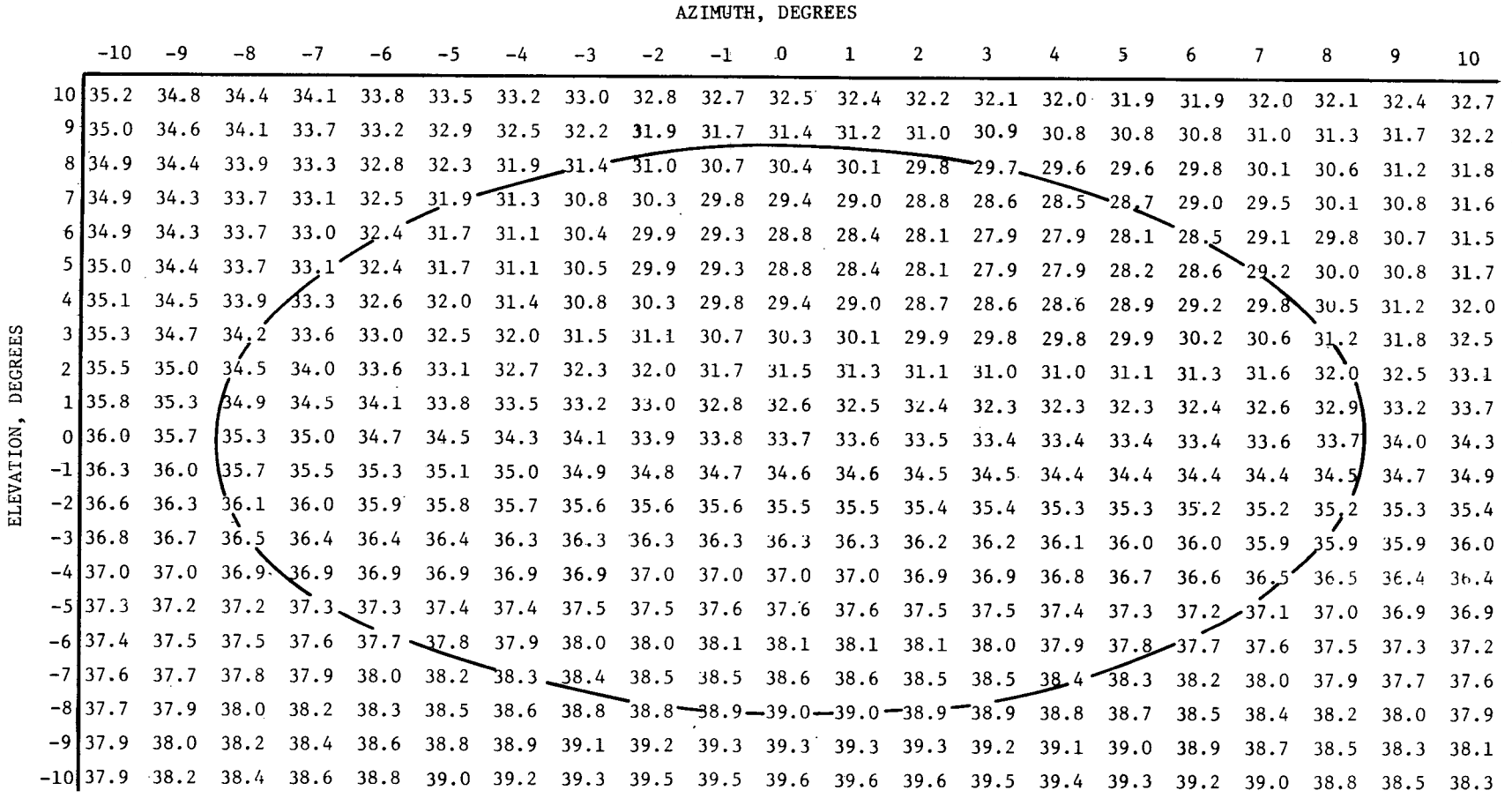

EL \ AZ	-10	-9	-8	-7	-6	-5	-4	-3	-2	-1	0	1	2	3	4	5	6	7	8	9	10
10	35.2	34.8	34.4	34.1	33.8	33.5	33.2	33.0	32.8	32.7	32.5	32.4	32.2	32.1	32.0	31.9	31.9	32.0	32.1	32.4	32.7
9	35.0	34.6	34.1	33.7	33.2	32.9	32.5	32.2	31.9	31.7	31.4	31.2	31.0	30.9	30.8	30.8	30.8	31.0	31.3	31.7	32.2
8	34.9	34.4	33.9	33.3	32.8	32.3	31.9	31.4	31.0	30.7	30.4	30.1	29.8	29.7	29.6	29.6	29.8	30.1	30.6	31.2	31.8
7	34.9	34.3	33.7	33.1	32.5	31.9	31.3	30.8	30.3	29.8	29.4	29.0	28.8	28.6	28.5	28.7	29.0	29.5	30.1	30.8	31.6
6	34.9	34.3	33.7	33.0	32.4	31.7	31.1	30.4	29.9	29.3	28.8	28.4	28.1	27.9	27.9	28.1	28.5	29.1	29.8	30.7	31.5
5	35.0	34.4	33.7	33.1	32.4	31.7	31.1	30.5	29.9	29.3	28.8	28.4	28.1	27.9	27.9	28.2	28.6	29.2	30.0	30.8	31.7
4	35.1	34.5	33.9	33.3	32.6	32.0	31.4	30.8	30.3	29.8	29.4	29.0	28.7	28.6	28.6	28.9	29.2	29.8	30.5	31.2	32.0
3	35.3	34.7	34.2	33.6	33.0	32.5	32.0	31.5	31.1	30.7	30.3	30.1	29.9	29.8	29.8	29.9	30.2	30.6	31.2	31.8	32.5
2	35.5	35.0	34.5	34.0	33.6	33.1	32.7	32.3	32.0	31.7	31.5	31.3	31.1	31.0	31.0	31.1	31.3	31.6	32.0	32.5	33.1
1	35.8	35.3	34.9	34.5	34.1	33.8	33.5	33.2	33.0	32.8	32.6	32.5	32.4	32.3	32.3	32.3	32.4	32.6	32.9	33.2	33.7
0	36.0	35.7	35.3	35.0	34.7	34.5	34.3	34.1	33.9	33.8	33.7	33.6	33.5	33.4	33.4	33.4	33.4	33.6	33.7	34.0	34.3
-1	36.3	36.0	35.7	35.5	35.3	35.1	35.0	34.9	34.8	34.7	34.6	34.6	34.5	34.5	34.4	34.4	34.4	34.4	34.5	34.7	34.9
-2	36.6	36.3	36.1	36.0	35.9	35.8	35.7	35.6	35.6	35.6	35.5	35.5	35.4	35.4	35.3	35.3	35.2	35.2	35.2	35.3	35.4
-3	36.8	36.7	36.5	36.4	36.4	36.4	36.3	36.3	36.3	36.3	36.3	36.3	36.2	36.2	36.1	36.0	36.0	35.9	35.9	35.9	36.0
-4	37.0	37.0	36.9	36.9	36.9	36.9	36.9	36.9	37.0	37.0	37.0	37.0	36.9	36.9	36.8	36.7	36.6	36.5	36.5	36.4	36.4
-5	37.3	37.2	37.2	37.3	37.3	37.4	37.4	37.5	37.5	37.6	37.6	37.6	37.5	37.5	37.4	37.3	37.2	37.1	37.0	36.9	36.9
-6	37.4	37.5	37.5	37.6	37.7	37.8	37.9	38.0	38.0	38.1	38.1	38.1	38.1	38.0	37.9	37.8	37.7	37.6	37.5	37.3	37.2
-7	37.6	37.7	37.8	37.9	38.0	38.2	38.3	38.4	38.5	38.5	38.6	38.6	38.5	38.5	38.4	38.3	38.2	38.0	37.9	37.7	37.6
-8	37.7	37.9	38.0	38.2	38.3	38.5	38.6	38.8	38.8	38.9	39.0	39.0	38.9	38.9	38.8	38.7	38.5	38.4	38.2	38.0	37.9
-9	37.9	38.0	38.2	38.4	38.6	38.8	38.9	39.1	39.2	39.3	39.3	39.3	39.3	39.2	39.1	39.0	38.9	38.7	38.5	38.3	38.1
-10	37.9	38.2	38.4	38.6	38.8	39.0	39.2	39.3	39.5	39.5	39.6	39.6	39.6	39.5	39.4	39.3	39.2	39.0	38.8	38.5	38.3

Figure 25. Ratio of Signal Power to Noise Density (P/η) for ηRFI = -180 dB/Hz Via TDRS W, dB-Hz

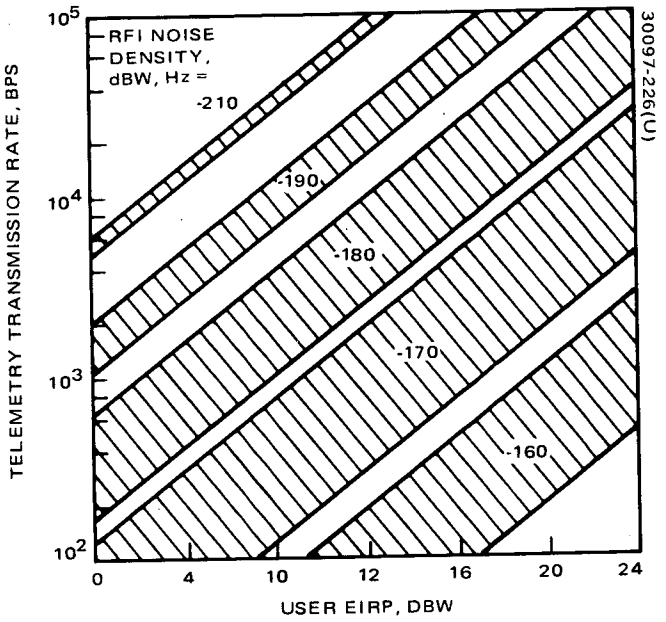

Figure 26. LDR Return Telemetry Performance (Single System User Satellite)

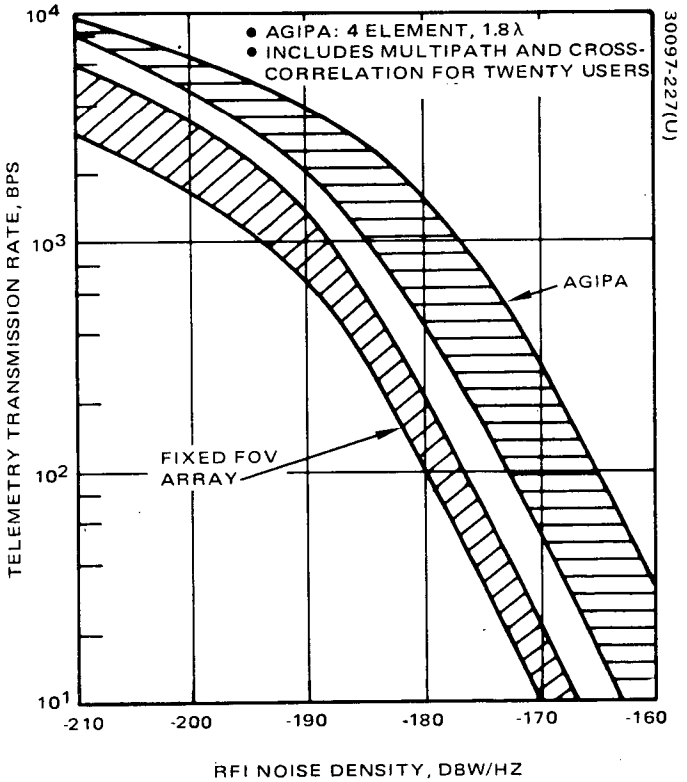

Figure 27. LDR Return Link Capability (4 dBW EIRP User Satellite)

3.2.2 Link Acquisition

There are two major aspects of link acquisition that were addressed in this study: 1) procedure and 2) performance analysis. The first is qualitative in nature and requires the establishment of the sequence of procedural steps required to achieve link acquisition. The second aspect naturally follows the first and requires analysis of the relationships between the many parameters to establish those parameters which are variable and to determine the major performance characteristics. Both aspects are discussed below.

3.2.2.1 Acquisition Sequence

Both the TDRS and user will have mechanically steerable antennas with relatively narrow beamwidths. The TDRS half-power beamwidth is approximately 0.4 degree. From Figure 16, it can be seen that in order to utilize the capability of the HDR service, the user will require an antenna with a diameter of 1 to 2 meters; this corresponds to a half-power beamwidth in the range of 1.5 to 0.8 degree. Radiation beamwidths this small require a sequence that result in each spacecraft lying and remaining in the beamwidth of the other. Correct continuous pointing is maintained by autotrack subsystems employing feedback.

To achieve acquisition, either the TDRS or the user spacecraft must transmit a Ku band signal to the other. This signal is then detected and detection followed by autotracking. Communication can then begin.

A prime objective in choosing the sequence is to allow the user to be initially passive. That is, with the user's transmitter off, and the user's antenna in an arbitrary orientation, the acquisition sequence must be started by ground control via the TDRS. Thus, the first commands to initiate action by the user must be transmitted via the TDRS by pointing its antenna such that the user lies within the beam. This may be possible with the narrow beam at Ku band, but from the pointing error budget of Table 9, the estimated 3σ uncertainty is 0.8 degree before calibration, which is approximately twice the half-power beamwidth. Thus, a wider beam must be used to be certain that the user lies within it. A logical choice was to use the dual frequency capability of the HDR/MDR antennas and begin acquisition by transmitting commands to the user at S band. The beamwidth at this frequency is approximately 2.7 degrees, which is significantly greater than the estimated 3σ error. The use of S band to initiate the acquisition requires the user to have a receiver and broad coverage antenna at this frequency. However, this may be required anyway in order to provide backup, direct-to-ground compatibility.

The user is commanded via his S band receiver to point a Ku band antenna at the TDRS with crude accuracy. The beamwidth of this antenna should be in the range of 3 to 5 degrees corresponding to a reflector

TABLE 9. POINTING ERROR BUDGETS

	3σ Angular Error, degrees (±)	
	TDRS	User
Spacecraft attitude stabilization	0.2	0.4
Alignment of antenna support*	0.1	0.1
Deployment mechanisms*	0.05	0.1
Thermal deflection of antenna support**	0.2	0.1
Antenna positioner	0.05	0.05
Antenna boresight alignment*	0.1	0.1
Boresight deflection due to thermal distortion**	0.1	0.1
Orthogonality of gimbal axis*	0.02	0.02
Accuracy of ephemerides	0.02	0.02
Operational time delays	0.2	0.5
Rss error	0.345	0.680
Maximum sum error	1.04	1.49

*These errors can be reduced by calibration.

**These time varying errors can be reduced after data analysis.

diameter in the range of 0.3 to 0.45 meter. The commanded pointing accuracy must then be in this range; from Table 9 this should present no difficulty. The user is then commanded to transmit via this broad beam antenna an unmodulated carrier which serves as a beacon for the TDRS. The TDRS is then commanded to perform a scanning search with its antenna over the angular region of user position uncertainty. With a high probability (discussed later), this search will result in a detection of the user signal which will cause the TDRS to automatically stop the search and begin autotracking. An unmodulated Ku band carrier is then transmitted via the TDRS antenna which is the beacon for the user. The user is then commanded, still via S band, to perform a similar scan search which will result in a detection of the TDRS beacon signal followed by an automatic switch to autotrack and a switching of the Ku band transmitter to the higher gain communication antenna. At this point, Ku band communication antennas on each spacecraft are automatically tracking signals transmitted by the other. One more command via S band may be used to transfer command reception to the user's Ku band receiver if desired, but for command reliability, it may be preferable to maintain the command link at S band.

In the above sequence, two Ku band user antennas have been mentioned: one with low gain (30 to 33 dB) for transmitting the beacon, and the high gain communication antenna for receiving the beacon signal from the TDRS and transmitting the return data via the TDRS. Thus, the low gain antenna is used only for transmission, while the high gain antenna is used for both transmission and reception and must provide the RF signals for autotracking. These user requirements are summarized in Table 10. It is expected that these two antennas will be rigidly attached to each other with their boresights aligned. A popular mechanical configuration uses a high gain cassegranian antenna with the low gain direct feed reflector mounted on the subreflector of the high gain antenna.

The alternate to scanning for signal detection is the general technique called beam broadening. With this method, the beam of the receiving antenna is made larger at the beginning of the acquisition sequence to ensure that the transmitting spacecraft lies within the beam. The transmitting antenna beam may also need to be broadened to ensure that the receiving spacecraft is illuminated.

Several methods are available for achieving varying beam sizes. These include 1) using separate antennas, 2) using a section of the main antenna, if an array antenna is used, or 3) changing the feed position such that the antenna beam is defocused. When antennas have a beam size which is a fraction of a degree, it is often advantageous to achieve beam broadening by using a second antenna with an area in the order of 1/100 of the main antenna. This second antenna may then cover the necessary angular sector to sense the transmitted signal. Once the signal has been sensed, the autotrack processing electronics directs the antenna positioner to align the beam of the smaller antenna toward the target. That is, the smaller antenna is boresighted on the target. Since the larger and smaller antennas have their electrical axes aligned, pointing the smaller antenna directly at the target also aligns the large antenna. The acquisition procedure then switches antennas, and the larger antenna develops error signals that cause it to be accurately boresighted on the target.

TABLE 10. USER REQUIREMENTS FOR HDR LINK ACQUISITION

1) S Band system with omni antenna for command

2) Dual-gain Ku band antenna (probably different antennas and feeds)

- Low gain: 30 dB, transmit only
- High gain: 47 dB, tracking feed, transmit, and receive

The major disadvantage of beam broadening is the additional RF and mechanical complexity because the RF error signals for autotracking must be generated for both beamwidths. Scanning requires no additional RF or mechanical complexity, but will cause additional gimbal wear. However, it is felt that this additional wear can be more easily accommodated by design than beam broadening. However, in the above discussed acquisition sequence, the use of two antennas on the user, one with a broader beam for a beacon, is a form of beam broadening. Since this broader beam is used only for transmission, most of the additional RF complexity is eliminated. The acquisition sequence is summarized in Table 11.

3.2.2.2 Scan and Detection Analysis

Typical patterns for scanning the search area are shown in Figure 28. The bar scan approach has the advantage of relatively simple pointing commands. Its disadvantage is that, for complete coverage of the search area, turnaround occurs outside the search area, thereby increasing scan time. A bar scan is also less efficient because it begins scanning over an area that has low probability of containing the signals, whereas, a spiral scan starts at the point of highest probability of finding the target. A spiral scan is most efficient in terms of early acquisition of the target, and the beam is always in the search area. The disadvantage of a spiral scan is that the positioner drive signal generation is more complex. However, since the same scan pattern will be used each time, the advantages of spiral scan in minimizing acquisition time outweigh the disadvantages of on-board signal generator complexity.

TABLE 11. HDR LINK ACQUISITION SEQUENCE

1) TDRS points dual-feed antenna at user ±1.0 degree accuracy

2) User-commanded via S band omnidirectional antenna to:

- Point dual gain Ku band antenna at TDRS - ±3 degrees
- Switch to low gain antenna mode
- Transmit unmodulated Ku band carrier

3) TDRS acquires user by antenna scan search and transmits Ku band beacon signal

4) User-commanded via S band to perform scan acquisition with high gain antenna followed by autotracking

5) User automatically switches transmitter to the high gain antenna

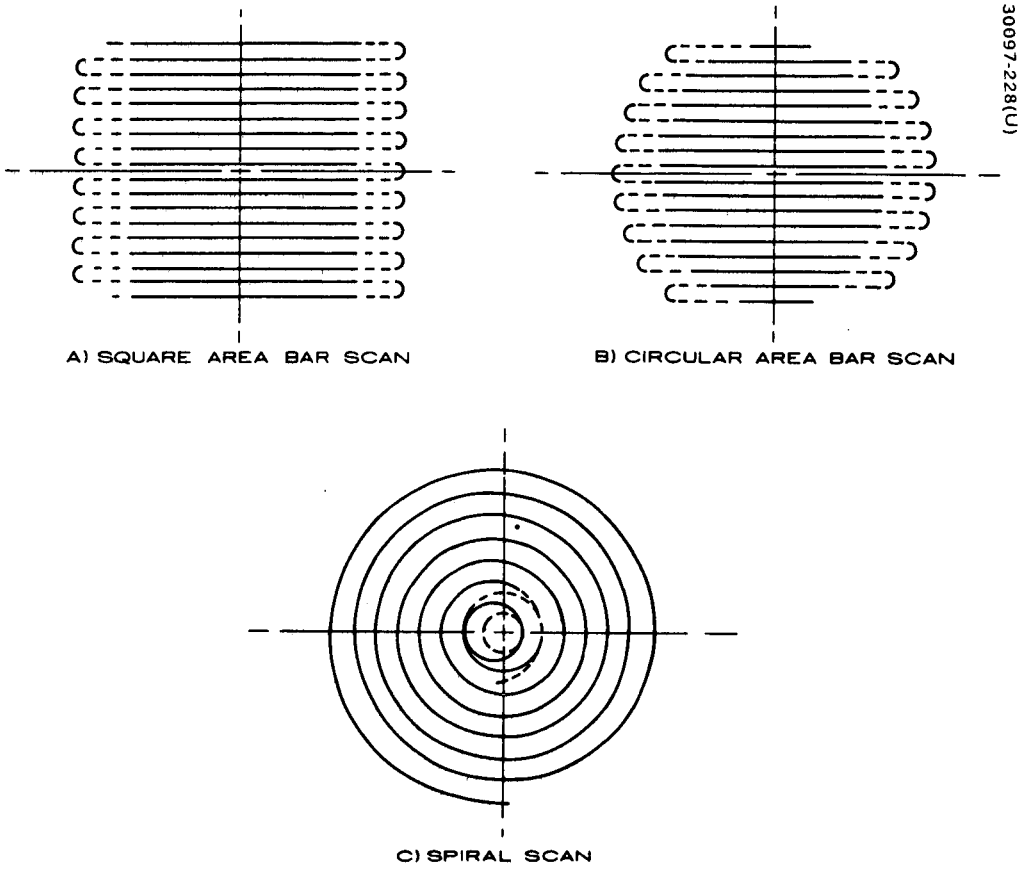

Figure 28. Scan Patterns

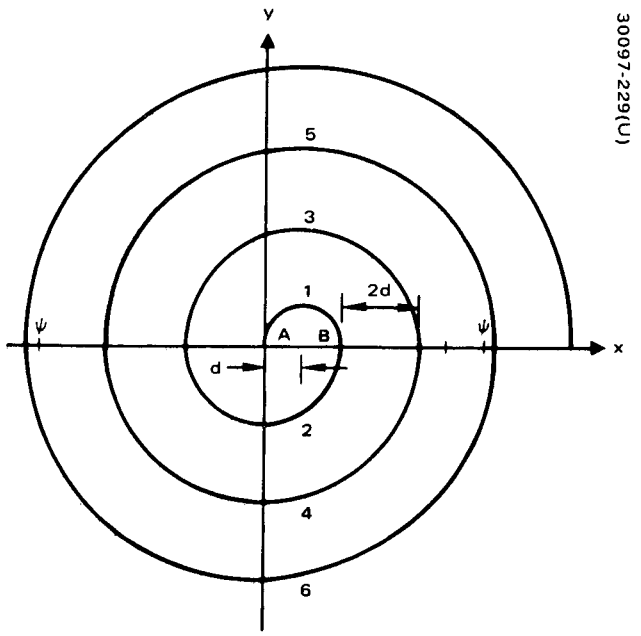

Figure 29. Spiral Pattern Consisting of Joined Semicircles

A scan pattern of interest is shown in Figure 29. The pattern consists of a set of semicircles with centers alternating between points A and B and diameters increasing in increments as shown. If the center of the antenna beam is to travel the pattern at a constant rate during each semicircle, the motion in the plane of Figure 29 is expressed by

$$\left.\begin{aligned} x_n &= nd\,(a - \cos \omega_n t) \\ y_n &= nd\,(-1)^{n-1} \sin \omega_n t \end{aligned}\right\} \qquad 0 \le t < \frac{\pi}{\omega_n} \qquad (1)$$

where

$$a = \begin{cases} 0 & \text{if n is even} \\ 1 & \text{if n is odd} \end{cases}$$

Two independent motors with orthogonal drive axes are used to position the antenna and hence their motion corresponds to the x and y coordinates of the figures. These positioners and the control electronics will have an angular rate limit, R, which will be assumed here to be the same for each motor drive. Thus,

$$|\dot{x}_n|_{max} = n\omega_n d = R = |\dot{y}_n|_{max}$$

If a maximum speed scan is to be achieved, then for the n^{th} semicircle

$$\omega_n = \frac{R}{nd} \qquad (2)$$

The motor drive signals will be the functions of Equation 1. The time, t_n, to trace the n^{th} semicircle is given by

$$t_n = \frac{nd\pi}{R}$$

And, the total scan time T_s is given time

$$T_s = \sum_{n=1}^{k} t_n = \frac{k(k+1)d\pi}{2R} \qquad (3)$$

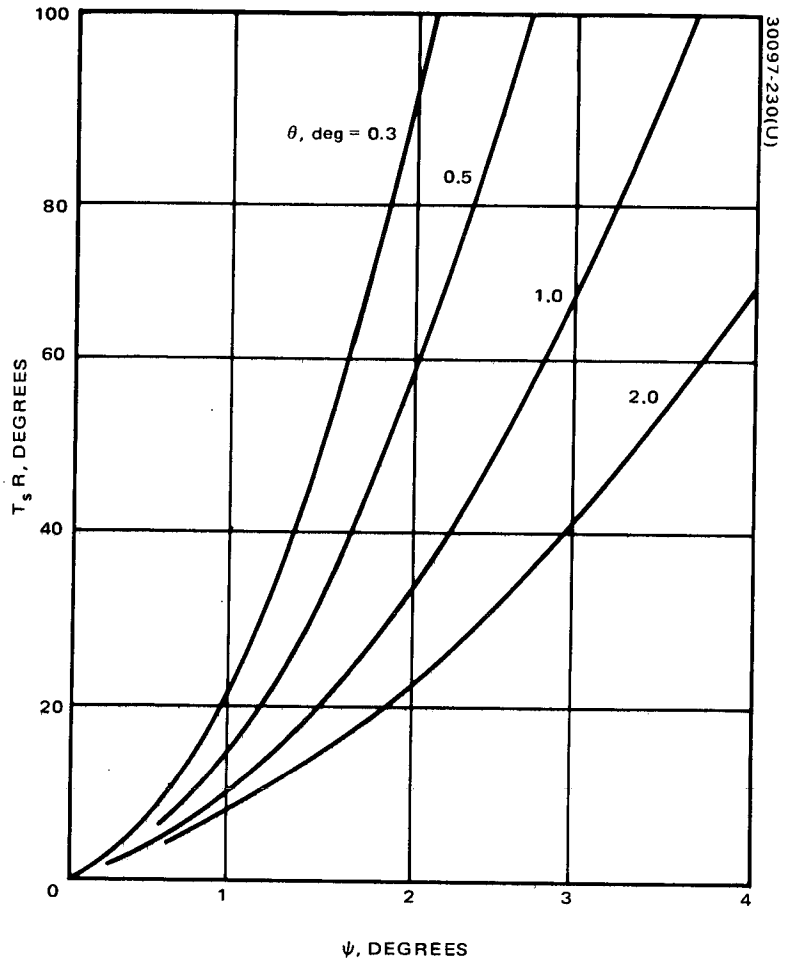

Figure 30. Search Time Parametric Curves

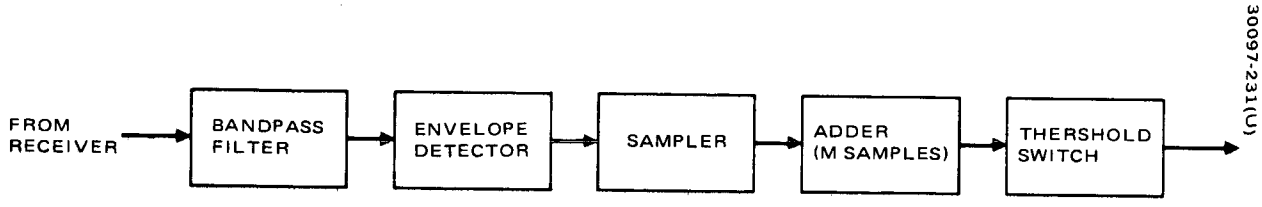

Figure 31. Signal Detector

where k is the number of required semicircle segments of the scan pattern.

Denoting by ψ, the half-angle of the cone to be covered by the scanning antenna beam, to ensure complete coverage by this area the number of required semicircles, k, is given by

$$k = 1 + \text{the next integer larger than } \frac{\psi}{d} \tag{4}$$

For reliable acquisition there should be overlap of the antenna beam 3 dB illumination area between adjacent semicircles. A conservative approach would be to make the angular distance d equal to one-fourth the 3 dB beamwidth, θ, i.e.,

$$4d = \theta \tag{5}$$

If this is done, the relationship between the scan area radius ψ, beamwidth, θ, maximum positioner rate, R, and total search time, T_s, can be approximated by letting $k = 1 + 4\psi/\theta_o$. The result is

$$T_s R = \frac{\pi\theta}{4}\left(\frac{8\psi^2}{\theta^2} + \frac{6\psi}{\theta} + 1\right) \tag{6}$$

This relationship is shown in Figure 30 for typical parameter values.

The maximum positioner rate for the TDRS is approximately 1 degree/second. If the same rate is assumed for the user, then for TDRS and user antenna beamwidths of 0.4 and 0.8 degree respectively, Figure 30 indicates the required search times corresponding to the estimated 3σ errors of Table 10 are approximately 6 and 8 seconds, respectively. Operational delays during the sequence are expected to be longer. If the scan radii, ψ, are increased to 1 and 2 degrees, respectively, for the TDRS and user for greater certainty of acquisition, the search times are 20 and 40 seconds, respectively.

The functional elements of the signal detector are shown in Figure 31. The envelope detector assumed in the analysis below is the square law device. Both linear and square law devices have been analyzed and shown to have nearly identical detection characteristics. The envelope detector is preceded by a bandpass filter and followed by a sampler. The sampler is, in turn, followed by an adder which sums the last m outputs from the sampler. A threshold switch is used to indicate a signal detection when the added output voltage exceeds a bias level, b.

Available statistical analysis is valid only if the samples of the detector output are independent. They may be considered to be independent if the sampling interval, t_s, is greater than the reciprocal of the input IF filter bandwidth, B, i.e.,

$$t_s \geq 1/B \tag{7}$$

In order to assure that the signal will remain within a beamwidth during a full cycle of the sample and add process, this cycle time, t_c, must be less than one-half the minimum time that a transmitter may lie in the antenna beam during the scan. Analysis of the scan motion of Figure 29 where Equation 5 is valid shows that the minimum time, t_{min}, for a transmitter to lie in the 3 dB beamwidth is given by

$$t_{min} \geq \frac{4d}{R} \tag{8}$$

and if Equations 5 and 8 are combined

$$t_{min} \geq \frac{\theta}{R} \tag{9}$$

Thus, a sample and add cycle period, t_c, must satisfy

$$t_c = mt_s \leq \frac{2d}{R} = \frac{\theta}{2R} \tag{10}$$

When no signal is present, the noise alone may cause the adder output to exceed the threshold level. The probability of error during a sample and add cycle, P_e, is the probability that this will occur and is given by

$$P_e = \int_b^\infty P_m(y)\, dy$$

where b is the normalized threshold level and $P_m(y)$ is the density function for the normalized adder output voltage and is given by

$$P_m(y) = \begin{cases} \dfrac{y^{m-1} e^{-y}}{(m-1)!} & y \geq 0 \\ 0 & y \geq 0 \end{cases}$$

In Reference 1, b is computed as a function of P_e and m.

A false alarm occurs during the search when the detector registers a signal detection and there is no signal present at the time. This happens if the output of the adder exceeds the threshold bias level due to noise alone. The probability of false alarm during one complete search is given by

$$P_{fa} = 1 - (1 - P_e)^r \tag{11}$$

where

$$r = \text{next integer greater than } T_s/t_c \tag{12}$$

From Equation 11, it follows that:

$$\left.\begin{aligned} P_e &= P_{fa} \qquad r = 1 \\ P_e &= \frac{P_{fa}}{r} \qquad r \geq 2,\ P_e r \ll 1 \end{aligned}\right\} \tag{13}$$

It may be noted from Equation 11 that $P_e \leq P_{fa}$. Thus, if $rP_{fa} \ll 1$ then $rP_e \ll$.

When the signal is present the probability of detection during a sample and add cycle, P_{dc}, is given by

$$P_{dc} = \int_b^\infty q_m(v)\, dv$$

where $q_m(v)$ is the probability density function of the adder output when both signal and noise are at the input. It is shown in Reference 2 that this integral may be expressed as

$$P_{dc} = 1 - T_{\sqrt{b}}(2m - 1, m - 1, \sqrt{mQ})$$

where T represents the incomplete Toronto function (see Reference 2) and Q is the signal-to-noise ratio at the envelope detector input.

The probability of acquisition, P_{acq}, satisfies the inequality

$$P_{acq} \geq P_A(1 - P_{fa}) \sum_{i=1}^{q} P_{dc}(1 - P_{dc})^{i-1} \tag{14}$$

The expression on the right is product of the probabilities that the transmitter is in the angular search area (P_A), that no false alarm will occur during a search, and that a detection will be made when the transmitter is in the 3 dB antenna beam. The parameter q is the total number of sample and add cycles that occur while the transmitter lies in the beam.

The probability of acquisition is greater than or equal to the right-hand expression because a detection will probably occur before the scan process is complete, and P_{fa} is the probability of a false alarm occurring anytime during the complete scan if no transmitter were in the search area. Substituting Equation 11 in Equation 14 and performing the summation

$$P_{acq} \geq P_A(1 - P_e)^r \left[1 - (1 - P_{dc})^q\right] \tag{15}$$

Equations 9 and 10 provide a lower bound on q, i.e.,

$$q_{min} = \frac{t_{min}}{t_c} \geq \frac{\theta}{mRt_s} \geq 2 \tag{16}$$

In almost all cases $P_{fa} \leq 10^{-5}$ by design, and from Equations 11 and 13, $P_{fa} \approx rP_e$ and so

$$(1 - P_e)^r \approx 1 - rP_e \tag{17}$$

A conservative design to satisfy Equation 7 is to let

$$t_s = \frac{2}{B} \tag{18}$$

Substituting this in Equation 16

$$q_{min} = \frac{t_{min}}{t_c} \geq \frac{\theta B}{2mR} \tag{19}$$

The inequality is thus strengthened by the use of q_{min}, i.e.,

$$P_{acq} \quad P_A(1 - P_e)^r \left[1 - (1 - P_{dc})^{q_{min}}\right] \tag{20}$$

Figure 32 shows the relationship between $q_{min} = t_{min}/t_c$ and the right-hand factor of Equation 20.

As an illustrative sample design, let

$$m = 100$$

$$P_A = 1$$

$$P_{fa} = 10^{-6}$$

$$P_{acq} = 0.9999$$

Letting $P_A = 1$ implies that the search area has been chosen large enough to ensure that the transmitting spacecraft lies within it. With $P_{fa} = 10^{-6}$ and $P_A = 1$

$$P_{acq} \geq 1 - (1 - P_{dc})^{(t_{min}/t_c)} \tag{21}$$

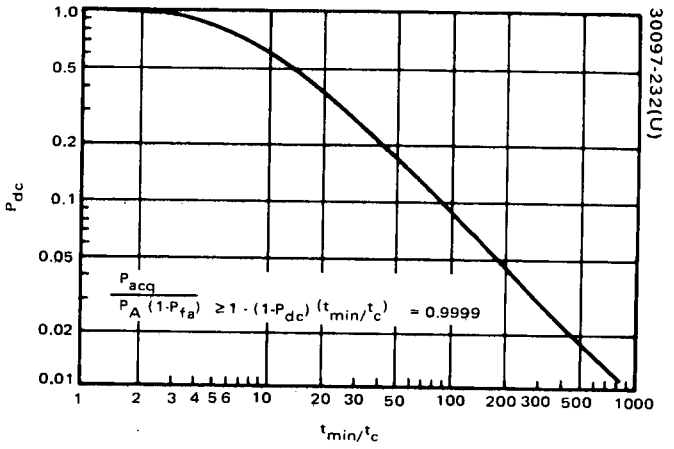

Figure 32. Detection Probability Versus t_{min}/t_c

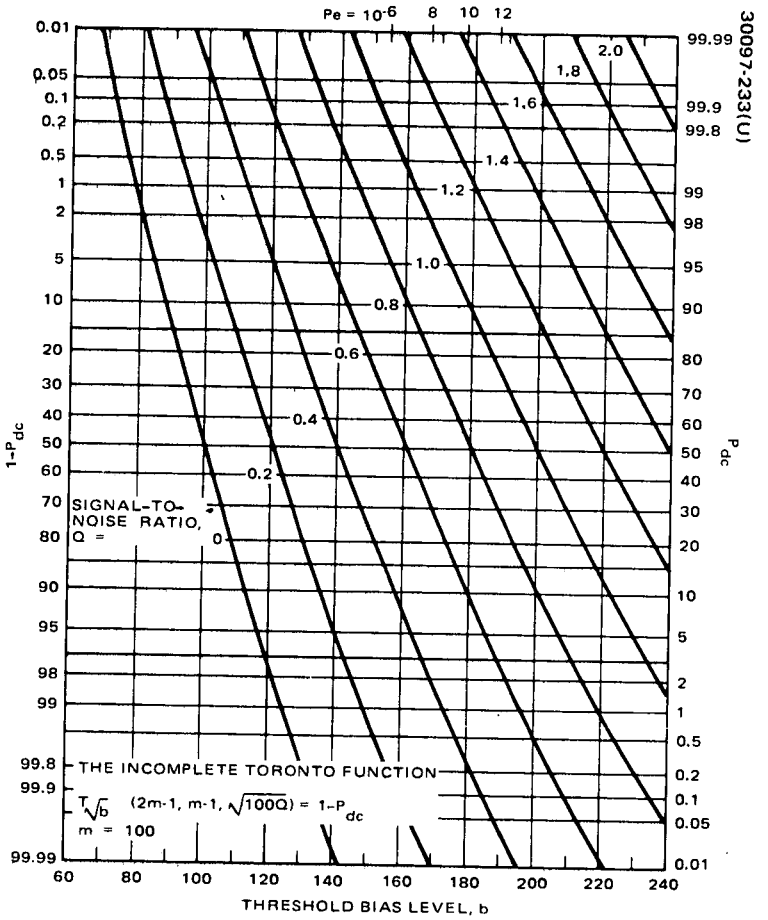

Figure 33. P_{dc} Versus Bias Level for Various Values of Signal-to-Noise Power Ratio

From the previous scan analysis it appears that the required search time, T_s, will be less than 100 seconds. It can be shown that the doppler shift at 14 GHz can be as large as ±400 kHz. Then allowing for oscillator instabilities, if a frequency search in addition to the scanning spatial search is to be avoided, $B \approx 10^6$ Hz.

If the sampling interval is chosen according to Equation 18, then from Equation 10

$$t_c = mt_s = \frac{2m}{B} = 2 \times 10^{-4} \text{ second}$$

From Equation 12 and the estimate $T_s \leq 100$ seconds

$$r = \frac{T_s}{t_c} \leq 50 \times 10^4$$

From Equation 13, the required P_e is given by

$$P_e \approx \frac{P_{fa}}{r} \geq \frac{10^{-6}}{50 \times 10^4} = 2 \times 10^{-11} \qquad (22)$$

As a conservative approach, let $P_e = 10^{-12}$. From Reference 1, the required threshold value, b, is 187.2.

The TDRS 3 dB beamwidth is approximately 0.4 degree and R is 1 degree per second. Thus $\theta/R = 0.4$ and this ratio is expected to be larger than 0.1 for the user spacecraft. Using the latter value in Equation 19 along with other numerical values mentioned above

$$\frac{t_{min}}{t_c} \geq \frac{\theta B}{2mR} \geq 500$$

From Equation 21 and Figure 32, the maximum required value of P_{dc} is 0.015.

Figure 33 shows a plot of P_{dc} versus bias level for various values of signal-to-noise power ratio, Q. As mentioned above for $P_e = 10^{-12}$, $b \approx 187$, and thus for $P_{dc} \geq 0.015$, $Q \geq 0.4$ (-4 dB).

For the TDRS, the transmitter power was chosen to be 100 mW for reliable acquisition. From the link budget of Table 3, the signal-to-noise ratio in a 10^6 Hz bandwidth is approximately 8 dB for a 1 meter user antenna diameter. Since the user is expected to have an antenna at least this large, the probability of signal detection when the TDRS is in the user's beam during the user's search is greater than 0.9999. The same is true for the search by the TDRS if the user's EIRP greater than 20 dB. The user's steerable beacon antenna will have a gain greater than 30 dB and his transmitter power will be larger than 1 watt as can be seen from Figure 16.

Conclusion

The conclusion of the above analysis is that:

1) The probability of acquisition success on each trial is extremely high, greater than 0.9999.

2) The maximum acquisition search time will be less than 1 minute. The average acquisition time will be less.

It should be noted that antenna slewing prior to the scanning search and other operational procedures may require several minutes, but these can be reduced by automating some functions and by prepositioning the user's antenna prior to stopping communication.

3.2.2.3 References

1) J. Pachares, "A Table of Bias Levels Useful in Radar Dection Problems," IRE Trans. on Information Theory, IT-4, No. 1 (1958) pp. 38-45.

2) J. I. Marcum, "A Statistical Theory of Target Detection by Pulsed Radar," with mathematical index, RAND Research Memo RM-754, 1 December 1947.

3.2.3 Ground Link Margin

The TDRS discussed in this volume provides nominally 9.8 dB margin for the return link from the TDRS to the Ground Station. This is 7.7 dB less than previous TDRS configurations. The forward link from Ground Station to TDRS can be provided with any desired margin with a sufficient transmitter power at the ground terminals. The lower margin in the return link was the result of a weight and space saving change from the configurations of Volumes 3 and 4 to a smaller ground link antenna. The lower margin results in more link outage due to attenuation during heavy rain.

There are two ways to reduce the link outage without increasing TDRS EIRP:

1) Use a ground station antenna larger than the currently suggested size with a 12.8 meter diameter. A 26 meter antenna would provide an additional 6 dB margin.

2) Provide ground terminal diversity with one or two additional terminals for receiving only.

The second method appears attractive from consideration of both cost and overall operational reliability.

To estimate the outage requires a model of the effects of weather on millimeter wave propagation and also rain rate statistics at the ground terminal site. An atmospheric effects model is given by Deerkoski (Reference 1). The USAF Handbook of Geophysics and Space Environments (Reference 2) gives empirical relations which permit data from Reference 1 to be extrapolated to the form shown in Figure 34. These data and the GSFC attenuation model then result in the plot given as Figure 35. The weather margin shown includes both signal attenuation and increased noise temperature for a 420 K receive system. With the design power level, the link outage is 0.6 percent or about 52 hours per year.

The use of ground station diversity against weather effects implicitly assumes that high concentrations of moisture, "rain cells," have limited spatial extent. The most recent experimental data on this concept have been obtained by Hodge (Reference 3) as part of the ATS-5 Millimeter Wave Experiment. Figure 36 shows experimental results during one storm with the terminals 8 km apart. The curve "Both" gives statistics for the smaller attenuation at the two sites. The divergence of the curves for the two sites separately provides a measure of the experimental error for this small data set. Figure 37 includes data for an entire year of measurements. The curves indicate that:

1) Diversity was of little value for small fade depths (small attenuations).

2) For 8 km separation and single site fades greater than about 6 dB, the diversity gain was sufficient to keep the effective fade to about 4 dB.

These results indicate that terminal separation of only a few kilometers may be acceptable. For preliminary design of a diversity system, it is therefore reasonable to assume that the probability of occurence of severe weather at two sites is statistically independent, even without excessive separation.

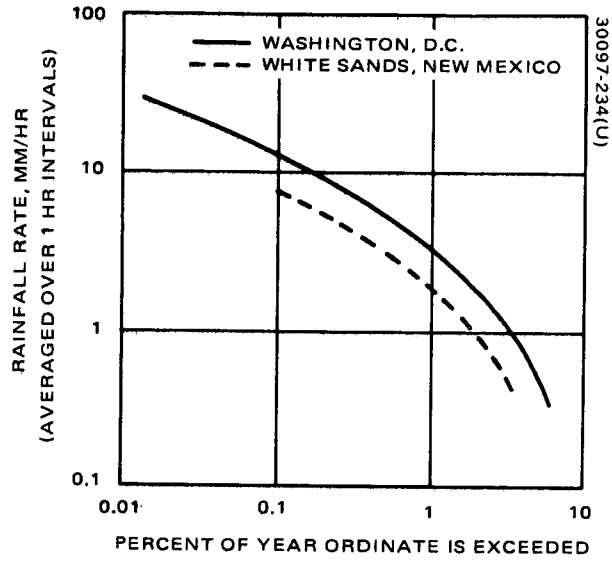

Figure 34. Rainfall Rate Distribution Data

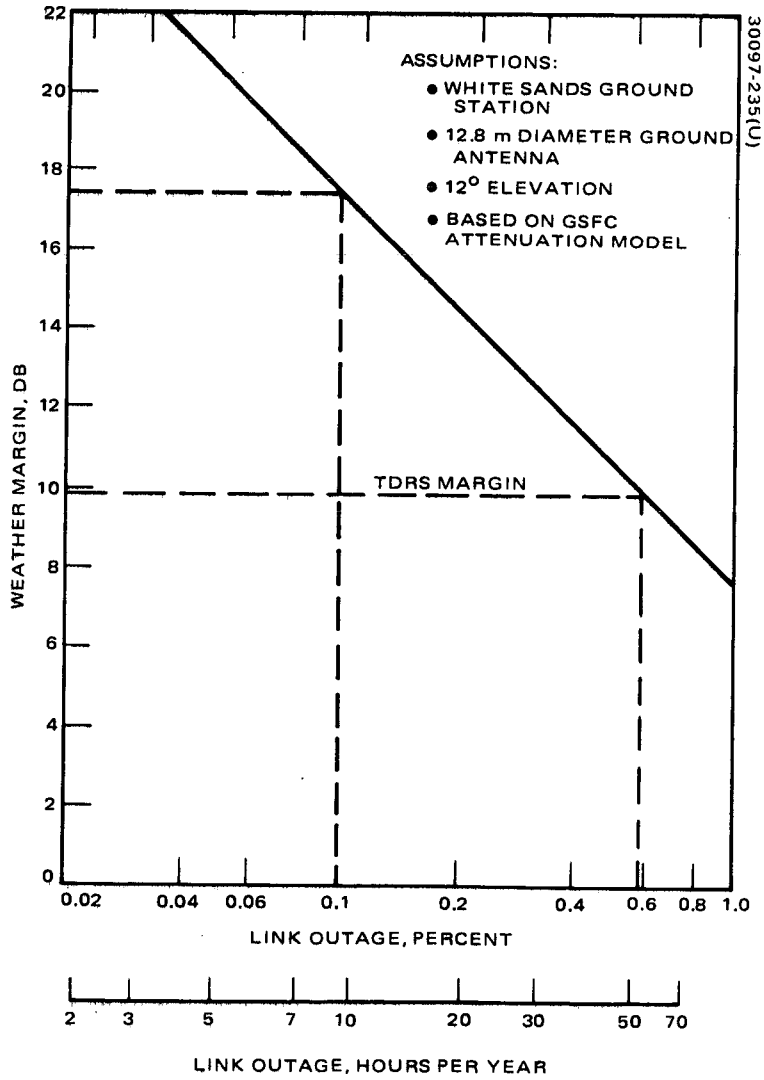

Figure 35. Weather Margin Versus Link Outage

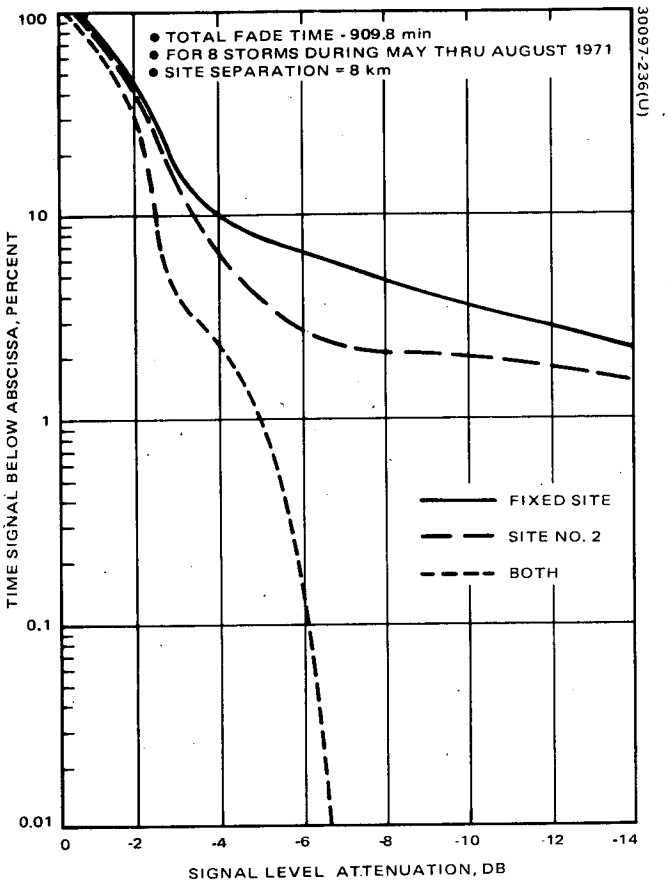

Figure 36. Fade Distributions for 8 km Site Separation (Hodge 1972)

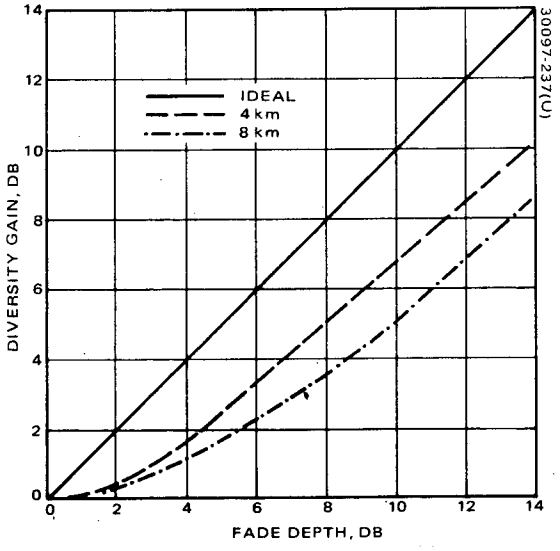

Figure 37. Diversity Gain Versus Single Terminal Fade Depth (Hodge 1972)

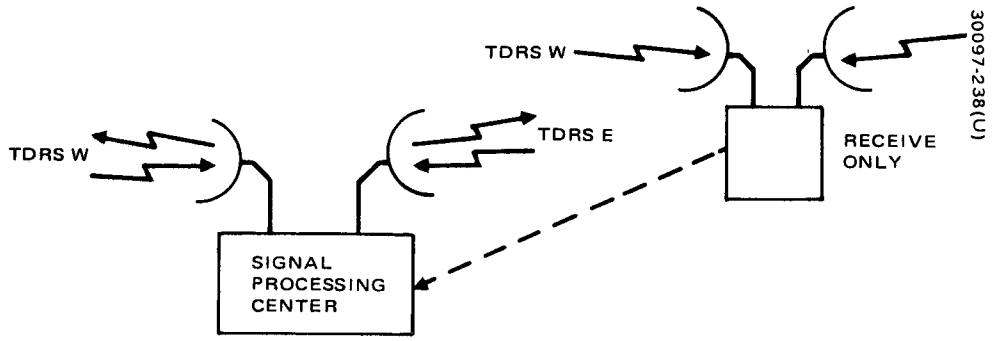

a) ALTERNATIVE 1: TWO SITES/FOUR TERMINALS

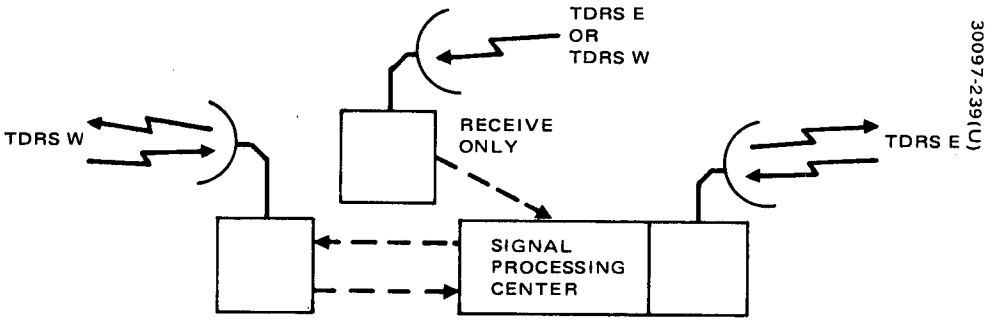

b) ALTERNATIVE 2: THREE SITES/THREE TERMINALS

Figure 38. Ground Station Diversity Alternatives

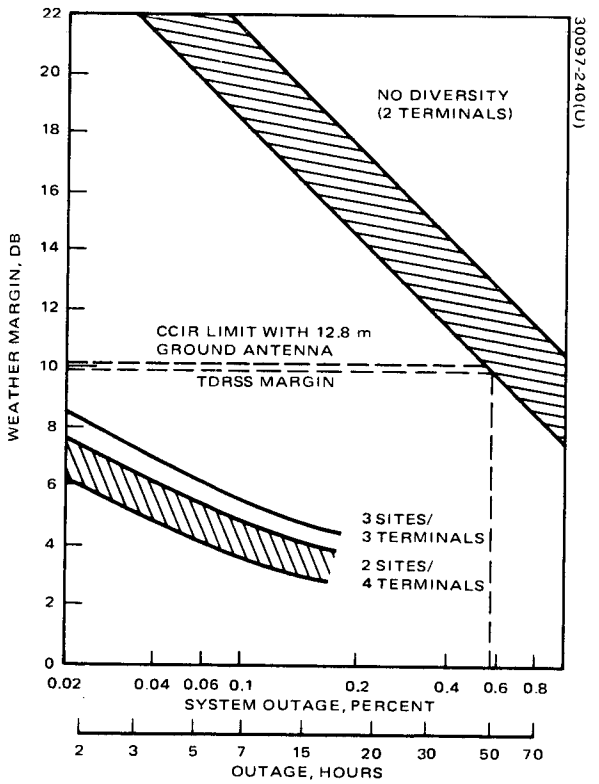

Figure 39. Ground Link Margin

Figure 38 shows two diversity schemes which were considered. The first alternative would entail addition of two terminals at a single remote site. They need only have a receive capability since there is no difficulty in providing uplink margin; this will provide considerable cost savings. The second alternative would use three sites with only one terminal at each site. Although this alternative requires only three terminals, data must be sent to and from one remote location and also received from the other, while the first alternative requires data transmission in only one direction from only one remote site. Table 12 shows the probability of outage for each of the alternatives. It is assumed that the links to both TDRSs are always required. The calculations assume that weather at different sites is statistically independent. It may also be possible that the attenuation seem by two antennas at a single site is statistically independent. The line of sight of the two antennas is nearly 180 degrees apart. The table shows entries assuming independent weather and also common weather. The results of Table 12 are shown in Figure 39 in terms of weather margin versus system outage. These results indicate that either diversity alternative will meet the desired system outage requirement of .1 percent. The two site/four terminal configuration is preferred for the reasons given above.

3.2.3.1 References

1) L. F. Deerkoski, et al, "Ku-band TDRSS Ground Antenna Study", GSFC, June 1970, X-525-70-200.

2) Shea L. Valley, ed., Handbook of Geophysics and Space Environments, Air Force Cambridge Research Laboratories, 1965.

3) D. B. Hodge, "The Use of Space Diversity in the Reception of Millimeter Wavelength Satellite Signals", The 1972 Spring URSI Session on Experiments Utilizing the ATS-5 Satellite compiled by L. J. Ippolito, GSFC, May 1972, X-751-72-208.

TABLE 12. SYSTEM OUTAGE PROBABILITY FOR GROUND DIVERSITY ALTERNATIVES

Configuration	Common Weather for Two Antennas at Single Site	Independent Weather for Two Antennas at Single Site
No diversity (one site/two terminals)	p^*	$2p-p^2$
Two sites/four terminals	p^2	$2p^2-p^4$
Three sites/three antennas	$3p^2-2p^3$	$3p^2-2p^3$

*p = probability of outage for a single antenna terminal

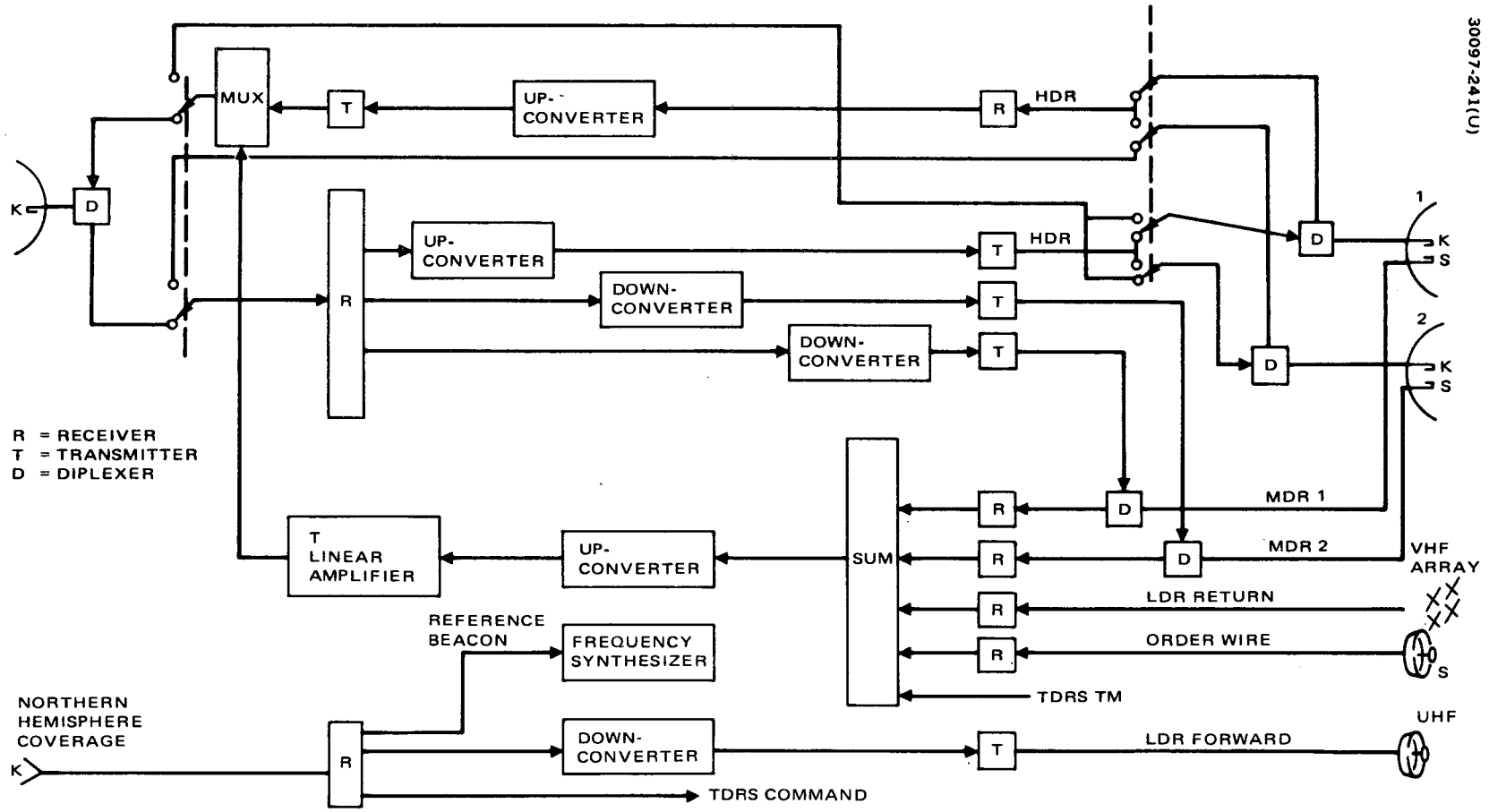

Figure 40. TDRS Repeater

3.3 TDRS REPEATER

Figure 40 is a simplified functional diagram of the repeater. The antennas on the left are for communication with the ground station and the antennas on the right are for communication with user spacecraft. The forward LDR channel, TDRS commands, and frequency reference beacon are received from the ground station via a northern hemisphere coverage Ku band horn as shown in the lower left of the figure. The LDR signal is upconverted and transmitted to users via the broad coverage UHF antenna. The command signal is sent to the TDRS decoder and the reference beacon to the frequency synthesizer to provide system coherency for all frequency conversions.

The HDR and two MDR forward channels are received from the ground station via the 1.43 meter reflector antenna with the Ku band feed. The MDR channels are appropriately downconverted to S band and amplified for transmission. The HDR channel is upconverted from the receive Ku band frequency to the transmit Ku band frequency as shown in the frequency plan of Figure 7b.

The two return MDR channels, the eight return signals from the LDR VHF array antenna, the order wire channel, and the TDRS telemetry are added together in frequency multiplex, upconverted to Ku band, and linearly amplified for transmission. Linear amplification is required to reduce intermodulation between channels and to allow adaptive processing at the ground station for up to 20 LDR users simultaneously. The return HDR channel is upconverted from the Ku band receive frequency to the Ku band transmit frequency and amplified in a saturated (i.e., limiting) amplifier for power efficiency. The outputs of the two power amplifiers are multiplexed and the resultant diplexed with the incoming combined forward MDR and HDR band for transmission to the ground station via the 1.43 meter Ku band dish.

The switches associated with the ground link signals and the HDR signal provide subsystem redundancy that will allow only slightly reduced service if one of the large reflector antenna subsystems should fail (including positioner, feed, and tracking electronics). The 1.43 meter antenna at the left of Figure 35 has only a Ku band feed and is the initial and primary ground link antenna. If it should fail, however, either 3.82 meter dual-feed antenna may be used for the ground link. If, for instance, antenna 2 were used, then antenna 1 would be used for the HDR channel and would be time-shared with MDR service. Lost would be the capability to provide the second two-way MDR link simultaneous with the other link, either MDR or HDR. The ability to provide two backup antenna subsystems for the ground link greatly enhances the system reliability and long life service potential.

If the primary ground link antenna operates as designed, then the switches allow the HDR channel to be provided by either of the dual-feed antennas. The major antenna parameters are summarized in Table 13. More detailed discussion of the repeater is presented in subsection 4.3.1.

TABLE 13. TDRS ANTENNA PARAMETERS

Link	Antenna Frequency, MHz	Antenna Diameter, meters	Minimum Antenna Gain over FOV, dB
Low data rate forward	UHF	1.43	12.5
Low data rate return	VHF	4.00	14.7
Medium data rate forward	S band	3.82	35.5
Medium data rate return	S band		36.2
High data rate forward	Ku band	3.82	52.8
High data rate return	Ku band		51.9
Order wire	S band	0.267	13.1
TDRS to ground	Ku band	1.43	45.0
Ground/TDRS	Ku band	Horns	18.5

3.4 USER EQUIPMENT

3.4.1 LDR and MDR Users

Both low data rate and medium data rate users will require spread spectrum transceivers. The carrier signals are modulated by binary PN sequences (codes), which in turn have been modulated by data. The use of PN coding for spectrum spreading accomplishes four objectives:

1) Allows code division multiplexing

2) Reduces multipath interference

3) Reduces the earth incident flux density (to meet CCIR requirements)

4) Improves range measurement accuracy.

All four of these reasons are important in the LDR system, and all but the first are important in the medium data rate system. The low data rate PN symbol (chip) rate is 614,400 chip/second in the allocated 1 MHz (400.5 to 401.5 MHz) band. The forward link bandwidth of the medium data rate service is 30 MHz, and the signal must be spread over most or all of this band to minimize the flux density. Thus, the MDR signaling rate may be more than 30 times greater than that of the LDR system. However, the transceiver (receiving/transmitting equipment) consists of the following major components, interrelated as shown in Figure 41 receiver, command data correlator, telemetry modulator, transmitter, interface buffers, and a signal acquisition, matched filter correlator.

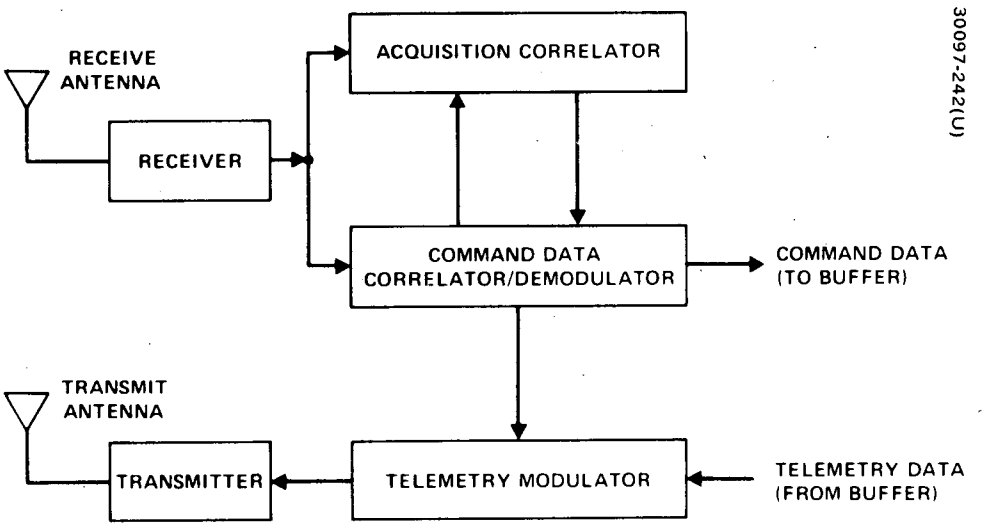

Figure 41. User Transceiver

The acquisition correlator permits rapid forward link signal acquisition and provides PN code timing to the command correlator, which maintains pattern and frequency lock after initial acquisition. The telemetry transmitter frequency may be phase locked to the received frequency for ranging, but may also be allowed to run free during telemetry data transmission enabling handover between TDRSs without interrupting data flow.

To operate with the TDRS system, a user spacecraft does not need to replace or modify its NASA ground station-compatible equipment, but must supplement it with the TDRS compatible transceiver and antennas. Two types of standard transceivers are envisioned, one for LDR users and one for MDR users. These transceivers can be connected with a switch to the regular command decoder and telemetry encoder. The choice between the ground station or TDRSS operation could be made any time during the user's mission by a simple command of the switch setting. If the data and command rates for both modes of operation are different, an interface buffer unit will also be required as part of the transceiver package.

In addition to the standard transceiver, the LDR users will probably require a UHF antenna. The VHF link to a TDRS is compatible in frequency with the user to ground station link.

Figure 42 presents a more detailed transceiver description with numerical values corresponding to the baseline parameters of LDR forward command and return telemetry links.

For this implementation, the acquisition correlator gives the following performance when the bit energy-to-noise density, E_b/η at the receiver is 0 dB, which is 10 dB below the link design value.

Mean time to threshold (synchronous signal output)	0.1 second
Probability of correct acquisition	0.99
Probability of a false synchronization output	0.01

In order for MDR users to realize the 1 Mbps capacity of the return link, a directive antenna will be required for expected transmitter power levels less than 30 watts. The relationship between user antenna gain and return data rate is shown in Figure 13. In order to allow communication during a major portion of the user's orbit, or whenever the user is visible to a TDRS, the directive antenna radiation must be steered. The most straightforward approach is to provide the capability to mechanically orient a single antenna structure; but whatever technique is employed, a steerable directive radiation pattern will be necessary for data rates near 1 Mbps.

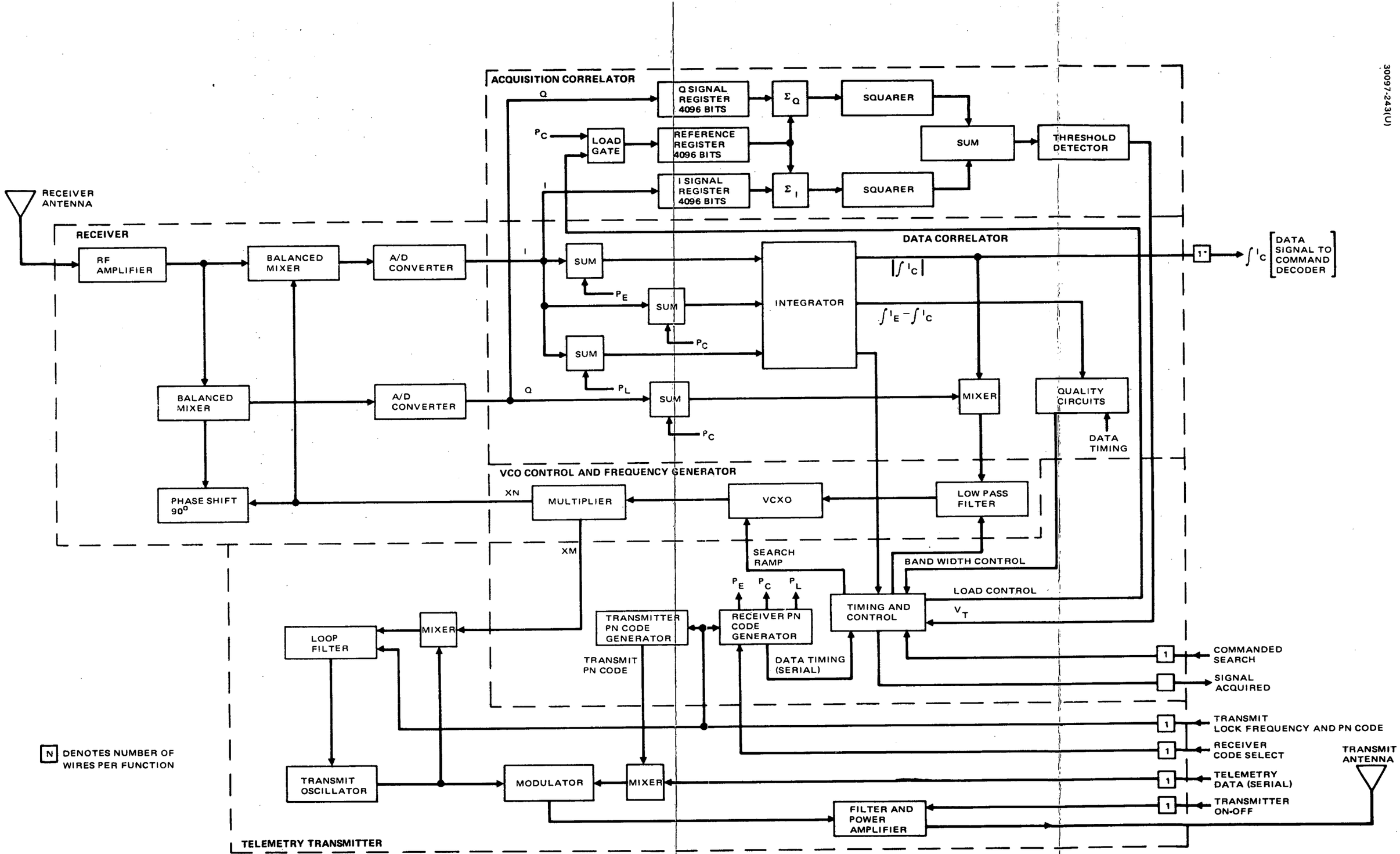

Figure 42. User Transceiver Detailed Diagram

FOLDOUT FRAME 1

FOLDOUT FRAME 2

3.4.2 HDR Users

Whereas the principal problem with the LDR and MDR links is code acquisition (i.e., signal synchronization), the principal problem of the HDR link is antenna beam acquisition and steering. The antenna half-power beamwidth will be less than 1 degree for most HDR users, necessitating special equipment for rapidly establishing the HDR user/TDRS link. A possible communication subsystem implementation is shown in Figure 43. The basic equipment required is as follows:

1) S band receiver with an omnidirectional antenna for command

2) Steerable, dual gain antenna

   - Low gain — transmit only
   - High gain — tracking feed, transmit, and receive

The dual gain antenna shown in Figure 43 consists of two separate antennas and feeds rigidly connected to each other with parallel boresights. Only the high gain antenna has a tracking feed. With this equipment the acquisition sequence is as follows.

1) The TDRS is commanded to point a dual-feed antenna at the user with ±1 degree accuracy and an unmodulated carrier is transmitted at Ku band.

2) The TDRS transmits the following commands at S band which are received, verified, and executed via the users S band omnidirectional antenna:

   - Point antenna at TDRS with ±3 degree accuracy
   - Switch power amplifier output to low gain antenna
   - Turn off carrier modulator
   - Turn on transmitter

3) The TDRS performs a spatial scan acquisition of the user carrier.

4) The user is commanded via S band to perform a scan acquisition of the TDRS signal (see step 1).

5) Following acquisition, the autotrack system is automatically activated, the user switches its transmitter to the high gain antenna and data transmission begins.

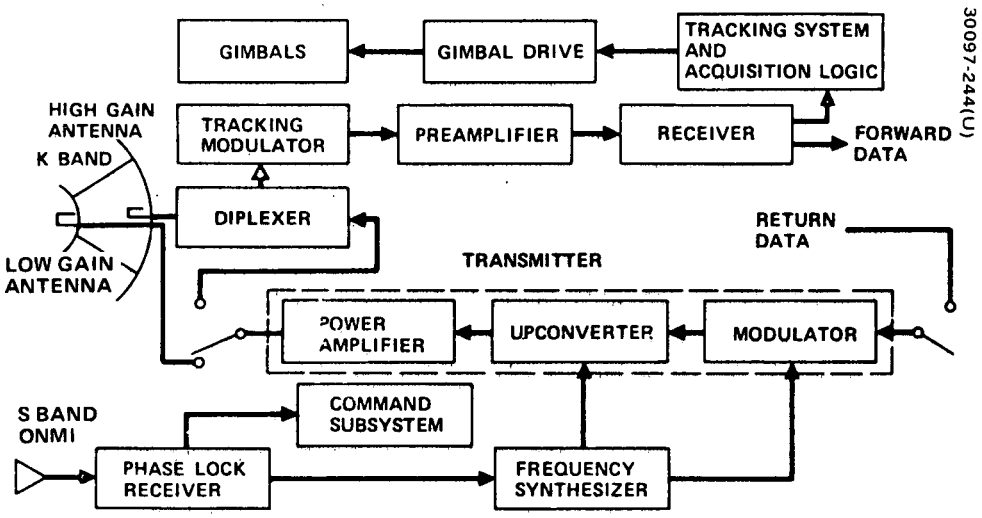

Figure 43. HDR User Communication Subsystem for TDRSS Operation

In Figure 43, an output of the S band receiver provides a reference for the user's frequency synthesizer. This is not required, but if a frequency reference properly adjusted on the ground based on ephemerides is sent to the user, the effect of doppler shift can be compensated and the acquisition time greatly reduced.

The maximum time required to perform steps 3 through 5 above is estimated to be 45 seconds. The antenna slewing of steps 1 and 2 will probably require more time. For instance, with the TDRS antenna slew rate of approximately 1 degree/second, slewing across the earth disc will require approximately 20 seconds. The user may be required to slew 180 degrees which would take 120 to 240 seconds, depending on its positioner capability. However, this delay could be eliminated by prepositioning the antenna for the next communication period at the end of the current period.

3.4.3 User Equipment Implementation

User transponder equipment may be constructed using design approaches described for the TDRS repeaters. The principal difference in the detailed design is that the user equipment must operate in the complimentary transmit and receive bands. Minimum mass designs are required to minimize the impact on user satellites. The power consumption of power amplifiers and transceiver equipment must also be minimized by using high efficiency components in their design and construction. Complete redundancy in all electronic equipment is included. Equipment mass and power parameters are summarized in Table 14.

Low data rate transceiver equipment is implemented with microwave integrated circuit construction. The receivers utilize a transistor preamplifier to achieve a moderate noise figure as RFI will generally limit the command link performance. Transmitters feature high efficiency transistor power amplifiers developing 5 watts of output power. Overall efficiency of the transmitter is estimated to be 50 percent. An omnidirectional whip array antenna may be used on satellites using the low data rate service. Pseudo-noise correlators are constructed with integrated circuits to minimize equipment mass and production cost. A crystal oscillator is provided for equipment operation prior to acquisition of the TDRS carrier which then provides the frequency reference for the transponder.

Medium data rate transceiver equipment at S band is also implemented with microwave integrated circuit construction. Command receivers for unmanned users utilize a transistor preamplifier to achieve a moderate noise figure. Higher data rates required for manned users are achieved by using a low noise parametric preamplifier and by operating the TDRS in the high power mode. A 5 watt transmitter is provided for unmanned user satellites. The required link performance of 1 Mbps may be achieved with a 5 watt transmitter and directional antenna with approximately 20 dB gain. The directional antenna is controlled by commands received through an omnidirectional antenna. A mechanical positioner with stepper motor drive is used to position the antenna. Applications requiring lower data rates may be implemented with an array of antennas which are switched to achieve beam

TABLE 14. USER TELECOMMUNICATION EQUIPMENT

Item	Number	Mass, kilograms	Power, watts
LDR User VHF/UHF		5.8	15.0
Receiver	2	1.0	1.0
Telemetry transmitter*	2	2.0	10.0
VCO control and frequency generator	2	0.3	1.0
Acquisition and data correlator	2	1.0	3.0
Antennas	1 Set	1.5	–
MDR User (1 Mbps) S Band		14.9	32.0
Command receiver	2	0.8	1.0
Telemetry transmitter*	2	2.7	20.0
Frequency synthesizer	2	0.3	1.0
Signal processor	2	1.0	3.0
Diplexer	1	1.7	–
Antenna, omnidirectional	1	1.0	–
Antenna, directional	1	1.4	–
Gimbal	1	4.2	–
Gimbal driver	2	1.8	6.0
HDR User (100 Mbps) Ku Band		27.2	62.3
Command receiver, S Band	2	0.8	1.0
Telemetry transmitter, S Band	2	2.7	(20.0)
Tracking receiver, Ku Band	2	5.1	5.8
Telemetry transmitter,** Ku Band	2	5.2	45.5
Frequency synthesizer	2	0.5	1.0
Signal processor	2	1.0	3.0
Diplexer, S Band	1	1.7	–
Diplexer, Ku Band	1	0.2	–
Antennas, S Band	1	1.0	–
Antennas, Ku Band	1	3.0	–
Gimbal	1	4.2	–
Gimbal driver	2	1.8	6.0

*5 watts RF power.
**12 watts RF power.

steering. Beams are broad and can be controlled by computer-generated ground commands. The MDR transceiver is also compatible with ground based satellite control and data acquisition facilities. Pseudo-noise equipment is provided. It is implemented with integrated circuit construction.

The high data rate user equipment consists of a Ku band transmitter, a Ku band tracking receiver, a Ku band directional antenna, and Ku band transceiver equipment for initial acquisition and contact with ground stations directly. The Ku band transmitter utilizes a TWT amplifier and a receiver implemented with waveguide circuitry. For a data link operating at 100 Mbps, an 8 watt transmitter operating into a 2 meter antenna is required. As the beamwidth is less than 1 degree, autotracking is employed after acquisition of the link is achieved. The antenna is positioned with a mechanical motor employing a stepper motor driver.

3.5 GROUND STATION DESIGN

The ground station is the interface element between the TDRS and the two control centers – GSFC and the TDRS Control Center. The general relationship of the ground station to the other elements is shown in Figure 44. Also shown in the figure are three major portions of the basic ground station: 1) a terminal for maintaining RF communication with TDRS east, 2) a terminal for maintaining RF communication with TDRS west, and 3) a common area containing demodulation and processing equipment, which will be applied to signals from both terminals.

The RF terminals are of conventional design, but the signal demodulation and processing equipment, although not new in concept, has not been previously applied in the complexity required for simultaneous multiple user communication via the TDRSS.

It should be mentioned that a third terminal may be required for communication with the in-orbit spare TDRS and for redundancy. This will require only a slight increase in the processing equipment and its configuration controls.

The terminals consist of five major portions: 1) the antenna structure, 2) the antenna tracking subsystem, 3) the Ku band RF/IF subsystem, 4) the S band backup system, and 5) the UHF antenna for TDRS tracking. The signal processing can be separated into 10 functions:

1) LDR user telemetry demodulation

2) MDR channel 1 telemetry demodulation

3) MDR channel 2 telemetry demodulation

4) HDR telemetry demodulation

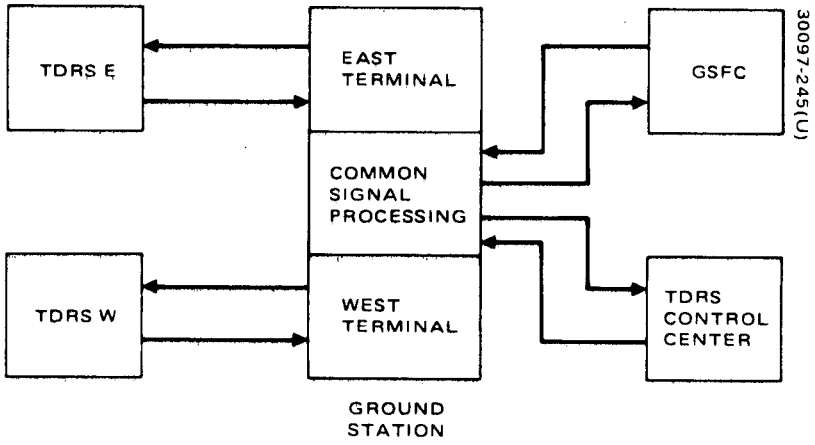

Figure 44. Overall Ground Station Concept and External Interfaces

5) LDR forward link modulation

6) MDR channel 1 forward link modulation

7) MDR channel 2 forward link modulation

8) HDR forward link modulation

9) TDRS telemetry, tracking, and command

10) User range and range rate measurements

3.5.1 Ground Terminal Design

The equipment and associated parameters for a terminal are listed below:

3.5.1.1 Antennas

- Ku band/S band antenna

  1) Reflector diameter, 12.8 meter (42 feet)

  2) Ku band cassegrain feed

  3) S band near-focus feed

  4) Polarization:

     a) Ku band, circular, C/CC

     b) S band, circular, C/CC

  5) Gain

     a) 13.5 GHz, 62 dB

     b) 15.0 GHz, 63 dB

     c) 2040 MHz, 46 dB

     d) 2220 MHz, 47 dB

  6) Pedestal type: azimuth/elevation

  7) Autotrack system: single RF channel amplitude comparison, monopulse type

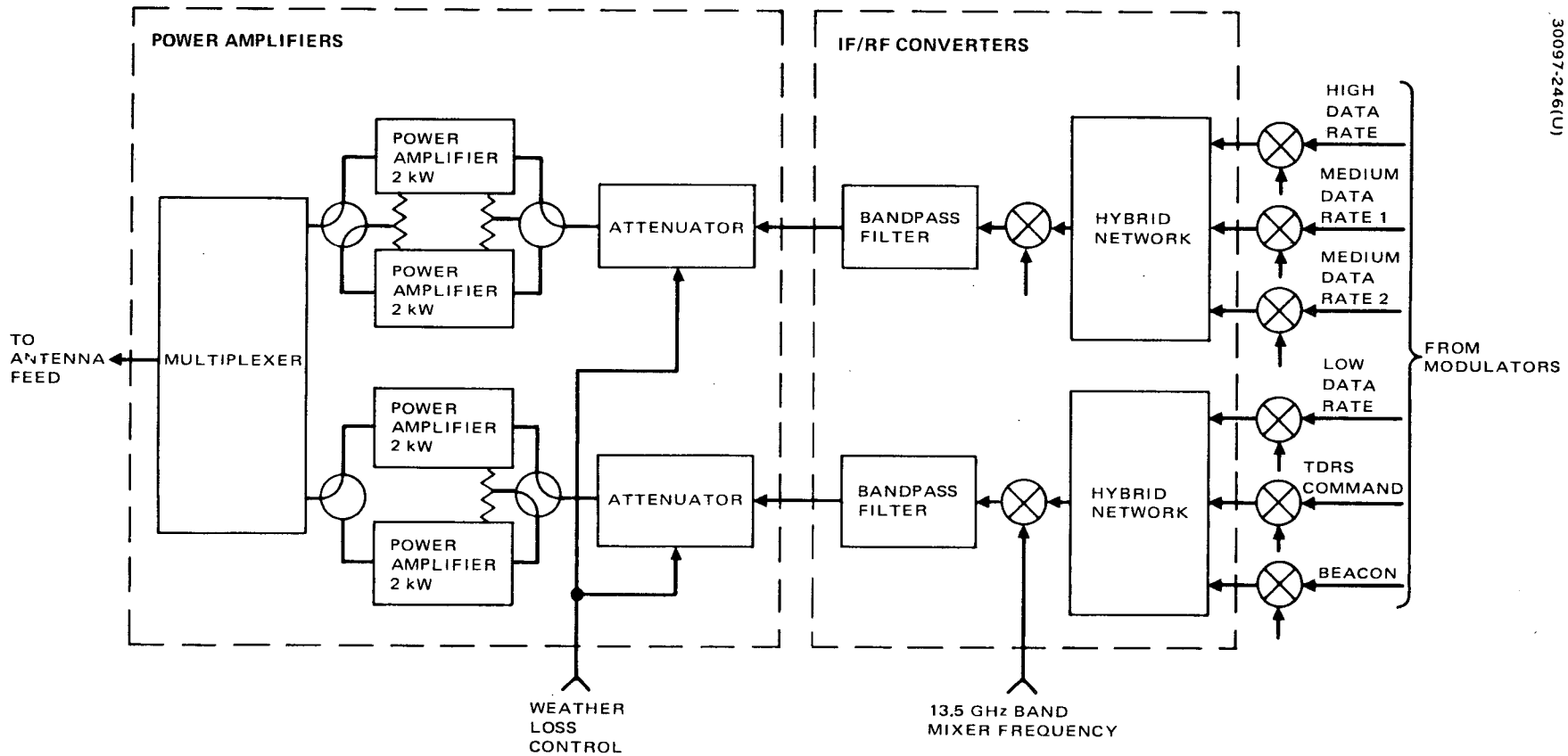

Figure 45. Power Amplifier and RF/IF Configuration

- UHF antenna for TDRS tracking

  1) Frequency, 400.5 to 401.5 MHz

  2) Gain, 5 dB

3.5.1.2 Receivers

- Ku band receiver

  1) Location, rear of reflector

  2) Noise figure, 3.9 dB

- S band receiver

  1) Location, within terminal structure

  2) Noise figure, less than 4 dB

- UHF receiver

  1) Location, within terminal structure

  2) Noise figure, less than 4 dB

3.5.1.3 Power Amplifiers

- Two 2 kW klystrons operational and two in standby

- The two HDR signals and three MDR signals are amplifier in one power amplifier; the LDR, TDRS command, and beacon are amplified in the other.

- Power output allocations at the Ku band antenna feed:

  LDR: 1 kW

  MDR: 600 watts per channel

  HDR: 1800 watts

  Beacon: 20 watts

  TDRS command: 20 watts

Figure 45 shows the forward link RF/IF equipment and power amplifier arrangement.

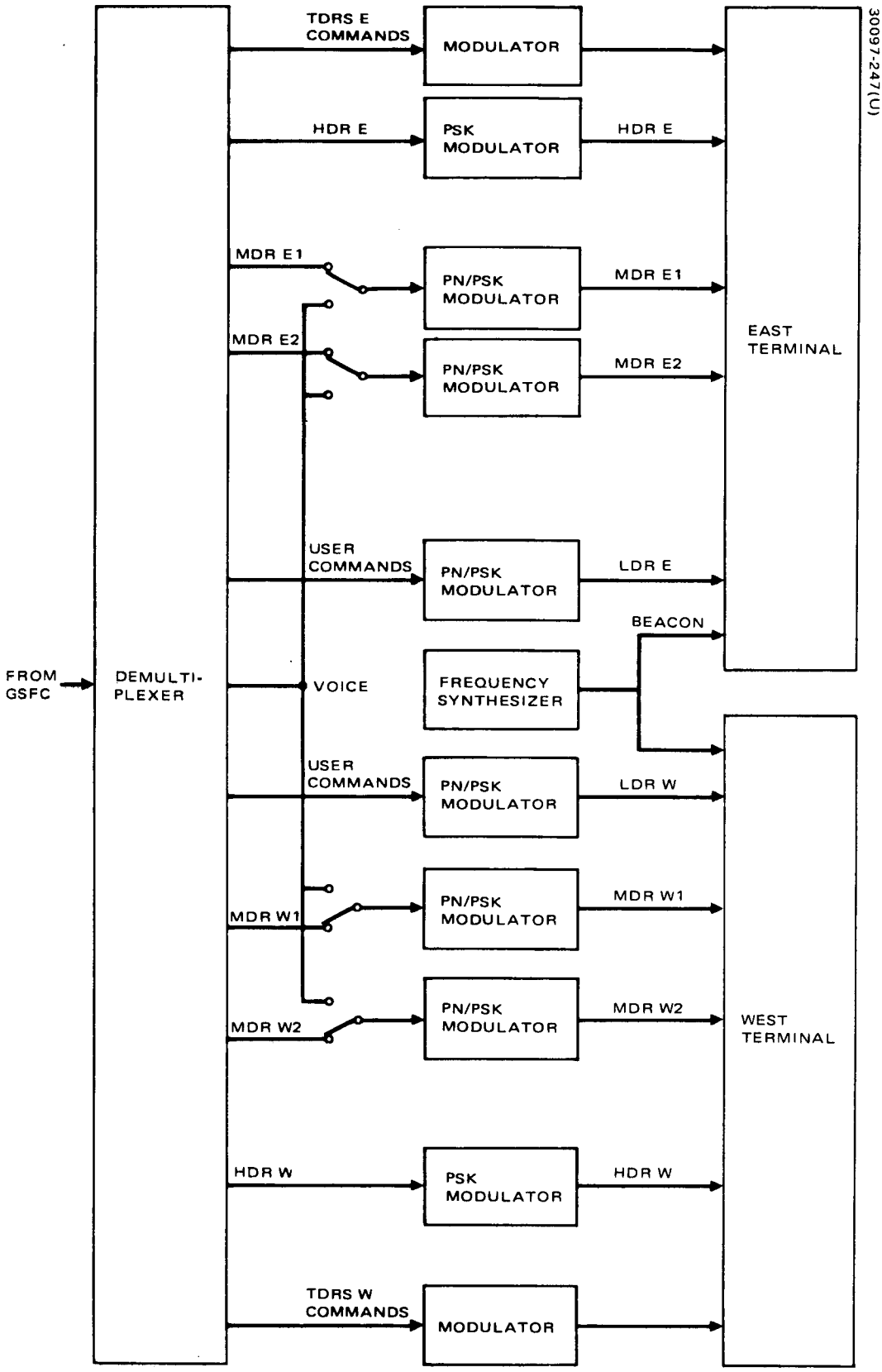

Figure 46. Ground Station Forward Signal Processing

3.5.2 Signal Processing

The ground station return signal processing equipment must separate the individual channels in the two signals from each terminal, demodulate the data signals, and then multiplex all data for transmission to the GSFC telecommunication control center. These functions are illustrated in Figure 46 where, for simplicity, range and range rate measurements have been made part of the general demodulation process. The forward signal processing as shown in Figure 47 includes demultiplexing the signals from GSFC, modulating the LDR and MDR with PN codes, IF carrier modulation of all signals, and transmission to the two terminals. The voice must be switched to the correct LDR or MDR channel as directed from GSFC.

The major task required for the signal processing equipment is one of integration, control, checkout, maintenance, and replacement provision. All equipment, except the LDR return channel demultiplexing and demodulation equipment, is conceptually conventional. The equipment and major parameters follow.

3.5.2.1 Forward Links

- LDR telemetry PN/PSK modulator
  1) Quantity, 2
  2) Rate, 614.4 kchips/s
- MDR PN/PSK modulator
  1) Quantity, 4
  2) Rate, 10 Mchips/s
- HDR PSK modulator
  1) Quantity, 2
  2) Rate, 50 Mbps
- TDRS telemetry
  1) Quantity, 2
  2) Type, three tone GSFC AM-FSK
  3) Bit rate 128 bps

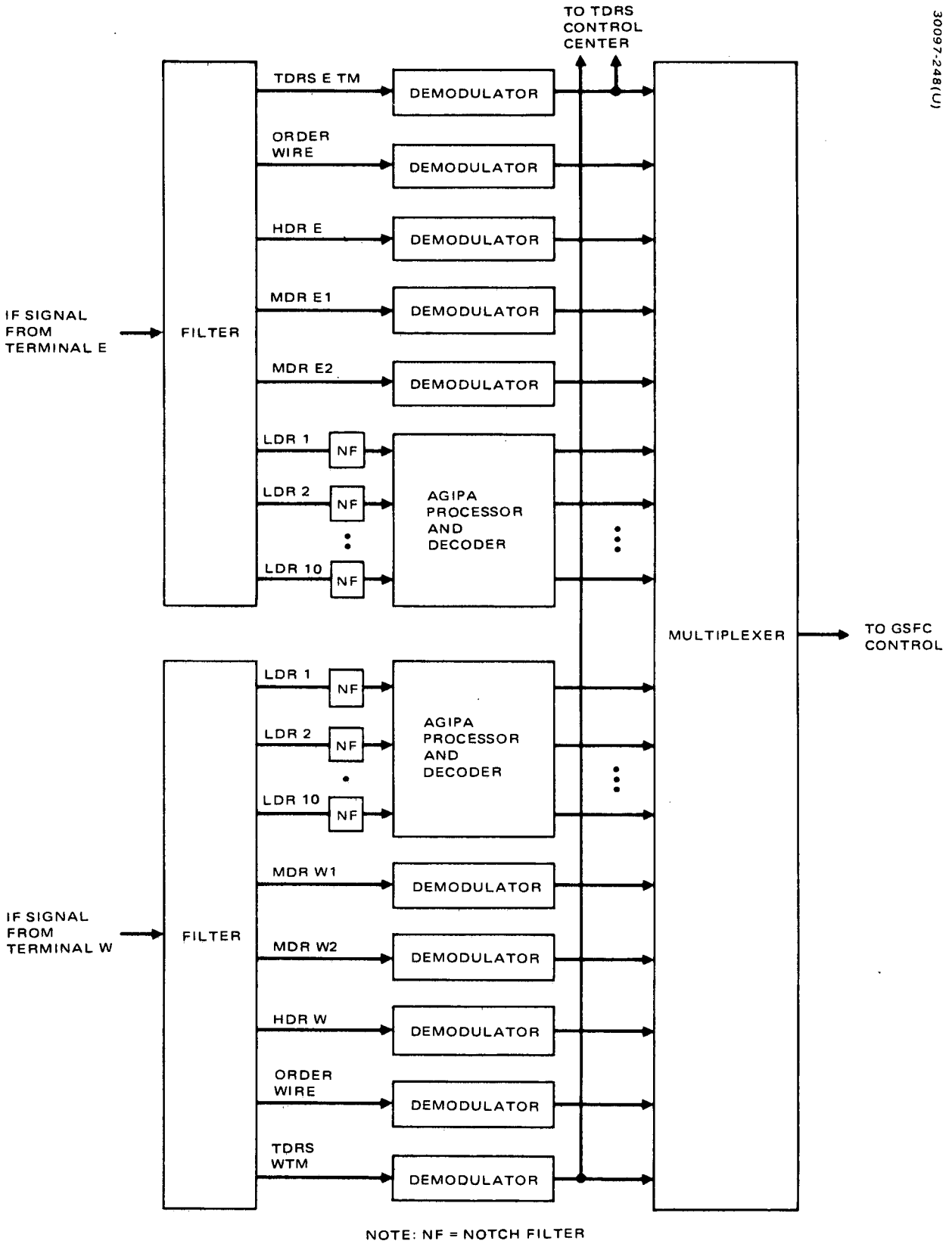

Figure 47. Ground Station Return Signal Processing

3.5.2.2 Return Links

- LDR telemetry: Notch filters will be used at IF in each LDR component signal as necessary to reduce high power, narrowband interference (see Figure 46). For each user the following equipment is required:
  - One AGIPA processor
  - One convolutional decoder
  - One range measurement unit
  - One range rate measurement unit

  The AGIPA processor includes the PN correlation process. A functional arrangement of the above equipment is illustrated in Figure 48.

- MDR: Biphase PSK correlation receivers must be used to demodulate the return signals and procude output bit streams corresponding to the current user spacecraft telemetry rates, a standardized but variable bit rate device is envisioned.

- HDR: A biphase PSK demodulator is required; the bit rate will depend on user requirements but rates up to 100 Mbps are possible.

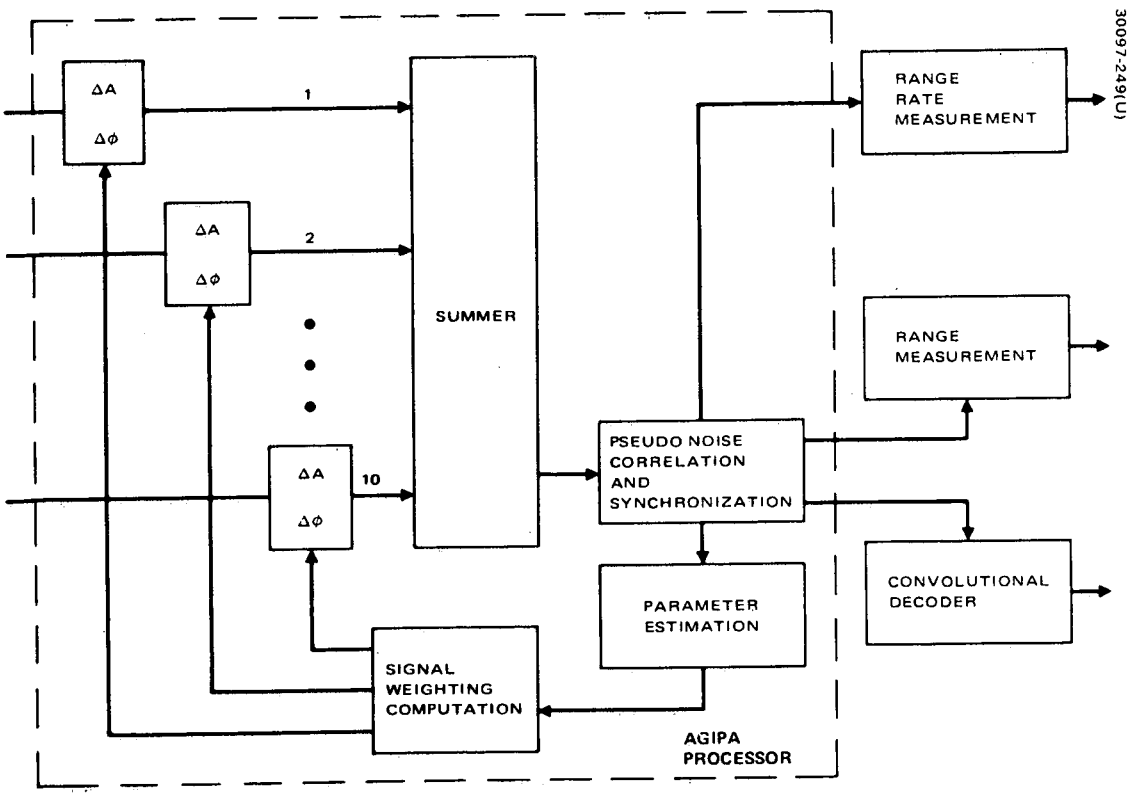

Figure 48. LDR Signal Processing

4. TDR SPACECRAFT BASELINE CONFIGURATION

4.1 CONFIGURATION

The Hughes Gyrostat stabilization concept has been employed to provide a fully stabilized platform for the payload while exploiting the simplicity and long-life advantages associated with spinning satellites. The two main elements of the spacecraft are the spinning rotor, comprising approximately 60 percent of the on-station vehicle mass, and the despun earth-oriented platform containing the communication repeater and its antennas. A rotating interface, consisting of conventional ball bearings and slip rings sustains the relative motion between the two bodies, permits signal transfer to take place, and affords an electrical path over which power from the solar panels and batteries can flow to the repeater payload.

Spin stabilization is accomplished by rotating the section of the spacecraft containing propulsion and power equipment at 100 rpm. The angular momentum developed provides a resistance to external torques and minimizes the number of attitude corrections required throughout the mission. The Gyrostat principle of stabilization is used to this design of the TDRS. This approach allows a large section of the spacecraft to be despun, thereby accommodating the antennas and communication electronic equipment required for this mission on the stabilized despun platform.

Figure 49 presents the baseline spacecraft configuration for the TDRSS Part II Delta launch vehicle. This spacecraft is designed to meet the payload mass and envelope restrictions of the Delta 2914 launch vehicle and to provide the maximum level of telecommunication service consistent with these restrictions and available spacecraft technology. The launch configuration is shown in Figure 50.

The despun section houses the communication equipment and some of the telemetry, tracking, and command equipment. Electronic equipment is mounted on a thermally controlled platform. In order to achieve a benign thermal environment for the communication subsystem and other critical equipment, a thermal control cavity is created inside the spinning solar cell array in which all temperature-sensitive equipment is placed. The aft end of the spacecraft around the apogee motor is sealed off by an insulating thermal barrier. This barrier has an external surface of stainless steel to protect the spacecraft from the intense heating caused by the apogee motor plume and from the axial RCS jet plume. The forward end of the rotating

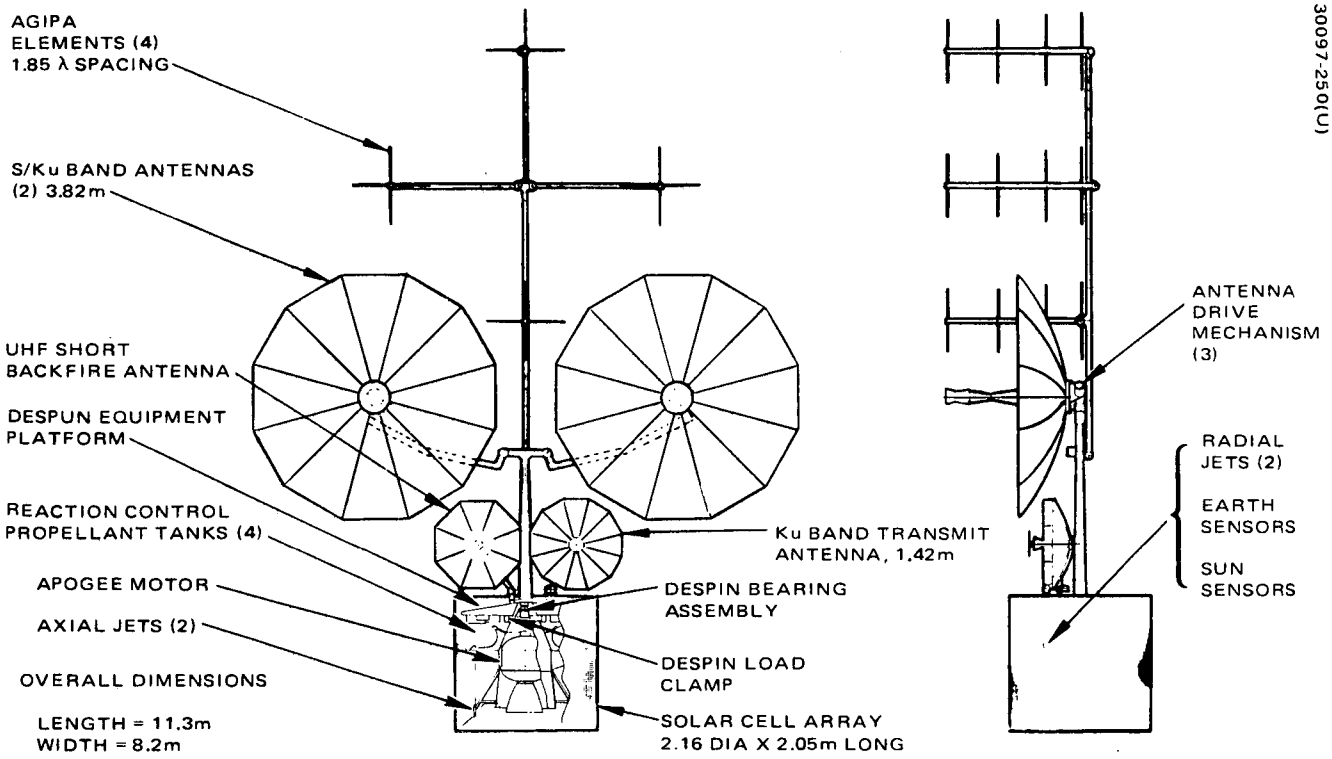

Figure 49. TDR Spacecraft Deployed Configuration

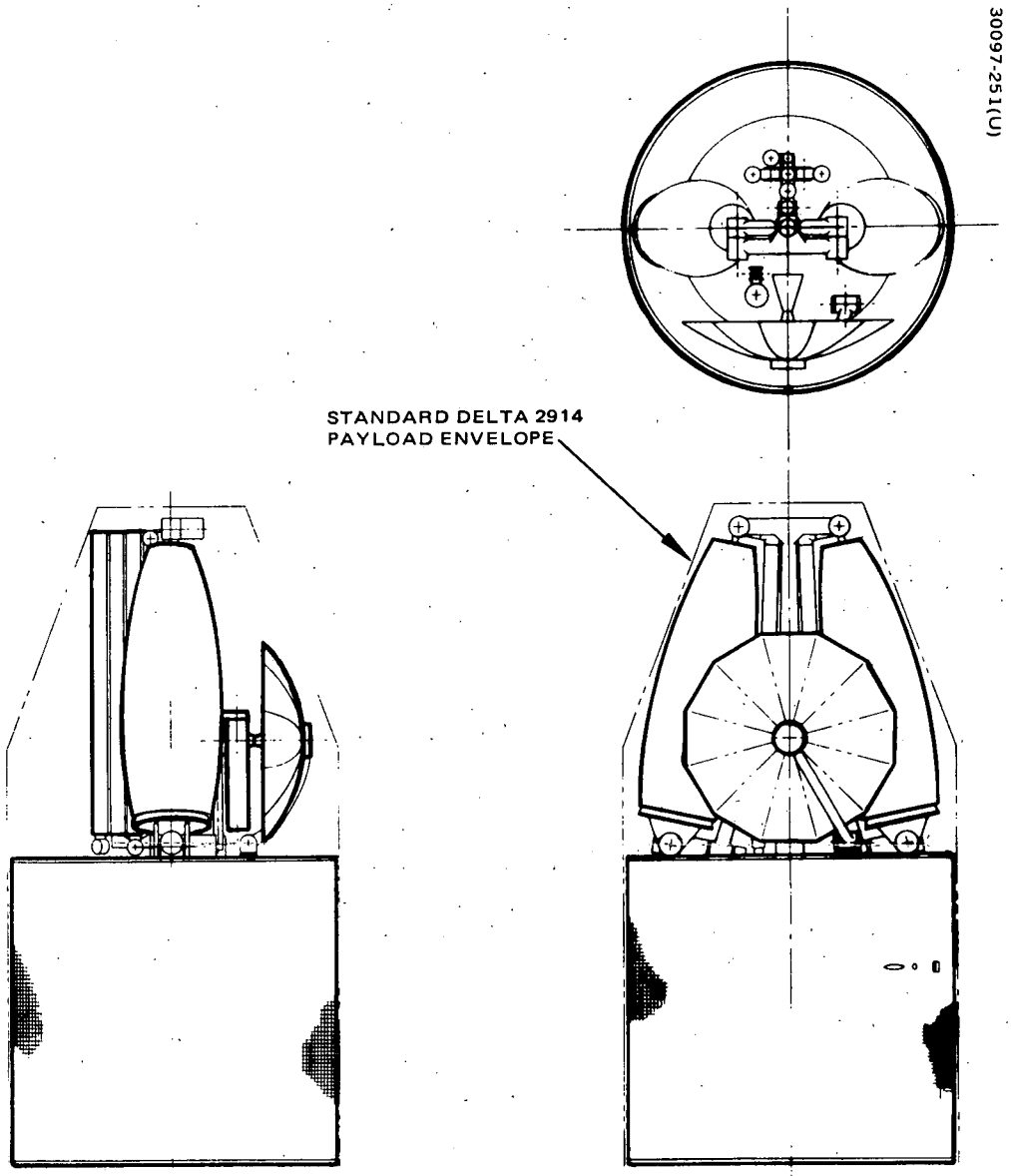

Figure 50. TDR Spacecraft Launch Configuration

drum cavity is sealed off by a spinning sunshield. This conical shell structure is covered with aluminized teflon to reject solar input while at the same time radiating the heat generated by the communication equipment. The spin of these primary thermal control surfaces provides a low gradient thermal environment for the communication electronics and primary spacecraft control elements.

Antennas are mounted off the platform on a mast type support structure. The LDR return link utilizes an AGIPA consisting of four VHF-Yagi elements. These are deployed on booms off the main support mast forward of the spacecraft body. LDR forward link is implemented with an UHF short backfire broad beam antenna which is deployed at the despun platform on a short mast. This antenna is 1.48 meters in diameter. Paraboloid reflector antennas 3.82 meters in diameter are provided for MDR and HDR links. They incorporate dual S/Ku band feeds so that the type of service is established by switching of appropriate repeater equipment. Stowage during launch is achieved by collapsing the paraboloid reflector and folding the supporting linkage. A fixed aperture Ku band antenna is provided for the TDRS to ground station link. It is 1.43 meters in diameter and is deployed on a short pivoted boom. All high gain antennas are provided with two-axis gimbals. Orderwire service for manned users is implemented through a broad beam S band short back fire antenna.

The spinning section supports and houses the propulsion, electrical power, attitude control, and some of the tracking, telemetry, and command equipment. The apogee motor is installed in the central thrust tube. Hydrazine tanks are mounted on ribs extending from the thrust tube to the solar cell array. Batteries, battery controllers, despin control electronics, and telemetry tracking, and command equipment are mounted on the ribs and small equipment platforms spanning the ribs. The aft end of the spinning section is sealed by means of a thermal barrier which protects the spacecraft equipment during apogee motor firing and minimizes heat loss during orbital operations. Attitude control sensors, the radial control jets, and umbilical connectors are installed in an annular section between sections of the solar cell array. The axial jets are mounted on truss supports and protrude through the aft thermal barrier.

The spacecraft is attached to the Delta payload attach fitting with a band release clamp. Launch loads are transmitted through a cylindrical thrust tube which supports the apogee motor and the spinning assembly of the spacecraft. A conical structure forward of the apogee motor picks up the despin bearing assembly outer housing. The inner bearing support structure transfers loads to the despin equipment support platform and antenna support structure. A load transfer clamp provides a more rigid load path during the early stages of launch. Immediately prior to third stage ignition, the clamp is released and the despin motor activated to provide a stable dual spin configuration during the third stage and apogee injection motor burns (a signal from the launch vehicle third stage sequencer is required). The equipment platform is spun slowly with respect to an inertial reference to minimize attitude perturbations during these burns. The spinning section is spun up by the spin rocket on the Delta third stage. Following

firing of the Delta third stage, the spacecraft is separated from the empty stage and then assumes its transfer orbit configuration. Following apogee injection and station acquisition, the spacecraft assumes its operational configuration upon receipt of commands to correct attitude, deploy antennas, and turn on equipment.

4.2 DESIGN FEATURES AND CONFIGURATION SUMMARY

4.2.1 Design Features

The Delta launched spacecraft baseline for Phase II provides enhanced communication capability relative to that configuration presented for Phase I of the TDRSS study. The significant changes include the use of an AGIPA antenna and repeater configuration for LDR users, the addition of a second MDR channel using a 3.82 meter paraboloid reflector antenna, and the addition of an HDR channel. Both MDR link antennas have dual feeds: at S and Ku band. Thus, the HDR link can be used via either antenna.

Elimination of LDR voice service and a reduction in LDR command transmitter power were required to further reduce the mass of the electrical power subsystem equipment. The LDR command channel is powered to provide 30 dBW EIRP for users up to 1000 km altitude orbits corresponding to a 20 degrees field of view at all times. A minimum of 28.2 dBW EIRP is provided for users in 5000 km orbits corresponding to a 31 degree field of view. A redirection in emphasis in subsystem design from maximizing the use of developed spacecraft components to minimizing the mass of spacecraft components has been required to achieve the communication goals established for this spacecraft configuration.

4.2.1.1 Repeater

The spacecraft is designed to achieve the mission with a high reliability by using redundancy for active components. Exceptions occur for items such as the apogee motor, structure, despin bearing assembly, and antennas where it would be prohibitive from mass considerations alone to provide redundancy. In these items, safety factors are employed in their design and assured by test programs. All electronic units are redundant in the TDRS configuration presented.

The VHF receivers associated with the AGIPA, LDR return provide light redundant downlink channels. This receiver incorporates lightweight surface wave bandpass filtering preceeded by preamplifiers which establish a low noise figure. Hybrid micro circuit packaging is also used to achieve low mass for the unit. The LDR forward link is implemented with redundant drivers and a bank of three power amplifiers of which only two are required. Thus no single electronic failure will cause a loss of mission objectives.

The S band transmitter and receiver from MDR users are capable of transmitting and receiving at any frequency within the designated bands providing essentially a "bent-pipe" capability. The instantaneous transmit

and receive bandwidths are limited to 10 MHz; however, these bands may be placed at any frequency within the specified frequency range in 5 MHz steps. A parametric amplifier followed by a transistor amplifier is used to maintain a low receiver noise temperature. The power amplifiers for the S band transmitter are solid state, providing an output power of 23.5 watts. This is reduced by the line losses to 12.5 watts at the antenna yielding the required 47 dBw EIRP.

The order wire S band receiver is designed as a return link which provides continuous coverage over the 31 degree field of view and offers the opportunity for any user to signal the earth station through the TDRS of his desire to use the main S band link. The order wire receiver uses an earth-coverage antenna to a frequency of 2218 MHz. The noise figure and antenna gain of this receiver allow approximately 1 kHz of data to be transmitted by the user to the ground station via the TDRS.

HDR users are provided a command and data return channel at Ku band. The forward link transmitter is implemented with a 100 mW solid-state amplifier which saves some mass relative to the use of TWT amplifiers. The return link receiver utilizes a TDA preamplifier to achieve a moderate noise figure. The TDRS/ground station links are also implemented at Ku band. The principal difference in equipment design is the use of TWT amplifiers for the downlink transmitters to meet communication data rate and link margin requirements.

4.2.1.2 TT&C

The telemetry, tracking, and command subsystem is derived from that used on the Intelsat IV. It features PCM and FM real time modes of operation for spacecraft telemetry. The PCM mode is used for all attitude, thermal, power, and status information, including command verification. Spinning and despun redundant encoders are interconnected by means of the electrical contact rings installed in the despin bearing assembly. Telemetry from the spinning encoder is interleaved with telemetry from the despun side on a word-by-word basis. The composite bit stream is converted to a Manchester code format which is then used to phase modulate either the S band telemetry transmitter of the telemetry carrier of the TDRS/ground station Ku band link.

The FM real time mode is used for transmitting attitude data (sun sensor pulses, earth sensors pulses, platform index pulses, and command execute pulses). The occurrence of a pulse coherently switches the frequency of an IRIG channel 13 subcarrier oscillator from its pilot tone to a different frequency, depending on the kind of pulse present. The output is connected via a slip ring to the despun encoder, the output of which phase modulates the telemetry transmitter of the primary telecommunication service system or the backup telemetry transmitter.

The S band transponder system will be compatible with the GRARR operational requirements to provide data for orbit determination during this phase. Once the spacecraft is on station, the S band transponder system will be used as a backup to the Ku band system in providing TDRS TT&C links to the ground station.

Spacecraft command is performed through two cross-strapped command systems. Redundant decoders are located on both the spun and despun portions of the spacecraft. A total of 255 commands are available for controlling the state of the rotor, while 127 commands are available for the despun platform.

A command transmission consists of a Ku band or S band carrier modulated by a sequence of tones at three discrete frequencies, designated 1, 0, and execute. The tones are amplitude-modulated with a 128/second clock. The demodulated FSK/AM output of the Ku band receiver and the S band command receiver drive both the despun and spinning decoders. Either of the redundant decoders on the despun and spinning side provide up to 128 pulse command outputs. The selection of the executing decoder is by unique decoder address. Command verification is provided by telemetry readout of the command register before sending the execution tone.

The command system is capable of executing jet firing commands in phase with the spin of the satellite. This is performed at the ground station by synchronizing the execute tones with sun or earth pulses received via real time telemetry. The repetitive command mode is also used for antenna pointing. Tracking commands are transmitted as required to maintain the antenna pointing at MDR user satellite. Antenna acquisition commands are also received prior to autotracking of HDR user satellites.

Extensive use of MOS-LSI circuitry is planned in order to achieve a minimum mass for the TT&C subsystem. Principal circuits using this technology are those performing digital and timing functions. Advantages of the technique include lower subsystem mass and improved reliability. This technology has been demonstrated on other space programs performed by Hughes.

4.2.1.3 Antennas

The TDR spacecraft configurations studied under this contract are characterized by large assemblage of antennas. This is necessary to provide the service and performance required by the TDRS system. The antenna technology required for this program includes extensive use of deployable, minimum mass construction.

An AGIPA configuration of four Yagi-elements is selected. The design presents a low area to incident sunlight, thereby minimizing the solar radiation pressure torques. The elements also lend themselves to low mass construction and ease of deployment. A moderate gain element

is selected, and although it does not meet the specified G/T for the LDR return link, it is shown (subsection 3. 1. 2. 1) to be adequate for performance in an RFI limited communication environment. A short backfire element is selected for the LDR forward link operating at UHF. This element develops the required performance with high efficiency and with minimum mass using rib and mesh construction.

The high gain S/Ku band antenna is a deployable rib-mesh design of 3. 82 meters (12. 5 feet) in diameter and f/D of 0. 4. Its surface contour is shaped by 12 aluminum ribs of 3. 82 cm diameter with tapering wall thickness between 0. 15 and 0. 30 mm. The surface contour precision of 0. 15 cm rms is accomplished by use of the double-mesh technique. The reflective (front) mesh is 0. 2 cm open (gold-plated chromel R knit mesh), and its contour between ribs is adjusted by tension ties to a back mesh of 1. 27 cm grid size. A redundant torque spring and motor drive system unfurls the antenna reflector in orbit as well as in earth gravity.

The Ku band transmit antenna is configured with 12 ribs. The double mesh technique is utilized to achieve a surface contour of 0. 25 mm rms accuracy. The front mesh openings are 0. 15 cm. The subreflector is constructed as a shaped honeycomb sandwich with fiberglass face sheets and 0. 025 mm aluminum foil for RF reflectivity. The reflector is locked to the antenna support mast during launch and gimbaled in orbit on a two-axis position drive.

The S band ranging transponder utilizes both omnidirectional and broad beam antennas. The receiver utilizes the omnidirectional antenna so that the backup TT&C will be operable in the event of other subsystem failures. The transmitter will initially utilize the omnidirectional antenna. Subsequently the transmitter will be switched to the broad beam antenna to enhance trilateration tracking at remote ground stations. The transponder antennas are installed on the despun portion of the spacecraft.

4. 2. 1. 4 Attitude Control

The attitude control system establishes the spacecraft attitude, provides a stable platform for antenna positioning, and monitors the orientation of the vehicle spin vector and despun platform azimuth for precision antenna pointing. Spin stabilization is used to absorb cyclic torque disturbances and to minimize the number and frequency of reaction jet firings required for orientation control. A large despun platform is provided for mounting antennas and associated electronics. The spacecraft spin axis is nominally oriented normal to the orbit plane.

This configuration features Gyrostat stabilization. This is a technique that allows a large mass to be despun and oriented with a high degree of precision and stability. Despin control is autonomous and uses earth sensor data to orient the despun section toward the center of earth. A magnet/pipper coil pair located in the bearing and power transfer assembly

establishes the relative phase relationship between the rotor and the platform. Nutational stability is provided through the passive nutation damper mounted on the despun platform, along with active control through the despin control system and the active nutation control system. The damper consists of a single degree of freedom magnetic tip mass pendulum supported on a cantilevered beryllium-copper torsion wire. By dimensionally controlling the torsion wire, the natural frequency of the pendulum can be adjusted to spacecraft nutation frequency.

Because of the importance of despin control to communication service and to nutational stability, an automatic rate control logic has been included. If, for any reason, the despin electronics is deprived of inertial reference information, the control logic will automatically switch to a rate hold mode wherein the spacecraft is controlled to maintain the most recent platform rotor relative rate.

The despin bearing and power transfer assembly (BAPTA) is the structural interface between the spun and despun sections. Its major structural components are also fabricated from beryllium. The bearings selected are 440C CEVM stainless steel angular contact bearings, 60 mm bore, extra light series with a nominal 25 degree contact angle. The bearing lubrication system consists of four sintered nylon reservoirs, two porous ball retainers, the bearing metal parts, and the internal walls of the motor/bearing subassembly. The oil used to lubricate the bearings is a mixture of Apiezon C and lead napthanate. The lubricant is vacuum-impregnated into the bearing parts prior to assembly. Redundant, brushless, resolver-commutated dc torque motors are provided. The motors are segment-wound on a common lamination stack, and two fully redundant resolvers are provided. Power and signal transfer from spun to despun sections of the satellite is accomplished with a dry-lubricated slip ring assembly.

4.2.1.5 Reaction Control

A bipropellant reaction control subsystem design is featured for this spacecraft configuration. This has been selected rather than the hydrazine monopropellant system designs used on current spin-stabilized satellites in order to conserve propellant mass. The thruster selected is the TIROC 1N which produces 1 newton of thrust using monomethyl hydrazine and nitrogen tetroxide propellants. The specific impulse is approximately 50 percent greater than that attainable with the catalytic decomposition hydrazine thrusters, thus reducing propellant consumption by 1/3. Prototype models of this thruster have been constructed and extensive testing has verified performance and lifetime. The subsystem is configured with two oxidizer and two fuel tanks, two radial and two axial thrusters. The mission can be achieved in the event of any single thruster failure, thereby assuring a highly reliable subsystem design.

Propellant for 7 years of spacecraft operations has been included. In the event that the solar cell array has not degraded to the point conservatively predicted and the spacecraft has not failed, the TDRS will continue to

function and provide relay service as specified. This will provide a longer time to write off development and deployment costs of the system, and the expected cost effectiveness of the system will be enhanced.

4.2.1.6 Apogee Motor

A high performance apogee motor is selected for the Delta launched spacecraft configuration. It is based on the use of a composite-modified, double-base (CMDB) propellant produced by Hercules, Inc. The selected propellant has been used in over 850 Hercules production motors. Its performance has been well characterized in over 65 static and 190 flight tests and has remained consistent in motors fired after a period of 7 years. This motor design saves 10 kg relative to motors produced by other manufacturers.

4.2.1.7 Electrical Power

Electrical power is provided by a spinning solar cell array. A portion of the solar array power is used to charge nickel-cadmium batteries to provide power during periods of solar eclipse and to supplement the power available from the solar cell array during period of peak demand. The solar array features the use of currently available 22 x 62 mm solar cells, 0.25 mm thick. The cells are covered with 0.15 mm ceria doped microsheet. The solar cell array provides 364 W, end of life, at summer solstice, and 397 W, end of life, at the beginning of the eclipse season.

The electric power subsystem configuration includes two batteries with active battery discharge control. The batteries are composed of 16 series cells. Battery discharge regulators boost the battery output to a nominal 25.5 volt line. The battery discharge regulator circuit is of the boost choke type and uses pulse width modulation. It has a minimum number of power transistors and requires minimum input line filtering. To reduce power transistor stress and to minimize output filter size, each circuit is two phase, with forced current sharing between phases.

The electrical power subsystem is sized to support a MDR voice service a minimum of 25 percent of the time. This limitation is incurred at the end of life during the summer solstice season and is also imposed during periods of solar eclipse. During the first 3 years, MDR voice service can be supplied 40 percent of the time while the spacecraft is in sunlight.

4.2.1.8 Structure

The structural design is based predominantly on the use of beryllium to conserve spacecraft mass. This material has been used in spacecraft structures for at least 5 years. Its principal advantage is obtained in primary structure where stiffness is a critical design condition. This applies to the thrust cone, equipment mounting platforms, and the antenna support mast.

The primary load carrying structure is divided into a spun and despun section. The spun section consists of a thrust cone and four equipment carrying ribs fabricated from beryllium. A thin circular magnesium plate is attached to the ribs to provide the shear transfer to torsional loading. The ribs provide the support for the solar panel which is fabricated from two-ply fiberglass facesheets with an aluminum honeycomb core. The despun section consists of a despun shelf of stiffened beryllium plate with six beryllium ribs on the forward side. The antenna mast structure is comprised of beryllium tubular elements.

4.2.1.9 Thermal Control

The thermal control subsystem is essentially a passive design consisting of surface finishes on structure and equipment, thermal barriers and shields, insulation blankets, and heaters for critical propulsion components. Bulk temperature control is achieved by coupling equipment radiatively with the spinning solar cell array and with radiators installed at the forward end of the spacecraft. The solar cell array assumes a benign temperature in the range of 285 to 295 K (except during eclipse) which stabilizes the temperature of components about that level. The aft end of the spacecraft is closed and protected from apogee motor plume heating by a stainless steel aft barrier. This barrier has hanovia gold on the surface that faces the spacecraft interior to minimize heat inputs to the spacecraft during apogee motor firing and to minimize heat transfer at this interface during all orbital steady-state conditions.

Most of the power dissipating units are grouped on a despun platform across the forward end of the solar panel. Platform dissipation is radiated to a despun intermediate radiating surface provided between the platform and space. The temperature performance is well within the equipment design range for the extremes in both season and operating mode. The wide range of allowable operating conditions is a desirable feature which allows equipment to be switched on as required to the limits of the available power supply.

Antenna masts and support booms are treated with a combination of aluminum foil and aluminized teflon strips to limit temperature gradients that would cause deflections of the structure. Primary emphasis is on the S/Ku band antenna supports where pointing accuracy is essential for system operation.

The apogee motor has an aluminized kapton multilayer insulation blanket to protect the spacecraft from postfiring thermal soakback. Additional thermal isolation is provided around the aft end and around and over the nozzle to limit undesirable local temperatures near the nozzle throat during the transfer orbit. In addition to this isolation, an active heater on the nozzle throat is provided in the baseline to assure adequate temperature control of this critical element.

4.2.2 Configuration Summary

4.2.2.1 Spacecraft Characteristics Summary

A list of spacecraft design characteristics is presented in Table 15. The spacecraft geometrical characteristics were shown on the configuration drawing, Figure 49.

4.2.2.2 Power Requirements

Electrical power requirements follow directly from the EIRP specifications and supporting equipment required for the mission. A summary of power requirements is given in Table 16. All links are continuous except for the MDR voice links, which are designed for partial usage. Initially the solar cell arrays produce sufficient power to allow continuous operation of the MDR voice and data service in the higher power mode and either a MDR or a HDR channel together with LDR service. At end of life, the available power will support a minimum of 25 percent operation of this combination of services during critical periods such as summer solstice and solar eclipse. The profile of power available from the solar cell array is shown over the spacecraft lifetime in Figure 51.

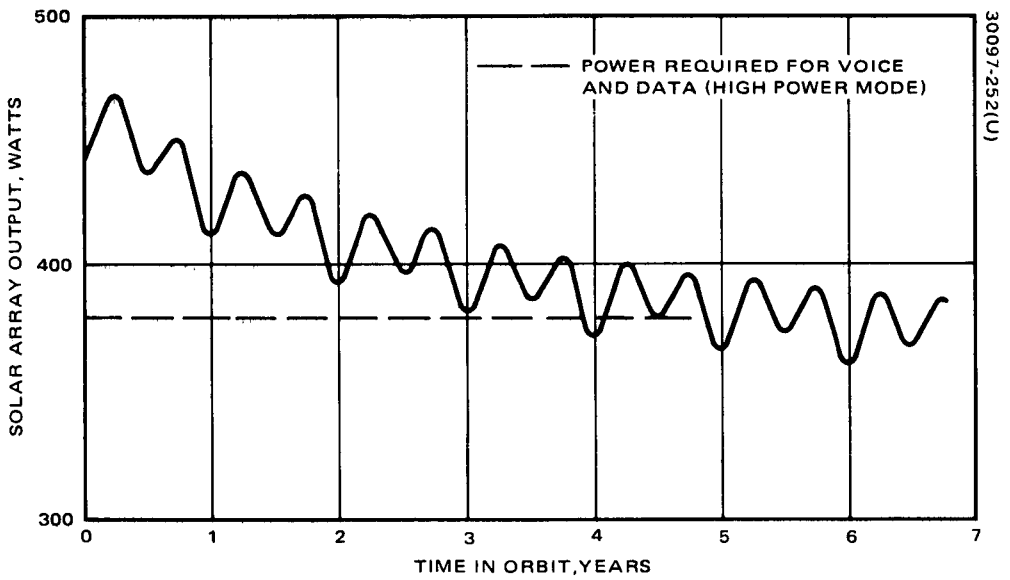

Figure 51. Available Solar Array Power

TABLE 15. TDR SPACECRAFT GENERAL SUMMARY

General	
Orbit	Synchronous, 7 degree initial inclination
Launch vehicle	Delta 2914
Payload fairing	Standard 2.44 m fairing (8 ft)
Design lifetime	5 years required/7 year design goal
Reliability	0.685 at 5 years
Station change maneuver	2 maneuvers, 4.3 degree/day
Configuration	
Stabilization	Hughes Gyrostat
Despun section subsystems	Antennas Repeaters Portion of TT&C
Spinning section subsystem	Electrical power Propulsion Attitude control Portion of TT&C
Structure	Uses aluminum and beryllium
Nominal dimensions	
• Height by width (antennas deployed)	11.3 x 8.2 m
• Diameter and length (rotor)	2.16 x 2.05 m
Mass, end of life (dry)	357.5 kg
Thermal Control	Thermal control cavity inside spinning solar cell array — passive design
Telecommunication Subsystem	
Low data rate user command	30 dBW EIRP, 400.5 to 401.5 MHz, 20 degree field of view
Medium data rate user command	41 dBW EIRP, 2035 to 2120 MHz
Medium data rate voice and data	47 dBW EIRP, 2035 to 2120 MHz
High rate user command	40 dBW EIRP, 14.75 to 14.85 GHz
LDR/MDR data return	44.8 dBW EIRP, 14.6 to 14.7 GHz
HDR data return	50.6 dBW EIRP, 14.9 to 15.1 GHz
Low data rate receive sensitivity	-14.5 dB/K
Medium data rate receive sensitivity	10.2 dB/K
High data rate receive sensitivity	20.2 dB/K
Order wire receive sensitivity	-15.2 dB/K
Ku band forward link sensitivity	-13.2 dB/K

Table 15 (continued)

Telemetry Subsystem	
PCM mode	
• Word length	8 bits
• Frame length	64 words (11 words subcommutated)
• Analog words	110
• Digital words	31
• Bit rate	1000 bps
• Code type output	Manchester
FM mode (attitude data)	
• Subcarrier frequency	14.5 kHz
• Data type	Real time pulses
• Modulation	FM
• Data transmitted	1) Sun pulses 2) North earth pulses 3) South earth pulses 4) Execute receipt
Command Subsystem	
Tones	1, 0, and execute
Input signal	FSK/AM
Bit rate	128 bps
Command capacity, despun	255
Command capacity, spun	127
Command verification	Telemetry
Command execution	Sun or earth pulses
Maximum command rate	Approximately 4/s
Antenna Subsystem	
Low data rate return (VHF)	4 Yagi element AGIPA
Low data rate forward (UHF)	Short backfire, 13.4 dB (20 deg)
Medium data rate, S-band	Paraboloid reflector, 35.2 to 36.2 dB
High data rate, Ku-band	Paraboloid reflector, 51.9 to 52.8 dB
TDRS to ground link, Ku band	Paraboloid reflector type, 44 dB
Ground to TDRS link, Ku band	Two horns, 18.5 dB
Transponder, S band	Omnidirectional and short backfire antennas
Order wire service	Short backfire type, 13 dB

Table 15 (continued)

Attitude Control Subsystem	
Stabilization type	Gyrostat type dual spin
Nutation control	Magnetic damper and despin control dynamics
Despin control	Earth center finding with earth sensors
Pointing accuracy	0.3 degree
Power and signal transfer	Dry lubricated, silver slip rings
Despin motor	Two independent brushless dc motors
Reaction Control Subsystem	
Propellants	Monomethyl hydrazine/nitrogen tetroxide
Thrusters	2-1N radial, 2-1N axial thrusters
Electrical Power Subsystem	
Sunlit power	
• Equinox, EOL	364 W
• Summer solstice (EOL)	397 W
• Maximum bus voltage	30 V (clamped by bus limiters)
Solar cells	
• Type	22 x 62 x 0.25 mm silicon n/p, 10 ohm-cm
• Cover glass	0.15 mm ceria doped microsheet
Batteries	
• Number	Two
• Type	Nickel-cadmium
• Capacity	10 A-hr
• Maximum DOD	60 percent
• Charge rate	c/15
• Trickle charge rate	c/60
• Minimum bus voltage	24.5 V
• Average eclipse power	183 W
Electronics	
• Battery charge control	Automatic or ground commanded
• Battery discharge control	Automatic
• Tap limiter activation voltage	29 to 29.5 V
• Bus limiter activation voltage	29.5 to 30 V

Table 15 (continued)

Apogee Injection Motor	
Type	Solid propellant, $I_{sp\ eff}$ = 298 s
Velocity of injection	1679 m/s
Spacecraft at separation	678 kg
Structure	
Thrust tube	Beryllium semimonocoque
Spun platform	Beryllium/magnesium
Despun platform	Beryllium
Antenna support	Beryllium
Solar array substrate	Aluminum honeycomb/fiberglass composite structure
Thermal control	Passive

TABLE 16. ELECTRICAL POWER SUMMARY

Equipment	Sunlit Operation			Eclipse Operation	
	Mode A Peak* 25.5 V	Mode B Equinox 26.5 V	Mode C Solstice 26.5 V	Mode D Peak* 24.5 V	Mode E Normal 24.5 V
HDR return transmit (Ku)	35.3	36.5	36.5	–	–
LDR/MDR return transmit (Ku)	10.5	11.1	11.1	10.1	10.1
HDR forward transmit (Ku)	6.6	6.8	6.8	–	–
MDR forward transmit 1 (S)	–	27.6	27.6	26.5	26.5
MDR forward transmit 2 (S)	104.5	–	–	100.5	–
LDR forward transmit (UHF)	114.0	119.0	119.0	–	–
Receivers, processors, etc.	37.8	39.4	39.4	36.4	36.4
Transponder (S)	2.1	26.0	26.0	2.0	2.0
Telemetry, tracking, and command	15.4	15.7	15.7	14.8	14.8
Antenna position control	11.9	12.0	12.0	11.4	11.4
Despin control	19.8	20.0	20.0	19.0	19.0
Thermal control	6.0	6.0	6.0	6.0	6.0
Power electronics	11.0	11.0	11.0	26.0	26.0
Battery charging	–	37.0	–	–	–
Distribution losses	7.0	7.0	7.0	4.0	4.0
Power required	381.9	375.1	338.1	256.7	156.2
Contingency	13.1	21.9	25.9	–	–
Power available	395.0	397.0	364.0	Batt.	Batt.

*Peak loads for 25 percent of time.

4.2.2.3 Estimated Spacecraft Mass

The estimated mass of the spacecraft and its components is presented in Tables 17 and 18. The estimates are based on flight proven equipment where applicable, and on comparison with developed equipment when design requirements force development of new equipment. Structural weights have been estimated from the size, loads, and characteristics of the selected materials. A contingency of 78.2 kg has been identified during the spacecraft definition study. This is approximately 8 percent of the total hardware mass exclusive of the apogee motor. This level of contingency is typical for a program new start and is considered adequate for the TDRSS mission.

4.2.2.4 Telemetry and Command Lists

Telemetry and command requirements are presented in Tables 19 and 20. A total capability of 64 words is provided for telemetry divided equally between the spun and despun section of the spacecraft.

4.3 SUBSYSTEM DESCRIPTION

The spacecraft configuration requires extensive use of low mass technology for all subsystems in order to achieve a telecommunication service level compatible with the overall TDRSS program objectives. Applicable technology and components developed in previous Hughes programs have been used to the maximum extent to provide a design that can be implemented with a high level of confidence.

The subsystem descriptions are organized as follows:

- Telecommunications
- Telemetry and command
- Antennas
- Attitude control
- Reaction control
- Electrical power
- Apogee motor
- Spacecraft structure
- Thermal control

TABLE 17. SPACECRAFT MASS SUMMARY

Subsystem	Mass, kilograms
Repeaters	68.2
Telemetry, tracking, and command	12.9
Antennas	53.0
Attitude control	20.0
Reaction control	10.5
Electrical power	41.1
Wire harness	15.0
Apogee motor, burned out	25.4
Structure	76.5
Thermal control	8.8
Contingency	26.1
Spacecraft, final orbit	357.5
RCS propellant	25.0
Apogee motor expendables	295.5
Spacecraft separation mass	678.0

TABLE 18. SUBSYSTEM MASS SUMMARY

Subsystem/Item	Quantity		Mass, kilograms
	Available	Required	
Repeater Subsystem			68.2
Receiver, command/LDR forward (Ku)	2	1	3.4
Receiver, HDR return (Ku)	2	1	5.9
Receiver, HDR/MDR (Ku)	2	1	5.1
Transmitter, LDR/MDR/HDR (Ku)	4	2	11.4
Transmitter, HDR forward (Ku)	2	1	4.0
Transmitter, LDR forward (UHF)	2/3	1/2 of 3	4.1
Receiver, LDR return (VHF)	16	8	5.4
Receiver, MDR return (S)	4	2	2.9
Transmitter, MDR forward (S)	4/6	2/4 of 6	11.6
Receiver, order wire (S)	2	1	1.9
Transponder (S)	2	1	4.0
Frequency synthesizer	2	1	8.5
Telemetry and Command Subsystem			12.9
Despun decoder	2	1	1.6
Despun encoder and multiplexer	2	1	2.5
Spun decoder	2	1	1.6
Spun encoder and multiplexer	2	1	3.3
Despun squib driver	1	1	2.5
Spun squib and solenoid driver	1	1	1.4
Antenna Subsystem			53.0
Paraboloid reflector (Ku)	1	1	1.4
Horns (Ku)	2	2	0.5
Paraboloid reflector (S and Ku)	2	2	17.8
Backfire (S)	2	2	1.0
Backfire (UHF)	1	1	2.0
AGIPA-YAGI (VHF)	4	4	8.0
Bicone (S)	1	1	1.0
Antenna positioner	3	3	12.6
Positioner controller	3	3	2.7
Coaxial waveguide			6.0
Attitude Control Subsystem			20.0
BAPTA	1	1	10.0
Earth sensors	3	2	2.2
Sun sensor	1	1	0.1
Despun control electronics	2	1	3.6
Accelerometer	2	1	0.3
Active nutation control electronics	2	1	1.5
Nutation damper	1	1	2.3

Table 18 (concluded)

Subsystem/Item	Quantity		Mass, kilograms
	Available	Required	
Reaction Control Subsystem			10.5
Tanks	4	4	4.0
Thrusters	4	3	0.3
Filters, manifold, valves			5.2
Pressurant			1.0
Electrical Power Subsystem			41.1
Solar cell array	1	1	15.9
Batteries	2	2	15.4
Battery discharge controllers	2	2	6.0
Battery charge controllers	2	2	0.9
Voltage limiters	6	4	2.7
Current sensor	1	1	0.2
Apogee Motor, Burned Out	1	1	25.4
Wiring Harness			15.0
Structure			76.5
Thrust cone assembly			24.0
Substrate			21.7
Despun compartment			10.0
Antenna support			14.0
RCS tank and thruster support			4.5
Balance mass			2.3
Thermal Control			8.8
Forward sunshield			2.2
Aft barrier			2.1
RCS tank wrap			0.4
RCS shields, blankets, and heaters			0.7
Apogee motor blanket			0.3
Paint			0.5
Despun sunshield			1.6
Despun mast blanket			1.0

TABLE 19. TELEMETRY CHANNEL ASSIGNMENTS

Main Frame Word	Spinning	Despun
0	Frame sync	
1		Frame sync
2	Decoder 1 command verify	
3		Decoder 1 command verify
4	Decoder 2 command verify	
5		Decoder 2 command verify
6	Status word 6	
7		Status word 7
8	Subcommutation (digital)	
9		Status word 9
10	Attitude determination	
11		Subcommutation (digital)
12	Attitude determination	
13		Subcommutation (digital)
14	Attitude determination	
15		Status word 15
16	Subcommutation	
17		Subcommutation
18	Subcommutation	
19		Subcommutation
20	Subcommutation	
21		Subcommutation
22	Subcommutation	
23		Subcommutation
24	Telemetry calibration	
25		Bus voltage
26	Bus current	
27		Antenna A azimuth*
28	Bus voltage	
29		Antenna A elevation*
30	Despin position torque commands**	
31		Antenna B azimuth*
32	Motor torque command**	

*Digital output increases when antenna steers toward north or west.

**Both torque command signals are connected to each encoder via OR circuits, since only one despin control electronics unit is on at a time.

Table 19 (continued)

Main Frame Word	Spinning	Despun
33		Antenna B elevation *
34	Motor 1 current	
35		Antenna C azimuth*
36	Motor 2 current	
37		Antenna C elevation*
38	Spare	
39		Spare
40	Spare	
41		Spare
42	Spare	
43		Telemetry calibration
44	Spare	
45		Spare
46	Spare	
47		Spare
48	Spare	
49		Spare
50	Spare	
51		Spare
52	Spare	
53		Spare
54	Spare	
55		Spare
56	Spare	
57		Spare
58	Spare	
59		Spare
60	Spare	
61		Spare
62	Spare	
63		Spare

*Digital output increases when antenna steers toward north or west.

Table 19 (continued)

Main Frame Word	Subcommutated Channel	
Status Digital Bit Assignment – Spinning		
6	–	Status Word 6 (8 bits) Spinning Encoder Bit 1 Spinning decoder 1 execute 2 Spinning decoder 2 execute 3 Spacecraft seapration 4 Spinup sequencer 1/2 OFF 5 Subframe count 6 Subframe count 7 Subframe count 8 Spare
8	0	Reaction Control Status Bit 1 Latching valve 1 OPEN/CLOSE 2 Latching valve 2 OPEN/CLOSE 3 Latching valve 3 OPEN/CLOSE 4 Spare 5 Spare 6 Radial valve heater ON 7 Axial valve heater ON 8 Spare
	1	Reaction Control and Apogee Motor Status Bit 1 Apogee motor 1 OFF 2 Apogee motor 2 OFF 3 Apogee motor 3 OFF 4 Apogee motor 4 OFF 5 Spare 6 Spare 7 Spare 8 Spare

Table 19 (continued)

Main Frame Word	Subcommutated Channel	
Status Digital Bit Assignment – Spinning (continued)		
8	2	TT&C Status Bit 1 Telemetry encoder 1 PCM mode 2 Telemetry encoder 2 PCM mode 3 Telemetry encoder 1 ON (spinning) 4 Telemetry encoder 2 ON (spinning) 5 Telemetry transmitter A ON 6 Telemetry transmitter B ON 7 Spare 8 Spare
	3	Electrical Power Status Bit 1 Trickle charge battery 1 OFF 2 Trickle charge battery 2 OFF 3 Spare 4 Spare 5 Set charge temperature limit 1 6 Set charge temperature limit 2 7 Spare 8 Spare
	4	Electrical Power Status Bit 1 Thermal charge limit set override 2 Voltage limiter 1 ON 3 Voltage limiter 2 ON 4 Voltage limiter 3 ON 5 Voltage limiter 4 ON 6 Spare 7 Spare 8 Reconditioning discharge ON

Table 19 (continued)

Main Frame Word	Subcommutated Channel	
Status Digital Bit Assignment – Spinning (continued)		
8	5	Controls Status Bit 1 Despin electronics 1 ON 2 Despin electronics 2 ON 3 Motor drive 1 ON 4 Motor drive 2 ON 5 ANC 1 ON 6 ANC 2 ON 7 Motor driver 1 low/high gain 8 Motor driver 2 low/high gain
	6	Controls Status Bit 1 Command limiter ON 2 Interlock enable 3 Rate command latch 1/2 4 Earth sensor 1 OFF 5 Earth sensor 2 OFF 6 Earth sensor 3 OFF
	7	Control Status Bit 1 Select earth sensor 1 2 Select earth sensor 2 3 Select earth sensor 3 4 SCL eanble 5 Spare 6 Spare 7 Spare 8 Spare

Table 19 (continued)

Main Frame Word	Subcommutated Channel	
Status Digital Bit Assignment – Spinning (continued)		
10	Code t_1 t_2 t_3 t_4 t_5 t_6 t_7 t_8 t_9 t_{10}	Status Word 10 (8 bits) Attitude Determination Measurement — Bit 1 2 3 4 5 6 7 8 Spin period 1 0 0 0 1 0 0 0 Sync control reference 0 0 0 1 1 0 0 0 Inner sun chord 0 0 1 1 1 0 0 0 Outer sun chord 0 1 0 0 1 0 0 0 North earth chord 0 1 0 1 1 0 0 0 South earth chord 0 1 1 0 1 0 0 0 Sun-N. earth separation 0 1 1 1 1 0 0 0 Sun-S. earth separation 1 0 0 0 1 0 0 0 N. earth to S. earth 1 0 0 1 1 0 0 0 Platform pointing 1 0 1 0 1 0 0 0
12	–	Status Word 12 (8 bits) Attitude Determination 1/2-16 bit word; bit 1 most significant bit
14	–	Status Word 14 (8 bits) Attitude Determination 1/2-16 bit word; bit 8 least significant bit of 16 bit word included in status word 12 and 14 and coded in status word 10
Analog Subcommutator – Spinning		
16	0 1 2 3 4 5 6 7	Battery 1 voltage Battery 2 voltage Battery 1 charge/discharge current Battery 2 charge/discharge current Battery 1 pack 1 temperature Battery 1 pack 2 temperature Battery 2 pack 1 temperature Battery 2 pack 2 temperature

Table 19 (continued)

Main Frame Word	Subcommutated Channel	
Analog Subcommutator – Spinning (continued)		
18	0	Spare
	1	Spare
	2	Spare
	3	Spare
	4	Spare
	5	Spare
	6	Spare
	7	Spare
20	0	Radial jet 1 temperature
	1	Radial jet 2 temperature
	2	Axial jet 1 temperature
	3	Axial jet 2 temperature
	4	Fuel tank 1 temperature
	5	Fuel tank 2 temperature
	6	Hydrazine 1 pressure
	7	Hydrazine 2 pressure
22	0	BAPTA temperature 1
	1	BAPTA temperature 2
	2	Apogee motor temperature 1
	3	Apogee motor temperature 2
	4	Sunshield temperature 1
	5	Sunshield temperature 2
	6	Solar panel temperature 1
	7	Solar panel temperature 2

Table 19 (continued)

Main Frame Word	Subcommutated Channel	
Status Digital Bit Assignment – Despun		
7		Status Word 7 (8 bits) Despun Encoder Bit 1 Despun decoder 1 execute 2 Despun decoder 2 execute 3 Subframe count 4 Subframe count 5 Subframe count 6 Spare 7 Spare 8 Spare
9		Status Word 9 (8 bits) Despun Encoder Bit 1 Spare 2 Spare 3 Spare 4 Spare 5 Spare 6 Spare 7 Spare 8 Spare
11	0	Communication Status Bit 1 Ku band receiver CMD/LDR forward A ON 2 Ku band receiver CMD/LDR forward B ON 3 Ku band receiver MDR/HDR forward A ON 4 Ku band receiver MDR/HDR forward B ON 5 Antenna tracking modulator driver select A/B (Antenna A) 6 Ku band receiver HDR return 1 A ON 7 Ku band receiver HDR return 1 B ON 8 Antenna tracking modulator driver select A/B (Antenna B)

Table 19 (continued)

Main Frame Word	Subcommutated Channel	
Status Digital Bit Assignment – Despun (continued)		
11	1	Communication Status Bit 1 Spare 2 Spare 3 Antenna tracking modulator driver select A/B (Antenna C) 4 Ku band receiver HDR return bandwidth 1 5 Ku band receiver HDR return bandwidth 2 6 Ku band receiver HDR return bandwidth 3 7 Ku band receiver HDR return bandwidth 4 8 Ku band transmitter HDR return 1 A ON
	2	Communication Status Bit 1 Ku band transmitter HDR return B ON 2 Ku band transmitter HDR return TWT select 3 Spare 4 Spare 5 Spare 6 Ku band transmitter MDR/LDR A ON 7 Ku band transmitter MDR/LDR B ON 8 Ku band transmitter MDR/LDR TWT select
	3	Communication Status Bit 1 Ku band transmitter HDR forward 1 A ON 2 Ku band transmitter HDR forward 1 B ON 3 Ku band transmitter HDR forward 1 power amplifier select 4 Spare 5 Spare 6 Spare 7 UHF transmitter driver A ON 8 UHF transmitter driver B ON

Table 19 (continued)

Main Frame Word	Subcommutated Channel	
Status Digital Bit Assignment – Despun (continued)		
11	4	Communication Status Bit 1 UHF power amplifier 1 ON 2 UHF power amplifier 2 ON 3 UHF power amplifier 3 ON 4 Spare 5 Spare 6 Spare 7 Spare 8 Spare
	5	Communication Status Bit 1 VHF horizontal receiver 1 A ON 2 VHF horizontal receiver 1 B ON 3 VHF horizontal receiver 2 A ON 4 VHF horizontal receiver 2 B ON 5 VHF horizontal receiver 3 A ON 6 VHF horizontal receiver 3 B ON 7 VHF horizontal receiver 4 A ON 8 VHF horizontal receiver 4 B ON
	6	Communication Status Bit 1 VHF vertical receiver 1 A ON 2 VHF vertical receiver 1 B ON 3 VHF vertical receiver 2 A ON 4 VHF vertical receiver 2 B ON 5 VHF vertical receiver 3 A ON 6 VHF vertical receiver 3 B ON 7 VHF vertical receiver 4 A ON 8 VHF vertical receiver 4 B ON

Table 19 (continued)

Main Frame Word	Subcommutated Channel	
Status Digital Bit Assignment – Despun (continued)		
11	7	Communication Status Bit 1 Spare 2 Spare 3 Spare 4 Spare 5 Spare 6 Spare 7 VHF receiver select up converter 8 VHF receiver frequency source select
13	0	Communication Status Bit 1 Order wire receiver A ON 2 Order wire receiver B ON 3 S band transmitter 1 A ON 4 S band transmitter 1 B ON 5 S band transmitter 2 A ON 6 S band transmitter 2 B ON 7 Spare 8 Spare
	1	Communication Status Bit 1 S band transmitter 1 high/low select 2 S band transmitter 2 high/low select 3 S band receiver 1 A ON 4 S band receiver 1 B ON 5 S band receiver 2 A ON 6 S band receiver 2 B ON 7 Spare 8 Spare

Table 19 (continued)

Main Frame Word	Subcommutated Channel	
Status Digital Bit Assignment – Despun (continued)		
13	2	Communication Status Bit 1 Spare 2 Spare 3 Spare 4 S band MDR receiver 1 step attenuator IN/OUT 5 S band MDR receiver 2 step attenuator IN/OUT 6 Spare 7 Telemetry encoder 1 ON 8 Telemetry encoder 2 ON
	3	Deployment Status Bit 1 Release support arm Ku band antenna 1 2 Spare 3 Spare 4 Release S/Ku band antenna arm 1 5 Release S/Ku band antenna arm 2 6 Release UHF antenna arm 7 Release AGIPA mast top lock 8 Release AGIPA mast bottom lock
	4	Deployment Status Bit 1 Release YAGI element 1 from support arm 2 Release YAGI element 2 from support arm 3 Release YAGI element 3 from support arm 4 Release YAGI element 4 from support arm 5 Release stowed YAGI element 1 6 Release stowed YAGI element 2 7 Release stowed YAGI element 8 Release stowed YAGI element 4

Table 19 (continued)

Main Frame Word	Subcommutated Channel	
Status Digital Bit Assignment – Despun (continued)		
13	5	Deployment Status Bit 1 Deploy dipole assembly YAGI element 1 2 Deploy dipole assembly YAGI element 2 3 Release UHF antenna from support arm 4 Deploy dipole assembly YAGI element 3 5. Deploy dipole assembly YAGI element 4 6 Spare 7 Spare 8 Spare
	6	Power Status Bit 1 Voltage limiter 1 ON 2 Voltage limiter 2 ON 3 Spare 4 Spare 5 Spare 6 Spare 7 Spare 8 Spare
	7	Communication Status Bit 1 Frequency synthesizer A on 2 Frequency synthesizer B on 3 Frequency synthesizer status 4 Frequency synthesizer status 5 Frequency synthesizer status 6 Frequency synthesizer status 7 Frequency synthesizer status 8 Frequency synthesizer status

Table 19 (continued)

Main Frame Word	Subcommutated Channel	
Status Digital Bit Assignment – Despun (continued)		
15		Status Word 15 Bit 1 Spare 2 Spare 3 Spare 4 Spare 5 Spare 6 Spare 7 Spare 8 Spare
Analog Sumcommutators – Despun		
17	0	Spare
	1	Spare
	2	Spare
	3	Spare
	4	S band power amplifier 1 temperature
	5	S band power amplifier 2 temperature
	6	S band power amplifier 3 temperature
	7	S band power amplifier 4 temperature
	0	Forward shelf temperature 1
	1	Forward shelf temperature 2
	2	Aft shelf temperature 1
	3	Aft shelf temperature 2
	4	Auxiliary battery voltage
	5	Ku band transmitter A temperature
	6	Ku band transmitter B temperature
	7	Heater bank A current

Table 19 (continued)

Main Frame Word	Subcommutated Channel	
Analog Sumcommutators – Despun (continued)		
21	0	Heater bank B current
	1	Heater bank C current
	2	Heater bank D current
	3	Spare
	4	Spare
	5	Spare
	6	Spare
	7	Spare
	8	Spare
23	0	BAPTA hub temperature 1
	1	BAPTA hub temperature 2
	2	UHF power amplifier 1 temperature
	3	UHF power amplifier 2 temperature
	4	UHF power amplifier 3 temperature
	5	UHF power amplifier 4 temperature
	6	Spare
	7	Spare

TABLE 20. COMMAND ASSIGNMENTS

Summary	Despun	Spinning
Communications	111	0
Deployment mechanisms	26	0
Antenna operations	12	0
TT&C	11	3
Power	3	17
Controls	0	26
RCS	0	22
Subtotal	163	68
Spares	92	59
Total	255	127

Communications

Despun

1) Frequency synthesizer, A ON, B OFF
2) Frequency synthesizer, B ON, A OFF
3) Frequency synthesizer, both OFF
4) Master oscillator select A
5) Master oscillator select B
6) Frequency synthesizer A frequency step for S band transmit local oscillator 1
7) Frequency synthesizer B frequency step for S band transmit local oscillator 1
8) Frequency synthesizer A frequency step for S band receive local oscillator 1
9) Frequency synthesizer B frequency step for S band receive local oscillator 1
10) Frequency synthesizer A frequency step for S band transmit local oscillator 2
11) Frequency synthesizer B frequency step for S band transmit local oscillator 2
12) Frequency synthesizer A frequency step for S band receive local oscillator 2
13) Frequency synthesizer B frequency step for S band receive local oscillator 2
14) Ku band receiver command/LDR forward, A ON, B OFF
15) Ku band receiver command/LDR forward, B ON, A OFF
16) Ku band receiver CMD/LDR forward, both OFF
17) Ku band receiver MDR/HDR forward, A ON, B OFF
18) Ku band receiver MDR/HDR forward, B ON, A OFF
19) Ku band receiver MDR/HDR forward, both OFF
20) Antenna tracking modulator driver select A (antenna A)
21) Antenna tracking modulator driver select B (antenna A)

Table 20 (continued)

22)	Ku band receiver HDR return 1, A ON, B OFF
23)	Ku band receiver HDR return 1, B ON, A OFF
24)	Ku band receiver HDR return 1, both OFF
25)	Antenna tracking modulator driver select A (antenna B)
26)	Antenna tracking modulator driver select B (antenna B)
27)	Antenna tracking modulator driver select A (antenna C)
28)	Antenna tracking modulator driver select B (antenna C)
29)	Ku band receiver HDR return 1 bandwidth select: 100 MHz
30)	Ku band receiver HDR return 1 bandwidth select: 50 MHz
31)	Ku band receiver HDR return 1 bandwidth select: 10 MHz
32)	Ku band transmitter HDR return 1, A ON, B OFF
33)	Ku band transmitter HDR return 1, B ON, A OFF
34)	Ku band transmitter HDR return 1, both OFF
35)	Ku band transmitter HDR return 1, select TWT A
36)	Ku band transmitter HDR return 1, select TWT B
37)	Ku band transmitter MDR/LDR A, ON, B OFF
38)	Ku band transmitter MDR/LDR B, ON, A OFF
39)	Ku band transmitter MDR/LDR, both OFF
40)	Ku band transmitter MDR/LDR, select TWT A
41)	Ku band transmitter MDR/LDR, select TWT B
42)	Ku band transmitter HDR forward 1, A ON, B OFF
43)	Ku band transmitter HDR forward 1, B ON, A OFF
44)	Ku band transmitter HDR forward 1, both OFF
45)	Ku band transmitter HDR forward 1, select paramp A
46)	Ku band transmitter HDR forward 1, select paramp B
47)	UHF transmitter driver, A ON, B OFF
48)	UHF transmitter driver, B ON, A OFF
49)	UHF transmitter driver, both OFF
50)	UHF power amplifier 1 ON
51)	UHF power amplifier 1 OFF
52)	UHF power amplifier 2 ON
53)	UHF power amplifier 2 OFF
54)	UHF power amplifier 3 ON
55)	UHF power amplifier 3 OFF
56)	VHF horizontal receiver 1, A ON, B OFF
57)	VHF horizontal receiver 1, B ON, A OFF

Table 20 (continued)

58)	VHF horizontal receiver 2, A ON, B OFF
59)	VHF horizontal receiver 2, B ON, A OFF
60)	VHF horizontal receiver 3, A ON, B OFF
61)	VHF horizontal receiver 3, B ON, A OFF
62)	VHF horizontal receiver 4, A ON, B OFF
63)	VHF horizontal receiver 4, B ON, A OFF
64)	VHF horizontal receivers, all OFF
65)	VHF vertical receiver 1, A ON, B OFF
66)	VHF vertical receiver 1, B ON, A OFF
67)	VHF vertical receiver 2, A ON, B OFF
68)	VHF vertical receiver 2, B ON, A OFF
69)	VHF vertical receiver 3, A ON, B OFF
70)	VHF vertical receiver 3, B ON, A OFF
71)	VHF vertical receiver 4, A ON, B OFF
72)	VHF vertical receiver 4, B ON, A OFF
73)	VHF vertical receivers, all OFF
74)	VHF receivers select upconverter A
75)	VHF receivers select upconverter B
76)	VHF receivers select frequency source A
77)	VHF receivers select frequency source B
78)	Order wire receiver A ON, B OFF
79)	Order wire receiver B ON, A OFF
80)	Order wire receivers, both OFF
81)	S band transmitter driver 1, A ON, B OFF
82)	S band transmitter driver 1, B ON, A OFF
83)	S band transmitter driver 1, both OFF
84)	S band transmitter driver 2, A ON, B OFF
85)	S band transmitter driver 2, B ON, A OFF
86)	S band transmitter driver 2, both OFF
87)	S band transmitter high level select
88)	S band transmitter low level select
89)	S band power amplifier 1, 2, and 3
90)	S band power amplifier 1, 2, and 4
91)	S band power amplifier 1, 3, and 4
92)	S band power amplifier 2, 3, and 4
93)	S band receiver 1, A ON, B OFF

Table 20 (continued)

94)	S band receiver 1, B ON, A OFF
95)	S band receiver 1, both OFF
96)	S band receiver 2, A ON, B OFF
97)	S band receiver 2, B ON, A OFF
98)	S band receiver 2, both OFF
99)	S band MDR receiver 1 step attenuator IN
100)	S band MDR receiver 1 step attenuator OUT
101)	S band MDR receiver 2 step attenuator IN
102)	S band MDR receiver 2 step attenuator OUT
103)	HDR/MDR/LDR antenna to A
104)	HDR/MDR/LDR antenna to B
105)	HDR/MDR/LDR antenna to C
106)	HDR S/Ku band antenna 1 to A
107)	HDR S/Ku band antenna 1 to B
108)	HDR S/Ku band antenna 1 to C
109)	HDR S/Ku band antenna 2 to A
110)	HDR S/Ku band antenna 2 to B
111)	HDR S/Ku band antenna 2 to C

Deployment Mechanisms	
Despun	
1)	Release support arm Ku band antenna
2)	Release S/Ku band antenna 1 arm
3)	Release S/Ku band antenna 2 arm
4)	Release UHF antenna arm
5)	Release AGIPA mast top lock
6)	Release AGIPA mast bottom lock
7)	Release YAGI element 1 from support arm
8)	Release YAGI element 2 from support arm
9)	Release YAGI element 3 from support arm
10)	Release stowed YAGI element 1
11)	Release stowed YAGI element 2
12)	Release stowed YAGI element 3
13)	Release stowed YAGI element 4
14)	Deploy dipole assembly YAGI element 1
15)	Deploy dipole assembly YAGI element 2

Table 20 (continued)

16)	Deploy dipole assembly YAGI element 3
17)	Deploy dipole assembly YAGI element 4
18)	Release S/Ku band antenna 1 from support arm
19)	Release S/Ku band antenna 2 from support arm
20)	Release UHF antenna from support arm
21)	Sever cable on S/ Ku band antenna 1
22)	Sever cable on S/Ku band antenna 2
23)	Sever cable on UHF antenna
24)	Unfurl by mechanical drive S/Ku band antenna 1
25)	Unfurl by mechanical drive S/Ku band antenna 2
26)	Unfurl by mechanical drive UHF antenna
	Antenna Operations
Despun	
1)	Step S/Ku band antenna 1 azimuth east
2)	Step S/Ku band antenna 2 azimuth east
3)	Step Ku band antenna azimuth east
4)	Step S/Ku band antenna 1 azimuth west
5)	Step S/Ku band antenna 2 azimuth west
6)	Step Ku band antenna azimuth west
7)	Step S/Ku band antenna 1 elevation south
8)	Step S/Ku band antenna 1 elevation south
9)	Step Ku band antenna elevation south
10)	Step S/Ku band antenna 1 elevation north
11)	Step S/Ku band antenna 2 elevation north
12)	Step Ku band antenna elevation north
	Telemetry, Tracking, and Command
Despun	
1)	Telemetry encoder 1 PCM mode
2)	Telemetry encoder 2 PCM mode
3)	Telemetry encoder 1 ON
4)	Telemetry encoder 1 OFF
5)	Telemetry encoder 2 ON
6)	Telemetry encoder 1 OFF
7)	Telemetry encoder 1 FM mode

Table 20 (continued)

8) Telemetry encoder 2 FM mode 9) Telemetry transmitter, A ON, B OFF 10) Telemetry transmitter, B ON, A OFF 11) Telemetry transmitters, both OFF
Power Subsystem
Despun 1) Voltage limiter 1 ON 2) Voltage limiter 2 ON 3) Voltage limiters OFF Spinning 1) Telemetry encoder A ON 2) Telemetry encoder B ON 3) Telemetry encoders both OFF
Power Subsystem
Spinning 1) Battery 1 charge ON 2) Battery 2 charge ON 3) Battery charge OFF 4) Trickle charge ON 5) Trickle charge battery 1 OFF 6) Trickle charge battery 2 OFF 7) Reconditioning discharge battery 1 ON 8) Reconditioning discharge battery 2 ON 9) Reconditioning discharge batteries OFF 10) Set charge temperature limit 1 11) Set charge temperature limit 2 12) Thermal charge limit set override 13) Voltage limiters OFF 14) Voltage limiter 1 ON 15) Voltage limiter 2 ON 16) Voltage limiter 3 ON 17) Voltage limiter 4 ON

Table 20 (continued)

Controls
Spinning 1) Earth sensors ON 2) Earth sensor 1 OFF 3) Earth sensor 2 OFF 4) Earth sensor 3 OFF 5) Select earth sensor 1 6) Select earth sensor 2 7) Select earth sensor 3 8) Motor drivers ON 9) Motor driver 1 OFF 10) Motor driver 2 OFF 11) Rate command latch 1 12) Rate command latch 2 13) Despin control electronics 1 and 2 OFF 14) Despin control electronics 1 ON 15) Despin control electronics 2 ON 16) Interlock enable 17) Interlock disable 18) Command limiter ON 19) Command limiter OFF 20) Motor driver 1 low gain 21) Motor driver 1 high gain 22) Motor driver 2 low gain 23) Motor driver 2 high gain 24) Active nutation control 1 ON 25) Active nutation control 2 ON 26) Active nutation control OFF
Reaction Control Subsystem and Apogee Motor
Spinning 1) Axial jet 1 2) Axial jet 2 3) Axial jets 1 and 2 4) Radial jet 1

Table 20 (continued)

5)	Radial jet 2
6)	Latching valve 1 OPEN
7)	Latching valve 1 CLOSE
8)	Latching valve 2 OPEN
9)	Latching valve 2 CLOSE
10)	Latching valve 3 OPEN
11)	Latching valve 3 CLOSE
12)	Apogee motor squib 1 (decoder 1)
13)	Apogee motor squib 2 (decoder 2)
14)	Apogee motor heaters ON
15)	Apogee motor heater 1 OFF
16)	Apogee motor heater 2 OFF
17)	Apogee motor heater 3 OFF
18)	Apogee motor heater 4 OFF
19)	Radial valve heater OFF
20)	Radial valve heater ON
21)	Axial valve heater ON
22)	Axial valve heater OFF

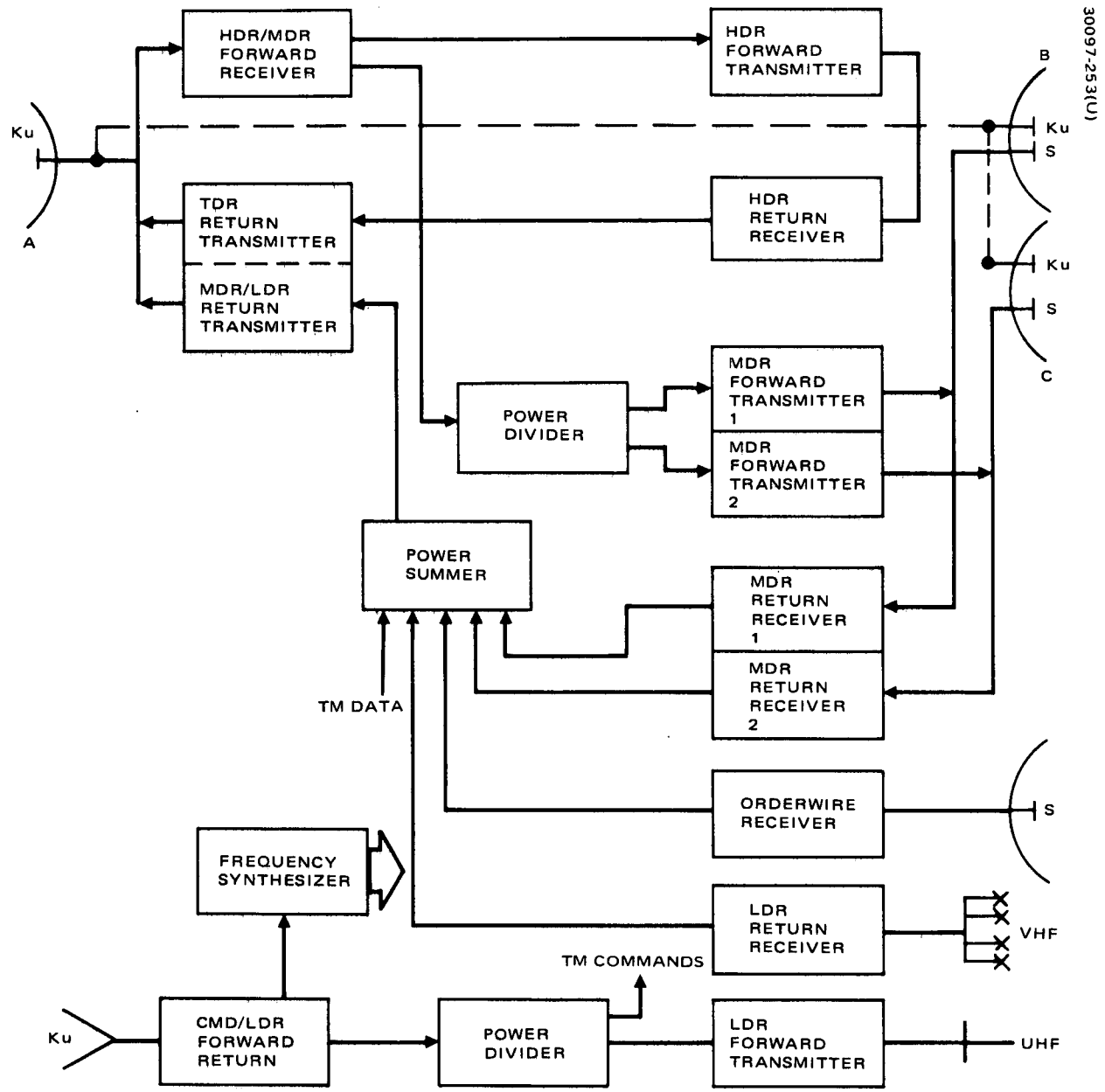

Figure 52. TDRS Telecommunications Repeater

4.3.1 Telecommunication Subsystem Description

The TDRS telecommunication service system is designed to provide low data rate (LDR), medium data rate (MDR), and high data rate (HDR) services. The low data rate return link includes a VHF AGIPA concept for RFI rejection. The MDR service is provided at S band with a capability for 2 kbps command data rate plus two voice signals to the Space Shuttle. Two simultaneous two-way channels are provided with a return link data rate capability of 1 Mbps. The S band services include an order wire receiver and a transponder for trilateration and backup TT&C operations. One HDR channel is provided at Ku band where adequate bandwidth is available for the 100 Mbps return link data rate. The space-to-space MDR and HDR links use two interchangeable dual-feed S/Ku band antennas. The TDRS telecommunication service subsystem characteristics are summarized in Table 21. Lack of space-qualified devices in some of the technology areas necessary for this configuration results in some developmental risk. These critical areas are discussed later. Most of the performance requirements can be met with state-of-the-art hardware devices.

The simplified block diagram of Figure 52 illustrates the TDRS repeater subsystem design configuration providing the required telecommunication service. The repeater is a frequency translation type providing coherent frequency translations at all bands and includes an S band order wire capability. Every active element in the repeater subsystem is redundant.

A multichannel Ku band receiver receives ground-transmitted command, LDR and beacon signals through an earth-coverage horn antenna. TDRS commands are sent to the TT&C subsystem, the beacon signal is processed and used to phase lock the frequency synthesizer to provide coherency. The LDR command data are distributed via a power divider to the UHF transmitter for frequency upconversion and radiation to user spacecraft. A multichannel Ku band receiver and high gain antenna are used for the two MDR channels and the HDR channel. The MDR signals are transmitted to the user spacecraft over two S band links. Upon return, the S band MDR data from user spacecraft are double conversion frequency translated to a Ku band link for transmission to the ground. A linear Ku band transmitter is used for MDR, LDR, and telemetry information. The HDR channel is transmitted to the user at Ku band and received at Ku band.

The VHF antenna is a four-element array utilizing the AGIPA concept to aid in suppressing RFI. The HDR and MDR user links utilize dual-feed parabolic reflectors, one for each MDR channel and a RF switch to select the antenna to be used for the HDR channel. Thus, the two antennas are shared between the MDR and HDR services.

Initial acquisition and TT&C backup functions are provided by an S band transponder.

TABLE 21. TELECOMMUNICATION SERVICE SUBSYSTEM CHARACTERISTICS

LDR Forward Link (to user)	
Forward link EIRP	30 dBW over 19.7 degrees FOV
Number of channels	One
Frequency	401.0 MHz
Coding	PN
Antenna	Backfire UHF
RF bandwidth	1 MHz
LDR Return Link (from user)	
Return link G/T	-14.5 dB/K
Number of simultaneous signals	Twenty
Frequency	136.5 MHz
Antenna	4-element AGIPA
RF bandwidth	1 MHz
MDR Forward Link (to user)	
Forward link EIRP	47 dBW, 41 dBW
Number of channels	Two
Frequency	Variable over 2038 to 2118 MHz
Instantaneous field of view	2.8 degrees
Antenna	Dual-feed paraboloid
RF bandwidth	30 MHz/channel
MDR Return Link (from user)	
Return link G/T	10.2 dB/K
Number of channels	Two
Frequency	Variable over 2220 to 2300 MHz
Antenna	Dual-feed paraboloid
RF bandwidth	10 MHz
Order wire G/T	-15.4 dB/K
HDR Forward Link (to user)	
Forward Link EIRP	40 dBw
Number of channels	One
Center frequency	14.81 GHz
Antenna	Dual-feed paraboloid
RF bandwidth	100 MHz
HDR Return Link (from user)	
Return link G/T	20.2 dB/K
Number of channels	One
Frequency	13.85 GHz
Antenna	Dual-feed paraboloid
RF bandwidth	200/100/50/10 MHz

Table 21 (continued)

MDR/LDR Return Link (to ground)	
Return link EIRP	44.8 dBW
Number of channels	Two MDR (10 MHz each) Eight LDR (1 MHz each) One TDRS telemetry One order wire
Frequency band	14.60 to 14.695 GHz
Antenna	Paraboloid
HDR Return (to ground)	
Return link EIRP	51.6 dBW
Number of channels	One
Frequency	14.96 to 15.16 GHz
Antenna	Paraboloid
MDR/HDR Forward Link (from ground)	
Forward link G/T	9.4 dB/K
Number of channels	One HDR (100 MHz) Two MDR (30 MHz)
Frequency	13.460 to 13.690 GHz
Antenna	Paraboloid – HDR MDR
RF bandwidth	230 MHz
TDRS Command Beacon, and LDR Forward Link (from ground)	
Forward link G/T	-13.2 dB/K
Number of channels	One LDR One beacon One command
Frequency	13.4 to 13.42 GHz
Antenna	Horn
RF bandwidth	20 MHz

The communication repeater receiver characteristics listed in Table 22 are those of typical current state-of-the-art hardware. The Ku band receivers having noise temperatures of 1170 and 2600 K are achieved using tunnel diode amplifiers and low noise mixers. Transistor low noise preamplifiers are used at VHF to achieve 420 K noise temperatures, and an uncooled parametric amplifier is used at S band for a 100 K noise temperature MDR receiver.

The transmitter characteristics are listed in Table 23. The required EIRP for each transmitter is shown and the major gain and loss contributors leading to the required dc power are listed also to illustrate the derivation of the total power required of each transmitter. The RF losses are summarized in Table 24 for both transmit and receive.

TABLE 22. RECEIVER CHARACTERISTICS

Receiver	Frequency Band	Bandwidth, MHz	Preamplifier Input Noise Temperature, K	Preamplifier Type
MDR/HDR	Ku	240	2600	None
HDR return	Ku	200/100/50/10	1170	Tunnel diode
Command/LDR forward	Ku	20	1170	Tunnel diode
MDR return	S	10	100	Parametric
Order wire	S	1	420	Transistor
Transponder	S	8	420	Transistor
LDR return	VHF	2	420	Transistor

TABLE 23. TRANSMITTER CHARACTERISTICS

Transmitter	Frequency Band	EIRP dBW	Antenna Gain, dB	RF Losses, dB	Power Amplifier			Total* Dc Power watts 24.5 V
					Output, watts	Efficiency, percent	Dc Power watts 24.5 V	
HDR return	Ku	51.6	45.3	2.7	8.5	33	25.8	33.9
HDR forward	Ku	40	52.8	2.7	0.1	2	5.0	6.3
LDR/MDR return	Ku	45.9	45.1	2.7	2.24	30	7.45	10.1
LDR forward	UHF	30	13.4	1.0	57.5	55	104	110
MDR forward	S	47/41	35.5	2.8/3.0	27/6.8	28/30	96.5/22.5	100.5/26.5
Transponder	S	20	13.5	1.5	6.3	30	22	24/2

*Includes upconverter, driver, EPC.

The repeater has several bands of operating frequencies and requires a variety of transmitters. The transmitters are the repeater's largest power consumer; therefore, design emphasis is placed on transmitter efficiency. All but the Ku band TWTs are solid-state devices. The Ku band forward transmitter uses an Impatt diode amplifier of ultra small configuration. The transistor power amplifiers used in the S band and UHF transmitters are operated at maximum efficiency and are paralleled to meet the total power output requirement. The TWT amplifiers are redundant and the transistor amplifiers are selectable as two of three to provide excellent reliability.

TABLE 24. RF LOSS SUMMARY

	Receive, dB	Transmit, dB	Remarks
K Band			
Ku waveguide	1.0	1.0	6 m at 0.165 dB/m
Rotary joints	0.3	0.3	0.1 dB each
Tracking modulator	0.6	0.5	Signal including transmit/receive diplexer
Antenna switching	0.3	0.3	Minimum loss
Redundancy switch	0.1	0.1	
Transmit diplexer	—	0.5	Ku return only transmit
	2.3	2.7	
S Band			
S band coax		1.3	9.75 m at 0.13 dB/m
S band flex joints		0.4	Two each at 0.2 dB
Transmit/receive diplexer	0.8	0.8	
Mode switch	—	0.3	High/low power
Isolator	—	0.2	High power only
	0.8	3.0	
VHF/UHF			
UHF low pass filter	—	0.4	
Cable loss	0.6	0.4	0.065 dB/m
Connectors	—	0.2	
Switch	0.2	—	
	0.8	1.0	

The repeater subsystem component mass is summarized in Table 25. The quantities represent the redundancy and spare components required to provide reliable telecommunication service. The dc power is also indicated for each active subsystem module.

4. 3. 1. 1 Telecommunication Repeater Design Description

The TDRS communication repeater subsystem is designed to provide LDR, MDR, and HDR links between the user spacecraft and a central ground station. The LDR link is accomplished at VHF frequencies using the AGIPA antenna system for RFI rejection. Two independent MDR links are provided at S band. Each link will allow voice signals plus data to be transmitted to a user spacecraft and up to 1 Mbps telemetry data to be returned. HDR services

TABLE 25. MASS AND POWER ESTIMATES FOR REPEATER COMPONENTS

	Spacecraft Quantity	Mass, kilograms	Dc Power, watts
Transmitter; LDR/MDR/HDR Return		11.4	44.0
Antenna switches	2	0.4	–
Multiplexer (two transmit and one receive)	1	0.4	–
TWT and EPC	4	8.2	42.4
Driver upconverter	4	2.2	1.6
Summer	1	0.2	–
Transmitter; HDR Forward		4.0	6.3
Antenna switches	4	0.8	–
Diplexer (transmit/receive)	1	0.2	–
Solid-state power amplifier	2	1.9	5.5
Driver upconverter	2	1.1	0.8
Receiver; Command/LDR Forward		3.4	2.1
TDA and bandpass filter	2	0.7	0.4
Mixer/amplifier and phase lock loop	2	2.5	1.7
Hybrid and divider	1	0.1	–
EPC	1	0.1	–
Receiver; HDR Return		5.9	5.0
Tracking modulator	2	2.2	1.7
TDA and switch	2	1.5	0.4
Mixer/amplifier/filter (redundant)	2	1.2	0.6
Tracking demodulator	2	0.9	1.8
EPC	1	0.1	0.5
Receiver; MDR/HDR Forward		5.1	5.8
Tracking modulator	1	1.1	1.7
BPF	1	0.1	–
Mixer/amplifier/filters	2	2.9	2.0
Tracking demodulator	2	0.9	1.8
EPC	1	0.1	0.3
Transmitter; MDR Forward		11.6	100.5/26.5
Driver	4	5.4	4.0
Power amplifier (four of six)	2	2.6	96.5/22.5
Diplexer and cable	2	3.4	–
EPC	2	0.2	–
Receiver; MDR Return		2.9	6.1
Preamplifier	4	1.6	5.0
Mixer/filter/amplifier/attenuator	4	1.2	1.0
EPC	2	0.1	0.1

Table 25 (concluded)

	Spacecraft Quantity	Mass, kilograms	Dc Power, watts
Receiver; Order Wire		1.9	1.7
BPF	1	1.1	–
Preamplifier	2	0.2	0.5
Mixer/filter amplifier/mixer amplifier	2	0.5	1.0
EPC	1	0.1	0.2
Transponder, S Band		4.0	24.0/2.0
Receiver	2	0.6	1.0
Transmitter	2	0.9	22.0
Frequency reference	2	0.3	1.0
Filter	1	2.2	–
Transmitter; LDR Forward		4.1	110.0
Driver	2	0.6	6.0
Power amplifier (three of four)	4	1.0	104.0
Summer and switch	1	0.5	–
LPF	1	1.0	–
Cable	–	0.9	–
EPC	1	0.1	–
Receiver; VHF LDR Return		5.4	7.9
Preamplifier/bandpass filter/amplifier	16	1.4	0.8
Local oscillator frequency source and selector	2	0.2	0.3
Preamplifier/mixer/amplifier	16	0.9	5.5
Bandpass filter/limiter/summer	1	0.7	–
Mixer/amplifier/filter	2	0.1	0.8
EPC	1	0.1	0.5
Cable and integrated package		2.0	
Frequency Synthesizer		8.5	7.8
Master oscillators and multiplier	2	8.4	7.3
EPC	1	0.1	0.5

are provided at Ku band with capability up to 300 kbps forward (to the user) and a 100 Mbps capability on the return link (from the user).

Repeater features include:

- Coherent frequency translations
- All active elements are redundant
- TWT high power amplifiers at Ku band

- Selectable Ku band transmitter/receiver and antenna combinations
- Solid-state S band, low power Ku band, and VHF power amplifiers
- Design includes IC and MIC components
- VHF AGIPA antenna concept in the LDR return link
- Ku band tracking antennas
- Low noise receivers with minimum complexity
- High efficiency transmitters

The following repeater design description is divided into groups of units according to their operating frequency. The repeater frequency plan shown in Figure 53 summarizes the operational bands.

The detailed block diagrams, Figures 54 and 55, show the inter-module connections necessary to accomplish the frequency cross-strapping and channel multiplexing within the repeater. Figure 54 includes all Ku band and UHF/VHF subsystem functions, and Figure 55 illustrates the S band subsystem. These units are described in detail in the following paragraphs.

Ku Band Repeater Units

The TDRS repeater subsystem units operating at Ku band consist of two transmitters and three receivers. Each of the receivers is designed to provide antenna tracking error signals derived from the antenna tracking modulators. The Ku band antennas used for the TDRS-user link are dual-feed S/Ku band parabolic reflectors interchangeable between Ku band transmitters and receivers.

The Ku band antenna tracking modulator is shown in Figure 56. The narrow beam Ku band antennas require precision tracking to maintain the HDR link performance requirements. This is provided by a ferrite switch module in the monopulse difference channel outputs from the antenna. The sum channel is diplexed with the transmitter and receiver, and the receiver input is therefore a composite signal containing data and tracking modulation. The tracking error signals are processed by a tracking demodulator in each Ku band receiver and applied to the antenna tracking control circuits. Dual switch drivers provide redundancy for the only active circuits in the modulator/diplexer.

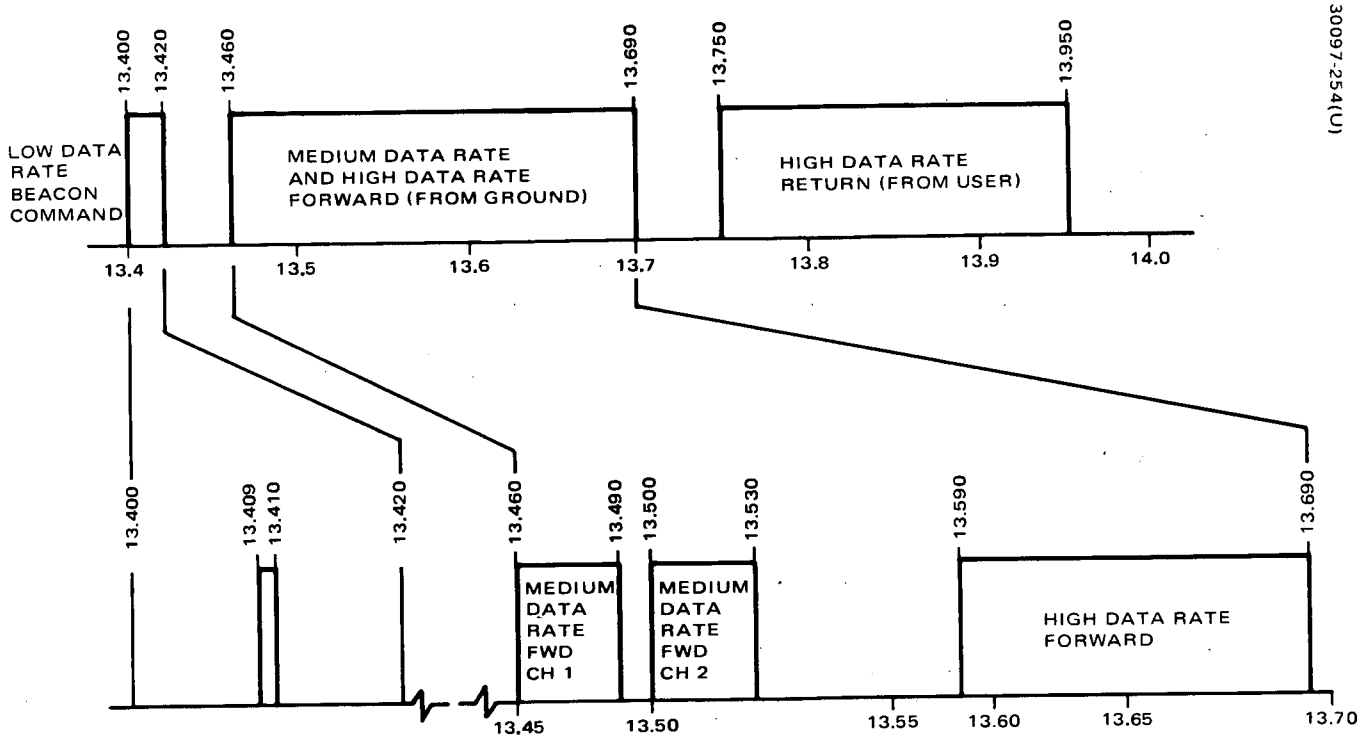

a) Ku BAND RECEIVE

Figure 53. TDRS Frequency Plan

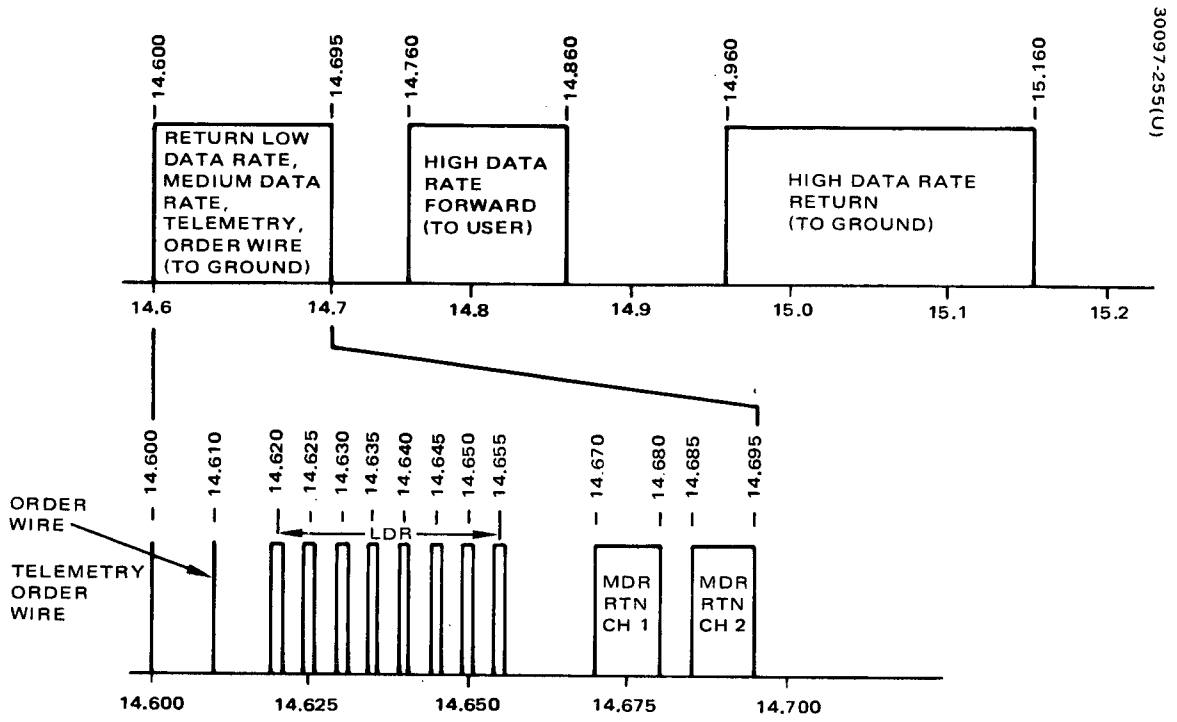

b) Ku BAND TRANSMIT

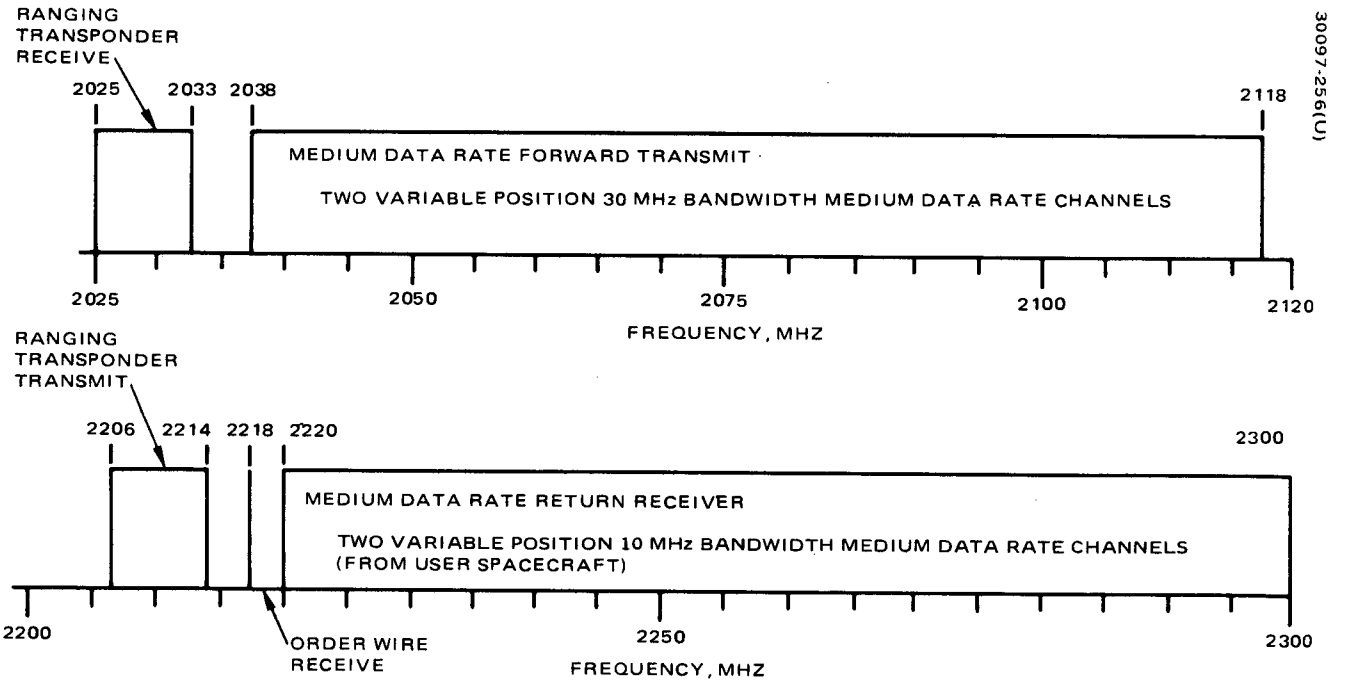

c) S BAND TRANSMIT AND RECEIVE

Figure 53 (continued). TDRS Frequency Plan

Figure 54. Delta Configuration - Communcations Repeater Ku Band and UHF/VHF Block Diagram

FOLDOUT FRAME 1

FOLDOUT FRAME 2

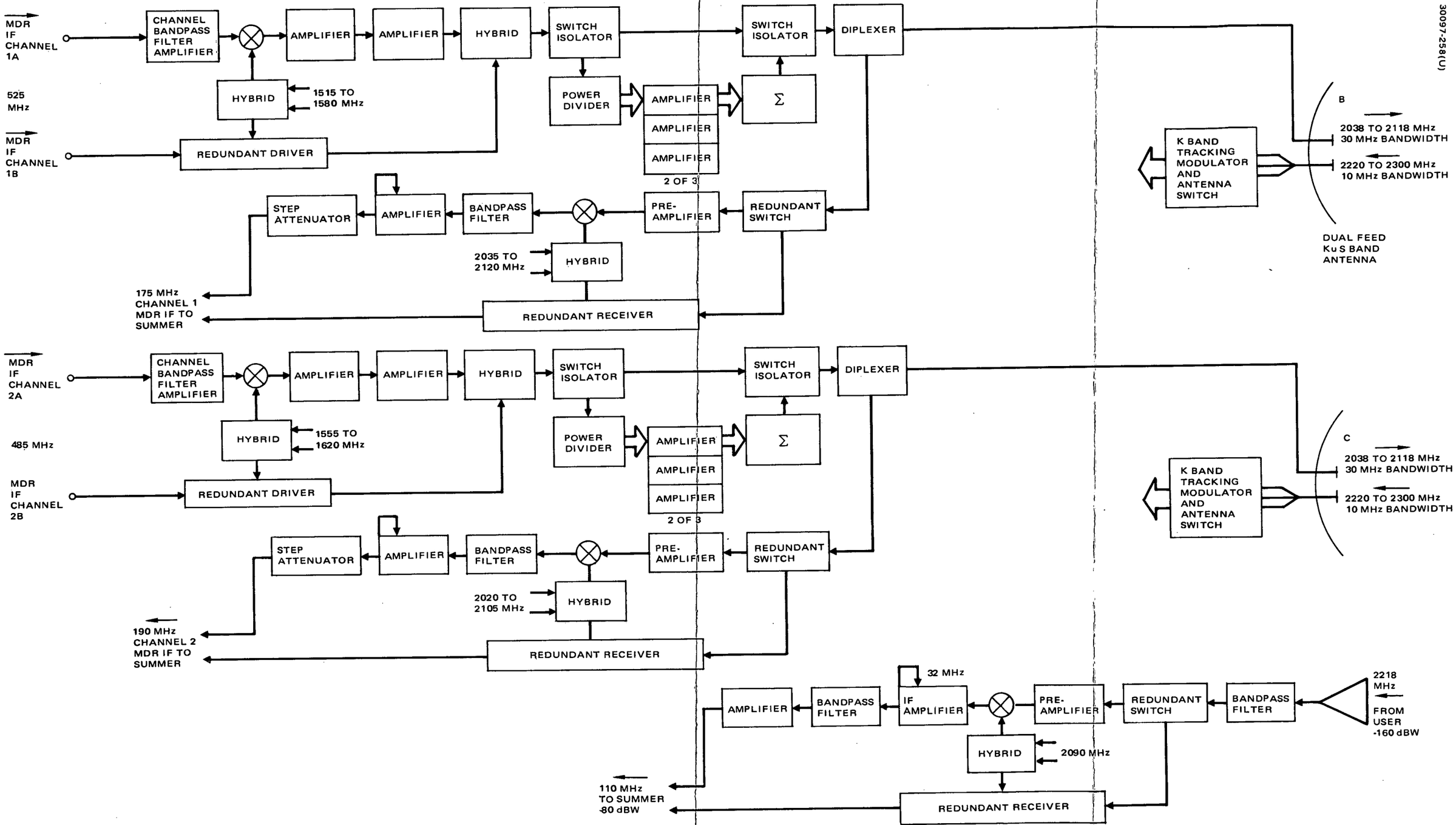

Figure 55. Delta Configuration - Communications Repeater S Band Block Diagram

FOLDOUT FRAME 1

FOLDOUT FRAME 2

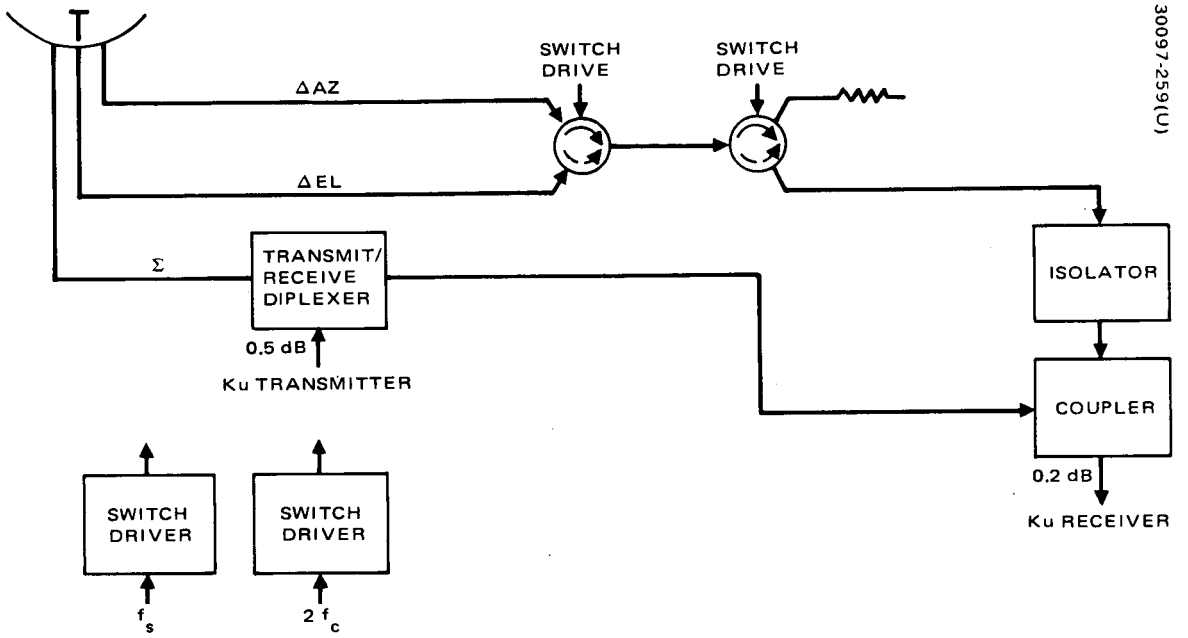

Figure 56. Ku Band Antenna Tracking Modulator/Diplexer

The antenna switching network is shown in Figure 57. The Ku band antennas may be used interchangeably with the Ku band transmitters and receivers. Two antennas have dual feeds for the two S band transmitters and receivers. A Ku band forward link and return link may be completed using any two of the three Ku band antennas. The switches are of the ferrite latching switch type, and this configuration or matrix represents the maximum switching capability within reasonable RF loss considerations. The switches will provide added assurance of a completed HDR link in the event of antenna deployment failure. Antennas A, B, or C may be connected to the ground link transmitter and receiver, and B or C to the HDR TDRS/user transmitter and receiver. The S band MDR transmitters and receivers are assigned specific antennas, B or C.

The upconverter and solid-state power amplifier of the HDR forward link transmitters are shown in the block diagram of Figure 58 for a single transmitter. The HDR channel signals leave the TDRS on a 14.81 GHz carrier. A 30 dB gain solid-state impact diode amplifier provides the -10 dBW required output. A 2 percent efficiency is predicted using complementary diodes. Three stages are required to achieve the necessary gain. Impatt diode devices have been effectively used for amplification to similar power levels at millimeter wavelengths.

The input signal level to the HDR return link receiver from user spacecraft is approximately -104 dBW on a 13.850 GHz carrier. Figure 59 is a block diagram of a return link HDR receiver two-stage preamplifier with a 1170 K noise temperature is employed consisting of a tunnel diode amplifier providing an overall gain of 24 dB. A receiver bandwidth of 200, 100, 50, or 10 MHz may be selected by ground command, thus enabling optimization of the link for any user bandwidth requirements.

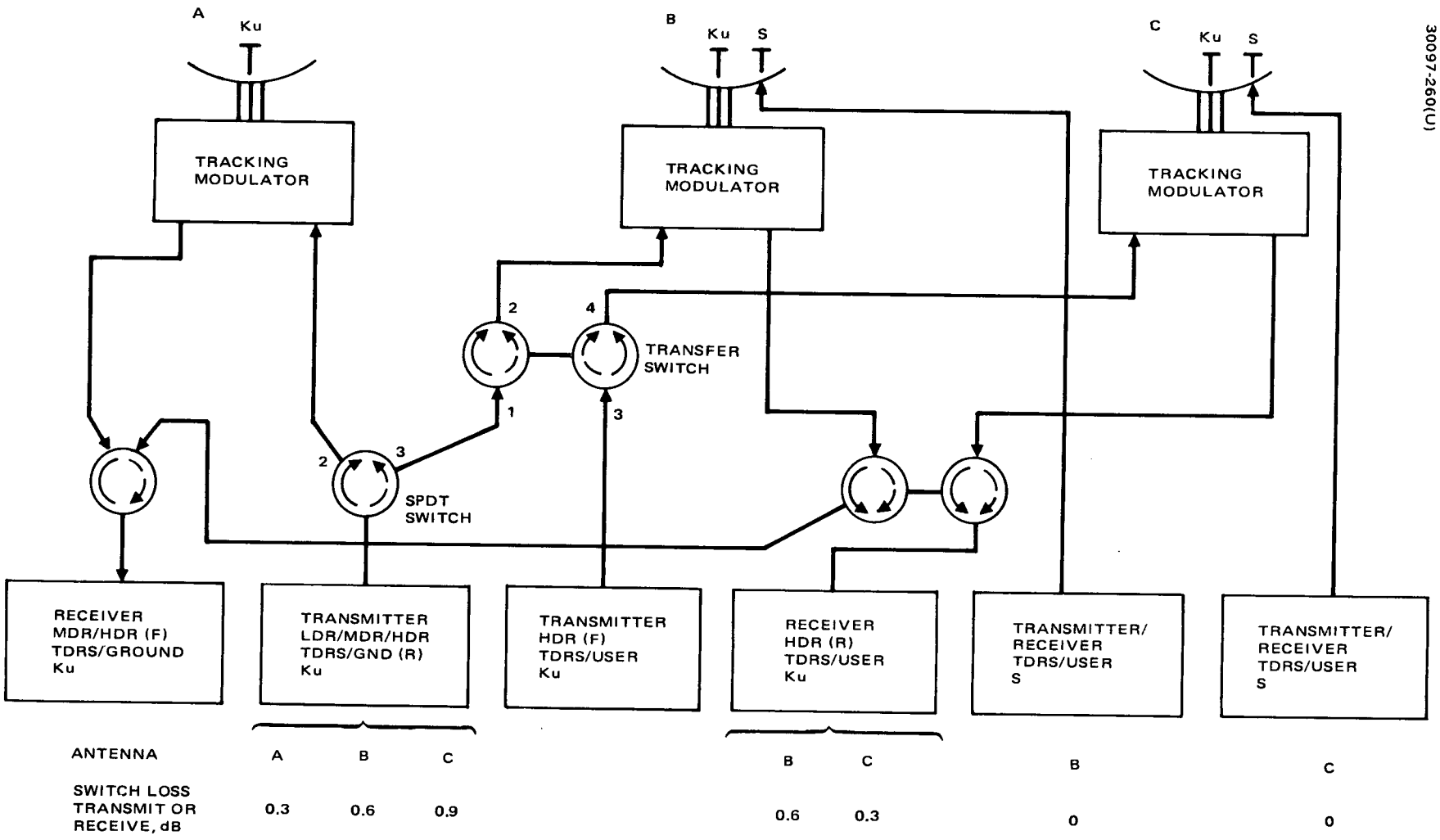

Figure 57. Antenna Switching Network

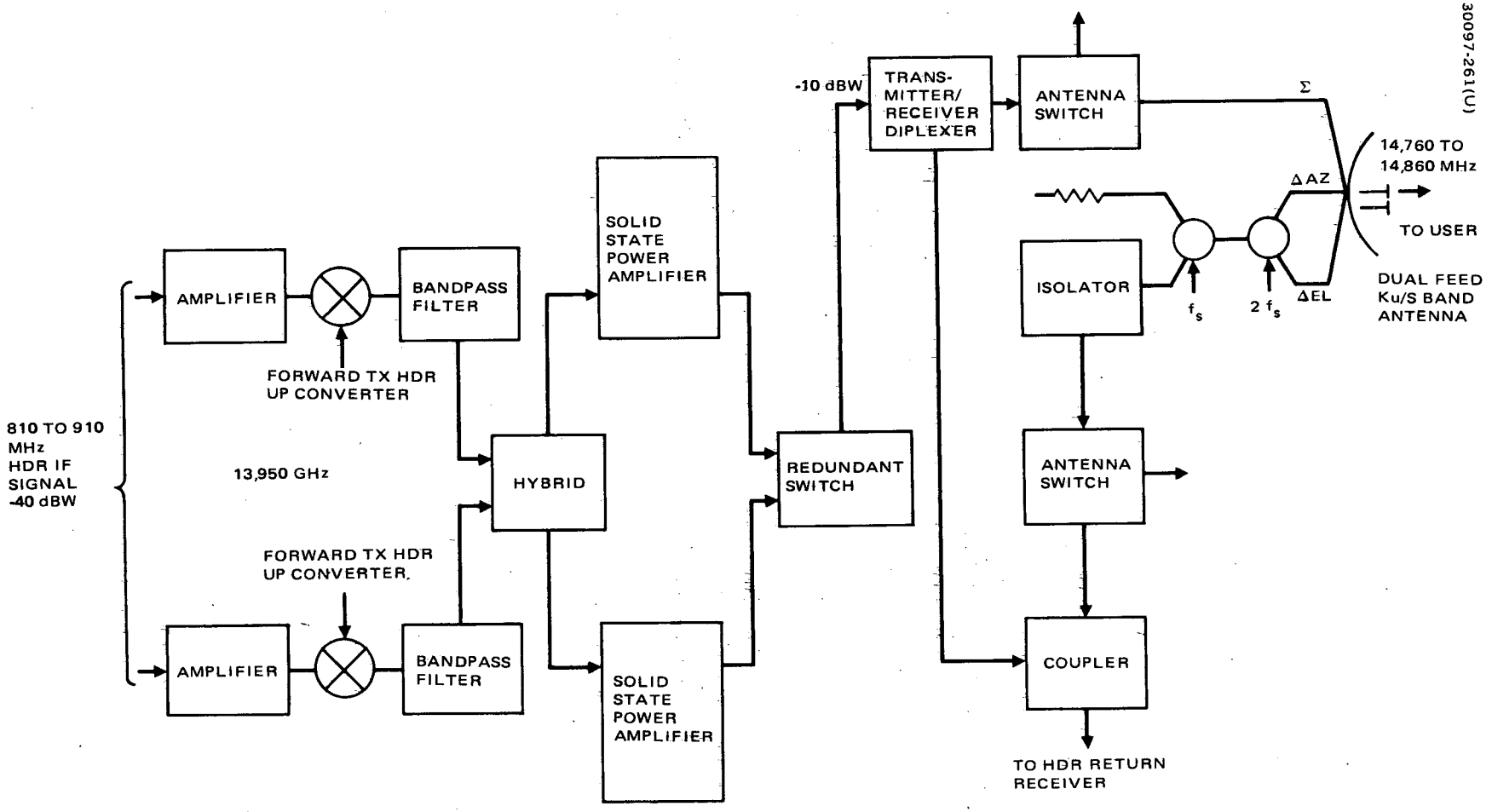

Figure 58. HDR Forward Link Transmitter and Upconverter

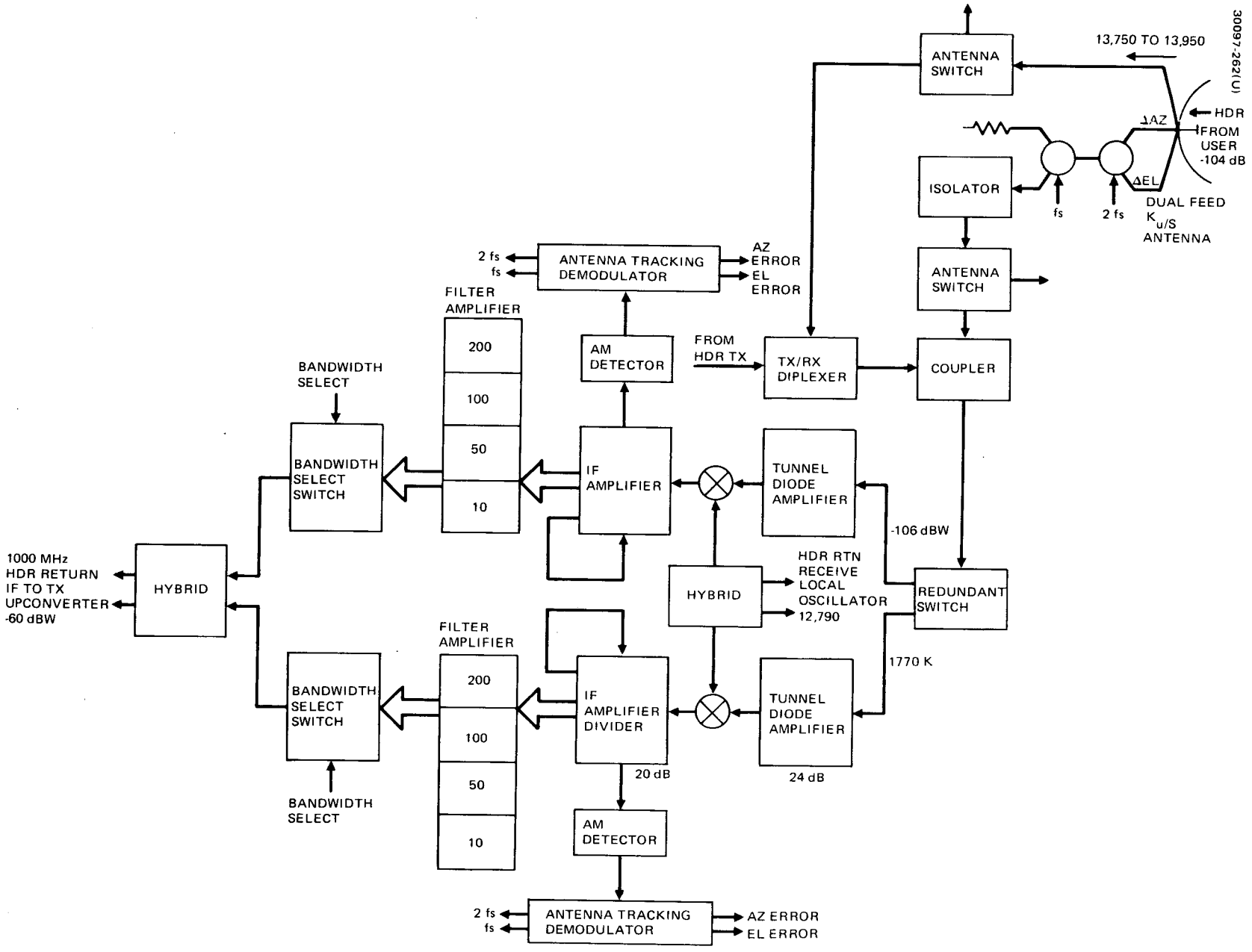

Figure 59. HDR Return Link Receiver

The data transmitted to the TDR spacecraft from the ground are received by two Ku band receivers. One receiver handles the HDR and MDR channels and the other handles the LDR channel, as well as TDRS telemetry command signals and the reference frequency beacon signal. The uplink MDR and HDR signals are received by a narrow beam Ku band parabolic antenna. Difference channel outputs are combined with the sum channel output after switching and phase shifting accomplished in the tracking modulator. Figure 60 is a block diagram of the MDR/HDR forward receiver.

This receiver processes the composite data and tracking signals through redundant mixer and amplifier filter circuits. The tracking modulation is processed in the antenna tracking demodulator to provide quadrature coordinate error signals. The demodulator is also the source of the two modulator switch driver signals. The receiver has no preamplifier and the noise temperature at the input bandpass filter is 2600 K. The moderate IF allows the use of transistor amplifiers for processing the tracking signal and increasing the drive level to the upconverter. The MDR and HDR signals are frequency-multiplexed and are selected through separate receiver filter amplifier circuits for each service. The MDR IF signals are distributed to the MDR forward S band transmitters and the HDR IF signals are connected to the HDR forward Ku band transmitter.

The uplink TDRS commands, LDR, and beacon signals are received on a low gain earth coverage horn antenna having 18.5 dB gain. The carriers are within the 13.400 to 13.420 GHz band and arrive with a signal level of approximately -115 dBW. Figure 61 is a diagram of the receiver. A tunnel diode preamplifier is used to establish a low noise temperature at the receiver input of 1170 K. Double conversion minimizes spurious responses. After a conversion to IF, the signals are separated and converted to a second IF. The beacon signal is used to phase lock a VCXO to the uplink carrier and establish a stable coherent reference signal as a source for all TDRS local oscillator and upconverter signals. The command/LDR forward link receiver is redundant and uses dual-series dissipative regulators. Hybrid circuit designs are used to minimize mass. The receiver data outpus (MDR, LDR, and TDRS commands) are distributed to their respective transmitters or processors via a six-way power divider.

The K band downlink MDR, LDR and telemetry signals are transmitted in the 14.60 to 14.69 GHz band, and the HDR channel uses the 14.96 to 15.16 GHz band. Figure 62 is a block diagram of the downlink transmitters.

The HDR and MDR/LDR return link transmitters use a 50 dB gain TWT. The HDR transmitter output is combined with the MDR/LDR transmitter output via a transmit diplexer to radiate from a common Ku band antenna. The MDR/LDR transmitter is operated in a linear region, at 5 dB backoff, since there are several data channels simultaneously amplified. The TWT saturated output power is 3.5 dBW for the MDR/LDR transmitter and for the HDR transmitter is 9.3 dBW.

S Band Repeater Units

The telecommunication repeater S band subsystem units provide the required MDR transmit and receive and order wire receive functions. There are two MDR transmitters and receivers allowing service to separate user spacecraft. A single transmitter/receiver design is illustrated by the block diagram of Figure 63.

The forward MDR IF signal is frequency-translated to S band for solid-state amplification to one of the two dual-feed S/Ku band antennas for transmission to a user spacecraft. The transmit frequency is selectable in the 2025 to 2120 MHz band by a commandable upconversion local oscillator frequency 1485 to 1580 MHz. The driver output is switched directly to the antenna in the case of low power mode operation or is switched to pass through a bank of transistor amplifiers which are summed to provide a high power output. The receiver employs a low noise parametric amplifier for the first stage, providing a noise temperature at the receiver input of 82 K. This is followed by a low noise transistor amplifier stage to provide a preamplifier gain of approximately 30 dB. The overall receiver noise temperature is estimated to be 100 K. The receiver is also frequency-selectable by command within the 2220 to 2300 MHz band. A step attenuator at the IF output controls the MDR return signal level driving the MDR return transmitter.

The order wire function is provided by receiving order wire signals at 2218 MHz and combining the data with the MDR and LDR IF signals for transmission on the Ku band downlink. Figure 64 is a block diagram of the order wire receiver. The order wire receiver is similar to the MDR receiver; however, it has a fixed frequency and narrow bandwidth. The single conversion utilizes mixing frequencies available from the frequency synthesizer to provide the proper IF. The receiver design includes redundancy and applies microstrip transmission techniques in the RF circuits to minimize mass.

VHF and UHF Repeater Units

The TDRS LDR service provides command transmission to at least 20 user spacecraft and telemetry data from 20 users simultaneously. Figure 65 is the LDR forward link transmitter block diagram. This transmitter features a solid-state driver with redundancy and a final power amplifier using hybrid coupled transistor amplifiers. A selectable, by command, group of three power amplifier outputs are summed by a switched Wilkinson summer to provide the required power output at 401 MHz. A helical low pass filter at the output attenuates the harmonic and spurious signal outputs from the transmitter. The overall amplifier efficiency is 55 percent and includes regulator losses and 3 percent allowance for space environment and life degradation.

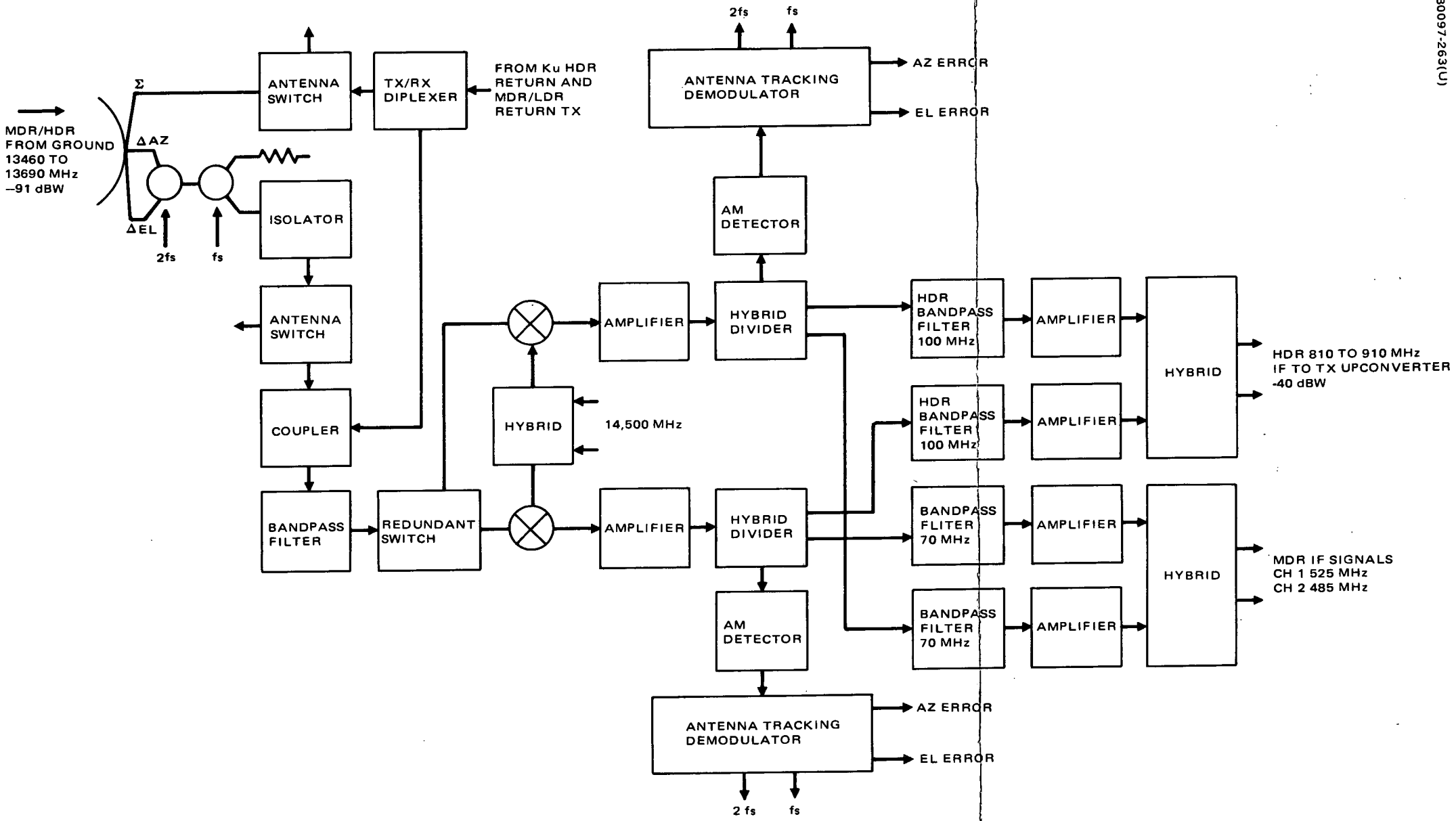

Figure 60. HDR Forward Link Receiver

30097-263(U)

FOLDOUT FRAME 1

FOLDOUT FRAME 2

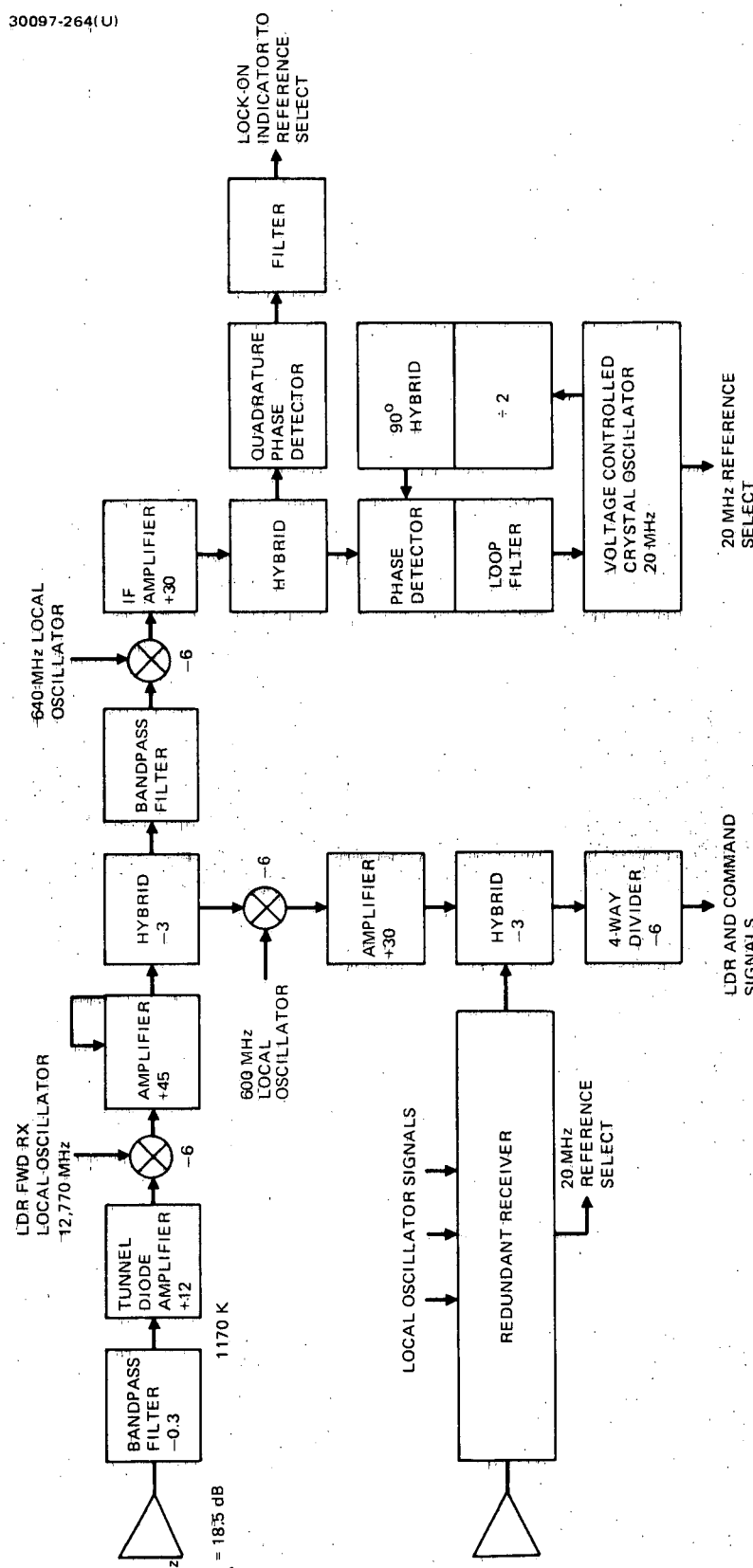

Figure 61. TDRS Command LDR and Beacon Receiver

The LDR return link uses a four-element AGIPA antenna to provide RFI rejection. The LDR receiver is designed to process the two outputs from each of the four AGIPA antenna elements independently through eight channels. The channels are frequency-translated to eight Ku band frequencies for transmission to the ground station in the MDR/LDR return link transmitter. High reliability is achieved by complete redundancy of all channels. This is illustrated in Figure 66, which also shows the transistor preamplifier and the acoustic surface wave RF bandpass filter (BPF). The IF channel filter bank is made up of monolithic crystal filters. The outputs are summed and upconverted to frequencies between 120 and 155 MHz. The eight channels are evenly spaced over this band with 5 MHz between center frequencies. Specific unequal frequency spacing may become necessary during detailed design to minimize intermodulation products. The LDR receiver contains an internal local oscillator frequency source to simplify the distribution of the many local oscillator signals required for the eight channel receiver. A 5 MHz harmonic generator, frequency multipliers, and amplifiers are combined to provide the ten local oscillator inputs between 85 and 120 MHz.

Frequency Synthesizer

The frequency synthesizer provides the necessary conversion frequencies for each of the receivers and transmitters in the TDRS communication subsystem. This requires a total of 14 frequencies to be derived from a stable crystal oscillator reference source. The primary reference source is a 20 MHz voltage controlled oscillator that is phase locked to an incoming pilot tone; the reference oscillator becomes a coherent frequency reference source. A secondary or standby reference source is also provided for use when the primary reference source is not phase locked to the incoming pilot tone. The secondary reference source is a quartz crystal master oscillator, temperature-controlled to maintain the required stability. The 14 output frequencies are generated by several solid-state multiplier chains. Three pairs of S band outputs are programmable in 1 MHz steps to provide repeater flexibility of user spacecraft interface frequencies.

All of the frequency synthesizer circuitry is straightforward in design. Extensive use of large-scale integration circuits will be made. Frequency divider integrated circuit breadboards developed for other space programs are directly applicable for this unit. Compact VCXO modules for the phase lock loop oscillators as required in the frequency synthesizer have been space-qualified. Wherever practical, monolithic crystal filters will be used to minimize circuit element mass, such as in the lower IF channel filters.

The dual regulator used for the frequency synthesizer, typical of those used throughout the repeater, is a series-dissipative regulator. This regulator design has exhibited excellent in-orbit performance and reliability on the ATS and Intelsat IV satellites. The regulators are designed with discrete component construction; however, the design is adaptable to hybrid microcircuit techniques. All TDRS regulators will have the same basic circuit topology with only small differences in command buffer logic.

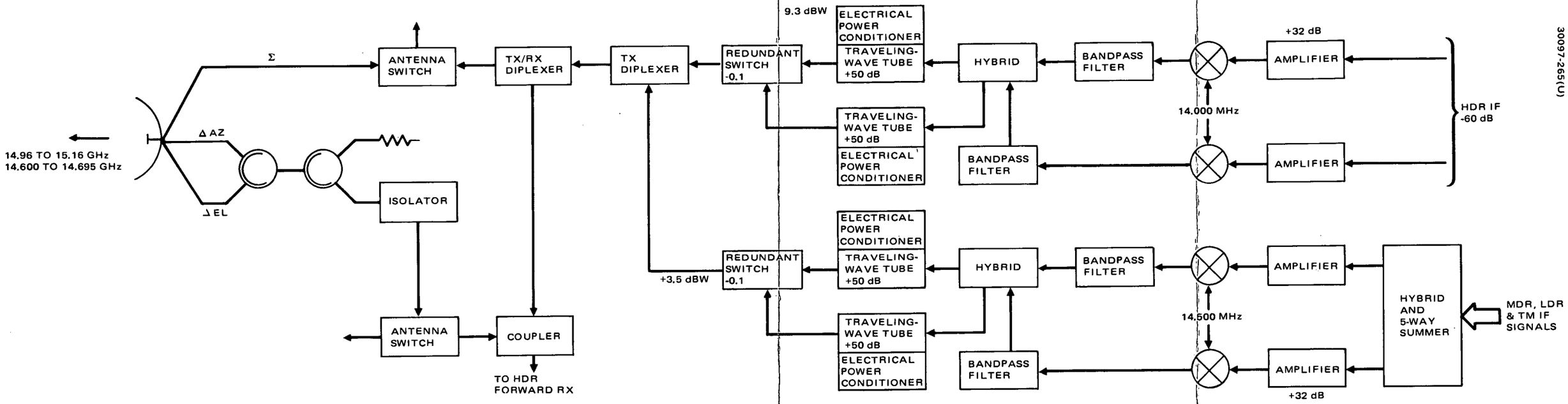

Figure 62. HDR and MDR/LDR Return Link Transmitter and Upconverters

30097-265(U)

FOLDOUT FRAME 1

FOLDOUT FRAME 2

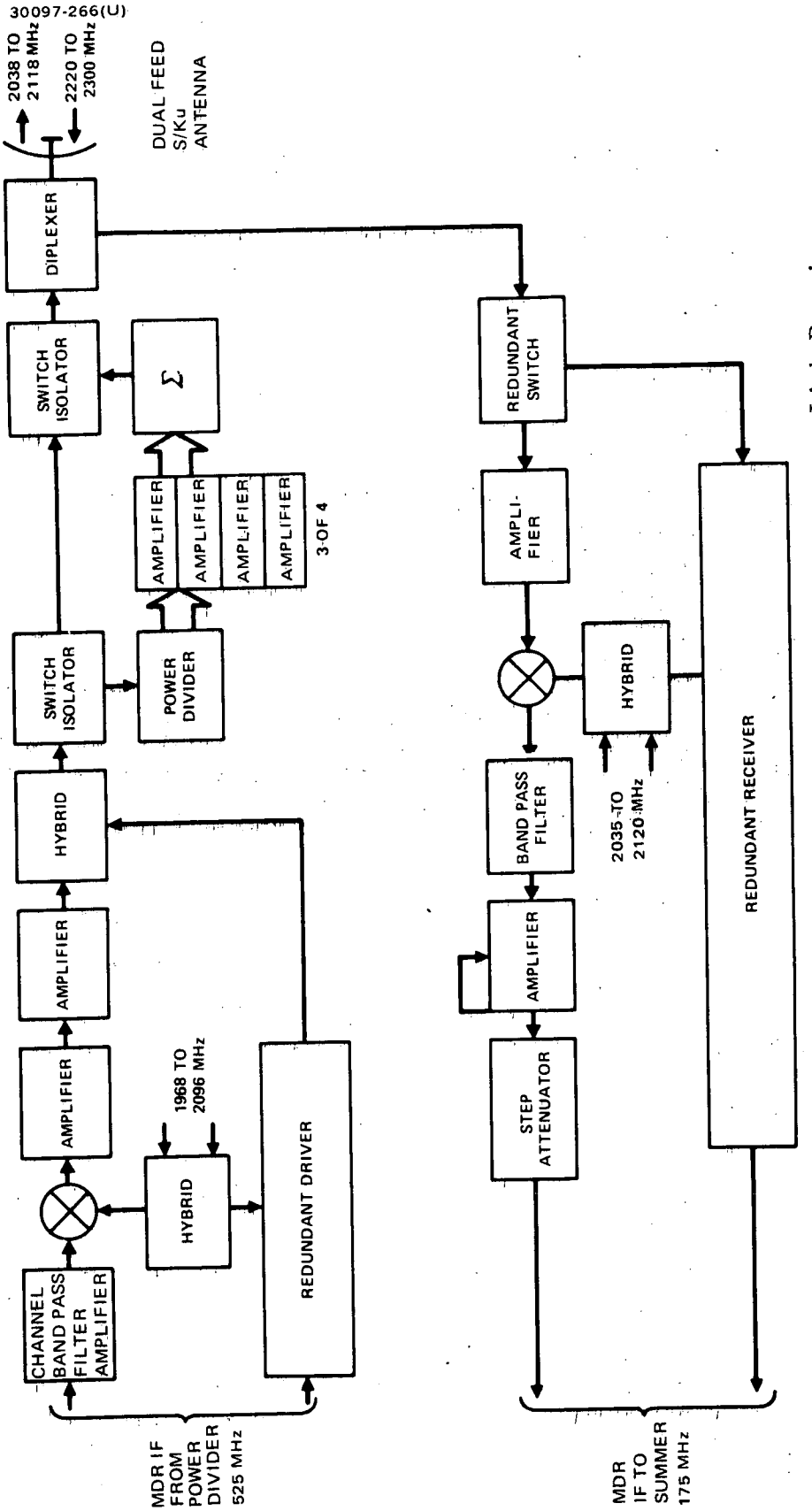

Figure 63. MDR Forward Link Transmitter and MDR Return Link Receiver

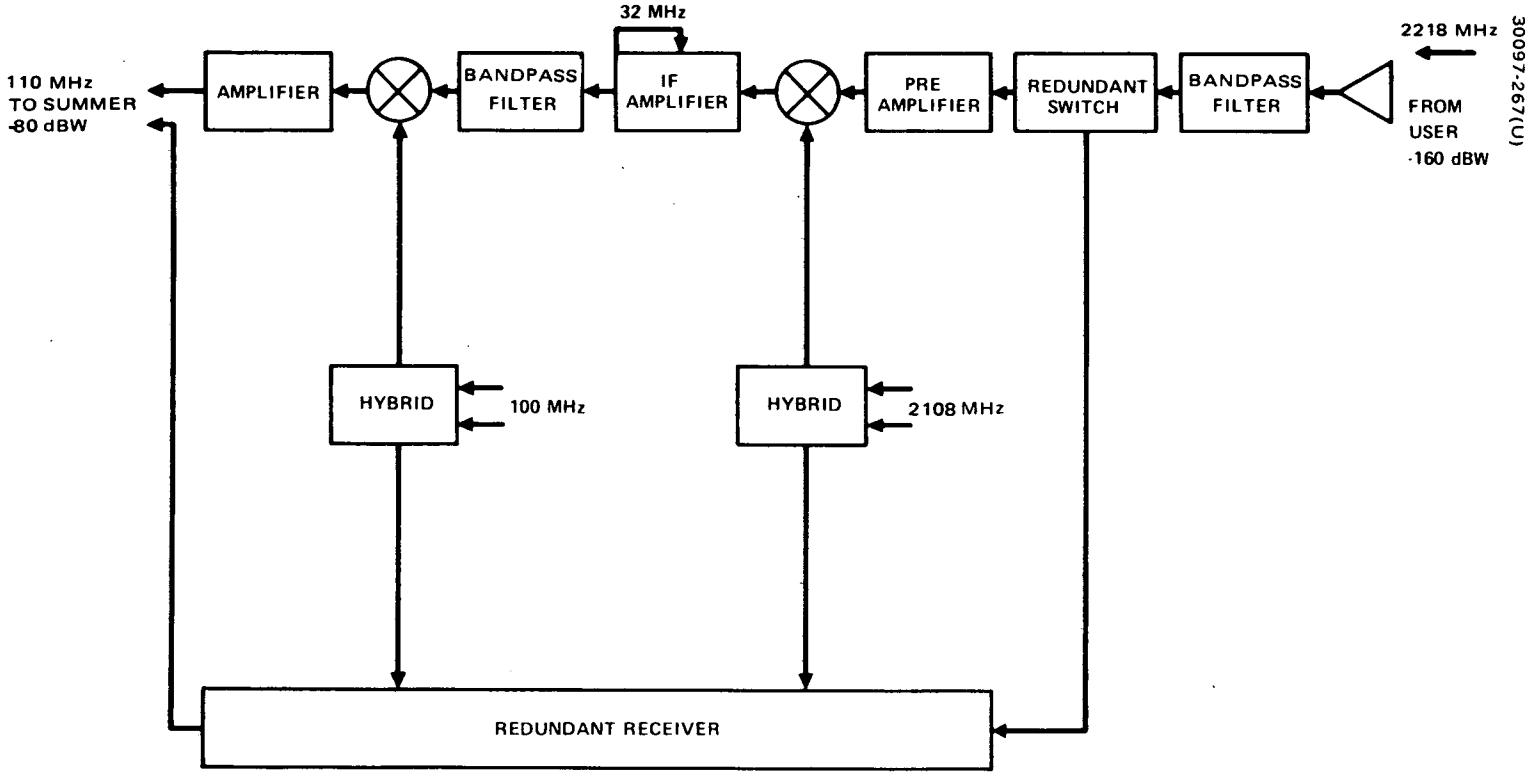

Figure 64. Order Wire Receiver

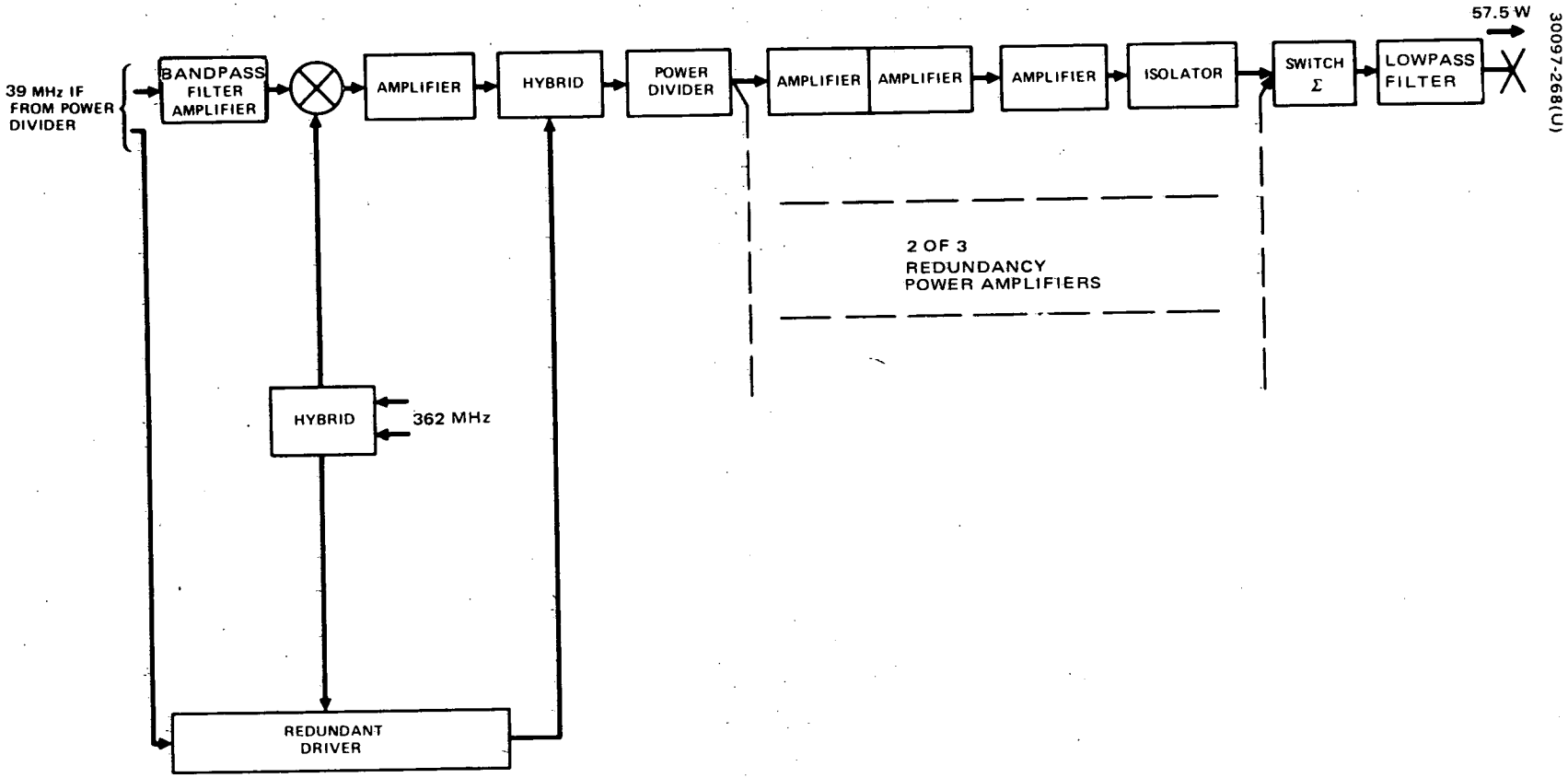

Figure 65. LDR Forward Link Transmitter

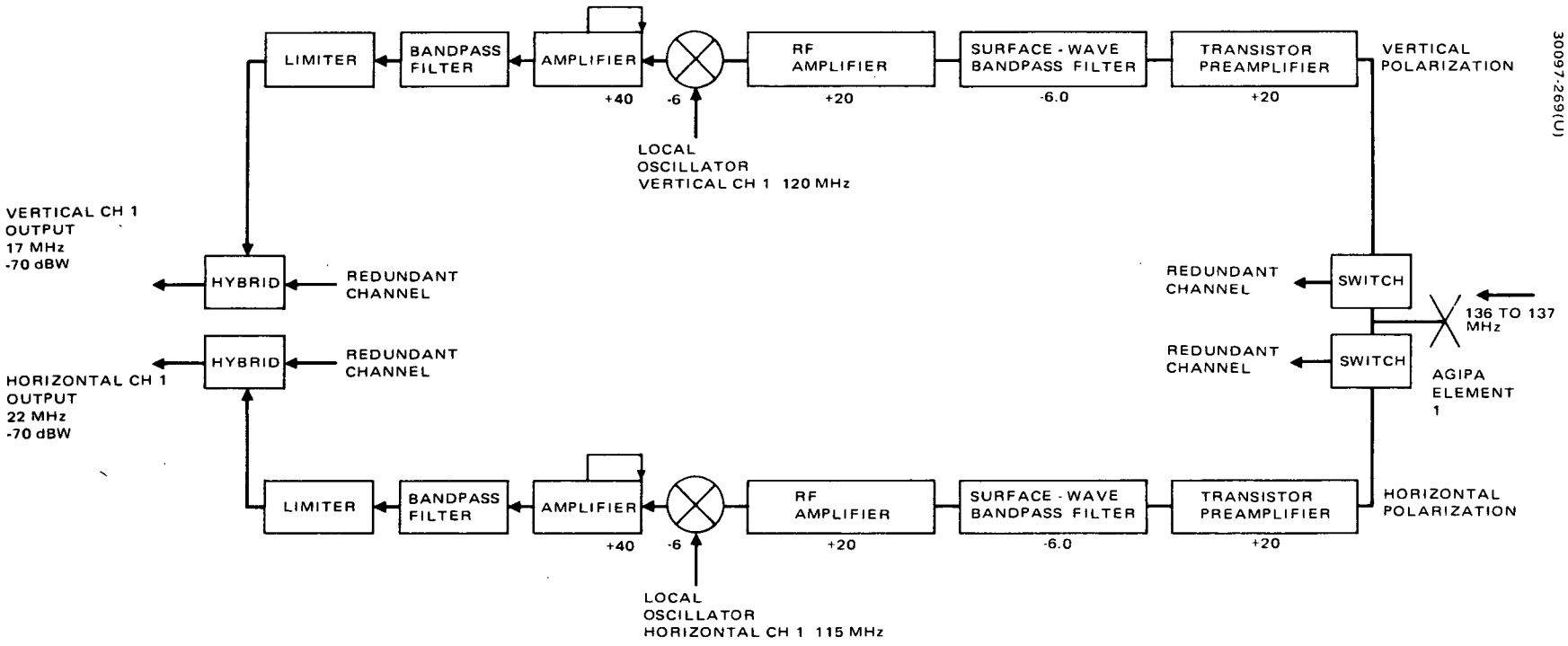

Figure 66. Redundant VHF Receiver

4.3.1.2 Telecommunication Repeater Advanced Technology Design Considerations

The Delta spacecraft configuration places severe demands on hardware design implementations by requiring minimum size, mass, and power, while providing nearly the same telecommunication services as larger spacecraft payload configurations. These demands have placed design emphasis on utilization of hybrid circuit and microwave-integrated circuit (MIC) technology with thick and thin film circuit components. Hybrid microcircuit techniques are also applied to IF circuit designs, voltage regulators, and power supplies. Digital control circuits utilizing metal-oxide semiconductor, large-scale integration circuits (MOS-LSI) are applied in the TT&C coders, decoders, and multiplexer designs, where applicable. When combined into an integrated package, the above microminiature techniques allow a design implementation of minimum mass.

There have not been many microminiature hybrid devices used to date in communication satellites or spacecraft in general; however, of those which have been used in recent communication satellite designs, there are not known failures in over 500,000 operating hours. High reliability is also substantiated by field test and life test results of Hughes missile and avionics subsystems using hybrid circuit designs. Compared to discrete circuit devices, the hybrid circuit failure rates are found better by a factor of 3 to 1. Therefore, the good reliability of the low mass microcircuit subsystems is a distinct advantage.

The technical risk areas of the repeater are related in part to the need for high efficiency power amplifiers and microwave multiplex filters with good rejection and low loss. These problem areas exist at all bands: Ku, S, and UHF. The thermal control and heat dissipation techniques require critical attention when microcircuit concepts are applied. For this configuration, the TDRS repeater components that require special design emphasis or that are classified as critical design items are:

1) Solid-state Ku band amplifier with 100 mW output and 2 percent efficiency

2) Ku band TWT amplifier with about 10 watts output and 32 percent efficiency

3) UHF power amplifier with 58 watts output and 55 percent efficiency using hybrid circuit technology

4) VHF receiver using preselector bandpass filter designs employing surface wave acoustic filter technology

5) S band paramplifier with a 100 K noise temperature

The microstrip techniques do not lend themselves to good filter designs because of the poor dielectric characteristics of the alumina substrate

material. Unloaded Qs of 200 to 300 are typical for microstrip filters; therefore, more conventional filter techniques are necessary for high Q multiple section filters such as used for the diplexer applications of the TDRS repeater. At UHF, some size and mass savings are proposed by using helical filter designs for the UHF low pass filter at the transmitter output.

The Ku band solid-state amplifier Impatt amplifier techniques are used for the HDR forward transmitter power amplifier. The requirement of 100 mW output at 14.7 GHz is achievable with present day silicon diodes. The 30 dB gain can be easily achieved with either a three-stage amplifier or a two-stage injection locked oscillator. The major technical design problem is achieving high efficiencies. For the 100 mW level output, present day design capabilities without special development yield about a 0.4 percent efficiency for an Impatt amplifier and 0.6 percent efficiency for an injection locked oscillator. Somewhat higher efficiencies result if hundreds of milliwatts output are used; however, there remains a large dc power requirement in either case. Development of smaller diodes could improve efficiencies by a factor of 1.5 to 2. These would be either silicon, complementary diodes, or gallium arsenide (GaAs) Schotky barrier diodes, both to be available soon. These diodes are capable of two to three times the efficiency of present silicon diodes. With diodes made to present day sizes, efficiencies of 1.5 percent for the amplifier and 2 percent for the oscillator design would be possible. If technology for making the new diodes smaller were developed, even higher efficiencies could be attained.

The TDRS TWT amplifiers would be developed as a scaled version of existing or presently under development spacecraft TWTs. The key performance parameter is efficiency. The 32 percent efficiency is achievable by operating the TWT at a voltage about 8 percent over that which corresponds to maximum gain. Thus, at the maximum efficiency operating point, there is a large average gain slope. The design objective would be to make the gain as flat as possible over the operating bandwidth. At Ku band, the gain slope could be as large as 0.5 dB over a 100 MHz bandwidth. If this becomes an excessive slope, then it would become necessary to use a dual pitch helix slow wave structure. The dual pitch helix has the pitch of the input section greater than the pitch of the output section. This effectively causes the input section of the TWT to be synchronous with the beam and the output section to operate at about 8 percent overvoltage. This gain slope compensation technique does not degrade efficiency and is presently applied in a number of X band and Ku band TWTs. Each TWT satellite application usually has such specific requirements that some new development is necessary; the TDRS TWT development should emphasize efficiency and low mass.

The low mass UHF power amplifier design assumes that hybrid circuit techniques will be advanced to a point where hybrid-coupled amplifiers may be integrated to form an extremely light package. The critical design problem in this regard is the method of heat dissipation and control. This, coupled with the problem of high efficiency in a small package, places the UHF power amplifier in the critical development item category.

The VHF multiple channel receiver associated with the AGIPA antenna requires a front end design having good noise figure with emphasis on minimum mass since there are great numbers of duplicate circuits. The most promising technical approach to meet these objectives is the use of a surface wave acoustic bandpass filter preceded by a low noise preamplifier of moderate gain. The critical development item in this design is the surface wave device which can provide a high rejection, steep slope filter characteristic. The insertion loss is moderately large, but should be tolerable with careful filter design and sufficient preamplifier gain. Current experimental developments indicate that surface wave bandpass filters will have performance capabilities applicable to most communication systems functions in VHF and low microwave regions. The major advantages of acoustic surface wave filters are small size, low cost, reproducibility, wide dynamic range, high Q, and good temperature stability.

Figures 67, 68, and 69 illustrate typical microcircuit technology packages applicable to TDRS, although developed for airborne applications at the Hughes microelectric technology facility. The UHF and VHF amplifier designs may be used throughout the IF circuits. S band microstrip techniques are illustrated in the circuit development breadboard photographs of Figures 70, 71, 72, and 73. These advanced concepts using thick film and thin film circuits will be developed into a complete integrated S band subsystem unit package. The low mass criteria for the Delta configuration repeater demand the utilization of these typical advanced microminiature packaging concepts.

4.3.2 Telemetry and Command Subsystem

4.3.2.1 Alternatives Considered

Before configuring the baseline subsystem for telemetry and command, several alternative configurations were considered. Principal among these tradeoffs were the following.

Centralized Versus Master-Remote Concepts

To meet the telemetry and command requirements of the TDR satellite, Hughes considered the use of a centralized system where all telemetry or command functions are centralized units such as the ones used on Intelsat IV satellites. Also considered was the use of a master-remote system where the telemetry and command functions are dispersed throughout the satellite by the use of remote units such as the ones used on the OSO satellite. Cost and mass were the factors considered in this trade, but the overriding consideration was mass. The master-remote concept for telemetry and command can be weight-effective for satellites above a certain minimum size and complexity; below this size the centralized concept proves to be more mass-effective. The size of the TDS satellite is such that a centralized concept is more mass-effective. This approach is also more cost-effective and was chosen for the baseline configuration.

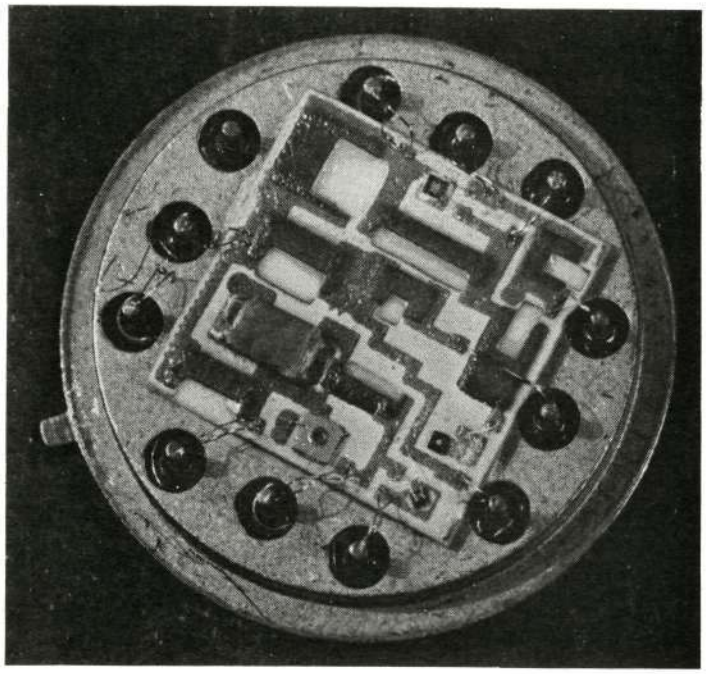

Figure 67. 150 MHz Amplifier (Photo 691624)

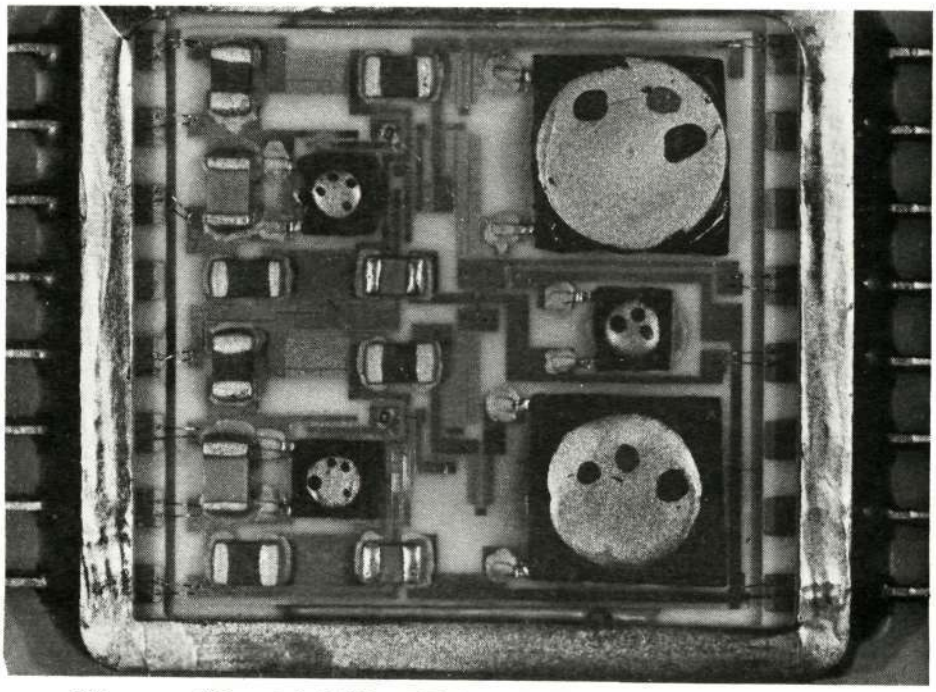

Figure 68. 30 MHz IF Amplifier (Photo 703739)

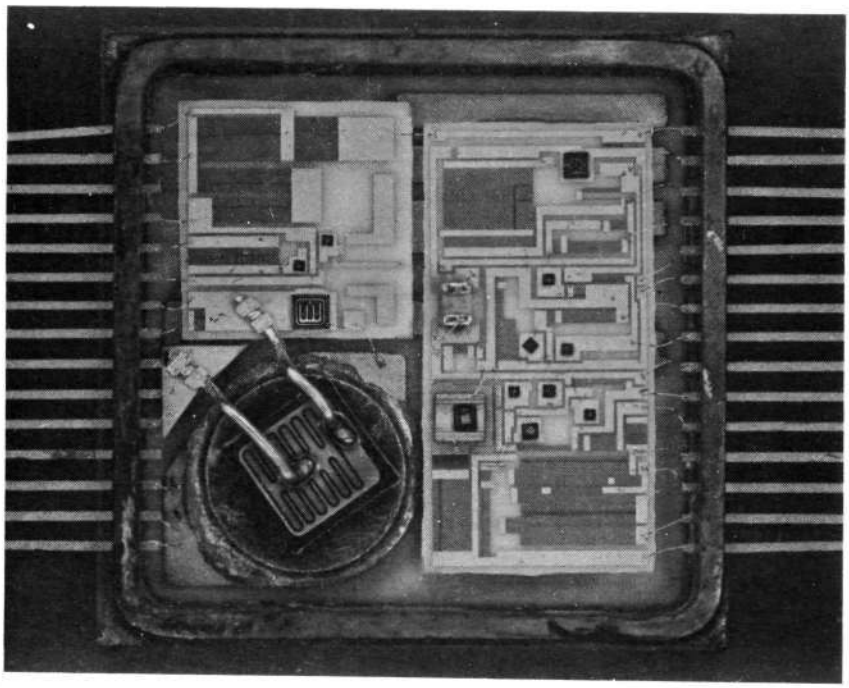

Figure 69. 30 Watt Power Regulator (Photo 4R20344)

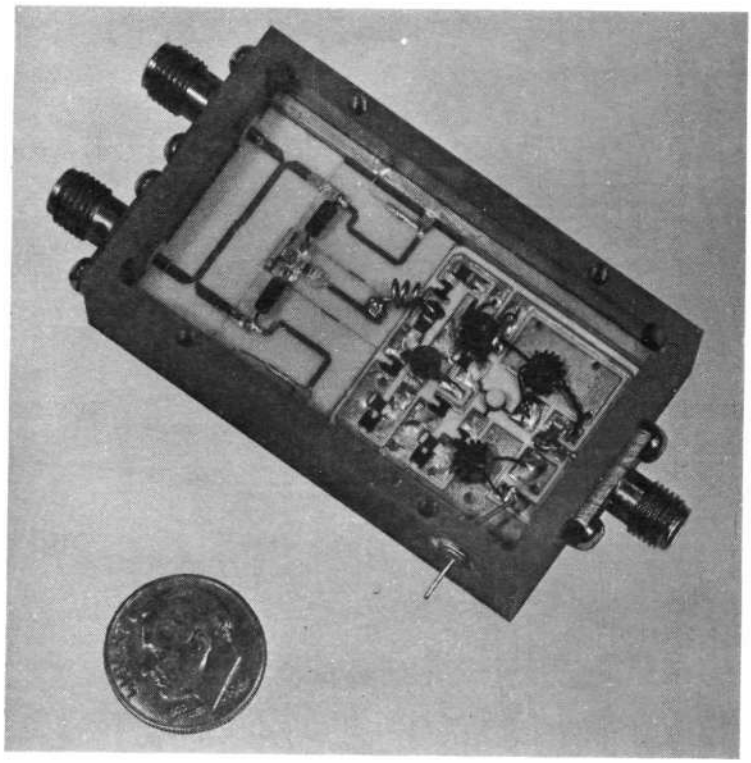

Figure 70. Mixer IF Amplifier (Photo 7317407)

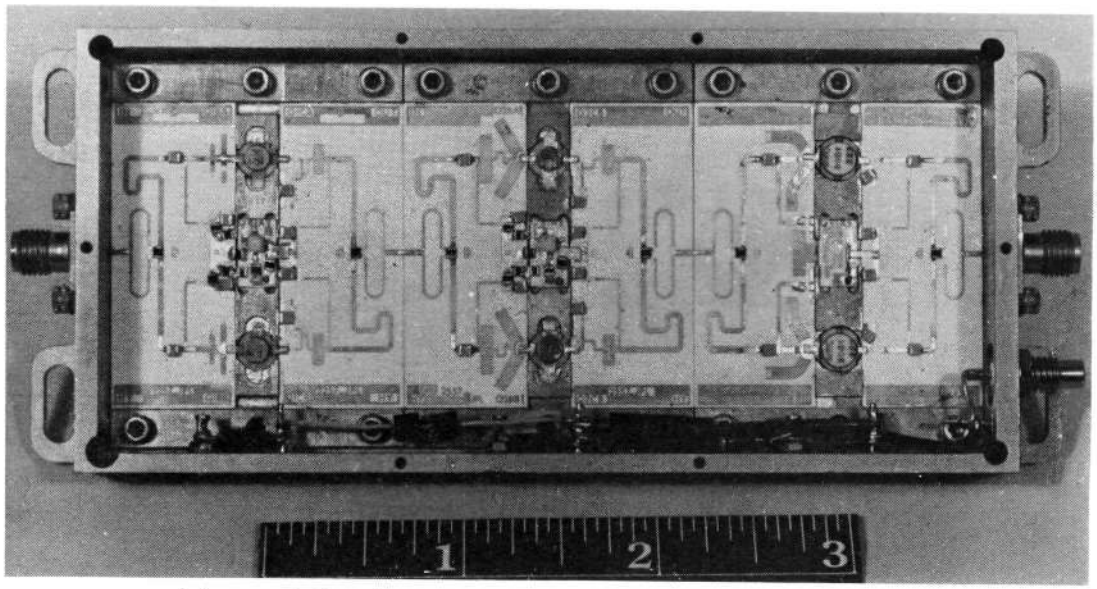

Figure 71. Driver Amplifier (Photo 7317363)

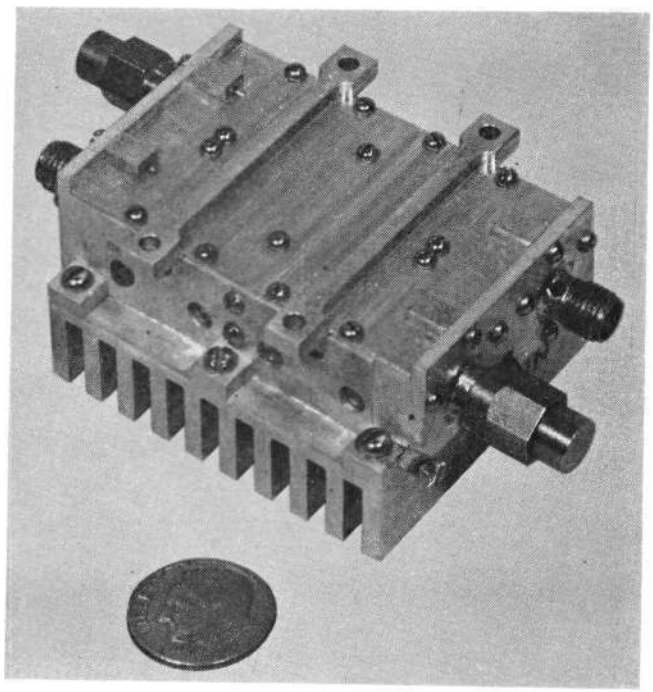

Figure 72. Power Amplifier (Photo 7317362)

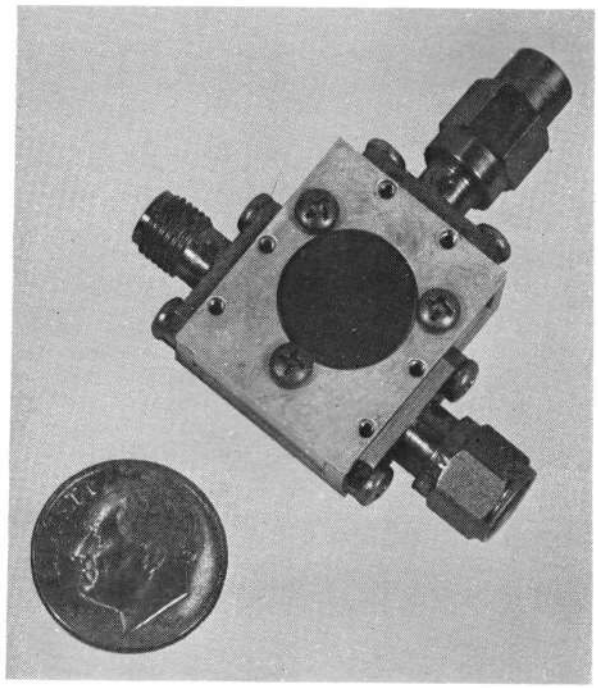

Figure 73. Isolator (Photo 7317358)

Real Time Execute Versus Automatic Execute for Commands

In compliance with the Statement of Work, Hughes has provided a standard GSFC AM-FSK command format, except that it includes a real time execution capability which necessitates the use of a third execute tone. This is the system used on other satellite systems such as ATS and Intelsat IV because it greatly reduces the complexity and mass of the satellite versus an automatic execute system. With the real time system, the requirement for a complex onboard attitude control and antenna pointing processor is eliminated. For these reasons real time execution was adopted.

4.3.2.2 Design Description

The primary telemetry and command requirements are to provide telemetry data and command control of the spacecraft using the GSFC standard telemetry and command formats. These requirements must be satisfied via either the primary telecommunication service system at the Ku band frequency or the backup telemetry transmitter and command receiver at S band. The S band transponder system will be compatible with the GRARR operational requirements to provide data for orbit determination during launch and injection phase. Once the spacecraft is on station, the S band transponder system will be used as a backup to the Ku band system in providing TDRS telemetry and command links to the ground station. The telemetry subsystem must provide data for the determination of performance, status, operational mode, attitude, and antenna pointing of the TDRS. The command subsystem must provide control of the spacecraft for selection of redundant units, operational mode changes, stationkeeping, and orientation of the spacecraft and the antenna. Figure 74 is a schematic diagram of the telemetry and command subsystem.

Command Subsystem

The units of the command subsystem, as shown in Figure 74, are fully redundant and cross-strapped so that either unit of every pair could fail completely without imparing the satellite's ability to receive and execute all commands. A command transmission consists of a microwave carrier modulated by a sequence of tones at three discrete frequencies, designated 1, 0, and execute. The tones are amplitude-modulated at 128 Hz. The demodulated output of the Ku band receiver and the S band command receiver drive both the despun and spinning decoders. Either of the redundant decoders on the despun and spinning side provides up to 128 pulse command outputs. The selection of the executing decoder is by unique decoder address. Command verification is provided by telemetry readout of the command register before sending the execution tone.

The command subsystem is capable of executing jet firing commands in phase with the spin of the satellite. This is performed at the ground station by synchronizing the execute tones with sun or earth pulses, received via real time telemetry. The repetitive command mode is used for antenna pointing and jet firings. Slewing is accomplished at a rate of 24 steps per second. Tracking commands are transmitted as required to maintain the antenna beam on the user satellite.

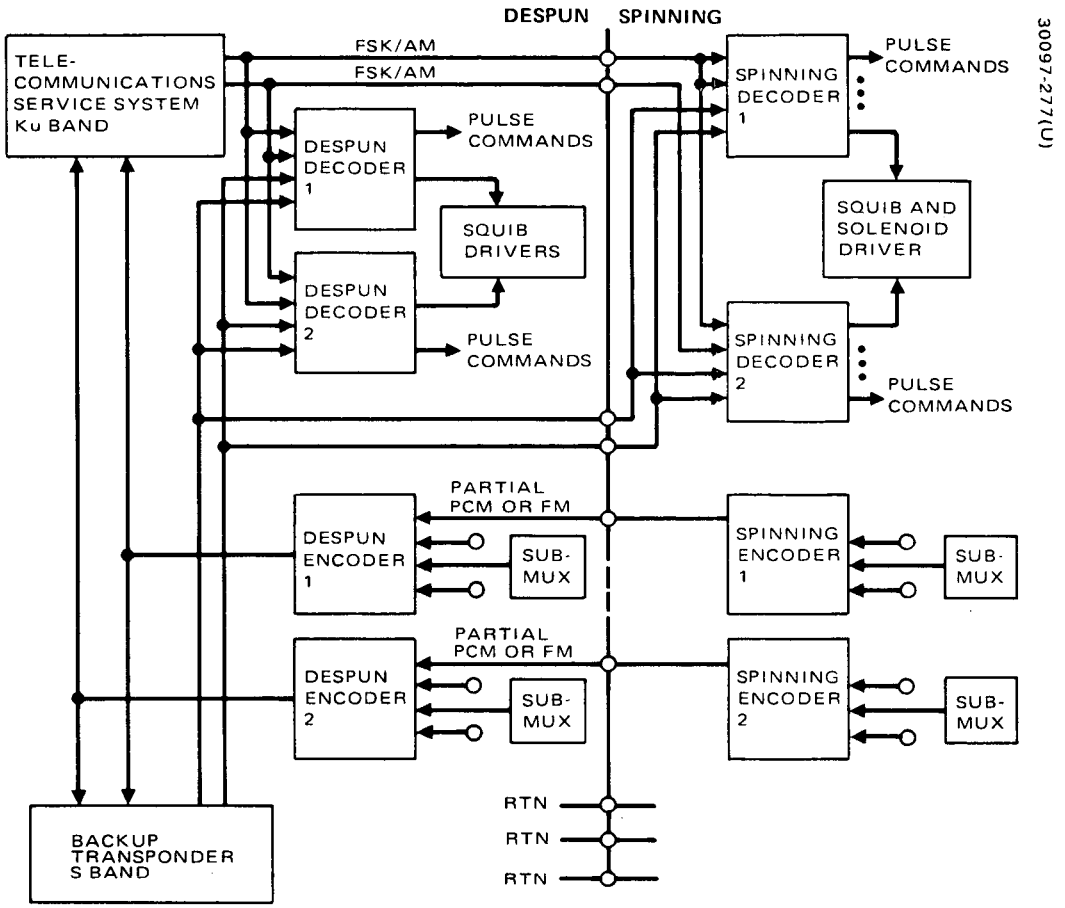

Figure 74. Tracking, Telemetry, and Command Subsystem

Signal and Word Format. The demodulated command from a receiver output consists of a sequence of 1, 0, and execute tone pulses; these are arranged as shown in Figure 75. For convenience, the 1 and 0 pulses will be referred to as bits since they convey binary information to the decoder logic circuitry.

The introduction portion of the command word consists of at least 16 0-bits followed by one 1-bit. During this time, a receiver is selected and the decoder registers and logic are reset. The decoder is then able to process the remainder of the command word. The next 8 bits comprise the address portion of the command word. The first 6 provide the coding for digital addresses. The address words are separated by a minimum Hamming distance of 2, so that a single error in the transmission or reception of a decoder address will not result in the successful addressing of a wrong decoder. To take advantage of the full command capability of the decoder design, spinning decoders have a unique address that differs from start of despun decoders. The last 2 bits are both ones, which ensures that the introduction sequence will never be repeated within the command word.

COMMAND GENERATOR CONTROL	FUNCTION PERFORMED	TONE	CODE	DURATION
ACTUATE XMIT				
	INTRODUCTION (CLEAR)	0	16 BITS	258 ms
		1	1 BIT	
	DECODER ADDRESS	0 AND 1	6 BITS	
		1	2 BITS	
	COMMAND	0 AND 1	8 BITS	
READ DECODER REGISTERS	COMMAND VERIFICATION VIA TELEMETRY			
ACTUATE EXECUTE				
	COMMAND EXECUTE	EXECUTE TONE	AS REQUIRED	VARIABLE TIME (40 ms FOR STANDARD SINGLE COMMAND)
ACTUATE CLEAR				
	CLEAR THE DECODER REGISTERS	0	16 BITS	133 ms
		1	1 BIT	

30097-278(U)

Figure 75. Command Format

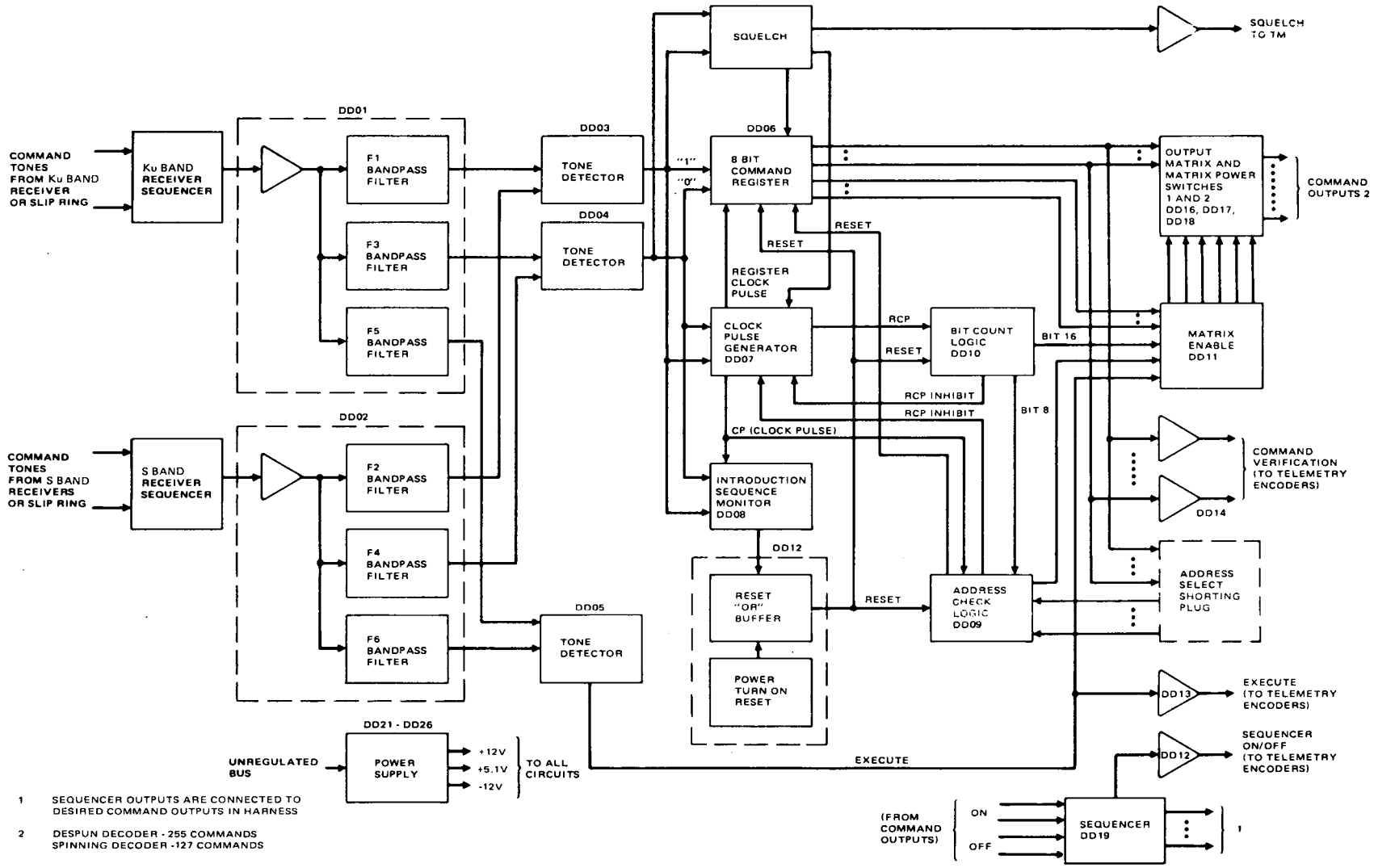

Figure 76. Despun or Spinning Decoder Block Diagram

The command itself consists of 8 bits. The 8 command bits are entered into a storage register for verification via telemetry. Once a command word is entered into storage, further processing of data bits is inhibited and an introduction format must be sent to clear the register. Upon receipt of the execute tone, a coincident pulse will occur on the decoder output line corresponding to the stored command. Execute tone pulses can be sent for as long or as frequently as required. After the command has been executed (or if necessary at any time during the commanding sequence), the commanding ground station resets and clears the decoder by repeating the introduction. As shown in Figure 75, the time necessary for introduction, addressing, and entering a command into the register is 258 ms. This means that the minimum time required before executing a command is 258 ms (even when bypassing the telemetry verification step).

Command Decoders. The despun and spinning decoders differ from each other in only the following particulars:

1) Despun decoders are implemented with more command outputs from the output matrix than from the spinning output matrix.

2) Each despun decoder contains a TWT sequencer.

3) Each spinning decoder contains a spinup sequencer.

In all other aspects, including method of operation, the despun and spinning decoders are identical. Both types, therefore, will be described with reference to the block diagram of Figure 76.

There are two receiver sequencers. Each feeds a set of 1, 0, and execute tone filters (six different frequencies). This arrangement provides positive identification of the command line (S or Ku band) being used for a given command, as each sequencer drives only one set. Cross-strapping is achieved by connecting the two corresponding tone filter outputs together at the input to their respective detector circuits.

The receiver sequencers sample the two S band and the two Ku band receiver outputs to select one that has a suitable output signal. The signal at the receiver output is shown in Figure 77. Tone filters are two-stage, stagger-tuned, passive, bandpass filters with -3 dB bandwidths of approximately 1200 Hz. The output of the first stage of each filter goes to the AM detector where the two signals are summed and the composite signal is full wave rectified and fed to a clock pulse generator which contains a narrow bandpass filter tuned to the 128 Hz bit rate. The output of the 128 Hz band pass filter is the demodulated AM, an 128 Hz sine wave with an amplitude proportional to the signal strength of the received AM-FSK signal. The 128 Hz sine wave is fed to a hard limiting circuit in the squelch circuit. The squelch circuit puts out a signal to enable the decoder processing when the input signal exceeds a preset threshold level. The 128 Hz sine wave is also fed to the clock pulse generator that generates the clock signals which drive the remainder of the demodulator.

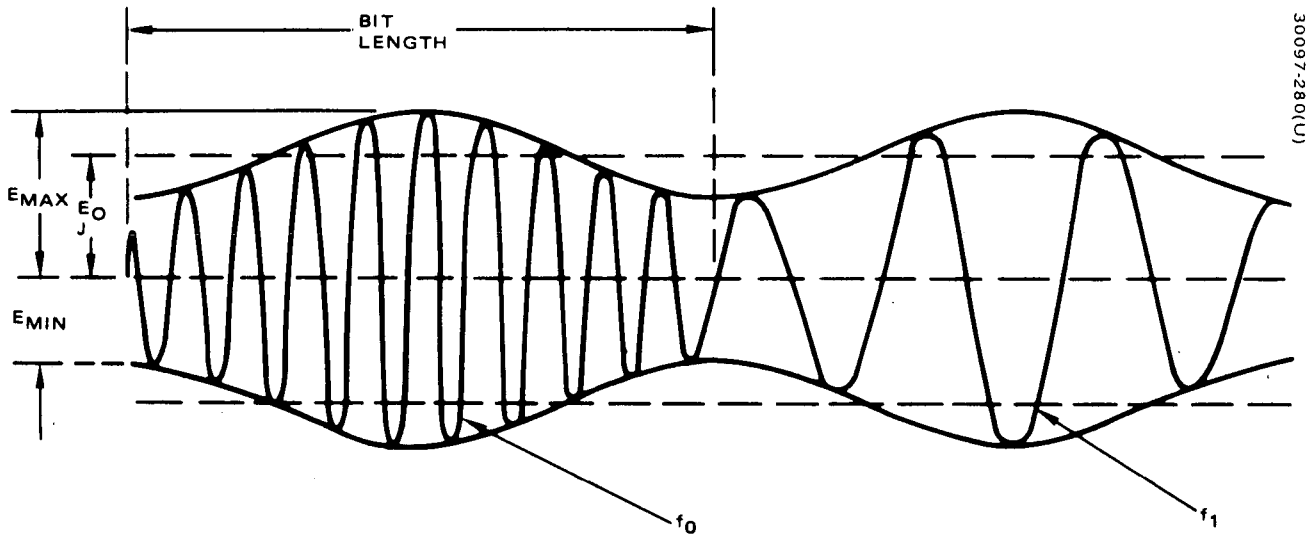

$$\text{MODULATION INDEX, } m = \frac{E_{MAX}-E_{MIN}}{2E_0} = 0.50 \pm 0.05$$

Figure 77. FSK/AM Signal Design

When power is turned on, the decoder is initialized by the power turnon reset circuit as follows: 1) the command register is cleared to all 0s (an illegal command), 2) the count register's count is set to zero, 3) the address check logic is reset, and 4) the full count logic is set to zero. Whenever an 0 or 1 tone pulse is detected, the clock pulse generator will provide a clock pulse (CP) to the introduction sequence monitor that checks the pattern of the incoming data. Upon receipt of eight or more 0s followed by a 1, it initializes the decoder in the same manner as the power turnon reset.

The command register is an 8 bit register. It receives 1s and 0s from the demodulator and RCPs (register clock pulses) from the clock pulse generator. Its output goes to the address check logic, output matrix, and to the telemetry buffers for parallel entry of its contents into redundant telemetry encoders.

The bit count logic provides a pulse to the address check logic when it has counted eight RCPs and a pulse to the full count logic when it has counted 16 RCPs. When the address check logic receives its pulse from the bit count logic, it checks the output of the command register (which now contains the address) and 1) if the address checks correctly, an enable signal is sent to the matrix enable or 2) if the address does not check, it inhibits further RCPs and clears the command register. Each decoder has an address plug that permits changing its address any time prior to launch. When the bit count logic has counted 16 RCPs, it inhibits further RCPs to prevent false clocking of the command register and also sends an enable signal to the matrix enable.

Use of two series matrix power switches prevents a single component failure in the matrix power switching circuitry from generating a false command. When both matrix power switches are enabled, an execute signal from the execute tone detector closes both power switches, causing a command pulse to occur on the output selected by the command portion of the command word. The command pulse is coincident with and lasts as long as the execute tone pulse.

Each despun decoder contains a TWT sequencer that, when turned on by command, times for a specified period, then generates a sequence of eight command-type output pulses spaced at 105 seconds, generates a second sequence of six pulses, and finally shuts itself off (it may also be commanded off, and thereby reset, at anytime during its cycle). The command-type outputs that each TWT sequencer generates appear on separate lines. Each line, in turn, is wired directly to selected command matrix output lines to execute those selected.

Squib and Solenoid Drivers. The squib and solenoid drivers actuate pyrotechnic and jet firing functions in the satellite. The squib drivers fire the apogee motor and bearing and power transfer assembly (BAPTA) release

squibs, and the solenoid drivers actuate the axial, radial, and spinup jet valves and the latching valve in the spinup jet line. There are four squib drivers and ten solenoid drivers that are capable of firing three squibs and driving eight pairs of solenoids. All of the squib drivers apply power to their respective squibs after specified delay times. The BAPTA clamp release squib drivers are commanded by redundant separation switches. The apogee motor squib drivers are each commanded redundantly by the spinning decoders. After mating of the spacecraft to the adapter, until actuation of the separation switches, all squib driver power inputs are directly connected to ground.

Telemetry Subsystem

The encoder units of the telemetry subsystem, as shown in Figure 74, are fully redundant and cross-strapped so that either unit or every pair could fail completely without impairing the satellite's ability to transmit all telemetry data. Normally, one encoder unit or the despun pair operates with one unit of the spinning pair. Two modes of data processing are used: PCM and FM real time.

The PCM mode is used for all attitude, thermal, power, and status information, including command verification. In the PCM mode, the spinning encoder receives, processes, and formats data originating on the spinning portion of the satellite. The output, which is connected across the spinning/despun via slip rings, is an 8 kHz biphase waveform from which a despun encoder recovers the nonreturn to zero (NRZ-L) bit stream and derives a coherent clock. The despun encoder gathers and processes data originating in the despun compartment, and alternates its bit stream word-by-word with the spinning encoder bit stream, then converts the composite NRZ-L bit stream to a Manchester code format. The converted stream is used for phase modulating a Ku band carrier within the telecommunication repeater on the despun side and modulates the backup VHF transmitter on the spinning side.

To accommodate the telemetry requirements of the satellite, the baseline Intelsat IV telemetry subsystem has been modified to include some subcommutated channels. In the main frame, one digital and four analog words on the spinning side and two digital and four analog words on the despun side are subcommutated.

The FM real time mode is used for real time attitude pulses (sun sensor pulses, earth sensors pulses, platform index pulses, and command execute pulses). The occurrence of a pulse coherently switches the frequency of an IRIG channel 13 subcarrier oscillator from its pilot tone to a different frequency, depending on the kind of pulse present. The output is connected via a slip ring to the despun encoder, the output of which phase modulates the Ku and VHF telemetry transmitters.

Spinning Encoder. In the PCM mode a spinning encoder conditions, multiplexes, and encodes the telemetry data originating on the spinning section of the satellite into a PCM bit stream. In the FM real time mode, the composite of real time pulses coherently switches the frequency of the SCO. All sequenced operations within the spinning encoder, including multiplexing, analog-to-digital conversion, attitude sensor pulse interval digitizing, and digital formatting, are timed by a 1.024 MHz crystal oscillator and countdown chain. The operation of the spinning encoder is described below with reference to Figure 78.

Multiplexers and submultiplexers provide analog and digital gating circuits to time multiplex the telemetry inputs. The telemetry inputs consist of bilevel and analog data with a normalized range of 0.00 to 5.12 volts. Both analog and digital signals are multiplexed with the same type of circuitry, the digital signals being treated as analog signals up to the output stage of the digital multiplexer, which converts them to standard logic levels. The analog multiplexer output is fed to a successive approximation type analog-to-digital converter that encodes each analog input into a serial 8-bit NRZ-L word, providing resolution of better than 0.5 percent of full-scale. The outputs of the analog-to-digital converter and digital multiplexer are combined at a data node to form the partial PCM bit stream.

The attitude data processor performs a sequence of ten time interval measurements (Figure 79), to facilitate the accurate and rapid determination of satellite attitude. Each measurement equals the number of cycles of a 32 kHz reference frequency, derived from the 1.024 MHz crystal oscillator, counted during the time of the interval being measured. The count is telemetered along with a 4 bit code identifying which measurement it represents. The inherent measurement resolution is ±1/2 period of the 32 kHz reference, or approximately 16 microseconds. Measurement T2, from the occurrence of a sun or earth pulse to the start of the next telemetry frame, is of particular significance. It allows a suitably equipped ground station to synthesize a pulse train at the spin rate and at a known phase with respect to the generation of pulses on board the satellite. Such a pulse train (which can also be derived from the FM mode telemetry) is required for synchronous pulsing of the spacecraft jets.

The biphase modulator converts the NRZ bit stream to a coherent biphase format, in effect adding an easily recoverable clock for use by the despun decoder. It also adds a double amplitude pulse once each frame to which the despun decoder synchronizes its frame timing.

When the encoder is in the FM real time mode, it accepts and processes various real time pulses and transmits their occurrences as discrete changes in SCO frequency. The frequency transmitted and the duration of transmission correspond to the particular group that includes the occurring pulse (Table 26). All of the tone frequencies are within the IRIG channel 13 band. If two pulses in different groups should occur simultaneously, priority gating of the pulses permits the occurrence of only one pulse to be transmitted.

The highest frequency group takes precedence. The most critical telemetry data are the attitude determination and execute pulses needed for spacecraft control. Except for a shared power supply and rotary transformer driver, the circuitry in the PCM path is entirely separate from that in the FM path to provide significant extra redundancy for these data.

Despun Encoder. In the PCM mode, a despun encoder conditions, multiplexes, and encodes the telemetry data originating in the despun compartment into a PCM bit stream, which it synchronizes and merges with the partial PCM from its associated spinning encoder. In the FM mode, a despun encoder switches the spinning encoder FM output to the telemetry transmitter. A comparison of block diagrams shows that the despun encoder (Figure 80) is identical in most respects to the PCM portion of the spinning encoder. In order to merge its PCM words with those of the spinning encoder, the despun encoder must derive its bit clock from the spinning encoder bit stream and synchronize the start of its telemetry frame with the spinning encoder double amplitude frame sync pulse. These tasks are performed, respectively, by the clock and data detector circuit and the sync detector circuit. If the clock detector is unable to derive a bit clock either because the spinning encoder has failed or has been commanded off, the clock selector will switch the despun encoder to its internal 1.024 MHz crystal oscillator so that despun telemetry may continue to be transmitted. The formatting logic performs the required merging of the partial PCM from the spinning encoder with despun encoder PCM. The combined NRZ-L bit stream is then coded into an NRZ-M waveform that biphase modulates the 32 kHz subcarrier output.

Component Physical Characteristics

Mass, power, and size data for selected components for the telemetry subsystem are listed in Table 27.

4.3.2.3 Performance

Telemetry and command performance characteristics are listed in Table 28. The command capacity may be divided as required between the spinning and despun sections of the spacecraft.

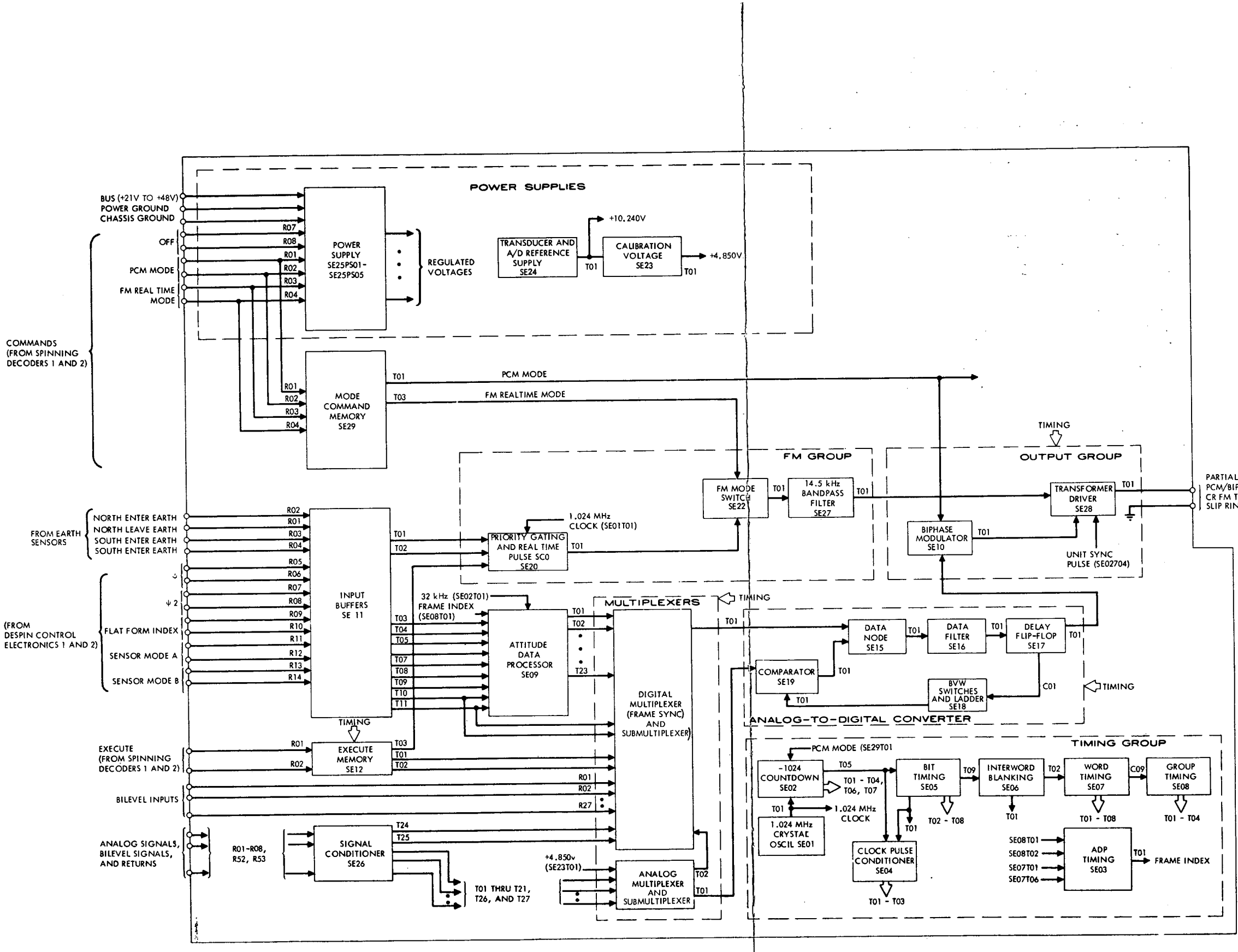

Figure 78. Spinning Encoder Block Diagram

FOLDOUT FRAME 1

FOLDOUT FRAME 2

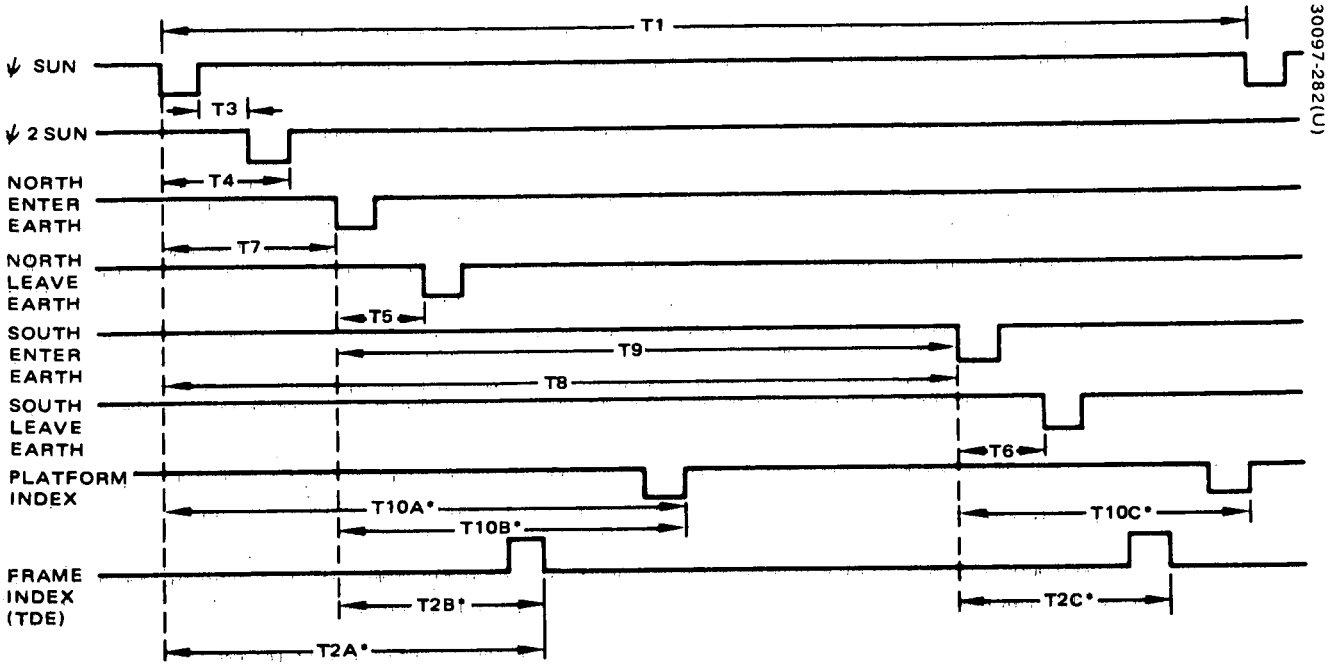

*THESE MEASUREMENTS ARE TAKEN RELATIVE TO THE SPECIFIC SENSOR IN USE AT THE TIME; THUS, A DENOTES THE MEASUREMENT TAKEN WHEN IN SUN MODE, B WHEN IN NORTH EARTH MODE, C WHEN IN SOUTH EARTH MODE.

Figure 79. Attitude Data Processor Time Interval Measurement

TABLE 26. FM MODE TRANSMISSION

Pulse	Frequency, kHz	Duration, ms	Remarks
Group 1			
Psi ( )	15.059	5	
Psi ( )	15.059	5	
Group 2			
North enter earth	14.222	10	
North leave earth	14.222	20 (exception)	For identification on ground
South enter earth	14.222	10	
South leave earth	14.222	10	
Platform index	14.222	10 to 120	Variable with spin speed
Group 3			
Command execute	13.838	Variable time	= execute duration (40 ms for standard single pulse)
Pilot Tone	13.474		Transmitted when no pulse is present

TABLE 27. TELEMETRY AND COMMAND COMPONENT PHYSICAL CHARACTERISTICS

Unit	Number per Spacecraft	Mass per Spacecraft, kg	28 Volt Bus		Size, centimeters			Program Identification
			Power Per Unit, watts	Spacecraft Standby Power, watts	Width	Length	Height	
Despun								
Decoder	2	2.7	0.9/1.8*	1.8	14.7	22.6**	6.9	HS 312 Mod
Encoder	2	4.2	4.0		14.7	22.6**	6.9	HS 213 Mod
Squib driver	1	2.5	–	–	14.7	15.2	3.6	
Spun								
Decoder	2	1.6	0.9/1.8***	1.8	14.7	31.0**	6.9	HS 312 Mod
Encoder	2	3.3	5.0	5.0	14.7	31.0**	6.9	HS 312 Mod
Solenoid and squib driver	1	0.9	–	–	14.7	34.3	3.6	HS 320
Latching valve – heater driver	1	0.5	–	–	6.6	8.9	7.4	

*Standby/execute.

**Standby unit.

***High power/low power

TABLE 28. TELEMETRY AND COMMAND PERFORMANCE CHARACTERISTICS

Parameter	Characteristics
Telemetry – Intelsat IV Type	
PCM Mode	
Work length	8 bits
Frame length	64 words main frame 11 words subcommutated (eight subcommutations)
Analog words	110
Digital words	31
Bit rate	1600 bps
Code type output	Manchester
FM Mode (Attitude data)	
Subcarrier frequency	14.5 kHz
Data type	Real time pulses
Modulation	FM
Data transmitted	1) Sun pulses 2) North earth pulses 3) South earth pulses 4) Execute receipt
Command – Intelsat IV Type, Modified	
Tones	1, 0, and execute
Input Signal	FSK/AM
Bit rate	128 bps
Command capacity, despun	255
Command capacity, spun	127
Command verification	Telemetry
Command execution	Real Time
Execution synchronization	Sun or earth pulses
Maximum command rate	Approximately 4/s

Figure 80. Despun Encoder Block Diagram

30097-283(U)

FOLDOUT FRAME 1

FOLDOUT FRAME 2

4.3.2.4 Technology Status

To obtain a low mass design, the LSI techniques are used for T&C units. Specifically, custom metal-oxide-semiconductor large-scale integration MOS-LSI was considered for these units. This technology has been developed at Hughes and at many other companies over the past several years. At Hughes, the custom MOS mask designs are done by the circuit design area with the use of a computer. The use of computer-aided design reduces time, cost, and manpower required for MOS-LSI development. The MOS chips designs are fabricated at the Hughes Newport Beach facility. This technology was first used at Hughes in 1964 to implement a digital differential analyzer (DDA) adder element which was used in operational space programs such as TACSAT, HS-318 and DSLS (ESSA). This technology was used by Hughes to implement much of the passenger service and entertainment system built for the McDonnell Douglas DC-10 commercial aircraft. It has recently been used in the designs of the remote decoders and remote encoders for the NASA Orbiting Solar Observatory (OSO) program.

Experience with this technology has proved that the best candidates for mass savings are the digital timing and control portions of a subsystem. Experience with other similar systems has shown that about 50 LSI packages of the commercially available TTL type can be replaced by one custom LSI chip design, with an accompanying net savings of about 0.23 kg. These rules of thumb were applied to redesign encoder and decoder units resulting in an approximate 5 kg mass savings for the subsystem.

4.3.3 Antennas

The baseline antenna subsystem consists of eight antennas as shown in Figure 81: the deployable VHF AGIPA antenna for the low data rate user return link, the deployable UHF band backfire antenna for the low data rate user forward link, two deployable S/Ku band high gain parabolic reflector antenna for both forward and return links of the medium and high data rate users, the Ku band parabolic reflector for the telemetry space to ground link, two Ku band earth-coverage horns for the command ground to space link, the S band backfire for the order wire and transponder function, and omnidirectional S band antennas for backup TT&C operation.

A lightweight rib mesh antenna design has been selected for use in the dual frequency S/Ku band, the Ku band, and UHF antennas. The open mesh approach achieves low mass and minimizes thermal effects on surface tolerances. A mechanical deployment system that provides uniform, controlled rib and mesh unfurling and allows gravity testing without adding special fixturing. The antenna design details have been generated by Radiation, Incorporated in response to a set of design requirements and configurational constraints specified by Hughes for the TDR satellite.

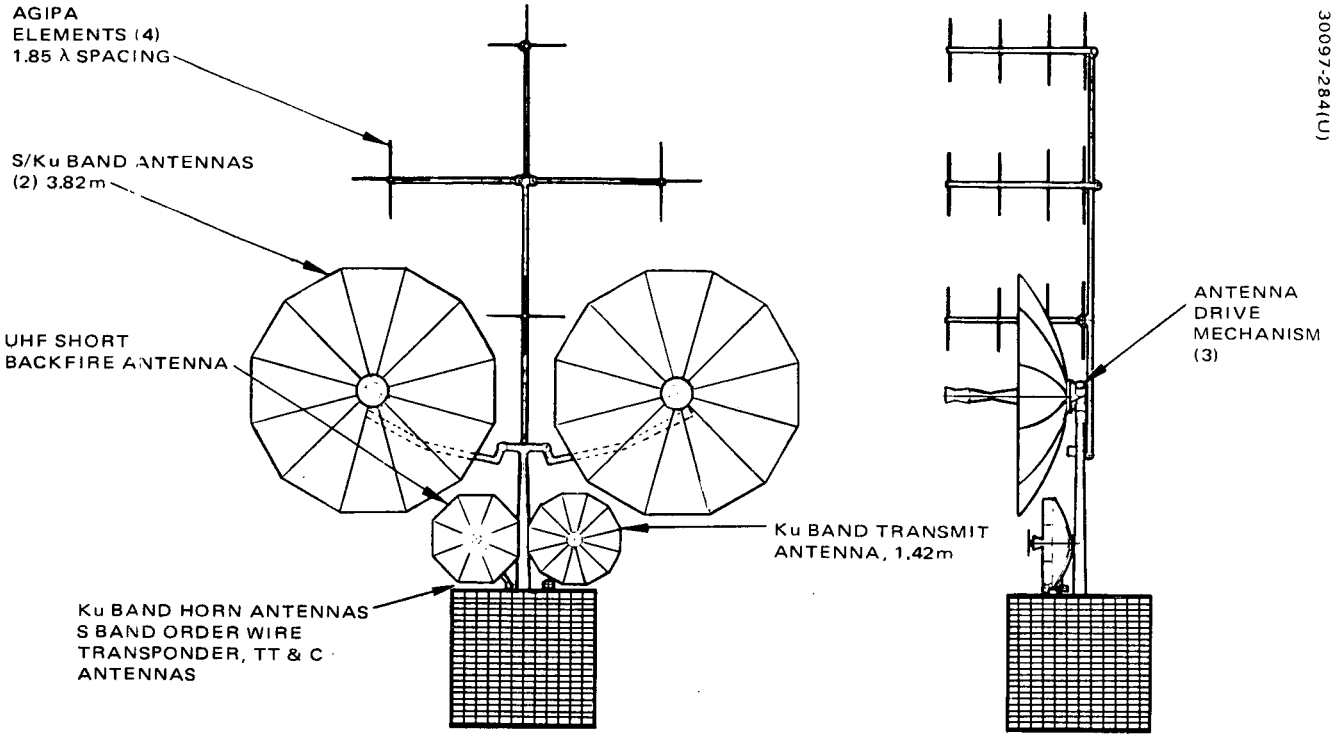

Figure 81. TDRS Antenna Configuration

The four-element AGIPA VHF antenna utilizes YAGI elements which have a low mass and low surface area for reduced solar pressure torques.

The primary objective in the antenna mechanical design is the attainment of minimum mass consistent with adequate structure strength, stiffness, and an antenna stowage within space available for payload. These parameters have been specified to be ±30 g quasi-static acceleration, 50 and 4 Hz minimum frequency for the stowed and deployed antennas, respectively.

During launch, transfer orbit, apogee injection and station acquisition all of the antennas are nested around a central support mast forward of the despun spacecraft platform in a volume compatible with the Delta 2914 payload fairing as shown in Figure 82a. After station acquisition, the AGIPA tiedown locks are released, and in the first step, one of the antenna deployment sequence, the central support mast of the AGIPA is extended to about 6 meters overall length. See Figure 82b. Three of the YAGI elements are fastened to the tip of this mast with support arms. The support links are rotated 90 and 180 degrees to position the array elements on a two wavelength circle. After orienting the four YAGI rods normal to the plane of the array, all dipole whips are released to establish the final AGIPA antenna configuration as shown in Figure 82c.

The deployment sequence is continued by releasing sequentially the platform tiedown locks on the support arms of the S/Ku band antennas. These support arms are hinged to the tip of the rigid center mast. The

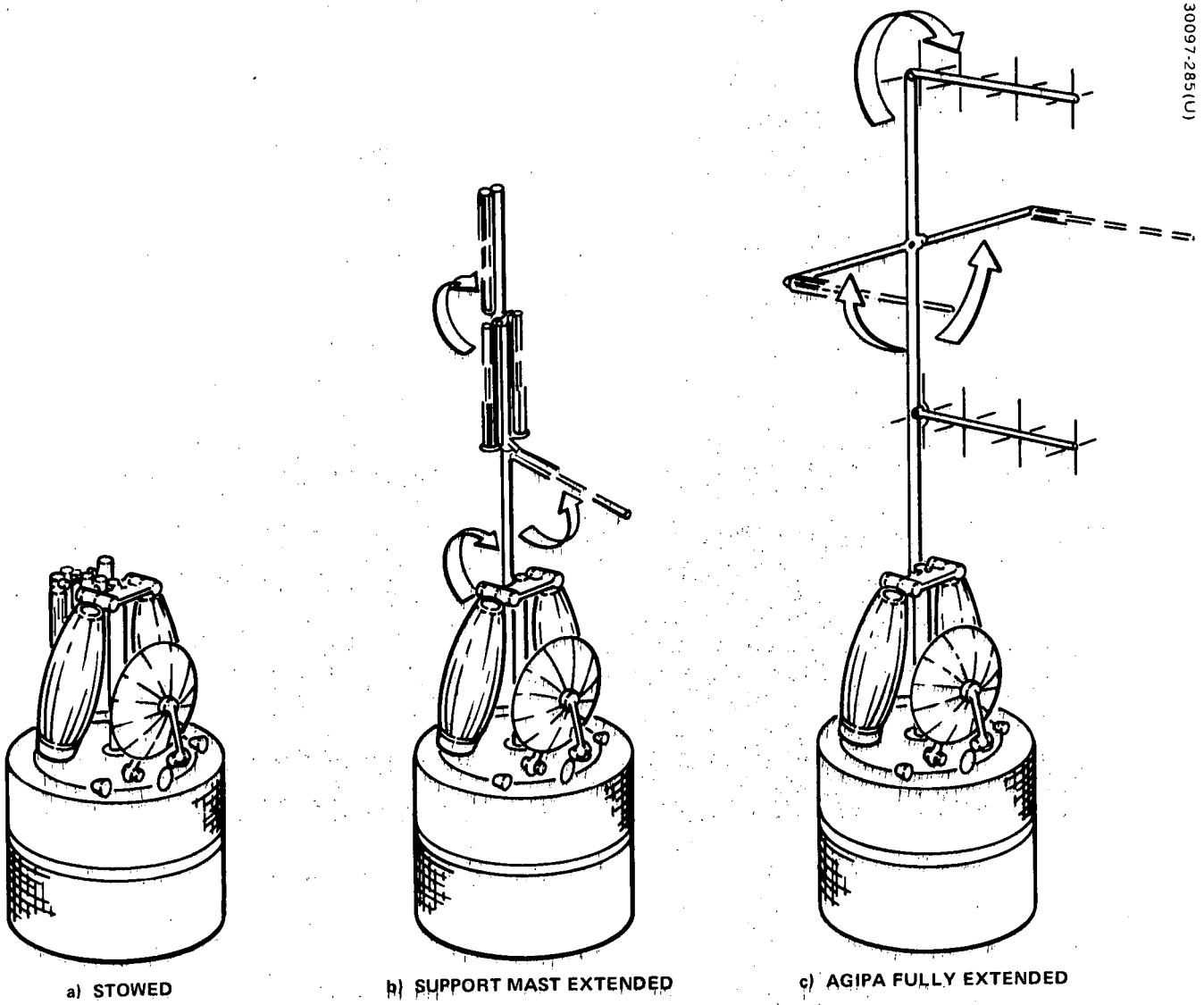

Figure 82. AGIPA Antenna Deployment Sequence

reflectors remain folded and attached to the supports while they rotate into position. Next, the UHF antenna support strut is unlocked, and is rotated on its platform hinge to position the UHF reflector. At this time sufficient clearance has been provided (as shown in Figure 83a) to pivot the ground link Ku band antenna 180 degrees on its two-axis gimbal drive. The UHF short backfire antenna reflector is unfolded after the Ku band rigid ground link antenna is pivoted 180 degrees in position. The spacecraft antenna configuration deployment is completed when the S/Ku band antenna reflectors are unfurled by their mechanical drive systems as shown in Figure 83b.

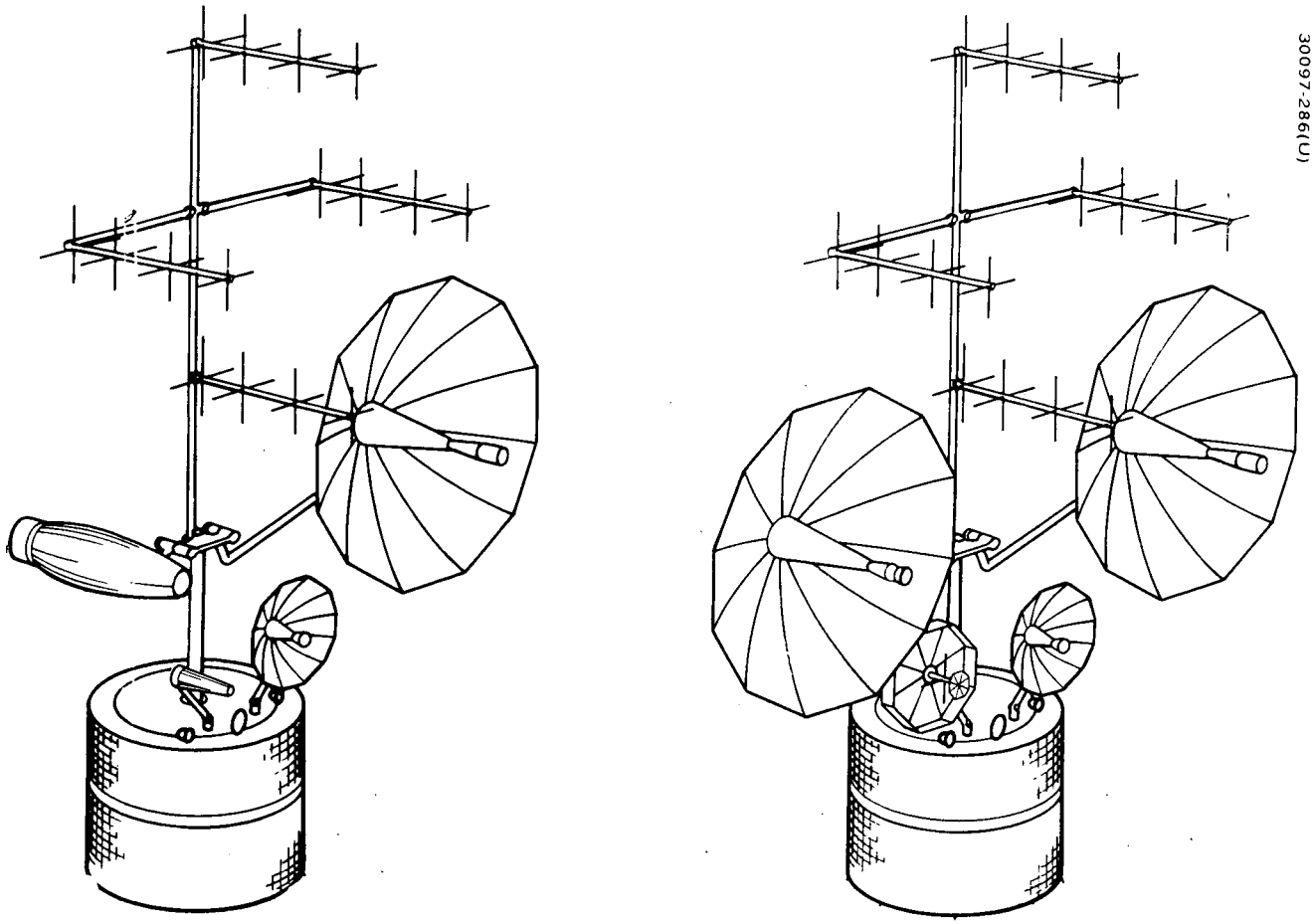

Figure 83. S/Ku Band Antenna Deployment Sequence

4.3.3.1 S/Ku Band Deployable Antenna

The S and Ku band dual frequency antenna selected for the TDRS is a deployable rib mesh design of 3.82 meter diameter. Its primary surface contour is shaped by 12 aluminum ribs of 3.8 cm in diameter and tapered wall thicknesses from 0.015 to 0.03 cm. The reflective mesh contour precision to within 0.025 cm rms is accomplished by using a secondary back mesh and adjustable tension ties between front and back mesh.

A central cone supports the S band feed assembly and the Ku band subreflector. The design features a cassegrainian configuration for the Ku band feed and a direct focal fed paraboloid reflector configuration at S band. The Ku band subreflector is dichroic and freely permits the transfer of the S band radiation from its feed located behind the subreflector. The antenna hub measures 45 cm in diameter and houses the mechanical deployment drive and linkage mechanism. Redundant torque spring and motor

drives unfurl the reflector in orbit as well as in a 1 g. The field rib dominated mesh antenna system was designed and tested by Radiation, Inc. Its mechanical and RF performance characteristics have been demonstrated in a NASA-sponsored program. Figure 84 illustrates the 3.82 meter diameter S/Ku band antenna reflector in its stowed configuration.

The number of ribs was based on a tradeoff study of surface tolerance, mass and deployed dynamic performance. Analyses indicate the deployed resonance exceeds the 4 Hz requirement with 12 ribs, and the use of fewer than 12 ribs was not considered practical because of gravity effects in positioning the reflective mesh. With fewer than 12 ribs, the mesh gore span between adjacent ribs becomes so large that gravity deflection of the mesh becomes significant and makes the setting of the reflector surface a difficult task. The rib walls are uniformly tapered from the 305 μm thickness midsection to 204 μm at the rib root and 152 μm at the rib tip. The tapering matches the rib strength to the moment profile of the rib loading in the maximum stress condition that occurs in the restrained stowed condition.

The reasons for the selection of the double mesh design for the S band antenna are illustrated in Figure 85. This figure shows antenna mass as a function of the surface accuracy for single and double mesh designs. The surface accuracy of the single mesh design directly depends on the number of ribs, while the surface accuracy of the double mesh is mass-independent since the surface accuracy is achieved through use of ties between the two mesh layers. The surface accuracy requirement of 1.53 mm rms total error dictates the use of a double mesh design for minimum mass.

The reflective mesh is constructed from five-strand bundles of 17.8 micron Chromel-R wire knitted into a wire screen. The front mesh is knitted with openings of 2 mm. This size opening was selected to ensure satisfactory RF reflectivity at 15 GHz. The back mesh is knitted with 1.27 cm openings. This size opening is sufficient to allow the back mesh to be utilized as a secondary drawing surface for contouring the front mesh while minimizing the antenna weight. The finished mesh is a low spring rate, elastic material. The use of this soft mesh with the rigid ribs results in a rib-dominated reflector surface which is relatively unaffected by changing mesh forces and orbital thermal variations throughout the antenna life. The mesh is attached to the ribs in a tensioned state of predetermined levels that are sufficient to ensure the mesh will remain in a flat, unwrinkled condition throughout the orbital life.

The double mesh technique essentially eliminates systematic surface error by reversing the front mesh bulge and pulling the front mesh to the back mesh as illustrated in Figure 86. The back mesh is separated from the front mesh by the rib diameter, and both meshes are tied by simple tension wires. By properly tensioning these tie wires, the reflector surface can be contoured to a precision parabolic shape. A surface accuracy of 0.0176 mm rms has been achieved on a 3.8 meter diameter reflector by Radiation, Inc.

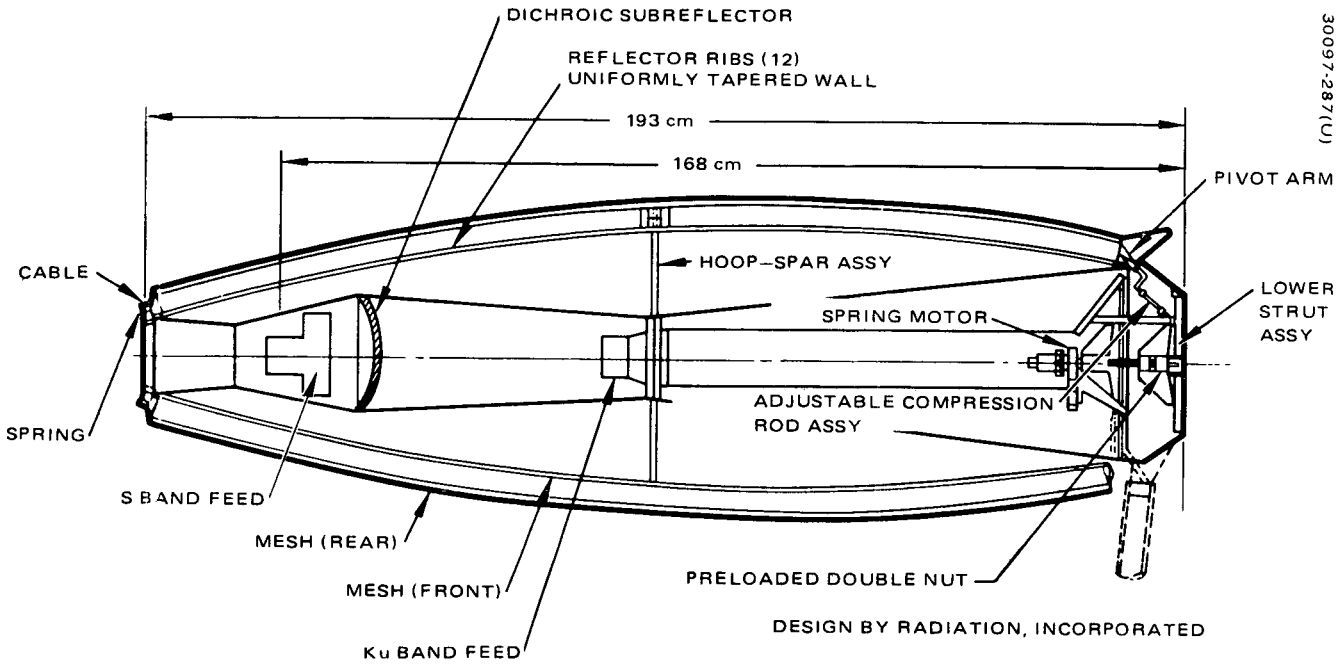

Figure 84. S/Ku Band Deployable Antenna

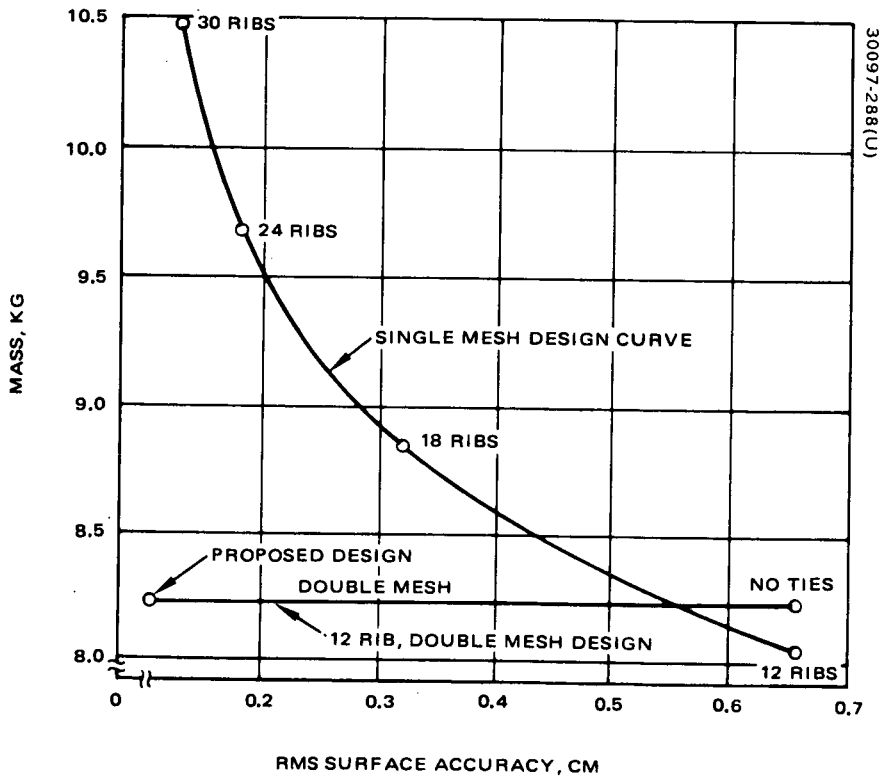

Figure 85. Mass Versus Surface Accuracy For Signal and Double Mesh 3.8 Meter Antenna

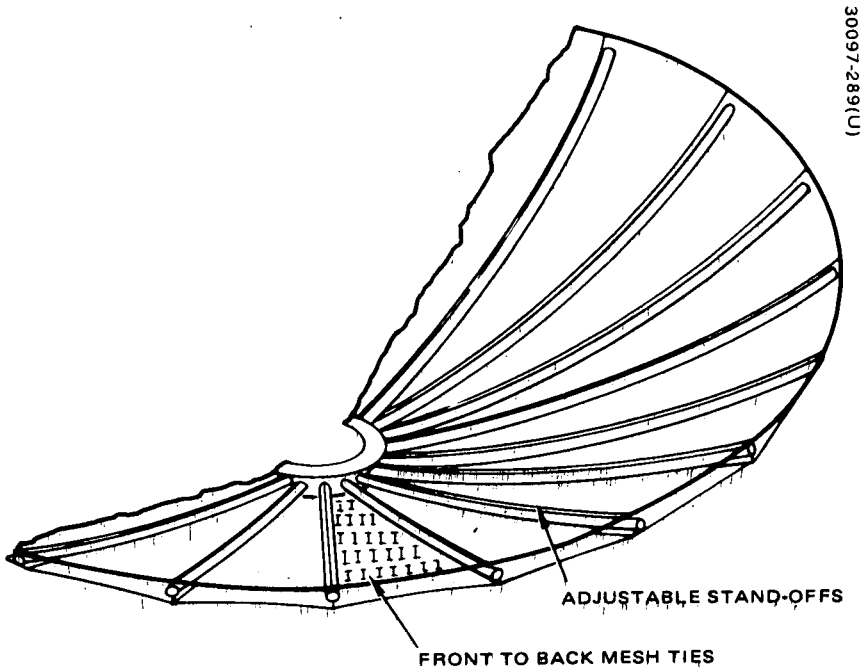

Figure 86. Double Mesh Concept

Deployment of the reflector from the stowed to the fully deployed position is precisely controlled to eliminate the transfer of any deployment energy to the spacecraft. The controlled deployment also prevents impact loading of the rib structures and mesh, thereby assuring that 1) the present parabolic surface is not distorted by the deployment action and 2) no mesh loading conditions result that exceed the mesh strength limits. The deployment mechanism utilizes redundant energy drive systems to rotate a ball-screw within a recirculating ball nut. The resultant linear motion of the ball nut serves to rotate each rib from the stowed to deployed position through the individual linkages to each rib. The primary drive of this system is a constant torque spring motor. The spring motor also provides a preload on the mechanism in the stowed condition. The spring motor provides sufficient energy to deploy the antenna in any orientation under gravity conditions. In a zero gravity condition, the spring motor capability exceeds the deployment energy requirements. The torque motors function then as dynamic brakes, controlling the deployment rate and requiring no electrical power. If required to deliver power, the motors can increase the torque to the ball-screw by as much as a factor of four.

Latching in the deployed condition is accomplished by driving the ball nut carrier and linkages through an over center condition (relative to the pivot arms). In this condition, the mesh tension forces, rib loads, spring motor, and pivot arm preload force the carrier against a mechanical stop. Any external loads that tend to restow the antenna only serve to further increase the loading of the ball nut carrier against the mechanical stop. This

TABLE 29. S/Ku BAND HIGH GAIN ANTENNA

Frequency Band	S Band		Ku Band	
Frequency, GHz	2.07	2.25	13.7	14.9
Aperture diameter, meters	3.82		3.82	
Aperture area gain, dB	38.4	39.1	54.7	55.6
Spillover and amplitude taper loss, dB	1.35	1.35	0.86	0.86
Phase loss, dB	0.14	0.14	0.04	0.04
Blockage loss, dB	0.19	0.20	0.08	0.08
Crosspolarization loss, dB	0.19	0.20	0.32	0.32
Radome loss, dB	0.19	0.10	0.16	0.16
Dichroic subreflector loss, dB	0.20	0.20	0.20	0.20
Surface tolerance loss, dB	0.02	0.02	0.32	0.36
Mesh I^2R loss	0.05	0.05	0.15	0.15
Hybrid loss, dB	0.20	0.20	N.A.	N.A.
Transmission line loss, dB	0.35	0.35	0.04	0.04
Feed and polarizer I^2R loss, dB	N.A.	N.A.	0.32	0.32
Comparator loss, dB	N.A.	N.A.	0.20	0.20
VSWR loss, dB	0.12	0.12	0.08	0.08
Total losses, dB	2.90	2.93	2.77	2.81
Total efficiency, percent	51.3	51.0	53.0	52.5
Antenna peak gain, dB	35.5	36.2	51.9	52.8
Half power beamwidth, degrees	2.5	2.3	0.37	0.34
Polarization sense	Circular	Circular (orthogonal)	Circular	Circular

toggle action eliminates the requirement for additional latching devices in the deployed condition and thereby improves reliability. A secondary advantage of the toggle latching is convenience during ground testing and handling. A reverse torque can be applied to the ball screw to back-drive the mechanism through the latching toggle action. The antenna can thus be remotely stowed during ground testing by reversing the current to the electric motors.

The RF performance characteristics for both the S and Ku band frequencies have been computed and are listed in Table 29.

4.3.3.2 Ku Band Antennas

The Ku band ground link high gain parabolic/reflector antenna Figure 87 consists of a 1.50 meter diameter rigid rib and mesh reflector and a multimode-horn feed with a cassegrainian subreflector all mounted on a two-axis positioner for beam positioning. A shaped reflector and multimode feed were chosen for high antenna efficiency. Large amplitude taper across typical reflector antennas is significantly reduced by distorting the shape of the subreflector away from a hyperboloid. Phase error thereby

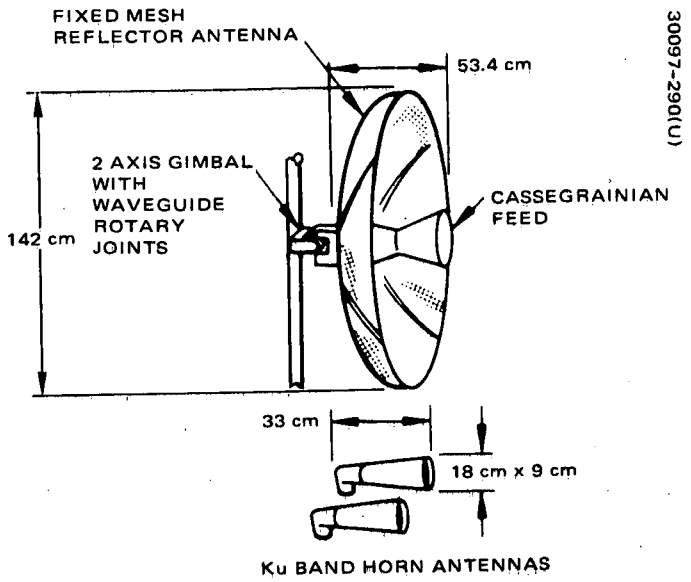

Figure 87. Ku Band Antennas, TDRS/Ground Links

occurring is corrected by slight distortions on the main reflector. Aperture efficiency improvements from 70 to 80 percent have resulted by employing this technique. A corrugated horn gives rise to the two modes needed to make this feed pattern symmetrical with very low sidelobes. The polarizer that generates a single sense of circular polarization consists of a waveguide orthomode tee for good impedance match and multiple iris phase shifter for good polarization ellipticity.

Two receive Ku band antennas will each cover the northern hemisphere with CP beams. The approximate beamwidth requirements are 9 by 18 degrees. An array of two fin-loaded pyramidal horn antennas is presently considered to be the most simple and proven approach toward satisfying the CP beam coverage requirements over the transmit and receive bands. The fin-loading at the horn aperture equalizes the E and H plane beamwidths, thereby providing CP over the full field of view, as well as at the beam peak. Each antenna assembly type utilizes a four-iris square guide polarizer and an orthomode tee. For simplicity, the unused orthogonal arm of the orthomode tee has been shorted out. Where the CP and VSWR requirements are stringent, it may be necessary to load this unused orthogonal arm.

Figure 88 illustrates the high gain Ku band antenna design. A set of 12 tubular aluminum ribs is used with the double mesh technique as described in the previous section to form the reflective surface. This rigid rib and mesh design weighs approximately one-third that of a solid reflector of sandwich construction.

The mesh material is the same type as that for the S/Ku band dish. The mesh surface tolerance is held to better than 0.0254 cm rms through use of the double mesh concept and adjustable rib standoffs. The smaller antenna dismeter and the rigid antenna construction allow accomplishing this surface accuracy.

The supporting ribs are 3.18 cm in diameter with a tapered wall of 0.0102 cm at the rib root to 0.0152 cm at the top. The ribs are made from 6061 T6 drawn aluminum tubing. The thermal control will consist of wrapping the ribs with multilayer (superinsulation) blankets. Each rib is supported in a boxed ring used as the hub. The hub is bonded to the feed support to become a rigid structure. It also serves as the interface flange to mount the antenna to the spacecraft. The support cone is made from aluminum sheet metal rolled and welded along a vertical seam. The final produce is etched to a 0.0152 cm thickness. Thermal control consists of multilayer blankets.

The subreflector is supported by a dielectric cone made from high modulus fiberglass and epoxy. The subreflector is made in a sandwich from using aluminum honeycomb core and thin wall skins of fiberglass covered with 0.00254 cm aluminum foil. Type 1160 aluminum foil is used for high conductivity and elongation properties.

The Ku band feed for the 150 cm reflector uses a multimode horn feed and a shaped 23 cm subreflector to produce a high overall antenna efficiency. The main reflector is also shaped for good phase efficiency. The feed horn and microwave components are made from aluminum plate that has been etched to a waffle pattern to maintain good stiffness to mass ratios. The entire assembly is dip-brazed together without any flanges to reduce mass in this area. This assembly is bonded in the support cone before the radome and subreflector are bonded into place. After alignment, the subreflector is bonded to give a single assembly. The radome is coated with an RF transparent space-qualified white paint for thermal control, while the back of the subreflector is covered with multilayer blankets. The RF performance predictions for the Ku band antennas are summarized in Tables 30 and 31. The mass of the total system is 1.40 kg as detailed in Table 32.

4.3.3.3 UHF Antenna

The UHF deployable mediam gain antenna design is of the short backfire type. It consists of two plane reflectors spaced approximately a half-wavelength apart with a dipole feed placed between them. The feed is a crossed dipole. The back reflector of the UHF antenna is 1.9 wavelength in diameter, and the front reflector is 0.6 wavelength in diameter for maximum gain.

The coaxial cable feed lines are 0.635 cm Alumispline by Times Wire and Cable Company. Stripline baluns are located at the base of the antenna post to generate the two orthogonal senses of circular polarization.

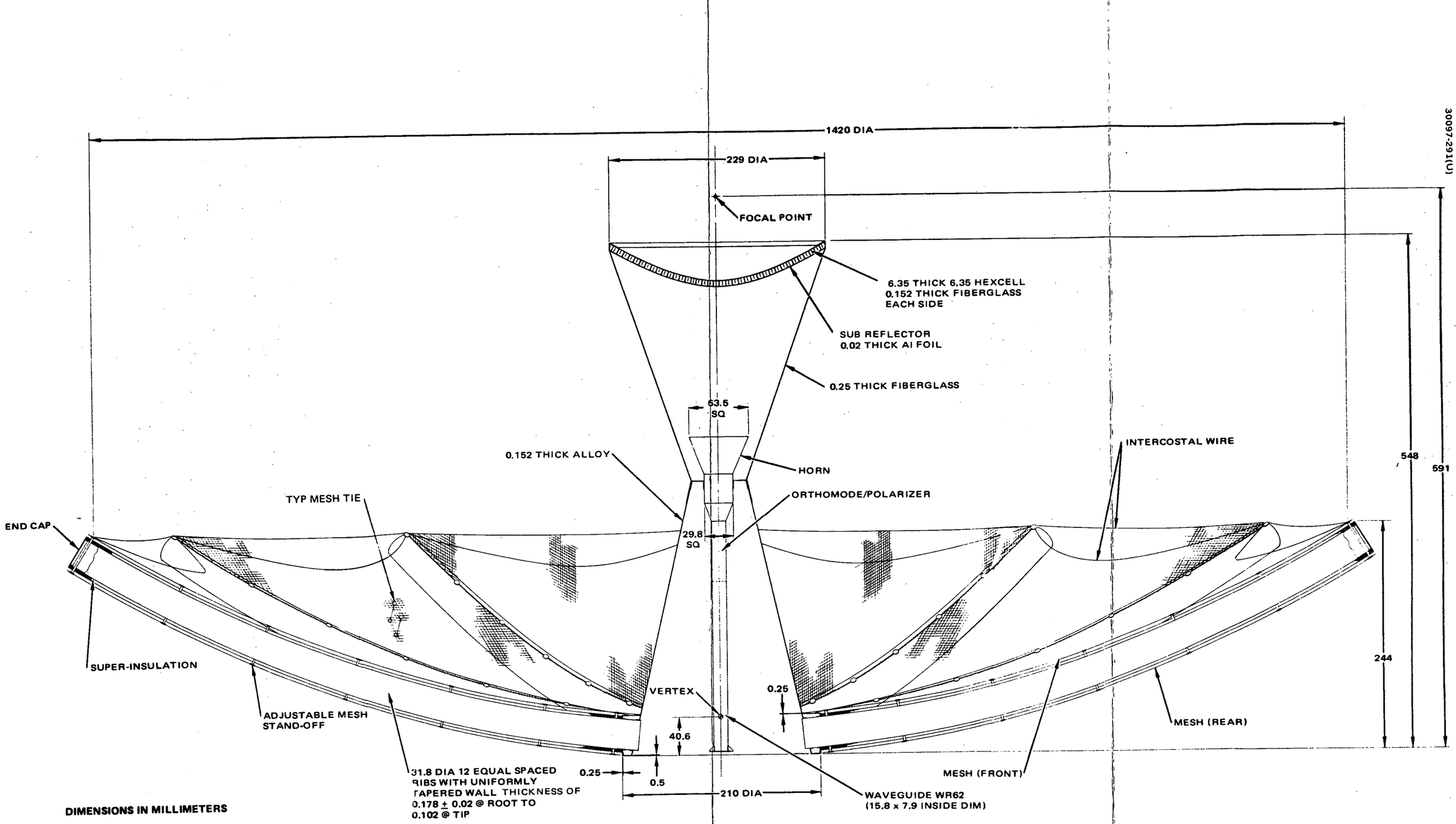

Figure 88. Ku Band Antenna

FOLDOUT FRAME 1

FOLDOUT FRAME 2

TABLE 30. Ku BAND REFLECTOR ANTENNA PERFORMANCE

Frequency		14.9 GHz
Aperture area gain ($4\pi A/\lambda^2$)		47.22 dB
Spillover and amplitude taper losses	0.86 dB	
Phase loss	0.05 dB	
Blockage loss	0.30 dB	
Reflector crosspolarization loss	0.02 dB	
Reflector surface loss (0.02 cm rms)	0.10 dB	
Reflector mesh I^2R loss	0.15 dB	
Horn I^2R loss	0.02 dB	
Polarizer and transition I^2R loss	0.30 dB	
Waveguide loss	0.04 dB	
VSWR loss (1.3:1)	0.08 dB	
Total losses		1.92 dB
Antenna peak gain		45.30 dB
Polarization		Circular

TABLE 31. Ku BAND HORN ANTENNA PERFORMANCE

Frequency		13.7 GHz
Aperture area gain ($4\pi A/\lambda^2$)		25.1 dB
Amplitude taper and phase losses	1.93 dB	
Horn I^2R loss	0.03 dB	
Polarization and transition I^2R loss	0.30 dB	
Waveguide loss	0.25 dB	
VSWR loss (1.3:1)	0.08 dB	
Total losses		2.59 dB
Antenna peak gain		22.5 dB
Antenna earth-edge gain (±9.1 degrees)		18.5 dB
Polarization sense		Circular

The primary reflective surface consists of a 0.64 cm grid Chromel-R wire mesh supported by eight tubular aluminum ribs. Since the reflective surface is flat in the deployed condition, the surface accuracy has little dependency on the number of ribs used. The governing parameters affecting the number of ribs are deployed frequency, weight, gravity effects on the mesh panels, and the surface area loss due to the noncircular shape of the perimeter.

TABLE 32. Ku BAND ANTENNA MASS BUDGET

Item	Mass, kilograms
Front mesh	0.21
Back mesh	0.06
Standoffs and ties	0.06
Ribs	0.31
Rib insulation	0.05
Subreflector	0.07
Support cone	0.34
Horn, polarizer, waveguide	0.22
Cone thermal blankets	0.07
Total mass	1.39

A secondary mesh surface, or fence, is used for improved RF efficiency. It is supported by secondary ribs hinged at the outer tip of each primary rib. The tendency of the mesh of this surface to scallop at the base and the tip of the secondary ribs is controlled by multiple intercostal wires and stepped tension values as described above.

The 8 antenna primary ribs are constructed from 1.91 cm diameter tubes with the wall thickness tapering from 204 microns at the root to 102 microns at the tip. The secondary ribs are 0.954 cm in diameter and have a constant wall thickness of 102 microns. The ribs are highly polished to provide the necessary thermal control. Unfurling of the antenna is accomplished by releasing pretensioned springs. The RF performance data predicted for the UHF reflector are show in Table 33.

TABLE 33. UHF ANTENNA PERFORMANCE

Frequency band	400.5 to 401.5 MHz
Aperture diameter	1.3 meters
Aperture gain*	15.0 dB
Reflector surface loss	0.02 dB
Reflector mesh I^2R loss	0.08 dB (0.317 cm)
Hybrid loss	0.16 dB
Coaxial cable loss	0.09 dB
VXWR loss (1.3:1)	0.08 dB
Total loss	0.43 dB
Antenna peak gain	14.57 dB
Antenna FOV gain (±13 deg)	12.50 dB
Antenna FOV gain (±15 deg)	11.82 dB
Polarization sense	Circular

*L. R. Dod, Backfire YAGI Antenna Measurements

4.3.3.4 AGIPA - VHF Antenna

A four-element YAGI array has been selected for the adaptive ground implemented phased array to provide the low data rate user return link. The YAGI elements are positioned in a square pattern on a 1.8 (wavelength) diagonal spacing forward of the spacecraft despun platform. The individual YAGI elements are 0.92 λ long and employ a set of four crossed dipole-reflectors, driven dipoles and directors. These dipoles are nested around a central support rod for launch. The four rods in turn are hinged to deployable arms which erect from the rigid spacecraft antenna mast (see Figure 89). The RF performance for the individual elements is illustrated in Figure 90 as determined from Jasik-Antenna Engineering Handbook.

4.3.3.5 S Band Transponder Antennas

An S band order wire antenna is used for initiating the user linkup. The antenna is identical to the UHF antenna, except scaled to S band. The reflector is made from perforated sheet metal for low cost and light weight. Single sense circular polarization is generated by slotfed crossed dipoles. Omnidirectional antennas are also provided to support backup TT&C operations.

4.3.3.6 Tracking Mechanisms

Motorized two-axis drives are used for the high gain S/Ku band antenna and the Ku band reflector positioning in azimuth and elevation. The selected position control elements are direct digital in operation and incorporate power off magnetic holding to permit power conservation by requiring spacecraft power only when the antenna is in motion. This magnetic detent is effective for each single step of the motor; therefore, no accuracy anomalies occur when power is removed.

The drive mechanism in Figure 91 is a two-axis positioner (elevation over azimuth) that moves its assigned load through ±16 degrees in azimuth and elevation. The two axes are driven by identical motor drive assemblies and are joined by a gimbal structure resulting in an elevation over azimuth configuration. The gimbal assembly is supported in each axis by the preloaded angular contact ball bearings of the motor drive assembly and by an outboard radial deep groove bearing. The bearing size is determined for launch load imparted to the mechanism, and bearing spacing is chosen sufficient to minimize error due to bearing runout. Dry film lubrication is used throughout the mechanisms for temperature range compatibility and to avoid the need for sealing the moving elements. The lubrication technique has been proven on previous Hughes programs and is amenable to the accuracy requirements and the torque capability of the drivers. The S band antenna positioner employs coaxial rotary joints for low RF loss (total of 0.2 dB). The Ku band drive mechanism has rotary waveguide RF power transmission across its axes.

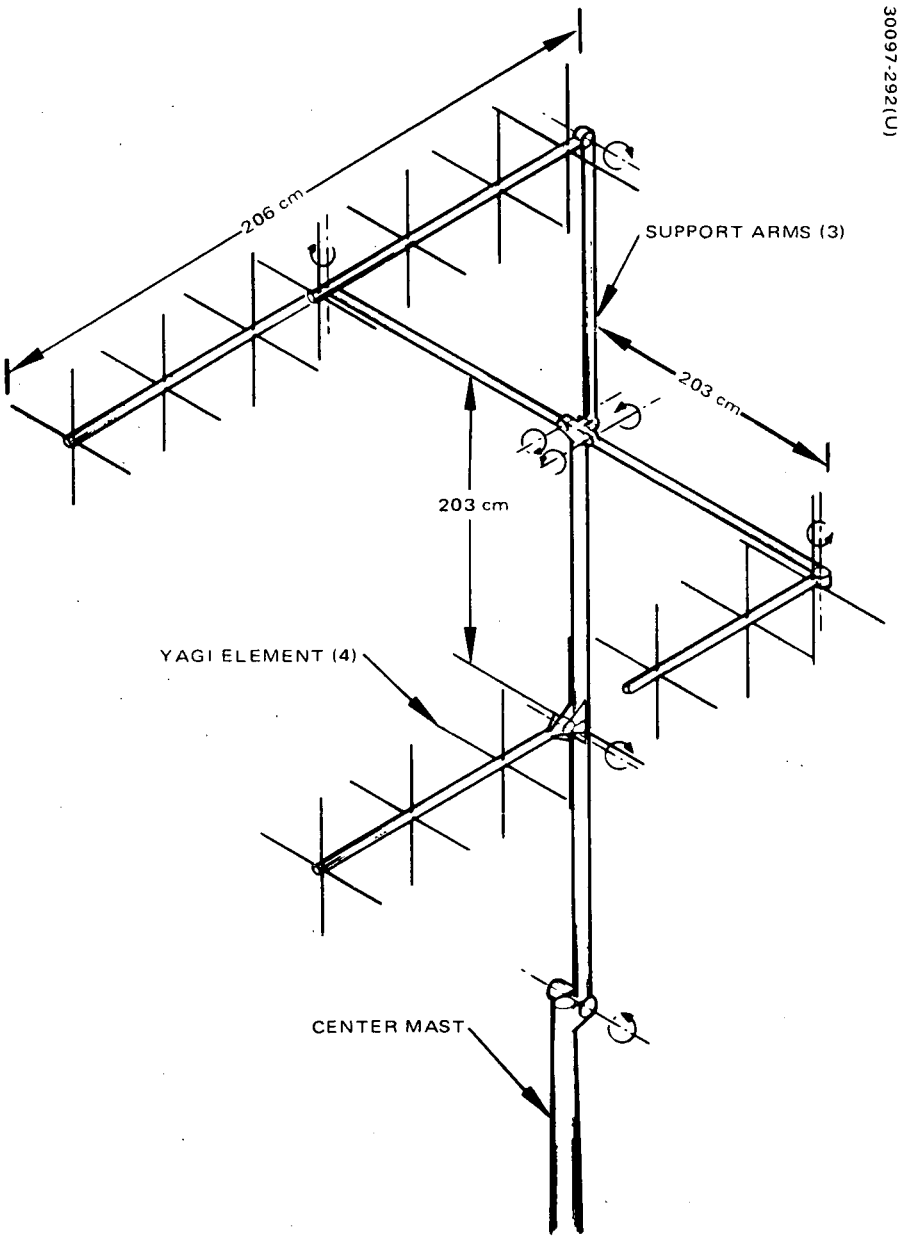

Figure 89. AGIPA Configuration

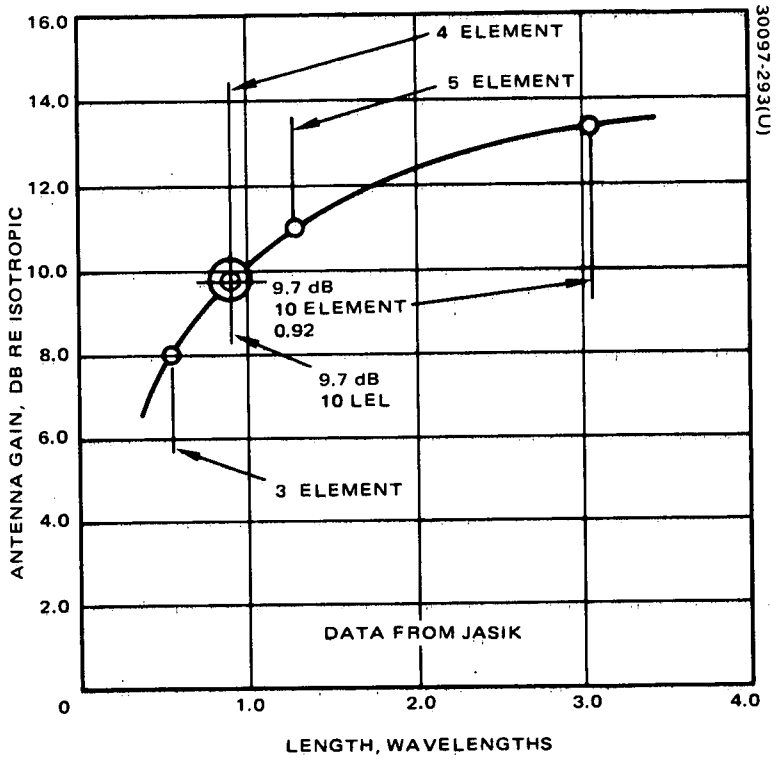

Figure 90. Yagi Antenna Gain Versus Length

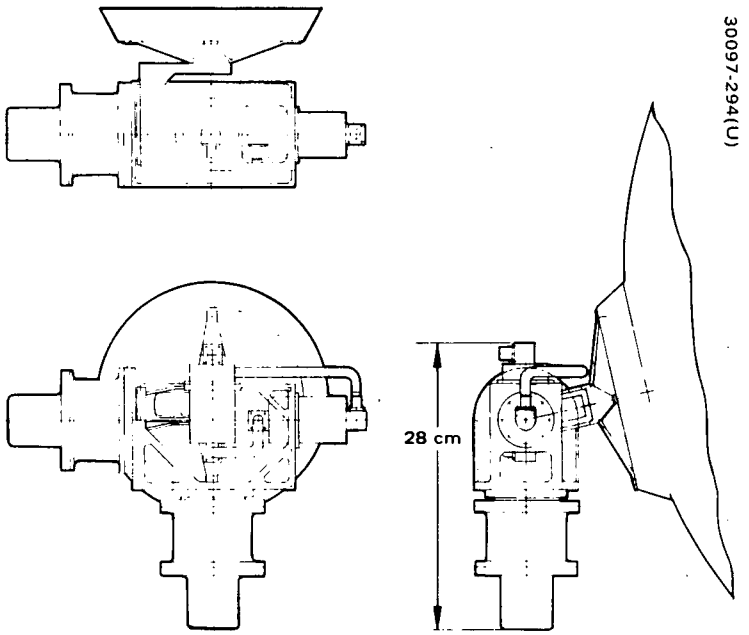

Figure 91. Two Axis Antenna Positioner

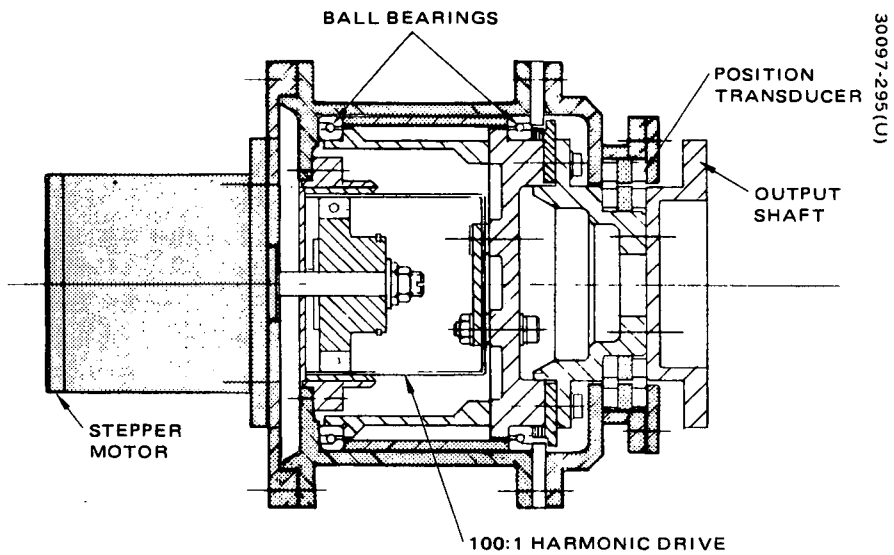

Figure 92. Antenna Positioner Drive Unit

The drive mechanism is powered by a permanent magnet, bifilar-wound, phase-switched stepper motor, producing 200 steps per revolution 1.75 degrees per step. The motor provides ample torque at stepping rates beyond the maximum required for this application and provides positive magnetic holding torque when power is removed. The transmission selected is a high ratio harmonic drive with a reduction of 144:1 resulting in a nominal gimbal movement of 0.0125 degree for each pulse to the stepper motor. The antenna positioner drive unit is shown in Figure 92.

4.3.4 Attitude Control

Attitude stabilization of the TDR spacecraft is achieved through vehicle gyroscopic stiffness developed by the spinning rotor, with both active control and passive energy dissipation on the despun platform assuring asymptotic stability of the spacecraft spin axis orientation. This Gyrostat concept has been successfully demonstrated during the TACSAT and Intelsat IV programs. The attitude control system establishes, monitors, and controls the vehicle spin axis orientation to provide a stable platform for antenna positioning, along with controlling the azimuth orientation of the despun platform for precision antenna pointing. The attitude control system is composed of the spin-axis control and despin control subsystems.

Spin axis attitude control functions include:

1) Establishment of a desired inertial spin axis attitude and maintenance of the attitude in the presence of external disturbances and orbital variations.

2) Provision for telemetry information to accurately determine the spin axis orientation by ground analysis of the telemetered data

3) Provision for dynamic stabilization of the desired spin axis attitude

The despin control functions include:

1) Control of the azimuth orientation of the despun platform to the required accuracy

2) Provision for platform rate stability in the event of loss of an inertial despin reference

3) Provision for dynamic stabilization of nutation

The design criteria involved in spin axis orientation control are:

1) Spin axis control subsystem must provide vehicle asymptotic nutational stability, with residual nutation consistent with antenna pointing accuracy requirements.

2) Nutation transients that occur in normal operation (such as those due to attitude correction maneuvers) must be rapidly damped.

3) Vehicle must be autonomously stable in failure modes involving large nutation angles.

4) Spin axis control requirements

• North-south error allocation	0.10 degree
• Orientation determination	0.02 degree
• System nutation damping time constant	5 minutes

Two stabilization principles are available for satisfying these requirements: The first is the energy sink criterion which states that a Gyrostat configuration with energy dissipation on the rotor may be made nutationally stable by providing sufficient energy dissipation on the despun portion. The second principle is that a Gyrostat configuration with an asymmetrical platform may also be stabilized nutationally using only torques applied by the despin motor. The energy sink analysis provides a means for estimating accurately the nutation damping or dedamping time constant associated with any passive dissipative device. Because the separate effects on system stability are only very weakly coupled, the total system nutation damping time constant may be calculated using a principle of superposition.

The despin control subsystem functions as a closed loop, autonomously operating control system that orients the payload antenna toward the earth while the rotor spins about an axis normal to the orbit plane. Table 34 summarizes the basic despin control system design criteria.

The motor torque requirement is established by both the desired margin over bearing friction torque and the torque necessary to overcome dynamic interaction torques that can arise during recovery from a temporary loss of despin control. The presence of a substantial cross product of inertia after deployment of the antenna payload leads to an interaction between spacecraft nutation and the despin control system. By proper design of the control loop dynamics, this coupling can be used to augment the primary attitude stabilization provided by the nutation damper.

The ability to recover automatically from a flat spin condition resulting from loss of despin control has been accommodated by incorporation of two features in the design of the despin subsystem.

1) The initial state of the despin subsystem is to be on when the bus voltage exceeds a certain minimum with both motor drivers active. For the flat spin condition with zero relative rate between platform and rotor, rate loop logic will command full saturation torque to both motors in the direction opposing friction.

TABLE 34. DESPIN CONTROL DESIGN CRITERIA

East-west error allocation	(3σ) 0.20 degree
Design life	7 years
Torque required per motor	2.712 Nm (Stall)
	0.814 Nm (at 100 rpm)
Nutation coupling	Stable coupling for all modes
Required modes of operation	Earth tracking
	Earth acquisition
	Rate command
	Ground override
	Rate hold
Initialization state	Select center earth sensor
	Both motor drivers on
	Zero commanded rate
	Low gain mode

2) The available motor torque for zero relative rate is sufficient to overcome the opposing dynamic torques due to residual rotor asymmetry and the effects of dedampers.

In addition to the normal earth pointing mode and acquisition mode, a ground control mode of inertial platform rate for transfer orbit operation and a ground override control mode for backup design control is desirable. Furthermore, if earth sensor pulses are temporarily absent, the despin system must maintain the platform rate at a small enough value to maintain linear operation of the nutation damper to ensure nutational stability.

4. 3. 4. 1 Baseline Design Description

Attitude Control

Figure 93 is a functional block diagram of the attitude control subsystem. It involves all components that determine and establish the spin axis orientation in inertial space and assure the spacecraft attitude stability.

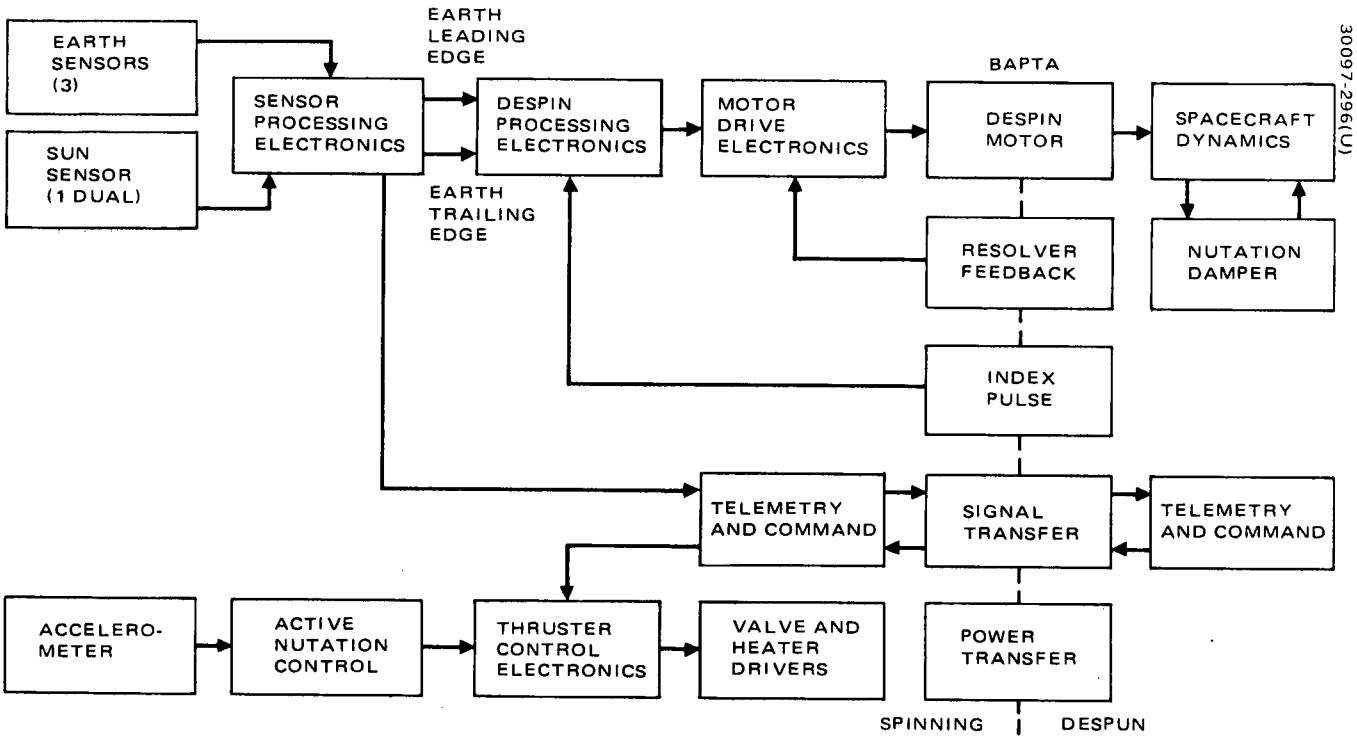

Figure 93. Attitude Control Subsystem Block Diagram

Determination and control of the spin axis attitude is similar to that used for TACSAT and Intelsat IV, using rotor mounted sun and earth sensors. The sun sensor provides pulse pairs for measurement of the angle between the sun line of sight and the spacecraft spin axis, while the earth sensors provide earth chord width information for attitude measurements. Corrections to the attitude are made using ground-commanded pulsing of the jets.

Sensor information for attitude determination is processed by the Hughes ATDET computer program currently used for on-orbit control of TACSAT I. This program models disturbance torques, sensor biases, and attitude commands, and produces a least squares fit of attitude to the data. Intelsat IV has demonstrated the adequacy of this system for spogee boost. by TACSAT I and Intelsat IV. The processing algorithm used permits on-orbit calibration of the sensors and updating of solar torque estimates.

Studies performed for Intelsat IV show that in the orbit normal attitude, during transfer orbit, attitude may be determined to 0. 2 degree (3σ) accuracy. TACSAT experience indicates that an on-orbit accuracy of 0. 02 degree (3σ) after calibration of sensor biases is achievable.

The TDRS attitude stabilization design incorporates despin control damping of nutation along with using the passive, platform mounted, eddy current nutation damper. The stability of the spin axis attitude is illustrated in Figure 94. The figure summarizes the nutation damping time constants for the individual elements of the attitude control subsystem as a function of nutation angle. Together these elements provide redundancy and substantial performance margin.

In addition to the techniques for stabilizing the nutation by action of internal elements, an active nutation control (ANC) loop using reaction jets has been incorporated to stabilize nutation in a failure mode or to reduce transient nutation during the apogee motor firing and antenna deployment phases of the mission. The ANC system is essentially the same as that used on Intelsat IV. It is provided as a backup during transfer orbit and as an extra margin of nutational stability during this critical portion of the mission. The method of actively controlling nutation is the following:

1) An accelerometer detects the presence of nutation and establishes the phase and amplitude of the motion with respect to a rotor-fixed coordinate system.

2) The accelerometer output signal is threshold-detected, amplified, and converted to a jet command.

3) The axial jet fires once per nutation cycle for some fraction of the cycle that results in the application of a transverse torque in opposition to the nutation motion.

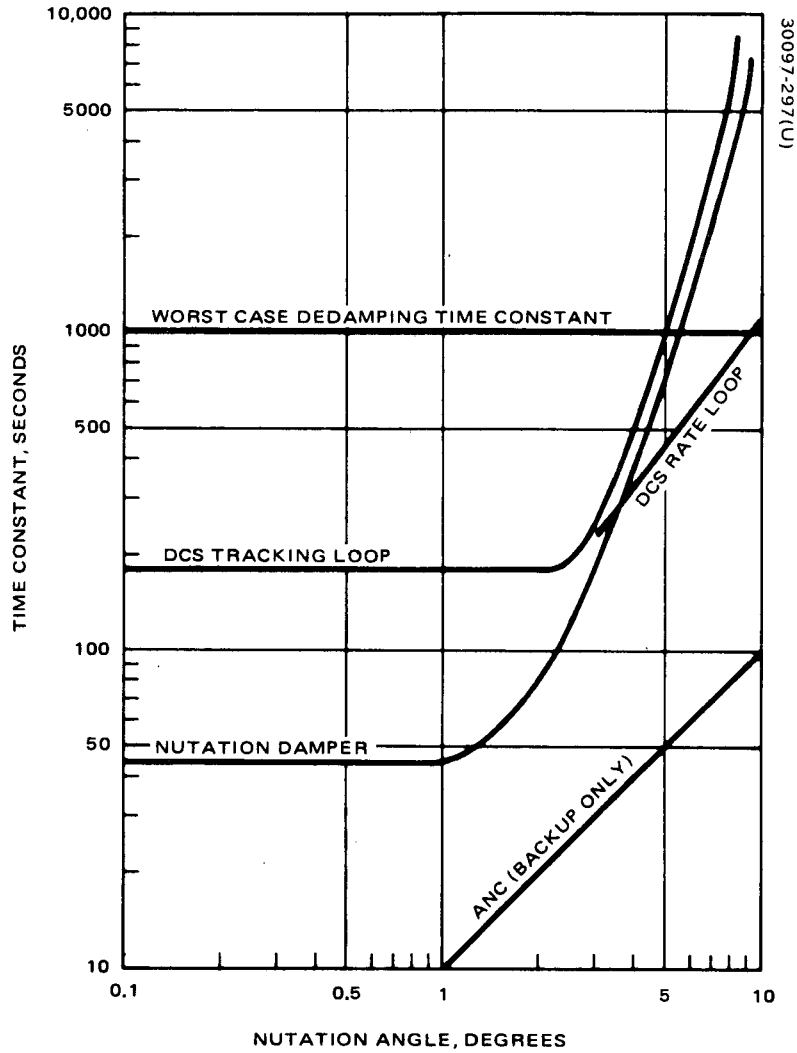

Figure 94. Stabilization Time Constants Versus Nutation Angle

The sensor that provides the desired turn-on and turn-off signals is a single-axis, force rebalance type accelerometer. The sensor provides a sinusoidal signal at rotor nutation frequency and an amplitude proportional to the nutation angle.

The signal conditioning unit (ANDE) monitors the accelerometer sinusoidal voltage (a lead filter rejects the dc component due to spin axis tilt and accelerometer misalignment), compares the negative portion of the filtered signal to a preset threshold level, and sends control pulses to activate the axial jet solenoid driver when the threshold voltage is exceeded. The duration of the jet command is directly proportional to the time interval during which the acceleration exceeds the threshold value.

On the Intelsat IV spacecraft, while the ANC system has not been required to maintain nutation stability during normal mission operation, the design implementation has been verified in orbit. Following the apogee motor burn on the F-4 spacecraft, the ANC system was observed in operation reducing the 1 degree nutation transient to threshold 0.4 degree. On the first two spacecraft, the ANC operation was not observed, but the accelerometer signals received shortly after thrust termination strongly suggest that the nutation was actively reduced to threshold.

Despin Control

Figure 95 is a simplified block diagram of the despin control subsystem (DCS). The DCS is composed of three major elements:

1) Earth Sensors – Three independent earth sensors are mounted on the spinning rotor and are used to supply rotor phase information relative to the earth center to the despin control subsystem. For on-station operation, only a single earth sensor is required for despin control. Use of three elevation orientations allows selection of the sensor to be used by ground command well in advance of sun or moon interference and provides adequate redundancy.

2) Bearing and Power Transfer Assembly – The bearing and power transfer assembly (BAPTA) provides electrical and mechanical interconnection between the spinning and despun sections of the satellite. The BAPTA consists of a bearing assembly, a motor drive assembly, and a slip ring assembly for signal and power transfer between the spun and despun sections of the spacecraft.

3) Despin Control Electronics – The despin control electronics (DCE) (shown in Figure 96) processes the inertial rotor phase information from the ground-selected earth sensor and the relative platform phase information from the MIP (sampled once every rotor spin revolution) and generates continuous control torque commands to the BAPTA torque motor. It contains both

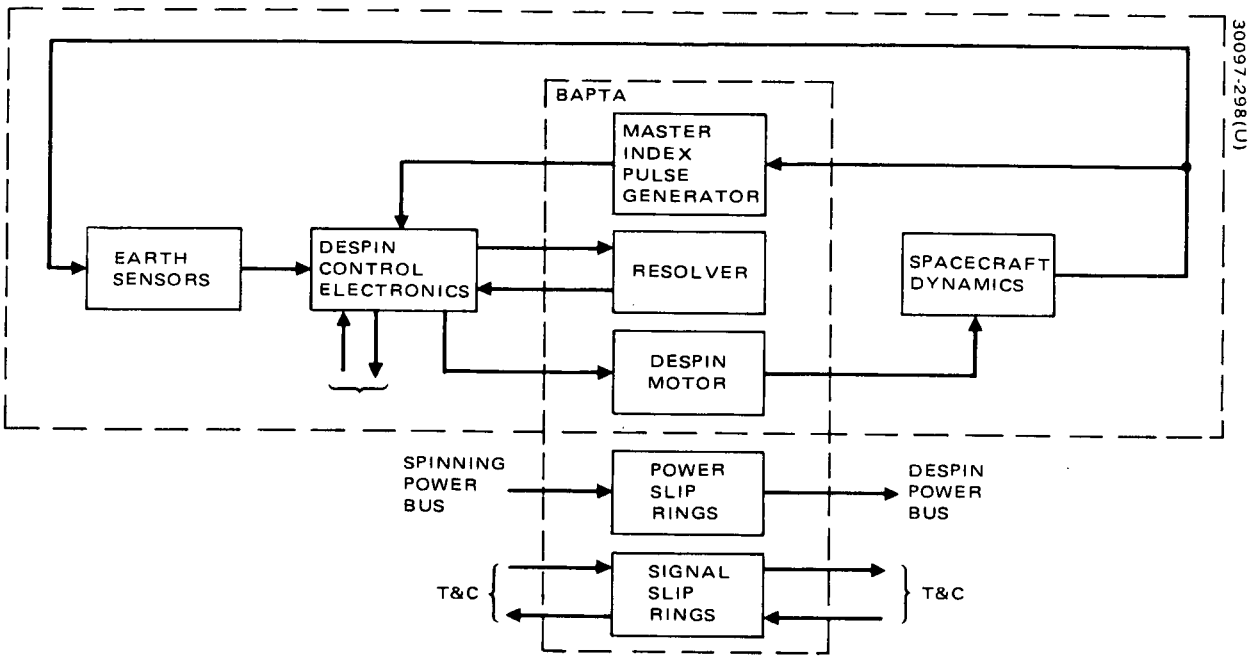

Figure 95. Despin Control Subsystem Block Diagram

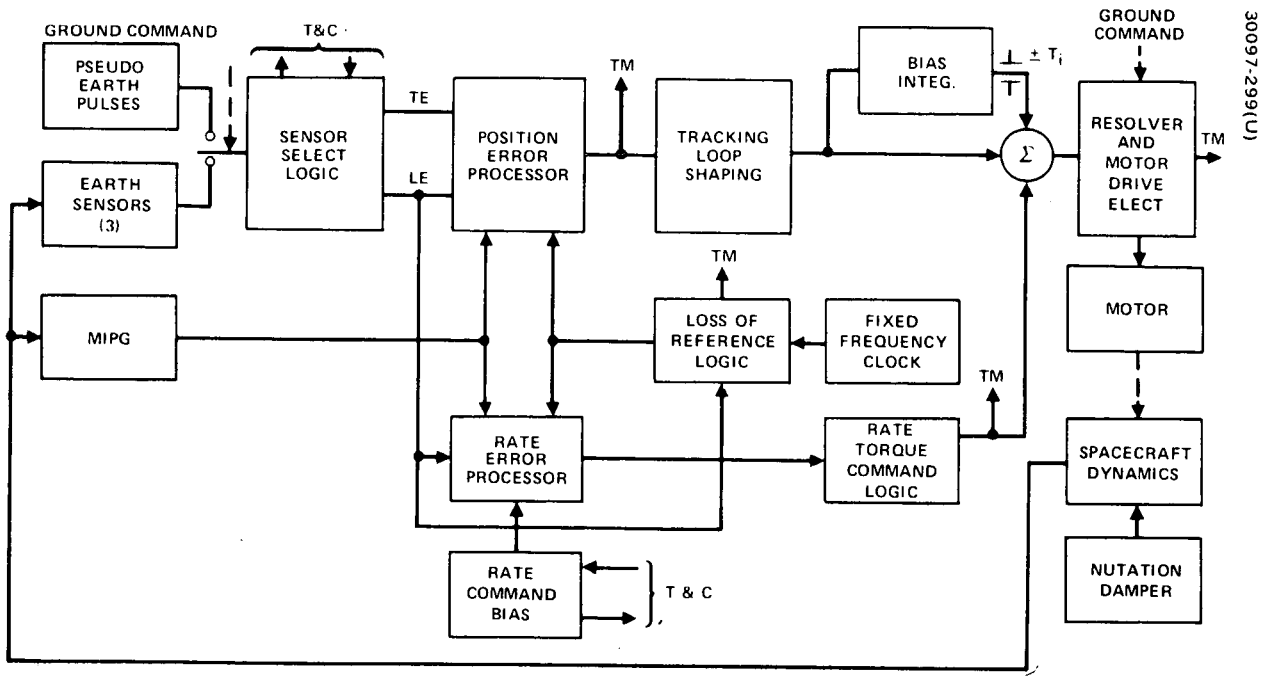

Figure 96. Despin Control Electronics Functional Block Diagram

rate and tracking loop control logic to ensure automatic despin of the platform and acquisition of the earth. The DCE contains the loss of sensor detection logic to provide platform rate stability in the event of loss of an earth sensor, and accepts ground commands for platform rate control and failure mode ground despin control.

The detailed design of each element in the attitude control system is given in subsection 4. 3. 4. 3.

Operational Modes. There are four basic operating modes for the despin control subsystem:

1) Normal earth tracking (low gain and high gain)

2) Controlled inertial platform rate

3) Pseudo-earth control

4) Rate hold mode

In the normal tracking mode the despin system aligns the despun antenna borewight to the center of the earth as sensed by the selected spinning earth sensors. Because of the wide variation in the platform inertia due to antenna deployment, a low gain tracking mode has been implemented for initial orbital operation of the despin subsystem. When the DCE is turned on, a lower control loop gain is activated. This gain provides good stability margins for the control system during transfer orbit and after antenna deployment. Once initial orbit is achieved and the antennas are deployed, a ground command to change to the higher gain mode is required.

The rate control mode uses an inner rate loop to ensure automatic despin and acquisition during initial rotor spinup and following apogee boost. A three-level ground-commandable ±12 and -24 degrees/rate bias is included in the DCE for controlling the platform rate prior to apogee boost in order to average the effects of platform cg offset. The magnitude of the maximum commandable rate torque is scaled to override the tracking loop and generate the desired platform rate.

In pseudo-earth mode, the tracking and rate loops operate using ground-transmitted leading and trailing edge pulses, which are locked in frequency to the rotor spin rate. The required spin synchronous pulse train is obtained by use of the sun sensor pulses which are available on real time FM telemetry. An additional sun pulse delayed by 14 degrees of spin phase from the telemetry sun pulse is created. This pulse train is then sent through the normal command channel to the despin control electronics. By controlling the phase of the channel to the despin control electronics. By controlling the phase of the retransmitted pulses with respect to the original sun pulse, the azimuth orientation of the payload antenna can be controlled.

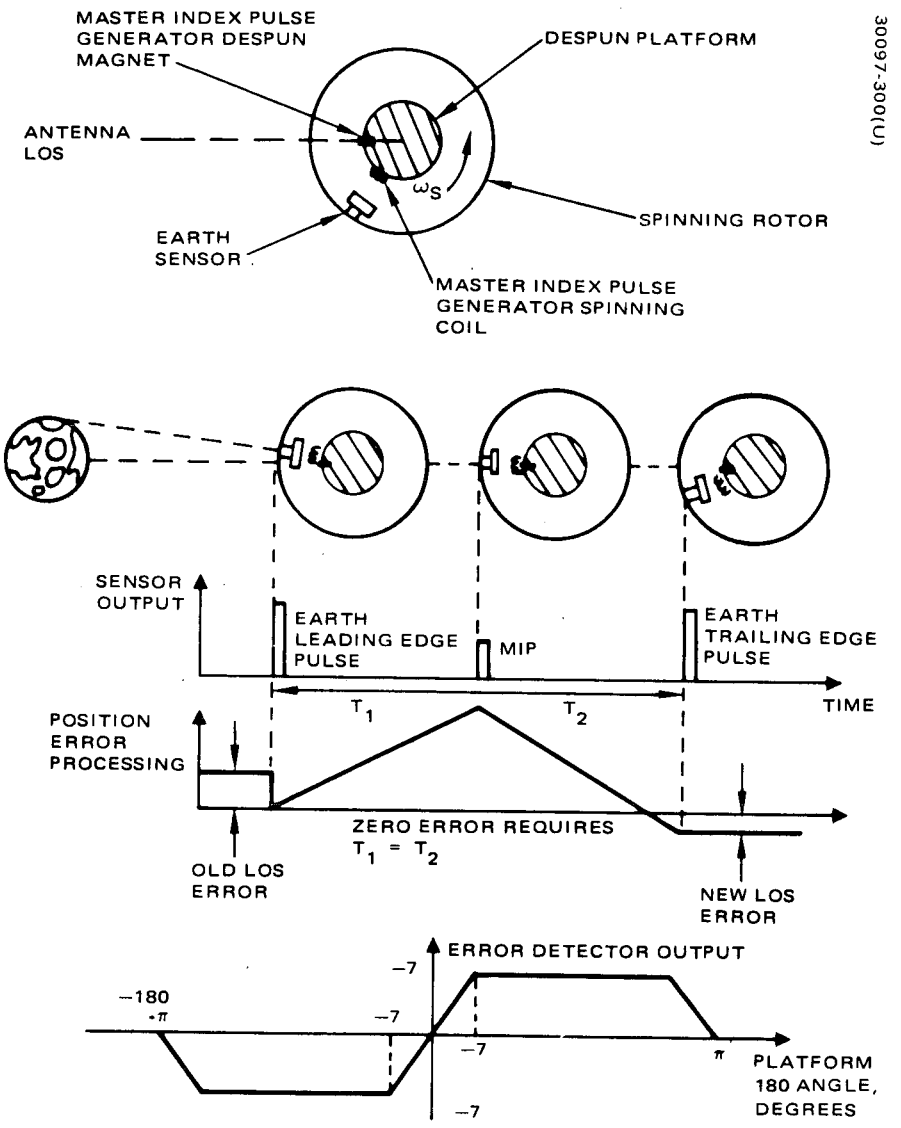

Figure 97. Formation of Despin Position Error Signal

In the event of loss of earth sensor pulses, automatic onboard logic will supply a once per revolution pulse to the rate control logic. The pulse frequency is based on a fixed clock rate (internal to the DCE) set to the nominal spin speed. Therefore, in event of a sensor loss, a slight platform rate will develop due to deviations in actual spin speed from the nominal. By ground commanding an alternate sensor, automatic despin and reacquisition will occur.

Signal Processing. Determination of the platform orientation is accomplished by means of an earth center-finding technique, similar to that used successfully in the TACSAT despin control system. The derivation of the pointing error signal is illustrated in Figure 97. The earth leading edge pulse from the selected earth sensor initiates a fixed rate integration within the error detector. At the occurrence of the MIP, the slope of the ramp is reversed. The earth trailing edge pulse from the sensor stops the ramp. If the MIP, which is aligned mechanically to the antenna boresight, occurs halfway between the leading and trailing edge pulses, the error is zero. Deviation of the MIP occurrence from the center earth position will result in a nonzero output of the error integrator as sampled at the earth trailing edge pulse. This sampled error (obtained once every rotor spin revolution) is directly proportional to the inertial angular east-west error of the despun platform. At the occurrence of the trailing edge pulse, the sensed error is held constant for the entire spin revolution and the integrator is reset to zero. This process is repeated at the occurrence of each earth leading edge pulse.

The linear range of the error detection is 7 degrees for north earth and south earth oriented sensors and 8 degrees for the center earth sensor. For errors beyond the linear range (as in the case when the platform is rotating), the sensed error is held at plus or minus the saturation value by the DCE. By use of an electronically generated delayed MIP, which is 180 degrees away from the actual MIP, the pointing error characteristic (as shown in Figure 97) can be achieved. This ensures the correct platform direction of rotation during acquisition for shortest acquisition time.

Determination of inertial platform rate (as is shown in Figure 98) is similar to the technique used for Intelsat IV and is accomplished by measuring the change in platform position over one rotor spin revolution. The rate logic utilizes the earth leading edge and MIP pulses along with a fixed frequency clock to digitally form this first-back-difference of position. At the occurrence of the earth leading edge pulse, an upcounter is set to zero and proceeds to count from the leading edge pulse to the MIP, using a crystal-controlled oscillator as the basic count clock. At the occurrence of the MIP, the number occurring in the upcounter is transferred to a downcounter and the downcounter is allowed to count from the next leading edge pulse to MIP. At the occurrence of each MIP, the number contained in the downcounter

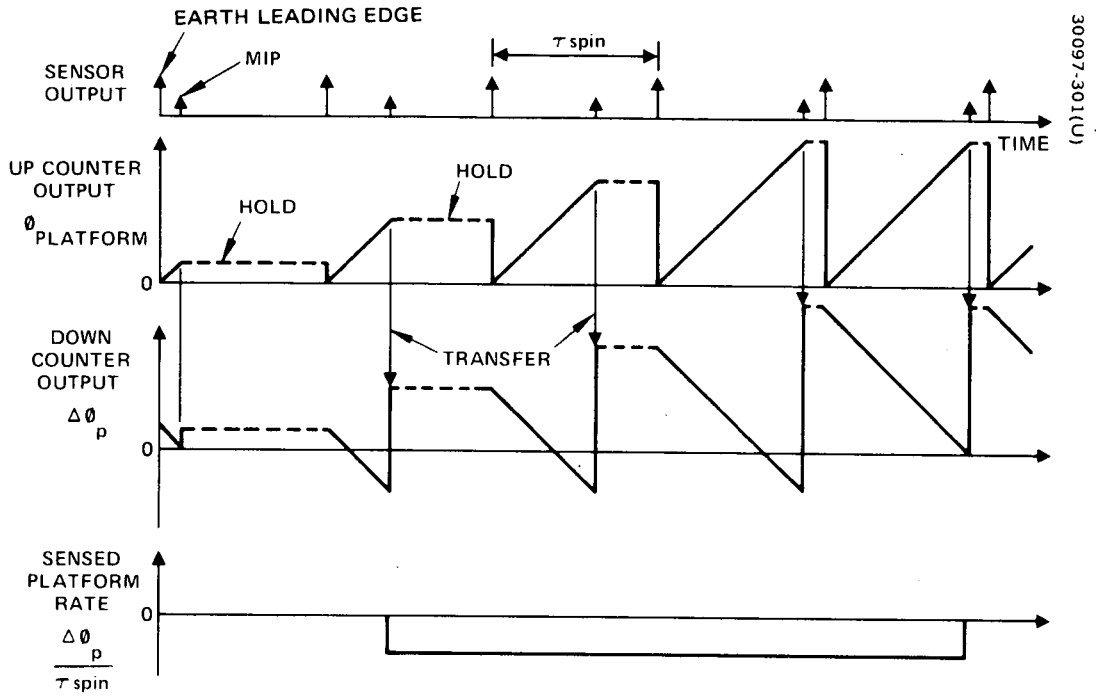

Figure 98. Rate Error Detection

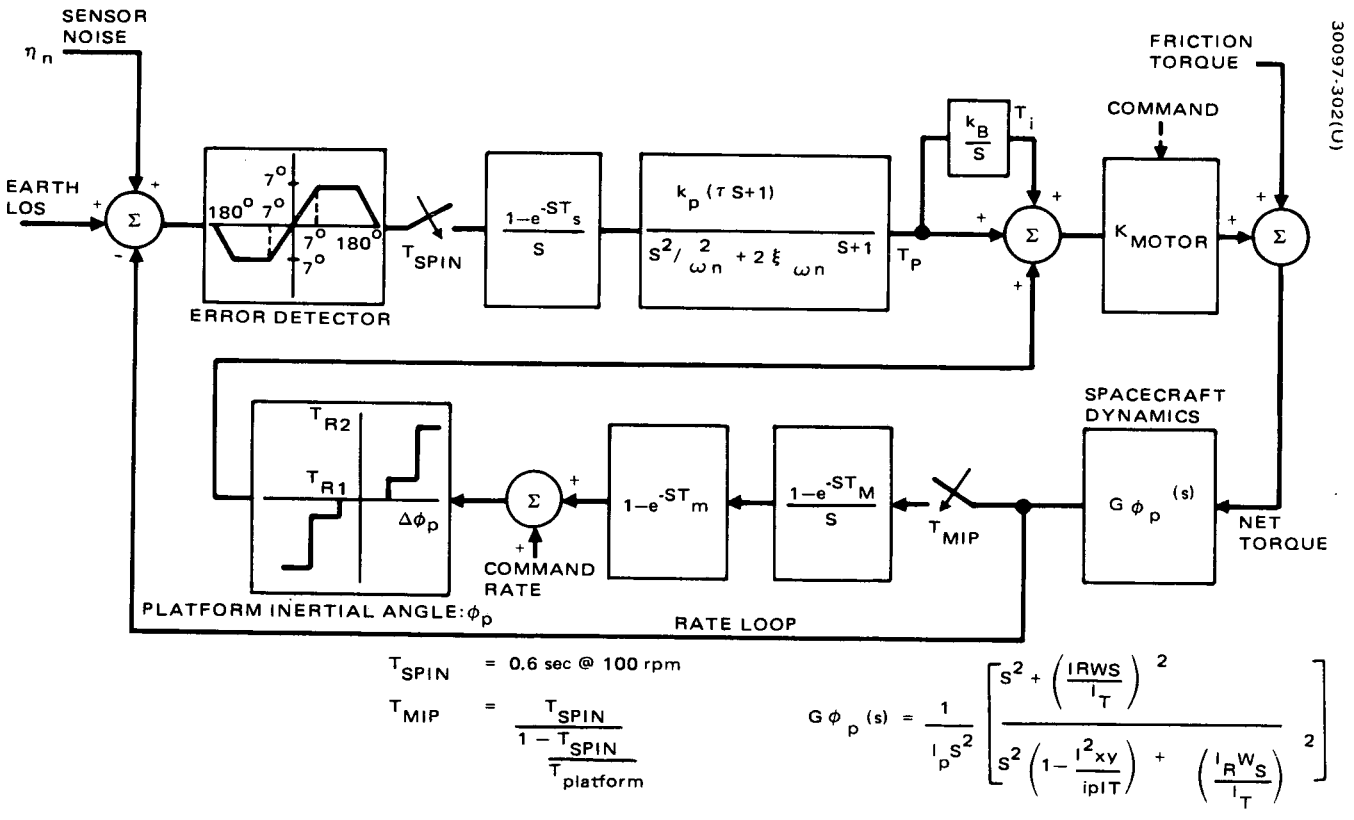

$$T_{SPIN} = 0.6 \text{ sec @ } 100 \text{ rpm}$$

$$T_{MIP} = \frac{T_{SPIN}}{1 - \frac{T_{SPIN}}{T_{platform}}}$$

$$G\phi_p(s) = \frac{1}{I_p s^2}\left[\frac{s^2 + \left(\frac{IRWS}{I_T}\right)^2}{s^2\left(1 - \frac{I^2_{xy}}{ipIT}\right) + \left(\frac{I_R W_S}{I_T}\right)}\right]^2$$

Figure 99. Despin Control Subsystem Analytical Model

represents the change in platform position over one sample. Thus, for a given spin speed the sensed rate can be determined from

$$\dot{\phi}_{\text{Platform}} = \frac{\Delta\phi_P/\text{sample}}{T_{\text{spin}}\ \text{s/sample}}$$

(spin period = 0.6 s at 100 rpm)

Since only the earth leading edge pulse and MIP are used in the rate error processing, the chordwidth variation does not affect normal rate loop operation.

The operation of the tracking loop is illustrated in the analytical model shown in Figure 99. The sampled and held output of the position error detector is used to drive an analog shaping network whose dynamics have been selected to provide stable closed loop pointing control and meet the despin system requirements. The resulting output of the shaping network is a torque command to the BAPTA.

The rate control loop is implemented as a bilevel deadband bang-bang controller. The two-level staircase prevents an undesirable limit cycle while providing rate loop nutation damping for large nutation angles, which would cause nonlinear tracking loop operation. During normal on-station operation, the tracking loop supplies all necessary pointing control and the rate loop is effectively deactivated, since the platform rates are well below the deadband value. The platform rate error is compared to one of four fixed ground-commanded levels at the input to the rate torque command logic. A nonzero rate command results in rate loop torques that override tracking loop torque such that the resulting platform rate is the commanded value plus or minus the small deadband value of the rate torque characteristic. The commanded rate mode is used during apogee boost to average out transverse torques caused by platform cg offset. The rate error processing accounts for all possible conditions of platform rate, pulse sequencing, etc. In particular, the rate sensing logic recognizes either the absence of MIPs, or MIPs at a very low rate, as a command for full negative motor torque. This logic provides the necessary torque command function for autonomous flat spin recovery.

The motor used in the despin control subsystem is essentially a two-phase 16-pole ac motor that requires in-phase sine and cosine driving voltages to generate the required rotating magnetic field. To operate as a dc motor, these sine and cosine voltages must be artificially generated. As is shown in Figure 100, this is accomplished by using a resolver in the BAPTA, which is essentially a transformer having both the primary and secondary windings on a stator element and with a transformer core rotor

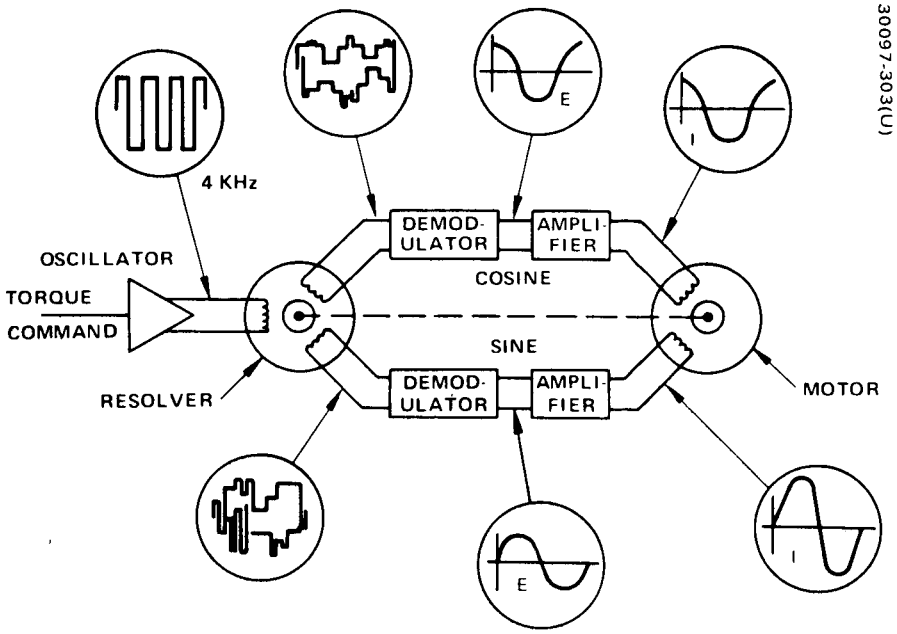

a) MOTOR DRIVE SYSTEM

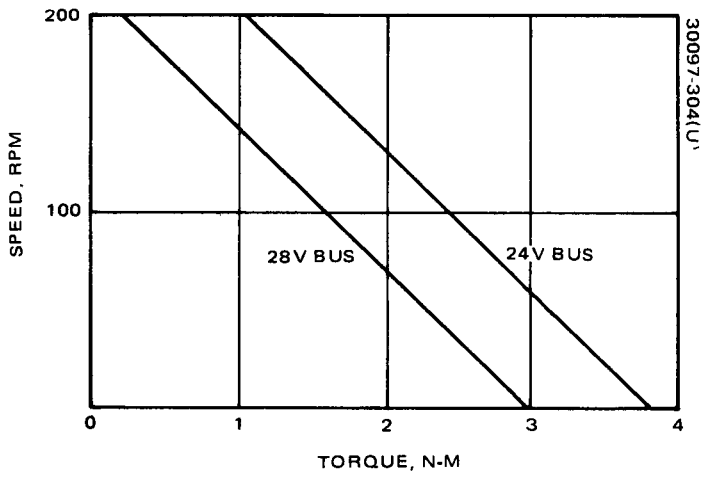

b) SPEED VERSUS TORQUE

Figure 100. Despin Motor Characteristics

design to provide a sinusoidal variation in the magnetic coupling between the windings as a function of the shaft rotation angle. A precise phase relation is maintained between the motor rotor and resolver by keying them to a common shaft. The resolver is excited by a 4 kHz carrier from the DCE. The sine and cosine resolver outputs are then synchronously demodulated to remove the carrier and amplified to drive the respective motor windings. The BAPTA motor has two sine and two cosine windings. One sine/cosine pair is driven by the motor driver circuits in a single despin control electronics unit. However, the DCE motor driver inputs are cross-strapped so that each DCE can drive either or both of the motor driver/motor pairs.

The available motor torque with a single motor driver active is shown in Figure 100. Under stall conditions (i.e., zero relative rotor/stator rate), the maximum torque is 2.98 newton-meters. As the relative rate increases, a back electromagnetic force (EMF) is developed in the motor stator windings; therefore, the torque is limited by the maximum available driving voltage, which is 19 volts at the motor winding under worst case end-of-life conditions (24 volt bus). At 100 rpm and at the expected BAPTA temperature of 294 K, the nominal friction level is 0.20 newton-meter. This implies a torque margin ratio of 7.5:1 for the low bus voltages for each motor.

When the DCE receives power, it turns on with several of the internal stages in preferred states. The DCE last utilized (ground command selected) is activated in the low gain mode. Both motor drivers are active and the ground mode logic is off. The rate bias is zero and center earth sensor is selected as the despin reference. This initialization logic is in part determined by the system requirement to recover automatically from a flat spin condition caused by battery failure upon exit from eclipse. The initialization logic described is compatible with normal spacecraft operation.

4.3.4.2 Despin Control Subsystem Performance Characteristics

Figure 101 shows the transmission of bearing friction variations to platform pointing error as a function of frequency for the tracking loop. As shown in the figure, the most sensitive region occurs for variations on the order of 30 seconds where the system transmission factor is 1 degree/newton-meter. This is a sufficiently low transmission factor, so that even relatively large friction variations would not cause loss of lock (maximum offset 7 degrees before losing lock). For lower frequencies, the feed forward integrator effectively nulls pointing errors due to friction, while at higher frequencies, the effect of inertia filtering dominates. On-station platform motion resulting from low level (-0.014 newton-meter rms) friction torque is negligible (-0.015 degree). This is a conservative estimate of expected torque noise based on in-orbit Intelsat IV data and ground test data.

The principal disturbance to platform pointing is the random error on the earth sensor leading and trailing edge pulses. The MIP pulse jitter is an order of magnitude smaller and negligible by comparison.

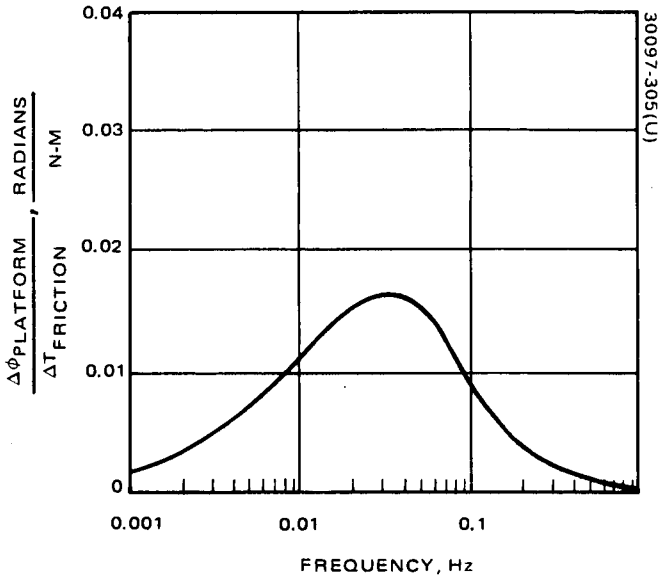

Figure 101. Platform Response to Bearing Torque Variations

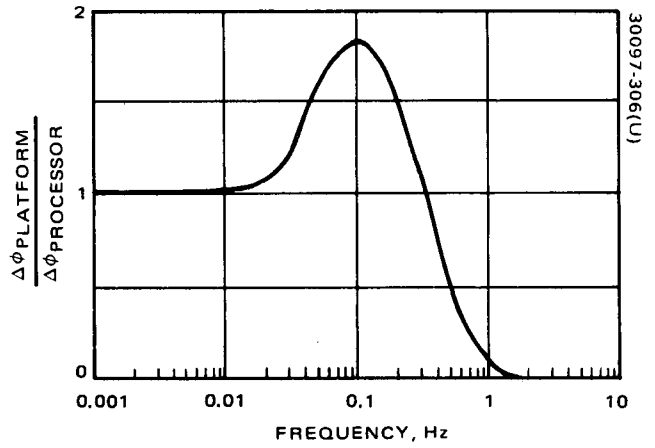

Figure 102. Platform Response to Sensor Phase Variations

Figure 102 shows the closed loop transfer function from sensor noise to platform pointing as a function of frequency for the proposed design. For a linear system, the noise transmission ratio (rms out/rms in) is simply the area under the square of the transfer function. The ratio for the tracking loop transfer function is 0.8.

The net transmission ratio, however, must also take into account an attenuation inherent in the LOS error processing. As discussed in a previous section, the azimuth error is determined by integrating at a constant slope up at the occurrence of the leading edge earth pulse and down at the occurrence of the MIP, until the occurrence of the earth trailing edge pulse. Any platform error will result in a change in MIP phasing with respect to the earth center. Analytically the error signal is

$$\phi_{\substack{\text{Platform}\\ \text{Error}}} = \int_{T_{LE}}^{T_{MIP}} S_o\,dt - \int_{T_{MIP}}^{T_{TE}} S_o\,dt$$

where S_o is a constant in degrees/s. With $T_{LE} \triangleq 0$,

$$\phi_{Error} = S_o \left[T_{MIP} - 0 \right] - S_o \left[T_{TE} - T_{MIP} \right]$$

$$= S_o \left[2T_{MIP} - T_{TE} \right]$$

if

$$T_{MIP} = T_{TE}/2 \text{ (i.e., the MIP is exactly between the earth pulses)}$$

then ϕ error = 0. If the MIP is off-center by one unit, the result of the up-down ramp will be a two-unit error. Thus, a scale factor of 0.5 is necessary in the subsequent electronics to form actual error.

For random, uncorrelated errors on both the leading and trailing edge pulses, the error in the LOS processor output voltage is $\sqrt{2}$ times the rms (or the 3 σ) noise on each of the two inputs pulses. However, with the scale factor reduction of 0.5, the net result in terms of input noise to the system transfer function is $\sqrt{2}/2$ or 0.707 of the sensor pulse jitter.

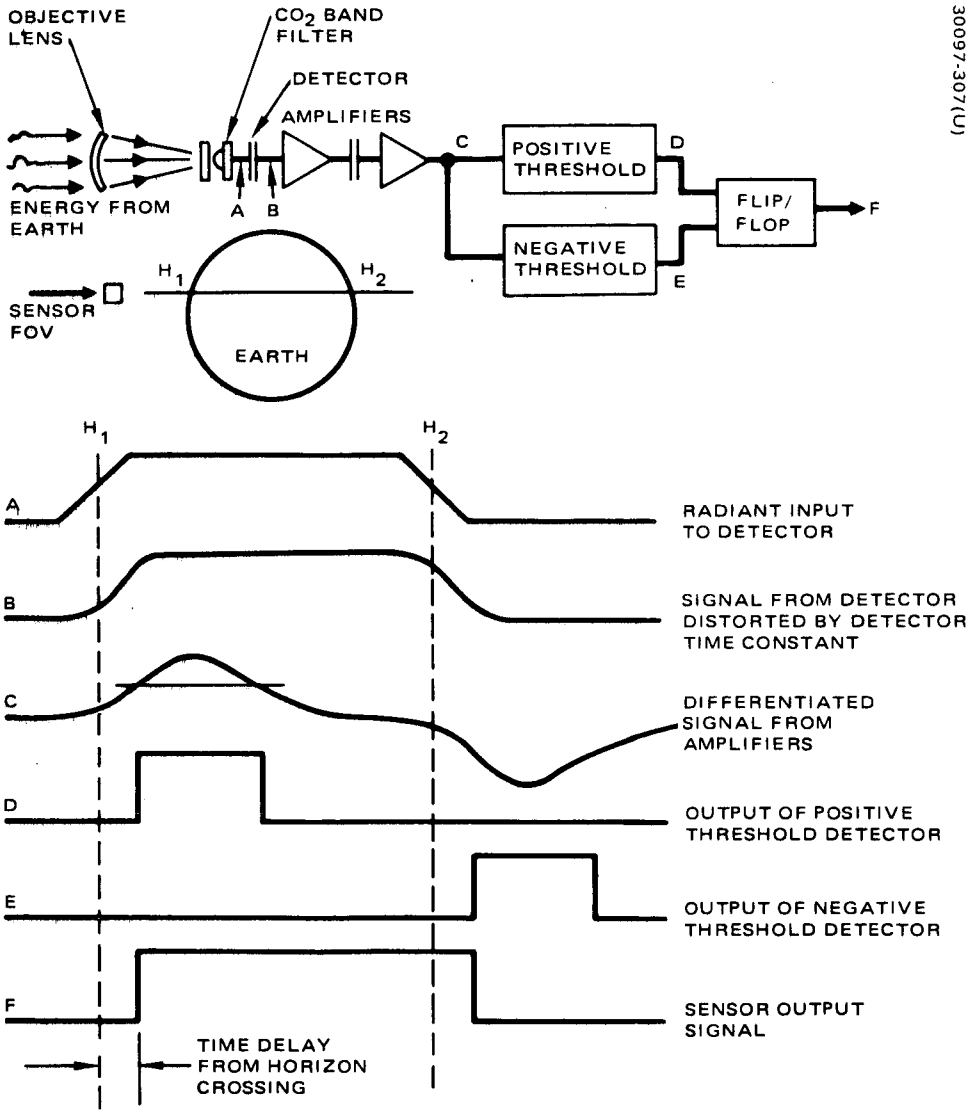

Figure 103. LMSC Type 8 Earth Sensor Block Diagram and Signal Processing

Combining the two attenuation factors, the net transmission from sensor pulse jitter to platform jitter is 0.57. For the worst case sensor noise of 0.1 degree (3 σ), the platform pointing would then be 0.05 degree (3 σ). These predictions, based on a simplified continuous data mode, have been verified using the analog simulation, as discussed below. The indicated performance is well within the allocation of 0.15 degree for platform jitter.

4.3.4.3 Component Description

The following section discusses the design of the individual elements involved in the attitude control system.

Earth Sensors

The given requirements call for three earth sensors oriented in line in azimuth and spaced in elevation such that the sun or moon cannot interfere with more than one sensor each at any time. The elevation orientations used in Intelsat IV, 0, and ±6 degrees from the plane normal to the spin axis, provide suitable separation of sensors. The sun passes through the scan path of each sensor twice per year and the moon passes through 27 times per year. All of these periods are predictable from ephemeris data, and sensor switching can be accomplished well in advance of requirements. Switching of sensors would be utilized where necessary to avoid sun and moon interferences, rather than require circuitry to inhibit the production of output pulses from scanning these sources. Such circuitry can minimize the number of times switching is required, but does not eliminate significant errors produced by scanning these sources when they near an earth edge. Without sun and moon discrimination circuits, the sensors are not damaged by sun exposure, but will produce output pulses when scanning the sun and the moon when it is very bright. The 0 degree sensor is used only for despin and the offset sensors are used for despin and attitude determination. Despin will be accomplished by centerfinding, using the space-earth (lead edge) and earth-space (trail edge) crossing pulses (or an earth-width pulse).

Known bias is allowable and <0.1 degree bias uncertainty is acceptable. Noise <0.1 degree at each earth edge crossing is desired. Satellite rotor spin rate would be 100 rpm +2 rpm. Proven technology, low mass and power, and high reliability have been emphasized. A satellite lifetime of 5 to 7 years is specified.

Figure 103 is a block diagram of signal processing of the sensor. The radiance of the warm earth is detected against the cold space background. The thermistor bolometer detector consists of an active thermistor flake immersed on a hemispherical germanium immersion lens and a compensating thermistor flake in the same package. The two thermistors are connected into a bridge network to which bias voltage is applied. The radiant energy is collected by a germanium objective lens, passes through a CO_2 bandspectral filter centered at 15 microns, and is focused on the active thermistor flake by the immersion lens. The change in resistance of the active thermistor flake produced by heat absorption when viewing the earth produces an offset voltage from the bridge. This signal is amplified, shaped, and differentiated

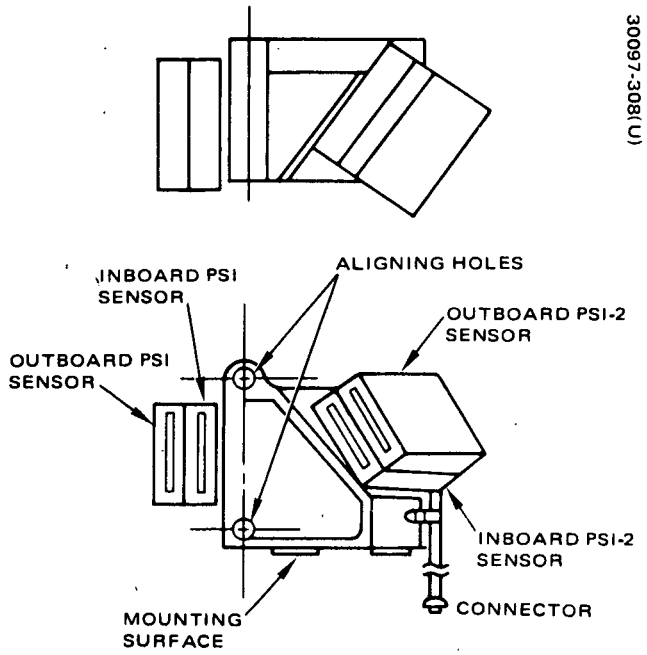

Figure 104. Sun Sensor Assembly Detail

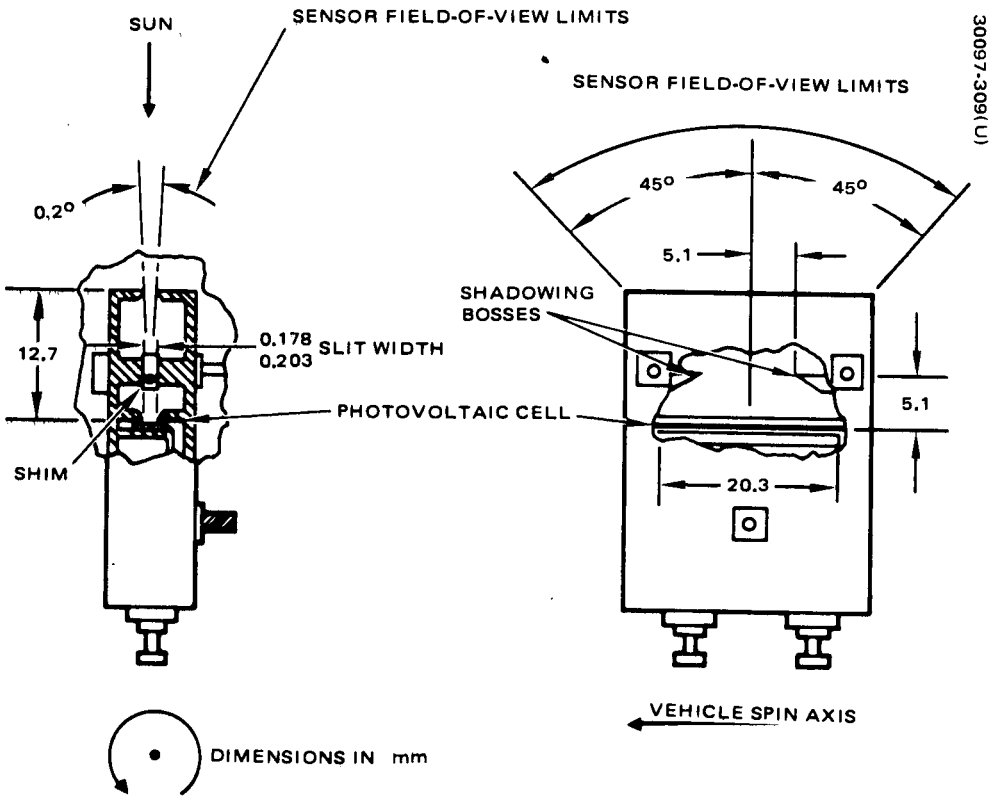

Figure 105. Single Sensor Unit Diagram

to produce analog-type pulses of opposite polarity at the leading and trailing earth edge crossings. A 5 volt amplitude rectangular output pulse is produced when the differentiator pulses trigger threshold circuits. The output pulse is started by the leading edge pulse and stopped by the trailing edge pulse. The threshold levels are variable and are set automatically at a percentage of peak of the differentiator pulses. This technique compensates for variations in earth radiance and almost eliminates error associated with fixed threshold levels due to such radiance variations.

Sun Sensor

The highly reliable sun sensor assembly provides redundant pulse pairs for determination of the spacecraft spin axis attitude relative to the sun within 0.2 degree. Identical assemblies have successfully flown on ATS, TACSAT, and Intelsat IV. The sensor is mounted to the spinning portion of the vehicle so that when the spacecraft spin axis is within 35 degrees of normal to the sunline, each sensor of the assembly produces one pulse per revolution. The angular relationship between a pair of sensors, ψ and ψ_2, is used as a measure of the polar sun angle between the sunline of sight and vehicle spin axis. The time relationship between the ψ and ψ_2 pulses is used to compute this angle. Sensor manufacturing and testing techniques have been developed during many Hughes spacecraft programs, making sensor fabrication and testing routine. All sensor parts and materials as presently used in the existing design are adequate for survival and reliable operation in the TDRS environments. The sun sensor provides accurate synchronization reference pulses used for attitude determination. Characteristics are listed in Table 35.

A sun sensor assembly (Figures 104 and 105) consists of four identical sensor units (redundant pairs) mounted on a precision bracket. Each pair of sensors provides two fan-shaped fields of view (0.2 by 90 degrees) whose planes are 35 degrees from each other. The plane of the field of view of one sensor (ϕ) is oriented parallel to the spin axis. The other sensor viewing plane, ψ_2, is inclined 35 degrees to the spin axis and rotated 35 degrees in azimuth from the ψ plane. As the sunlight enters the sensor field of view, an n/p silicon photovoltaic cell is illuminated. A voltage pulse is generated when the sun passes through the field-if-view plane. The electrical output signal from the sensor is a function of the input energy from the sun which

TABLE 35. SUN SENSOR CHARACTERISTICS

Field of view	35 degrees from ϕ = 90 degrees
Accuracy	0.2 degree spin azimuth reference
	0.2 degree sun angle measurement
Power	none
Mass	0.11 kg assembly
Redundancy	Redundant ψ and ψ_2 pairs
Reliability	0.9999 per ψ and ψ_2 pairs (5 years)

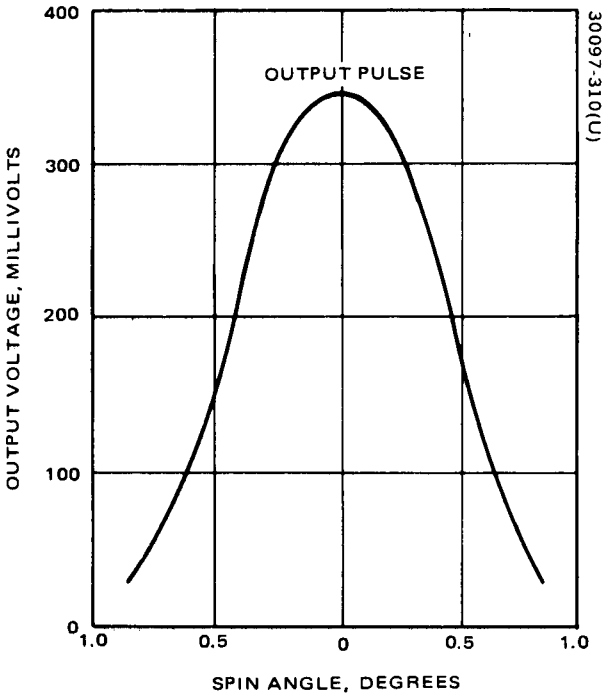

Figure 106. Typical Sensor Output Pulse

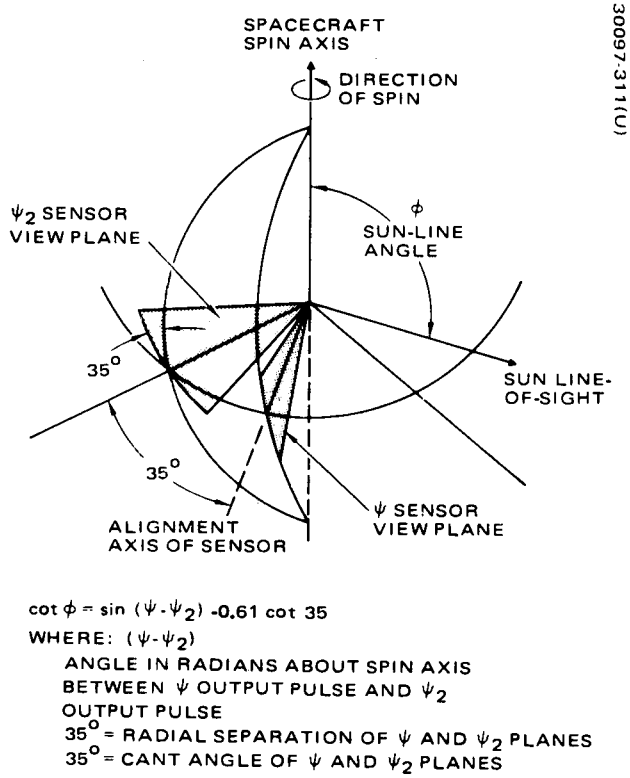

Figure 107. Sun Sensor Geometry

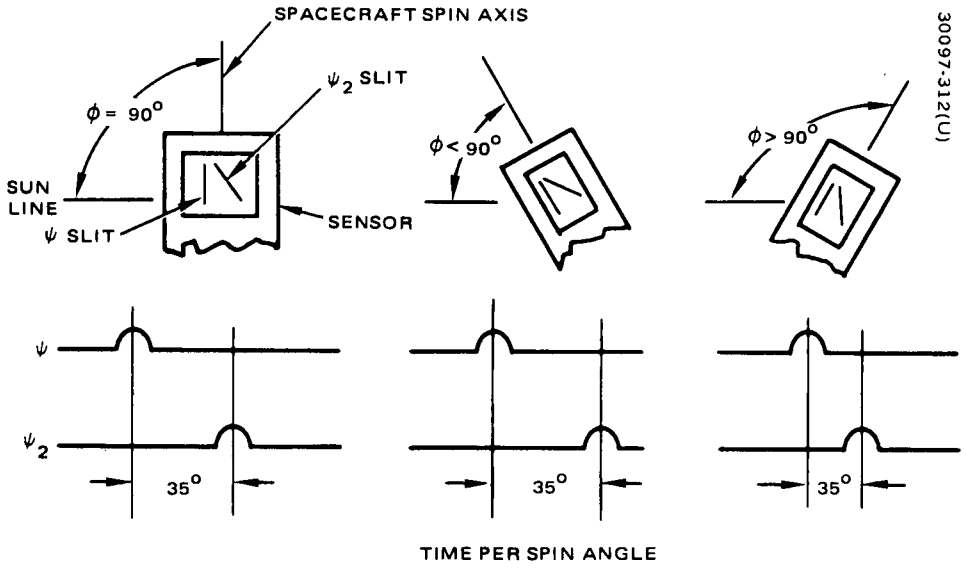

Figure 108. Phase Versus Output Timing

falls on the cell, the one kilohm load resistor and the diode loading effect of the unilluminated area of the cell. The field of view of each cell is ±45 degrees from the normal to the cell surface for specified output amplitudes.

The sensors are located on the rotating portion of the spacecraft so that the sensors produce one pulse per revolution when the spacecraft spin axis is within ±35 degrees of normal to the sunline. The width of the field of view of each sensor element in conjunction with the 0.5 degree angular size of the sun results in nominal pulse width of approximately 1.25 degrees at the 100 mV thresholding level. Due to the 35 degree inclination of the ψ_2 sensor, its nominal pulse width is 1.5 degrees. A typical output pulse is shown in Figure 106. The angular relationship between the ψ and ψ_2 sensors is used to measure ϕ, the polar angle between the sunline and vehicle spin axis. The formula that related the angle ϕ to the time of occurrence of the ψ and ψ_2 pulses is given in Figure 107. The pulse time relationship of the ϕ and ψ_2 pulses as a function of the spacecraft attitude to the sunline is shown in Figure 108. The nominal attitude accuracy of the sensor is ±0.5 degree without calibration. With both prelaunch and in-flight calibration, and by smoothing the data over a number of measurements, the sun angle uncertainty is reduced to approximately 2 degrees.

Nutation Damper

The proposed nutation damper is a scaled-down version of the unit employed on the Intelsat IV program. Figure 109 illustrates the damper and its essential design features. This eddy current damper comprises a single-axis permanent magnet pendulum subassembly suspended from a torsion rod, an aluminum alloy conducting vane for eddy current dissipation, and a supporting framework structure. Eddy currents generated in the vane by the moving magnetic tip provide the energy losses. The torsion rod provides the torque to restore the pendulum to the equilibrium position.

The torsion rod is machined from beryllium-copper wire stock. This material has been employed successfully in eddy current nutation damper designs for the Intelsat IV. The torsion rod element concept was conceived at Hughes following the demonstrated inability of commercially available flexible pivots to survive the dynamic loading environment of launch simulating vibration tests. The ability of the damper to provide very precise control of spacecraft pointing is due to the unique design combination of torsion rod, bonded solid lubrated journal bearings, and pendulum-rotor-journals. One end of the torsion rod is fixed to damper structure; the other is attached to the pendulum rotor. The pendulum rotor/torsion rod subassembly is suspended via large radial clearance journal bearings. In a 1g field, pendulum rotor journals contact lubricated bearing bores. However, in a zero g environment, and in the absence of external accelerations, the torsion rod acts to lift the pendulum rotor journals off the bearing bore surfaces, thus eliminating coulomb friction and allowing energy dissipation to continue as spacecraft nutation angles approach zero. The damper magnetic tip mass employs a cast Alnico VM permanent horseshoe magnet and two vanadium

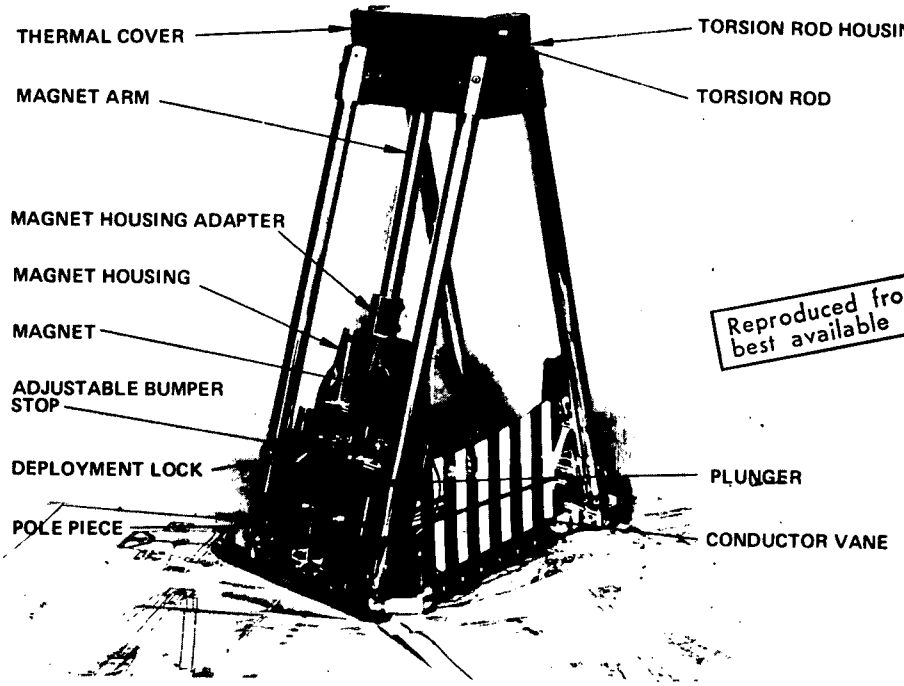

Figure 109. Nutation Damper

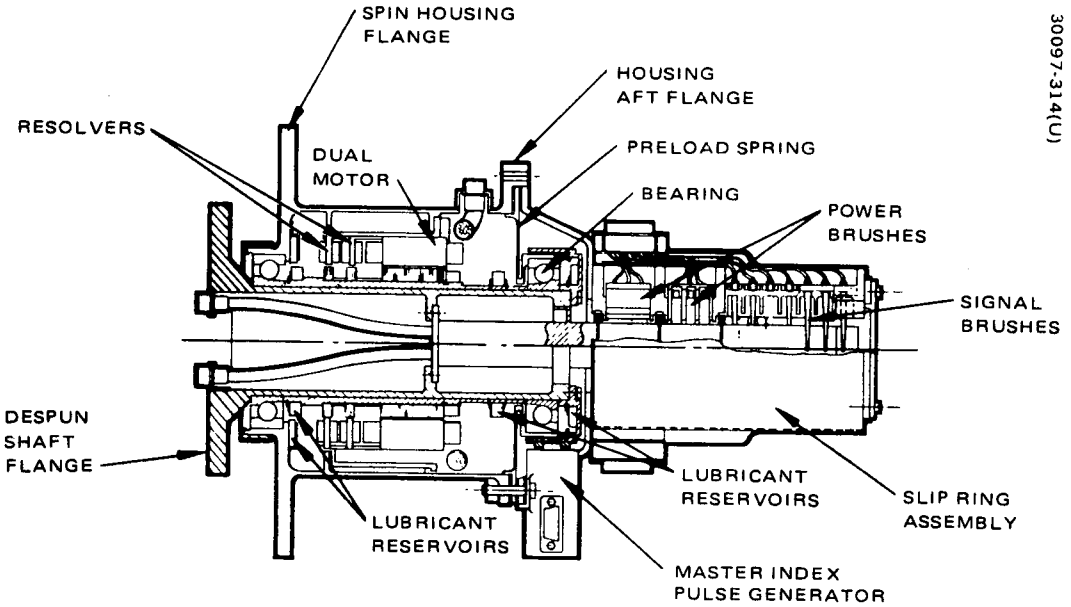

Figure 110. Bearing and Power Transfer Assembly

permendur pole pieces. The pendulum arm stiffness and the journal/bearing radial clearance preclude contact between magnet pole pieces and conducting vane during worst case mission lateral accelerations and thermal gradients.

The damper pendulum subassembly is caged during spacecraft launch by means of a pyrotechnic lock mechanism attached to the damper structure. This precaution is taken to preclude excessive dynamic loading and possible damage to the torsion rod and pendulum rotor bearing lubricated surfaces. Following spacecraft separation and prior to spinup, the damper pendulum is uncaged and the damper passive energy dissipation commences. During spacecraft apogee boost, the uncaged amper may experience full pendulum excursion to soft spring-loaded stops. The axial thrust load presents no problem for the damper suspension system, as the torsion rod deflects in bending to allow rotor journals to contact bearing bores which carry the load.

Bearing and Power Transfer Assembly

The BAPTA provides all mechanical and electrical interfaces between the spun and despun sections of the satellite. The assembly, shown in cross-sectional view in Figure 110, consists of five major components:

- Bearing and BAPTA structure support the despun platform and antenna during orbital operations.
- Brushless torque motor, despins and controls pointing of the antenna in response to torque commands from the despin control electronics (DCE).
- Master index pulse generator (MIPG) provides one pulse per revolution (from each of two redundant coils) to the DCE for relative angle (antenna pointing) information.
- Slip ring assembly (SRA) provides electrical power and signal transfer across the rotating joint.

The BAPTA design characteristics are summarized in Table 36.

The bearings selected for the TDRS BAPTA are 440C CEVM stainless steel angular contact bearings, 60 mm bore, extra light series (95 mm outside diameter), with 19 balls, each 0.0103 meter (13/32 inch) diameter, with a nominal 0.436 radian (25 degree) contact angle. The bearings selected are essentially identical in size and geometry to those used in the Anik I despin assembly. Torque noise data from the Anik I program are thus directly applicable. Measurements on a completed Anik I flight unit revealed a maximum peak-to-peak torque fluctuation due to bearings of approximately 0.005 N-m. The BAPTA is electrically isolated at each of its mounting surfaces (minimum of 10,000 ohms resistance) such that stray currents cannot pass through the bearings. Both the spinning and despun interfaces are insulated for redundancy. Additional protection is provided by grounding the spinning and despun BAPTA structure through a slip ring such that static charge can not build up and cause trickle current discharge through the bearings.

TABLE 36. DESPIN BEARING ASSEMBLY CHARACTERISTICS

Bearings	
Type	Angular contact
Contact angle	25 degrees
Material	440 C stainless steel
Size	60 mm bore, 19 to 0.0103 m diameter balls
Motor	
Type	Brushless dc, resolver commutated
Stall torque	3.8 Nm available each motor
Running torque	2.4 Nm available each motor
Slip Ring Assembly	
Power transfer	Two rings, six brushes per ring
Signal transfer	Twelve rings, two brushes per ring
Length	42 cm
Mass	10 kg
Reliability	0.99 for 7 years operation

Power and signal transfer from spun to despun sections of the satellite is accomplished with a dry-lubricated slip ring assembly utilizing coin silver rings and 85 percent silver, 3 percent graphite, 12 percent molybdenum disulfide composite brushes. The dry-lubricated slip ring technology employed in the TDRSS is the result of extensive long-term ground vacuum testing conducted to support the development of power transfer assemblies for previous programs.

The brushless, resolver commutation dc torquer motor assembly proposed for the TDRS BAPTA consists of two redundant motors, segment-wound on a common lamination stack, and two fully redundant resolvers. The motor is sized for a good margin of available torque above the BAPTA friction torque to enhance system reliability. This avoids the possibility of despin control loss due to unexpected bearing friction or marginal flat spin recovery capability. Motor internal construction is essentially identical to the successful Anik I design. Features of the motor design include firmly anchored and potted lead wires, sealed protective covers over motor and resolver windings, potted laminations to provide lamination support and good heat dissipation characteristics, and a metal sleeve over the magnets

to provide a smooth polished surface at the air gap. A final grinding of all critical diameters is performed after assembly of the rotor and stator. This provides a continuous smooth, highly concentric air gap and facilitates final cleaning and inspection operations. Alnico IX permanent magnets are used for maximum field strength and high coercive force to preclude demagnetization under maximum stall torque conditions.

Commutation control of the dual wound brushless motor is provided by a redundant pair of electromagnetic resolvers, one for each set of motor windings. Each resolver consists of a stator and rotor, rigidly mounted and precisely aligned to the structures that support the motor stator and rotor, respectively. The rotor is built of high permeability iron laminations and has eight poles. The stator contains a primary excitation coil and a pair of secondary (sine and cosine output) windings on a laminated iron structure.

The MIPG consists of a single housing enclosing two physically separate (for redundancy) coil wound permanent magnets and is mounted on the spinning housing. Each coil provides one pulse per revolution as the magnet passes a soft iron exciter on the despun shaft. The location of the zero crossing of each pulse is calibrated with respect to the BAPTA mirrors, thus providing relative angle information between spun and despun sections.

Despin Control Electronics

The despin control electronics uses information derived from earth sensor signals and the master index pulse (MIP) signal to control the despin motor torque by controlling motor current. Figure 111 is a block diagram of the DCE.

When the platform rate is zero and pointing at the earth, the position error controls motor current. The position error processing circuitry receives the selected pulse from one of the three earth sensors or the ground command substitute, the master index pulse (MIP) from the MIP electronics and the delayed MIP pulse (which occurs 283 ms after the MIP pulse) from the rate logic. The analog position error measurement circuit generates a bipolar proportional error signal based on the position of the MIP within the earth pulse. Outside this linear range, the position error signal is saturated. The position error signal is proportional to the time position of the MIP between LE and TE.

Appropriate shaping of the position error signal is provided by the shaping circuit and the limiting integrator. The shaped position error signal is used as the torque command input to the motor driver. A simple, proportional power amplifier was chosen for the brushless dc motor drive in keeping with the design goal of minimum complexity.

Once each rotor revolution, the position error measurement circuit determines the time position of the MIP pulse within the earth pulse as an analog voltage. The voltage is stored between measurements and shaped with active filters to provide a shaped position error signal.

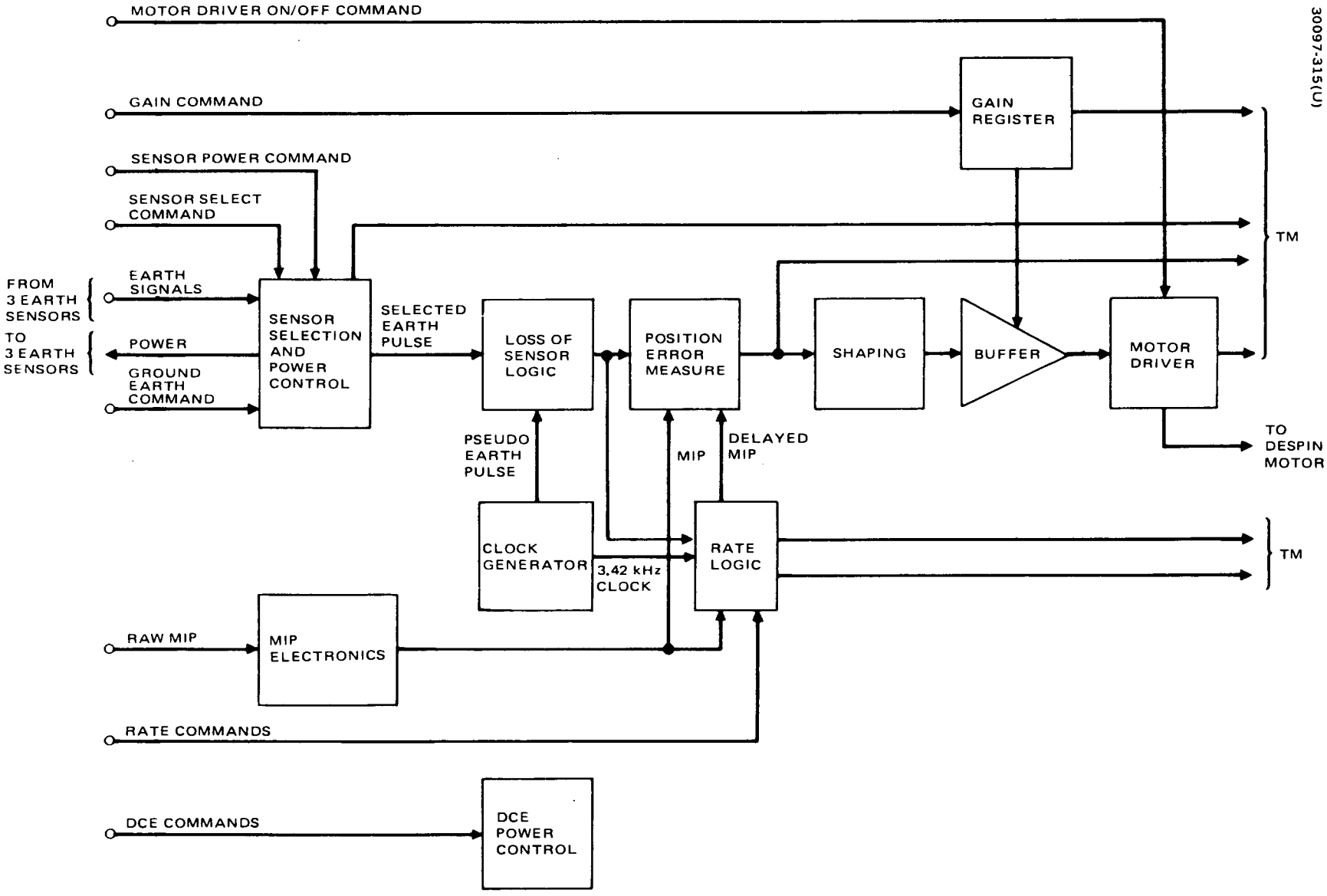

Figure 111. Despin Control Electronics

Figure 112 is a block diagram of the position error processing with waveforms. The figure shows the integrator control logic receiving the earth pulse and the MIP and delayed MIP. When the time interval between the delayed MIP and the MIP overlaps the earth pulse, the error integrator output will have a positive slope. When the time interval from the MIP to the delayed MIP overlaps the earth pulse, the error integrator slope will be negative. After the earth pulse, the resulting integrator voltage is sampled and held and the integrator is reset to zero. This results in a position measurement characteristic as shown in Figure 113. Error reversal at a point opposite the null ensures that the platform will always return to null by the shortest path. The shaping transfer function, which processes the error signal, consists of a dominant, low frequency zero term and two higher frequency poles. Proportional plus limited integral shaping is also provided to null steady-state friction torque. The shaping is realized using active RC networks. Two loop gain settings are selected by ground command. Power turnon resets the low gain setting.

The motor driver will be compatible with a dc brushless motor-resolver combination. The configuration, which is similar to that used on HS-312 and HS-333, is shown in Figure 114. The torque signal into the motor driver is modulated onto a square wave and used to drive the resolver. The carrier is generated by the oscillator. The resolver mounted on the motor shaft produces sine and cosine outputs as a function of the motor rotor to stator angle. These outputs are synchronously demodulated and become inputs to the power amplifiers. The power amplifier is a simple proportional design in keeping with the minimum complexity goal. Current sensing is used to provide true current command drive to the motor independent of speed and for telemetry. The driver will deliver sufficient current to the motor to provide full stall torque capability required for flat spin recovery.

Either or both motor drivers can be selected by ground command. Restoration of bus power after an outage will cause both drivers to turn on. The motor driver cross-strapping is configured such that a single demodulator output may drive its own power amplifier, the redundant unit power amplifier, or both. The motor driver line switch provides current limiting to protect the motor from demagnetization.

When the platform is spinning, the motor current is controlled by the rate logic. The rate logic uses a digital measurement technique to determine the first back difference of platform position resulting in a delta angle measurement. Because the rotor rate is close to constant, this delta angle is interpreted as platform rate.

The rate logic configuration shown in Figure 115 is similar to that used on Intelsat IV. The control logic receives the earth pulse, the MIP pulse, and the DCE clock. At the occurrence of the earth pulse, the upcounter is loaded with the minus 4 degrees/s. Thus for a commanded rate of zero, the initial upcounter value is -4 degrees/s. The upcounter is allowed to count from the earth pulse to the MIP. (When the MIP is within about 80 degrees of the earth pulse, the delayed MIP is used instead of the MIP to avoid bad measurements due to MIP earth pulse crossover.) A crystal-controlled

oscillator provides the basic count clock. The number in the upcounter is now transferred to the downcounter and the downcounter is allowed to count from the next earth pulse to MIP. The number in the downcounter now represents the first back difference or platform rate minus the initial 4 degrees/s offset. Underflow from the downcounter is detected and 3 bits are decoded as follows. If the re is no underflow, then the platform rate is more negative than -4 degrees/s and full spinup torque is applied. With underflow, the 3 bits are decoded to determine if the rate is between -4 and -2 where 1.356 N-m of spinup torque is applied or between -2 and 2 where no torque is applied, or between +2 and +4 where 1.356 N-m of despin torque is applied. If the decoder determines the rate to be greater than +4 degrees/s, then the downcounter is stopped and full despin torque is applied.

The upcounter and downcounter are operated simultaneously so that a rate sample is available once each rotation. Two special cases occur when the MIP rate is outside the dynamic range of the dual counter technique; that is, when the MIP rate is greater than twice or less than half of the earth pulse rate. When no MIP or delayed MIP occurs between LE pulses, the control logic causes zero to be transferred into the downcounter. This ensures underflow and a detected rate of greater than -0.195 rad/s so full despin torque is applied. When four or more MIPs plus dealyed MIPs occur between LE pulses, the control logic commands a digital/analog sample right after the LE pulse. This results in no underflow so full spinup torque is applied.

The design provides for commanded rate operation. Flipflops are used to store the rate command of zero or any of three nonzero rates. Power turnon will reset the rate command to zero. Command rate status is telemetered. At the occurrence of the earth pulse, the upcounter is loaded with the negative of the commanded rate. Thus, the platform rate will be controlled to a value that compensates for this offset, resulting in the desired platform rate.

The loss of sensor logic uses a simple 2 bit counter that counts the 1.66 Hz pseudo-earth signal and is reset by the selected earth pulse. If three pseudo-earth signals are counted without an earth pulse, then it is assumed that the sensor signals are not useful and the pseudo-earth pulse is substituted for the selected sensor signal. Reoccurrence of the sensor pulse restores the normal operation.

There are two redundant DCE units, only one of which is turned on at a time. Magnetic latching relays will remember the selected unit despite power loss. The selected DCE unit is cross-strapped to drive either or both motor drivers. After separation, both motor drivers will come on when the power bus comes up. Both can also be commanded on together and commanded off individually.

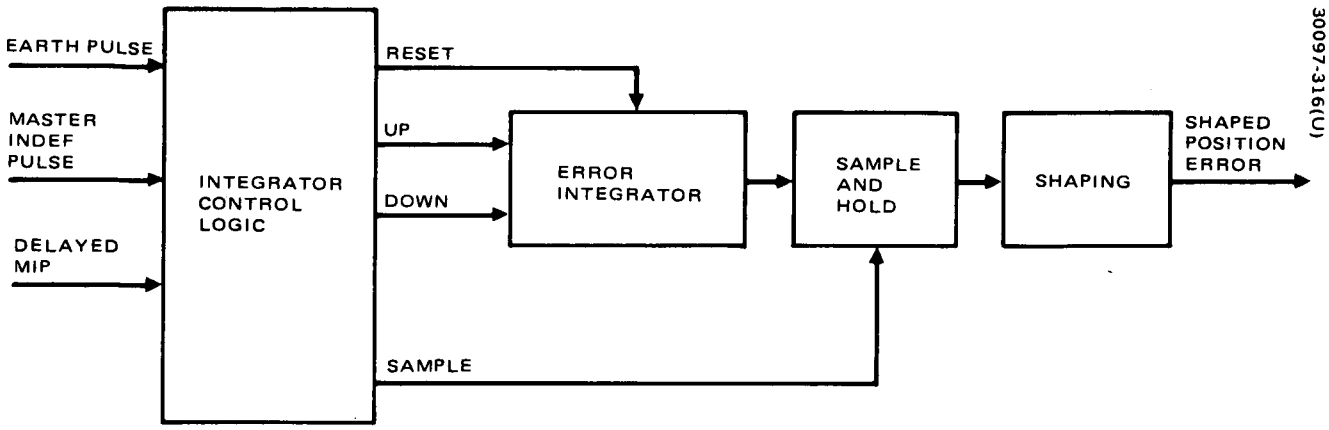

Figure 112. Error Measurement Circuit Block Diagram

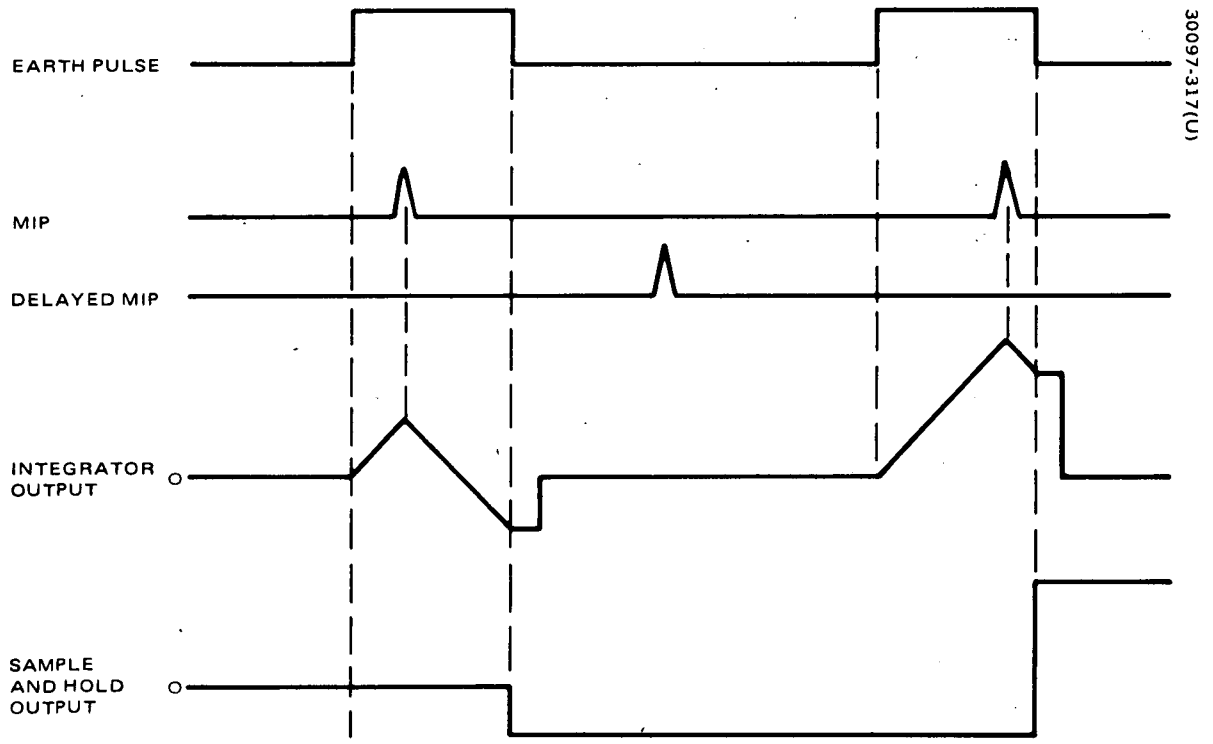

Figure 113. Position Error Measurement Circuit Waveforms

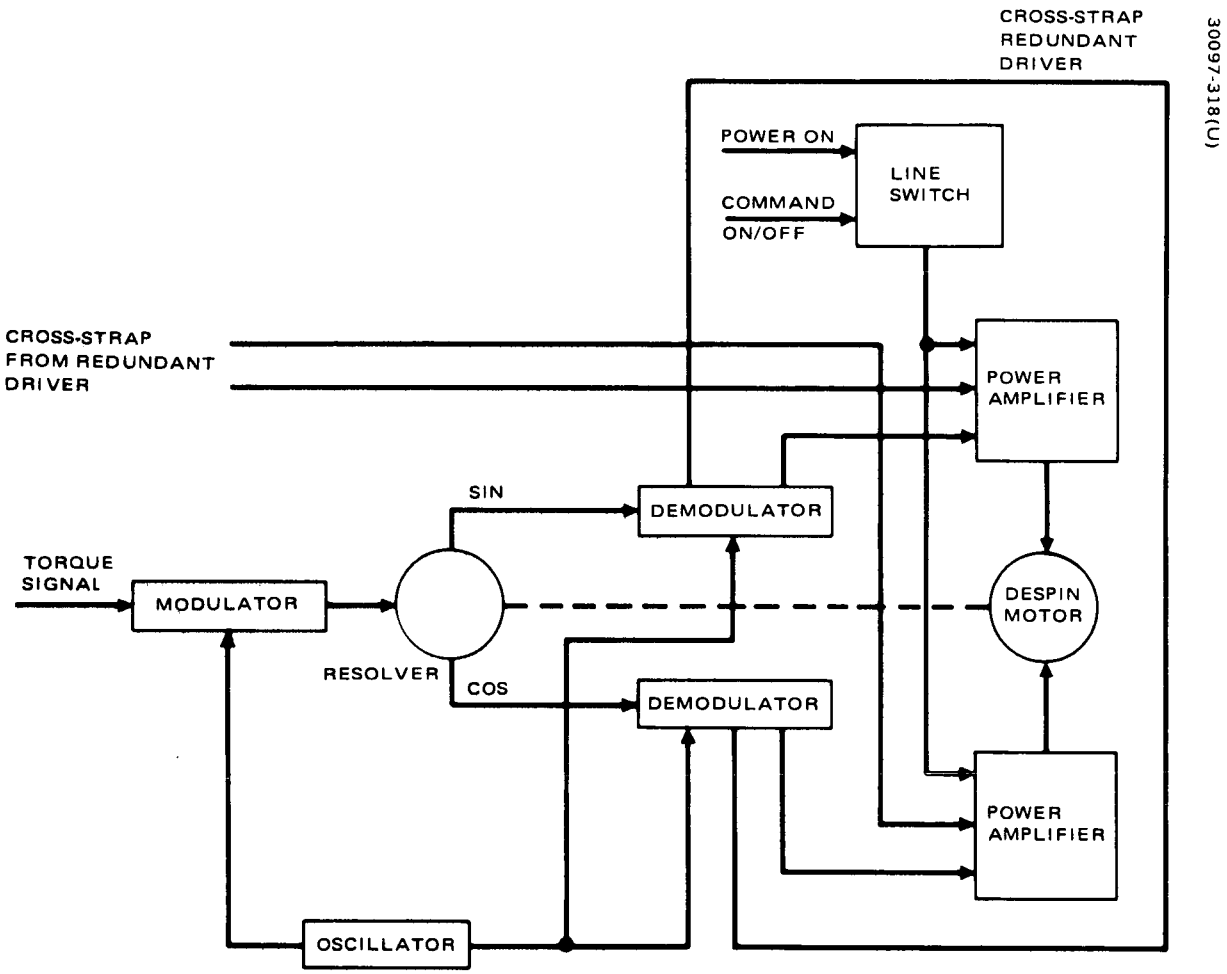

Figure 114. Motor Driver Block Diagram

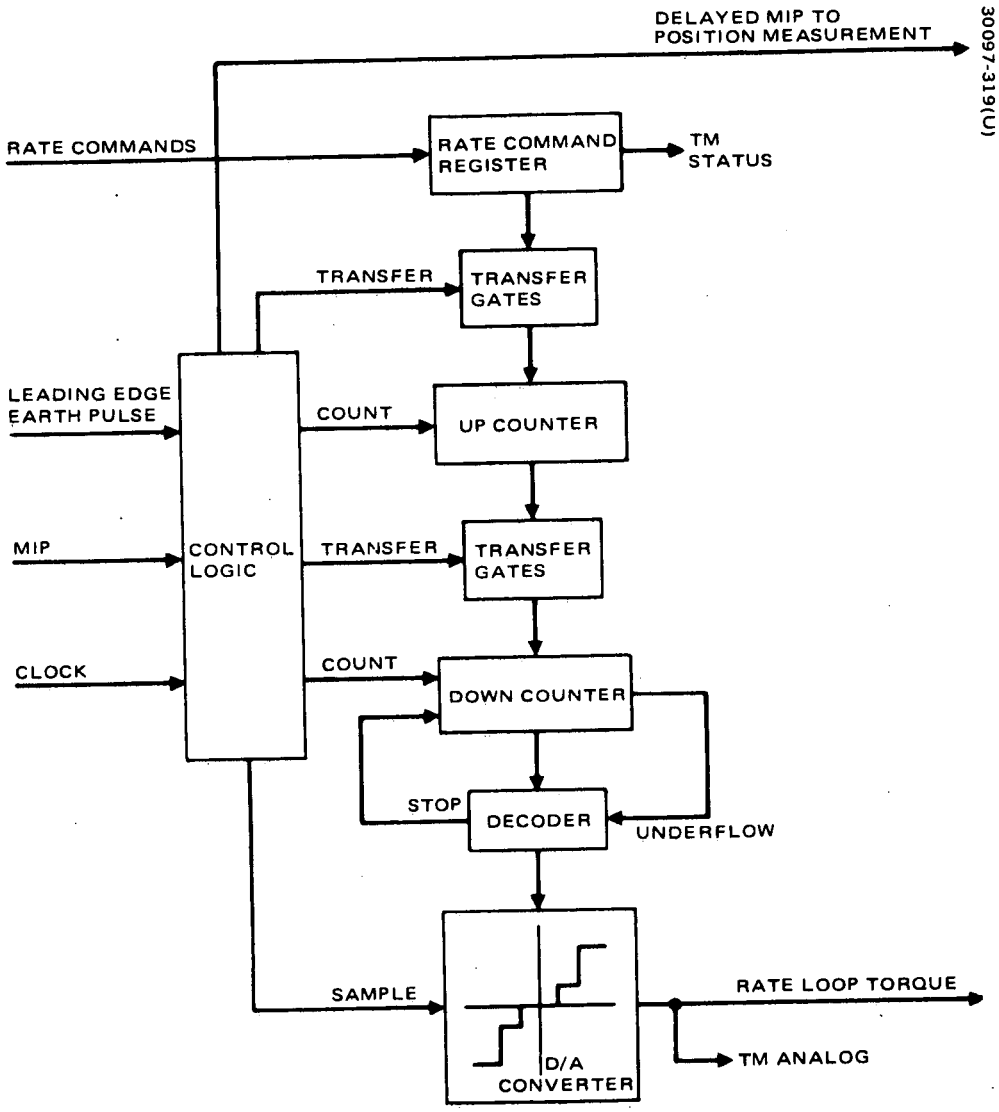

Figure 115. Rate Logic Block Diagram

4.3.4.4 Technology Status

The design and implementation of the TDRS attitude and despin control subsystem are based on proven technology from such programs as TACSAT I, Intelsat IV, and the Canadian Domestic Communication Satellite, Anik I. The basic Gyrostatic stabilization technique was proven with the flight of TACSAT I and continued to prove successful on all Intelsat IV flights. All mechanical elements of the TDRS subsystem involve flight-proven hardware. Control techniques and analytical performance predications have been verified from observation of the in-orbit behavior of both TACSAT I and Intelsat IV spacecraft. The following summarizes the technology status of the various elements of the subsystem.

Bearing and Power Transfer Assembly

The BAPTA design selected is the result of extensive background and years of experience in design, fabrication, test, and orbital operation of despin assemblies for TACSAT, Intelsat IV, and Anik I communication satellites. The TDRS subsystem design represents the best available technology applicable to highly reliable despin assemblies, where each detail has evolved through several generations of analysis and test. This wealth of background experience provides high confidence in meeting the BAPTA functional requirements with minimum risk of development difficulties.

Earth Sensors

The proposed earth sensor for TDRS subsystem has been flown on the TRW Intelsat III and DSCS II programs and therefore represents flight-proven hardware. The circuit functions are similar to the sensor flown on Intelsat IV.

Sun Sensor

The proposed sun sensor has been flown successfully on ATS, TACSAT, and Intelsat IV. More than 30 of these units have been built and tested; no failures have occurred in any sensor of this type flown on Hughes satellites.

Nutation Damper

The TDRS subsystem nutation damper represents a scaled version of the damper successfully flown on Intelsat IV. In-orbit studies of its nutation damper characteristics have been made and found to be in agreement with analytical predictions.

Active Nutation Control

The ability to actively control nutation using reaction jets and a rotor-mounted accelerometer was developed and proven for Intelsat IV. he ANC performance has been verified during in-orbit testing.

Despin Control Electronics

The control techniques and electronic hardware involved in the despin control subsystem are derived from the flight-proven hardware of TACSAT I and Intelsat IV. The basic elements and their derivation are as follows:

Position error detection	TACSAT
Control shaping	TACSAT
Rate control loop	Intelsat IV
Motor drive	Intelsat IV

The hardware fabrication and assembly techniques are the same as those used on TACSAT and Intelsat IV and being used on Anik I.

4.3.5 Reaction Control Subsystem

The RCS is a blowdown bipropellant type design. The hypergolic reaction of monomethyl hydrazine and nitrogen tetroxide produces hot gas, developing impulse for all required velocity and attitude control maneuvers, except for the orbital injection maneuver which is performed by the apogee motor.

The RCS provides the capability to perform the maneuvers shown in Table 37. As indicated in the table, injection trim and station change dominate all other maneuvers.

Most maneuvers will be initiated and terminated by ground command. Automatic attitude control will be initiated and terminated by on-board logic. Synchronizing the firing commands with sun sensor information will properly phase maneuvers. Each thruster command pulse will be 0.075 second at a spacecraft spin speed of 100 rpm. Table 38 summarizes the maneuvers, thruster utilization, and source of firing command. Cumulative impulse repeatability is ±7 percent when the thruster is operated in the pulsing mode.

TABLE 37. RCS PROPELLANT REQUIREMENTS

Operational Requirement	Magnitude	Propellant, kilograms
Preapogee motor orientation	132 degrees	1.4
Postapogee motor orientation	121 degrees	1.1
Solar torque compensation	—	5.2
Injection trim	55.5 m/s	7.7
Stationkeeping east-west	15.0 m/s	2.2
Station change	51.3 m/s	6.9
Jet misalignment effects	—	0.5
Total propellant required	—	25.0

TABLE 38. RCS MANEUVER SUMMARY

Maneuver	Thruster Used	How Initiated
Attitude Control		
Nutation control	Either axial, pulsing	Automatic firing
Attitude drift	Either axial, pulsing	Ground command
Reorientation	Either axial, pulsing	Ground command
Velocity Control		
Stationkeeping	Either radial, pulsing	Ground command
AKM performance anomaly	Either radial, pulsing	Ground command
Booster performance anomaly	Either radial, pulsing	Ground command

Figure 116 shows the arrangement of the reaction control subsystem. It is a redundant design (except for propellant), selected to provide a high reliability with a minimum of components. Malfunction of any single valve or thruster will not result in loss of subsystem function. The RCS is assembled as a unitized, all-welded system, with the stainless steel body valves joined into the system by means of diffusion-bonded, coextruded titanium-to-steel transition joints. The only mechanical joints in the RCS are the thrust chamber-to-propellant valve interfaces and the redundantly sealed fill and drain valves.

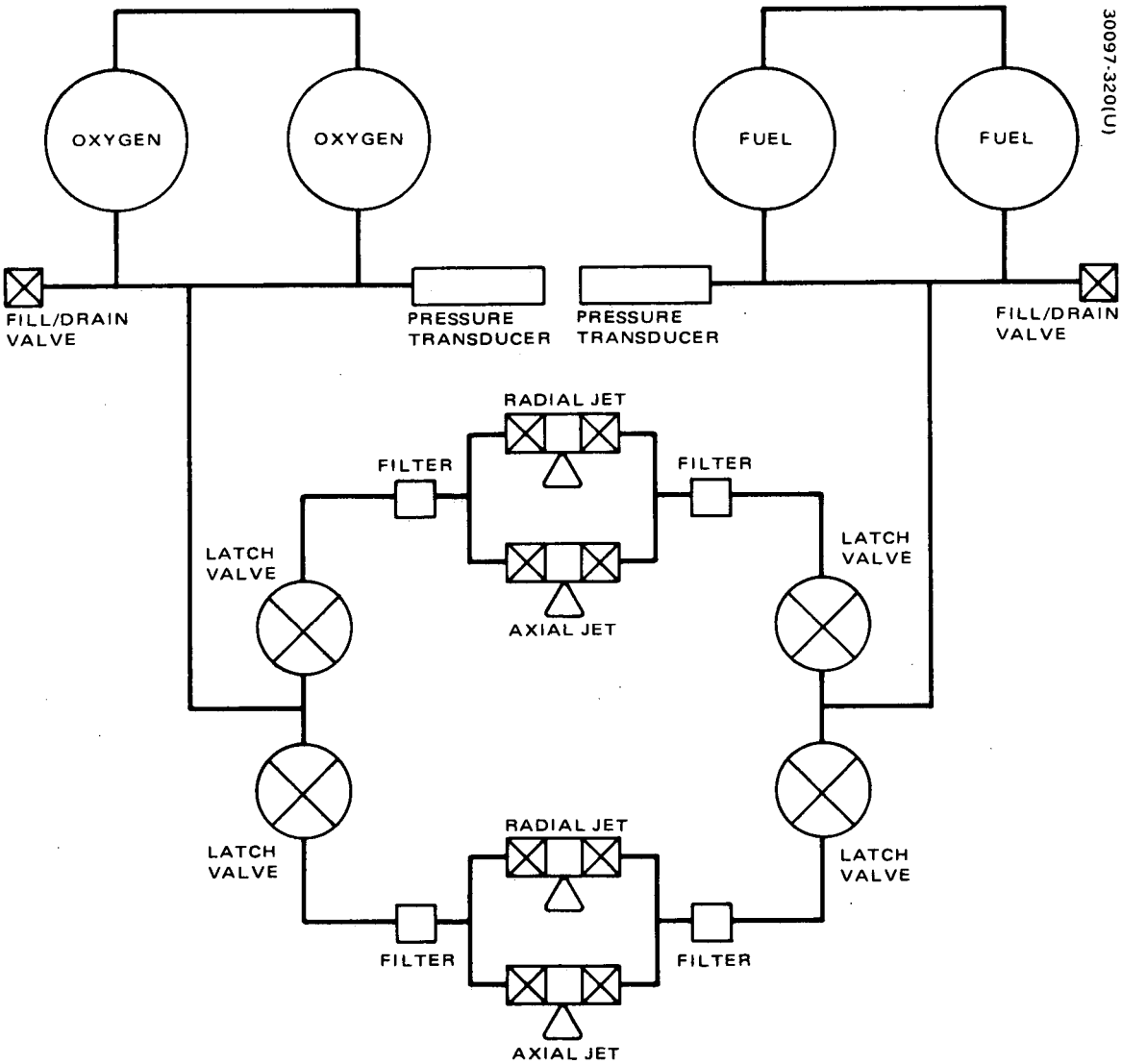

Figure 116. Reaction Control Subsystem Schematic

TABLE 39. RCS COMPONENTS

Component	Number/ Spacecraft	Unit Mass kilograms	Manufacturer	Previous Program Qualifications
Thruster, 1 N	4	0.075	Arbeitsgemeinschaft Für Raketentechnik und Raumfahrt and der Universität Stuttgart E.V.	New component
Propellant valve all thrusters	8	Included in thruster mass	—	New component
Tanks	4	1.0	—	New component
Filters	4	0.14	Vacco Industries	HS-312, HS-318, HS-333
Latching valves	4	0.27	Carleton Controls Corporation	HS-312, HS-318
Fill/drain valves	2	0.18	Hughes Aircraft Company	HS-312, HS-318, HS-333
Transducer	2	0.14	Edcliff	HS-312, HS-318, HS-333, ATS, HS-308
Lines and fittings	2	1.45	Hughes Aircraft Company	HS-312, HS-318, HS-333
Transition tubes	—	Included in lines and fitting masses	Nuclear Metals Division Wittaker Corporation	HS-312, HS-318, HS-333
Welded tees	—	—	Hughes Aircraft Company	HS-312, HS-318, HS-333

The components to be used in the RCS were initially developed for a monopropellant hydrazine system and have been used extensively in such systems. All materials used in these components which are wetted by the propellants are compatible with both the monomethyl hydrazine and the nitrogen tetroxide. Thus these previously developed components (tanks, fill and drain valve, pressure transducer, latch valve, and filter) can be incorporated into the bipropellant system. Table 39 summarizes the component mass, previous use, and number required per spacecraft.

The bipropellant thruster and associated propellant control valves have been developed during an intensive 6 year program by Arbeitsgemeinschaft Für Raketentechnik Und Raumfahrt and der Universität Stuttgart E. V., Stuttgart, West Germany. The propellant control valve employs an electromagnet to draw a flexure mounted poppet away from the valve seat. The valve is held closed by the spring flexure force. When power is applied, the electromagnetic forces overcomes the flexure spring forces and the valve opens. When power is removed, the valve closes.

Redundant pairs of axial and radial 1 newton thrusters are provided. All utilize a unique propellant injection scheme that allows extremely rapid ignition and combustion of the fuel and oxidizer to produce hot gases which are expelled through a converging-diraging nozzle to produce thrust. The bipropellant thruster, including propellant valves which have been produced, is capable of delivering more than 1 million seconds of steady-state operation with the external case temperature never rising above 400 K. On the other hand, the thruster (including valves) has demonstrated the capability to deliver over 10 million duty cycles with thrusting times as low as 3 milliseconds and impulse bits as low as 2.7×10^{-3} N-s repeatable to ±6 percent. The demonstrated specific impulse ranges from 260 seconds for very short duration pulses to 290 seconds for steady-state operation. The propellant valves developed in conjunction with this thruster have demonstrated over 1 billion cycles without failure.

Tests performed with the thruster have shown that the impulse bit produced is a linear function of valve on time from 3 milliseconds to greater than 150 milliseconds. In addition, the thruster has demonstrated the ability to operate in an unregulated blowdown mode with tank pressure varying from 2.76 MN/m^2 down to 0.69 MN/m^2 and mixture ratios of 1.5 to 2.5.

The thruster itself is illustrated in Figure 117. It incorporates a tangential propellant injection scheme near the nozzle end of the combustion chamber. There is one fuel port and one oxidizer port, each pointing in the same rotational direction. This injection scheme then drives a vortex flow in the chamber. The high g forces near the chamber walls keep the propellants in the liquid state as they flow along the wall, thus providing the wall with film cooling. The injection near the throat also serves to cool the throat. Once the propellant flows to the head end of the chamber, it is turned to the center of the vortex where propellant combustion takes place. The ability of this injection scheme to keep the walls cool enables the propellant valves to be attached directly to the sides of the chamber, thus minimizing the propellant dribble volume and allowing the very short pulse times. The Air Force Rocket Propulsion Laboratory currently has a program underway designed to confirm the performance figures quoted for this thruster.

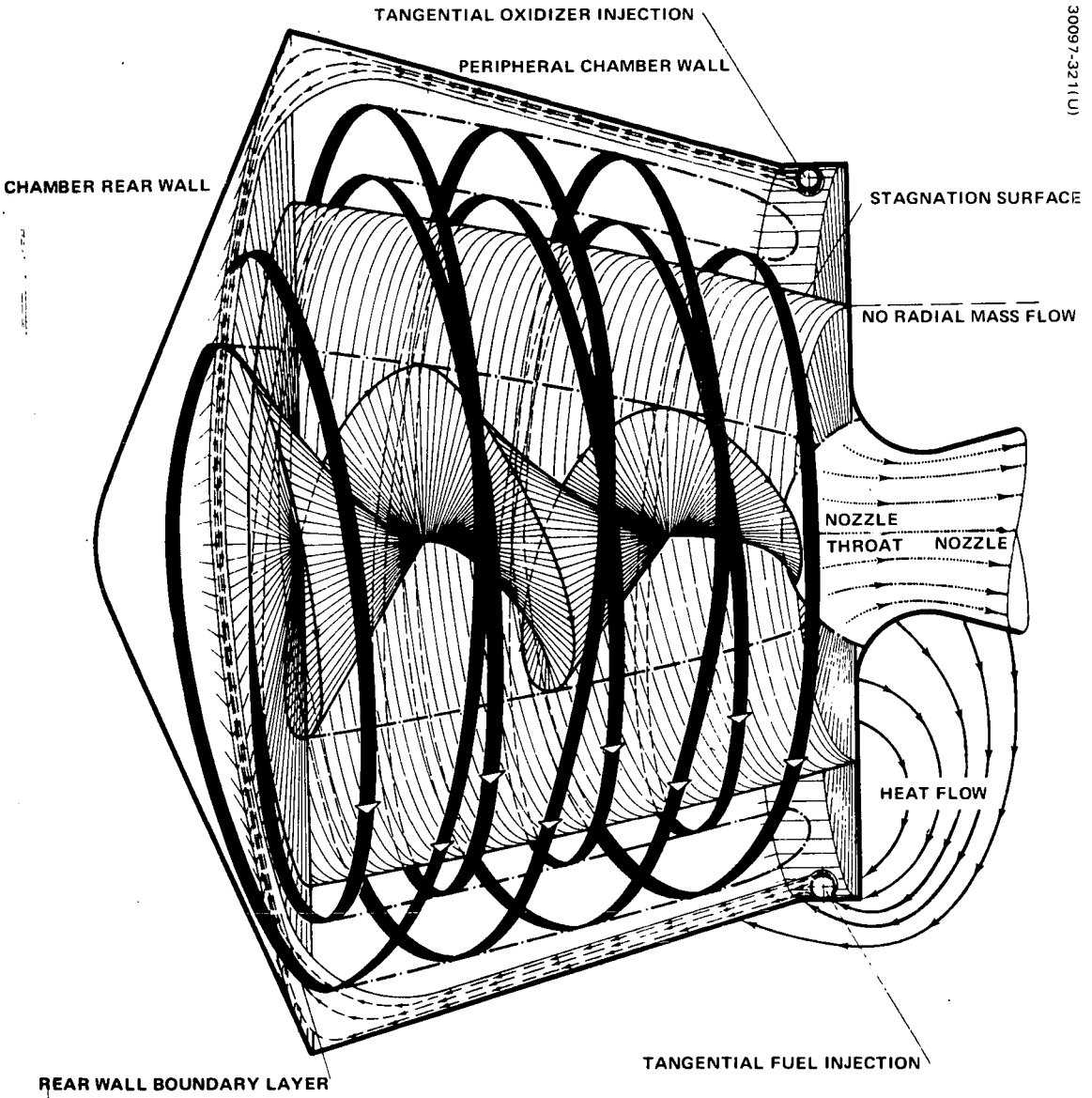

Figure 117. Functional Principle of Triroc-Rocket Engine

The four propellant tanks operate in the blowdown mode and employ no propellant management devices. The liquid gas interface is controlled by the centrifugal forces resulting from spacecraft spin. The tanks, made of 6AR-4V titanium alloy, are conispherical, welded structures. A typical tank is shown in Figure 118. Each has two ports — a liquid outlet at the apex of the conical section and a gas port, 180 degrees opposed. The included angle of the conical section is 85 degrees. This permits total removal of liquid by spinning (in orbit) or by gravity (during ground operations). At launch, each fuel tank will contain approximately 4.2 kg of monomethyl hydrazine and each oxidizer tank will contain approximately 8.3 kg of nitrogen tetroxide. Each tank will be sized to allow an overload capability of approximately 15 percent so that the tanks can be topped off to match launch vehicle payload capability at time of launch, thereby providing some excess maneuvering capability or propellant redundancy.

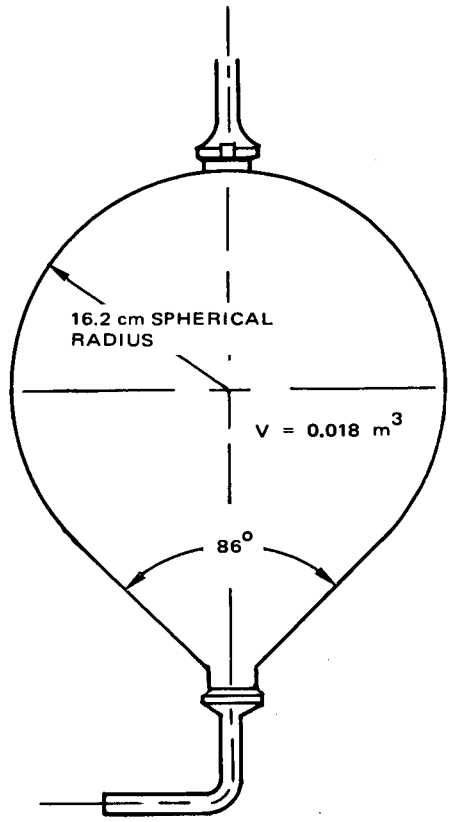

Figure 118. Propellant Tank

Each of the four latching valves is housed in a welded stainless steel body. As shown in Figure 119, a Belville spring provides the force to latch the valve in either the open or closed position, after removal of power from the actuation solenoid. The valve seat is a stainless steel to teflon interface. Moving parts are isolated from propellant contact by a welded metal bellows, which also balances poppet loads. All are normally closed, except during maneuvers.

A high capacity filter, with 10 micrometers absolute rating, is provided downstream of each latch valve. Figure 120 illustrates the construction of this filter. It consists of electrochemically etched discs mounted concentrically on a perforated tube. The entering fluid exits through the tortuous paths etched into the discs which are encased in a welded titanium housing.

Separate potentiometer type transducers in which pressure is sensed by an aneroid capsule of stainless steel is used to measure the fuel and oxidizer tank pressures. The deflection of this capsule is transmitted through a pushrod to the wiper of a linear-wound resistance element. An exploded view of this transducer is shown in Figure 121.

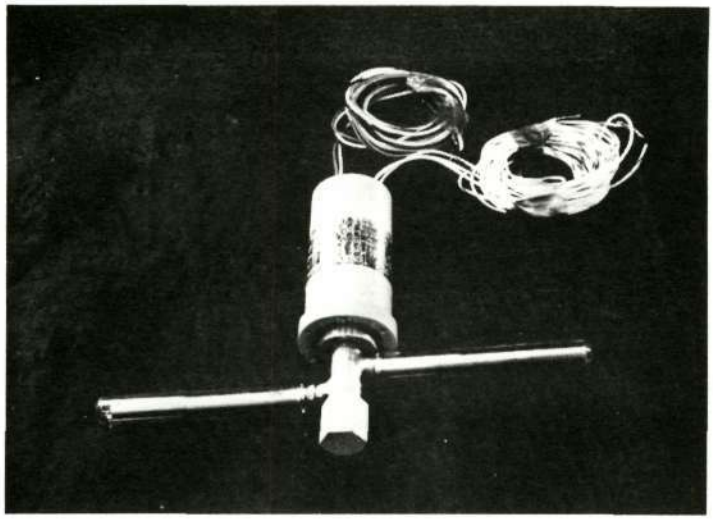

a) Assembled Configuration (Photo A27887)

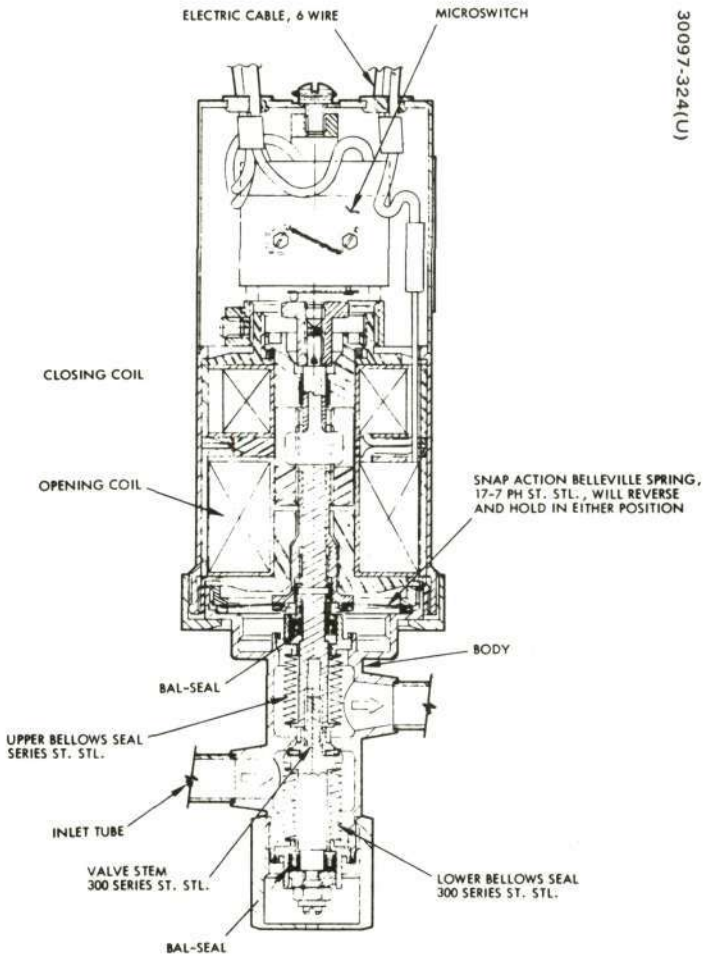

b) Cross Section View

Figure 119. Propellant Latching Valve

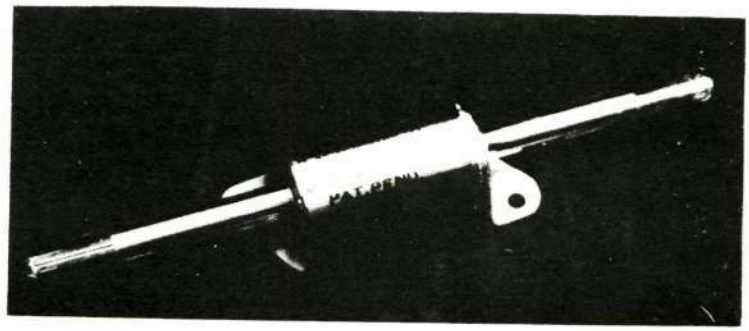

a) Assembled Configuration (Photo A27890)

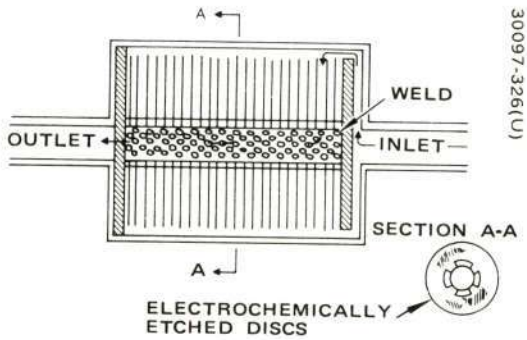

b) Cross Section View

Figure 120. High Capacity Filter

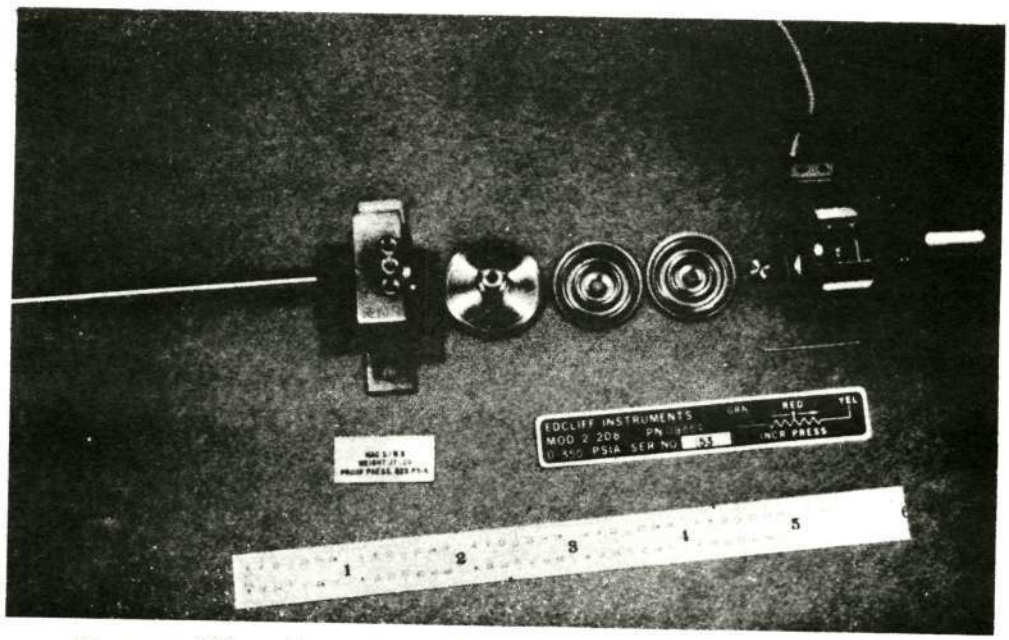

Figure 121. Pressure Transducer (Photo 30097-327)

a) Assembled Valve (Photo ES29087)

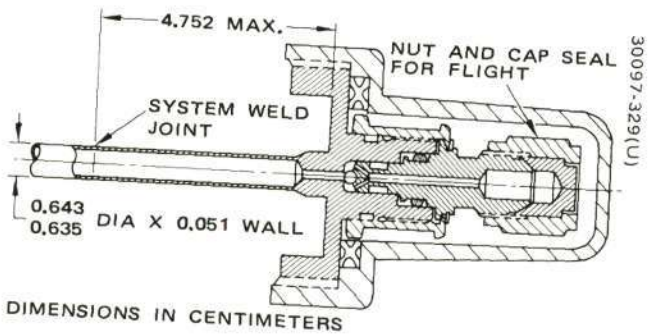

b) Cross Section View

Figure 122. Fill/Drain Valve

A manually operated and direct acting fill and drain valve is used for both the fuel and oxidizer portions of the system. Each of the two valve inlets is size-coded to ensure that each side is filled with the proper propellant. This valve is shown in Figure 122. The primary seal is formed between a tungsten carbide ball and the titanium body. Since these materials permit the application of high closing torques, zero leakage is achieved repeatedly. A redundant mechanical cap seal is installed for launch.

Propellant and gas manifolds are fabricated from seamless tubing, (0.63 cm outside diameter and 0.05 cm thick walls) of 6 Al-4V titanium alloy. Branch lines are accommodated by tee fittings. Stainless steel components are welded into the system by means of transition joints. These coextrusions of 6 Al-4V titanium and 304L stainless steel provide a transition of properties from one to the other. All connections are butt-welded by an automatic tube welded that produces preprogrammed, continuous tungsten inert gas (TIG) welds without the use of sleeves, rings, or filler material.

4.3.6 Electrical Power Subsystem

The electrical power subsystem supports operation of all payload and spacecraft subsystems. It is designed to provide payload power continuously for a minimum of 5 years for command and data relay to users. In addition, a voice relay will be provided to orbiting and manned spacecraft. With a manned spacecraft in an approximately 100 minute orbit, an S band forward voice link can be operational no less than 25 percent of the time. Voice operation on the return links is unrestricted in terms of power utilization. Table 40 shows the power requirement for the different operating modes for both the sunlit and eclipse portion of the orbit. These power requirements include approximately a 5 percent margin which is reserved for future growth.

TABLE 40. ELECTRICAL POWER SUMMARY

Equipment	Sunlit Operation			Eclipse Operation	
	Mode A Peak* 25.5 V	Mode B Equinox 26.5 V	Mode C Solstice 26.5 V	Mode D Peak* 24.5 V	Mode E Normal 24.5 V
HDR return transunit (Ku)	35.3	36.5	36.5	–	–
LDR/MDR return transunit (Ku)	10.5	11.1	11.1	10.1	10.1
HDR forward transunit (Ku)	6.6	6.8	6.8	–	–
MDR forward transunit 1 (S)	–	27.6	27.6	26.5	26.5
MDR forward transunit 2 (S)	104.5	–	–	100.5	–
LDR forward transunit (UHF)	114.0	119.0	119.0	–	–
Receivers, processors, etc.	37.8	39.4	39.4	36.4	36.4
Transponder (S)	2.1	26.0	26.0	2.0	2.0
Telemetry, tracking, and command	15.4	15.7	15.7	14.8	14.8
Antenna position control	11.9	12.0	12.0	11.4	11.4
Despin control	19.8	20.0	20.0	19.0	19.0
Thermal control	6.0	6.0	6.0	6.0	6.0
Power electronics	11.0	11.0	11.0	26.0	26.0
Battery charging	–	37.0	–	–	–
Distribution losses	7.0	7.0	7.0	4.0	4.0
Power required	381.9	375.1	338.1	256.7	156.2
Contingency	13.1	21.9	25.9	–	–
Power available	395.0	397.0	364.0	Batt	Batt

*Peak loads for 25 percent of time.

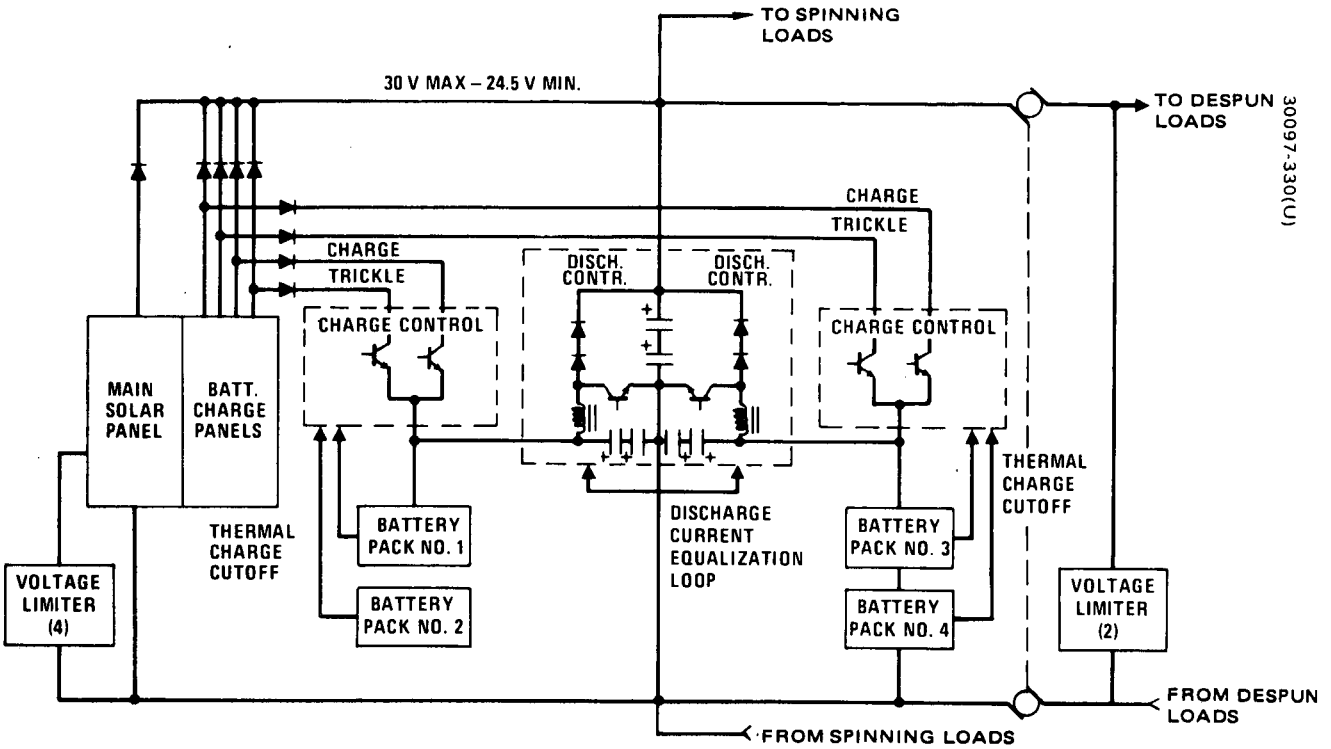

Figure 123. TDRSS Baseline Power Subsystem Block Diagram

The basic configuration of the power subsystem is shown in Figure 123. The power subsystem has two batteries with 16 cells each. Each battery is composed of two battery packs. The cells are 10 A-hr in size. The battery output is boosted by a boost discharge regulator to 25.5 volt nominal regulated voltage. Both batteries are required for complete mission success. Each battery is equipped with redundant discharge circuits for reliability. To provide high reliability, two cells in each battery are permitted to fail shorted without loss of the battery. Power system operation with battery power augmentation during operation mode A will result in very shallow battery discharges.

The solar array will automatically charge the batteries. During battery charging, the solar array voltage will be 26.5 volts or higher. The batteries are charged at C/15 rate. Between eclipse periods, the batteries are trickle-charged. The trickle charge rate selected is C/60. The equivalent battery charge current provided by the solar array to the two batteries is 60 watts. The solar panel output is 364.0 watts at summer solstice and 397 watts 23 days before equinox.

Bus voltage limiters maintain solar panel output voltage below 30 volts independently of load after emerging from eclipse and provide a minimum heat dissipation on the despun platform during launch and orbit acquisition and also during powered-down operation. Two types of limiters are used. The tap limiters shunt out selectable sections of the solar array

and function primarily to hold the bus voltage below 29.5 volts under full load and posteclipse periods and to dump surplus panel power in the panel itself for thermal control purposes. The bus limiters shunt the complete bus and function to limit bus to 30 volts and to provide heat for the despun shelf to keep its temperature within an acceptable limit under light load conditions.

Redundancy is employed in functional components of this subsystem, as well as piece parts, to ensure high reliability for a 5 year mission. A weight saving is accomplished by allowing 60 percent battery depth of discharge. Complete redundant battery discharge circuits are used. Since the probability of a battery open circuit failure is considered negligible, only protection against battery cell short circuit or cell fading is provided. The battery discharge regulator is designed for satisfactory operation even with two shorted cells in a battery. This regulator will operate from a minimum battery voltage of 17 volts at end of discharge.

The selected configuration is a compromise between requirements for low mass and high reliability. The power subsystem hardware selected is similar or identical to that used in other Hughes spacecraft, and therefore represents a minimum development risk. The power subsystem mass is listed in Table 41 and design characteristics are summarized in Table 42.

TABLE 41. POWER SUBSYSTEM ESTIMATED MASS

	Weight, kilograms
Solar array, excluding substrate	15.9
Batteries (two)	15.4
Battery discharge controllers (two)	6.0
Battery charge controllers (two)	0.9
Voltage limiters (six)	2.7
Current sensors	0.2
Total	41.1

TABLE 42. POWER SUBSYSTEM DESIGN CHARACTERISTICS

Solar Cell Array	
Length	2.05 meters
Diameter	2.16 meters
Cells	2.2 x 6.2 cm x 0.25 mm (10.0 mil) ohm-cm
Covers	2.2 x 6.2 cm x 0.15 mm (6.0 mil)
Batteries	
Number	2 with 16 cells each
Capacity	10 A-hr
Discharge cycles — eclipse	450 (60 percent D.O.D.)
Battery Controller	
Current sharing tolerance	5%
Rated output current	5 A
Battery input potential	16 to 22 V
Voltage Limiter (maximum bus potential)	30 V

TABLE 43. SOLAR ARRAY DESIGN

Number of panels:	1
Size	
Diameter	2.16 meters
Length	2.05 meters
Mass (excluding substrate)	15.9 kg
Solar cells	2.2 x 6.2 x 0.025 cm
Base resistivity	10 ohm-cm
Solar cell cover	0.15 mm (6 mil) thick
Nominal cell voltage (near maximum power)	0.445 V
Nominal cell current (near maximum power)	0.447 A
Temperature	Function of location and season
Radiation degradation	
Current	0.885
Voltage	0.930
Fabrication Loss	
Voltage	1.00
Current	0.97
Ripple	0.98
Effective illuminated area in current	0.318
Curvature edge defects, current	0.962
Solar angle	32 degrees
Seasonal intensity	
Summer solstice, current	0.888
Autumnal equinox, current	0.993
23 days before autumnal equinox, current	0.969
Coverslide darkening, current	0.98
Diode drop	0.8
Panel harness drop	0.2 V

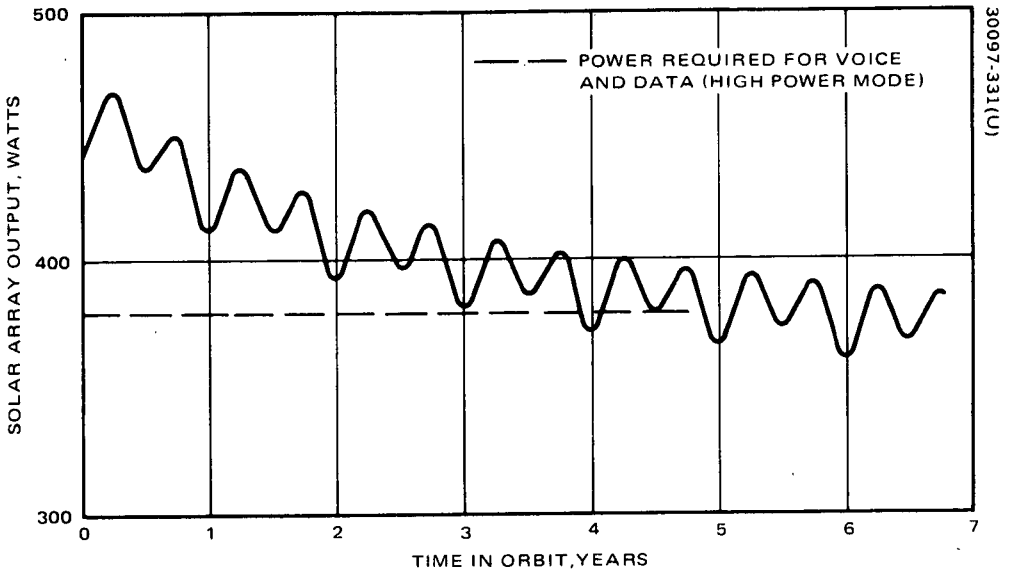

Figure 124. Available Solar Array Power

4.3.6.1 Solar Cell Array Design

The solar cell array design was optimized to achieve the required power output at the lowest mass. It provides end-of-life power of 364 watts at summer solstice and 397 watts 23 days before equinox. The solar array performance is illustrated in Figure 124. The design voltage is 26.5 volts. The solar array utilizes design techniques, fabrication methods, and materials previously employed by Hughes that have been confirmed by in-orbit data from TACSAT, ATS, and Intelsat IV, and FRUSA programs.

The solar cells are 2.2 by 6.2 cm, 10 ohm-cm base resistivity, n/p type and are 0.25 mm (10 mil) thick cell with 0.15 mm (6 mil) coverglass. The array is 2.16 meters in diameter at the substrate and 2.05 meters long, with a mass of 15.9 kg excluding the substrate. A total of 135 cell strings are in parallel and each string is 68 cells long, resulting in a total of 9180 cells. The solar array design factors are shown in Table 43. These design factors were developed over the entire family of spinning synchronous orbit solar panels and verified by flight data.

In order to achieve the most efficient solar cell array design, a parametric mass optimization was completed. Cell thickness, base resistivity, and cover thicknesses were optimized to provide minimum system mass for end-of-life conditions. The Hughes computer analysis essentially consists of altering cell characteristics, and compensating with greater or less panel area to maintain the same end-of-life power. All mass elements were included, such as cells, covers, cell array accessories, substrate, and spacecraft-related mass. The lowest mass system includes the thinnest available large area solar cell-cover combination. Since the cost of the

large area solar cells increases rapidly with decreasing cell thickness, a combination of 0.25 mm (10 mil) cells with 0.15 mm (6 mil) ceria doped microsheet cover was considered the best design choice.

A number of pertinent solar array design factors are discussed below.

Coverslide Degradation

Although an ultraviolet filter protects the coverslide adhesive from discoloration, some degradation in light transmission occurs. This results from ultraviolet irradiation from sources such as the sun and appears in the coverslide coatings and in the adhesive. A degradation factor of 0.98 is assumed.

Configuration and Geometrical Effects

The effects of cylindrical geometry and fabrication losses must be considered in the design. Corrections for the effects of geometry on current require a $1/\pi$ projection of the array surface. Calculations of projected solar panel area assume that a solar cell performs directly as a function of the cosine of the incident angle. This is not precisely the case because of cell mismatch and edge loss effects so an angle of incidence effect factor of 0.962 must be included.

Fabrication Effect

Fabrication and assembly losses result from the interconnection of the solar cells into the series parallel arrays, and are expected to degrade the current by a factor of 0.97 based on actual performance measurements obtained on the Intelsat IV and Telesat Programs.

Orbital Effects

In synchronous orbit, solar intensity varies from 135.1 mW/cm^2 at summer solstice to 144.3 mW/cm^2 at winter solstice. Since the axis of the satellite is parallel to the axis of the earth, the satellite experiences a maximum of 30.5 degree inclination at the solstice condition. The worst orbital condition, therefore, is summer solstice where the intensity is lowest and the angle of inclination the greatest. Corrections for intensity are made by multiplying the cell output at air mass zero by the ratio of the intensities (0.968). To correct the cell output for the angle of inclination, the current is multiplied by the cosine of the angle of inclination. The resulting correction factors for several pertinent mission dates are summer solstice 0.888, equinox 0.993, and 23 days before the autumnal equinox (eclipse season) 0.969.

Miscellaneous Corrections

Because most of the loads on the spacecraft may be considered constant current, the solar panel must be capable of satisfying these loads even at the lowest point in any output ripple. Ripple may arise from two areas: 1) that caused by uncompensated cutouts, cell output differences, etc., or

2) that caused by nonuniform degradation resulting from micrometeoroids damage, etc. Therefore, corrections are made on current for the effect of ripple (0.98). Consideration is also given to the 0.8 volt drop across the blocking diodes and to the 0.2 volt drop in solar cell array wiring.

Radiation Effect

The methods used by Hughes to compute natural and artificial radiation effects on solar array power output have been verified extensively with orbital flight data. The computational methods have been described in Hughes Phase I Final Report and only a brief summary will be included in this report.

The Hughes radiation environment calculation establishes for base line a "reference" equivalent 1 MeV electron fluence for the space environment. This reference 1 MeV electron equivalent fluence will cause the same damage to a 12 mil (0.30 mm) thick 10 ohm-cm solar cell as the actual space environment. In a given space environment, the damage to a solar cell is dependent on cell thickness, base resistivity, and coverglass thickness.

Large amounts of radiation damage data are available from cells bombarded with 1 MeV electrons. Because of this, it is a relatively simple matter to predict damage once an equivalent 1 MeV fluence has been determined.

The effective equivalent fluence is used in Figure 125 as an independent variable. The damage coefficient has been calculated for protons and electrons by measuring the diffusion length before and after irradiation. These damage coefficients are for bare cells on which the radiation is normally incident. Figure 125 represents the Hughes interpretation of the data of Martin, Statler, and Ralph from their paper, "Radiation Damage to Thin Silicon Solar Cell," dated 1967. The environment must be converted to include the effect of coverslips and base resistivity before finding the solar cell degradation from this figure. Degradation for both 10 ohm-cm and 2 ohm-cm base resistivity cells is calculated in the following steps:

1) A baseline reference 2.1×10^{14} equivalent 1 MeV electron fluence is established for a 12 mil (0.30 mm) thick 10 ohm-cm cell with 12 mil (0.30 mm) cover for a 5 year mission in synchronous orbit.

2) Effect of change in coverglass thickness is calculated. A change from 0.30 to 0.15 mm thick coverglass thickness on the 10 ohm-cm (0.30 mm) thick cell reduces the protection and more low energy electrons and protons will cause damage. The resultant fluence is 4×10^{14} equivalent (1 MeV) electrons.

3) With this fluence, the degraded power of a 10 mil (0.25 mm) thick 10 ohm-cm cell is found to be 82.5 percent in Figure 125.

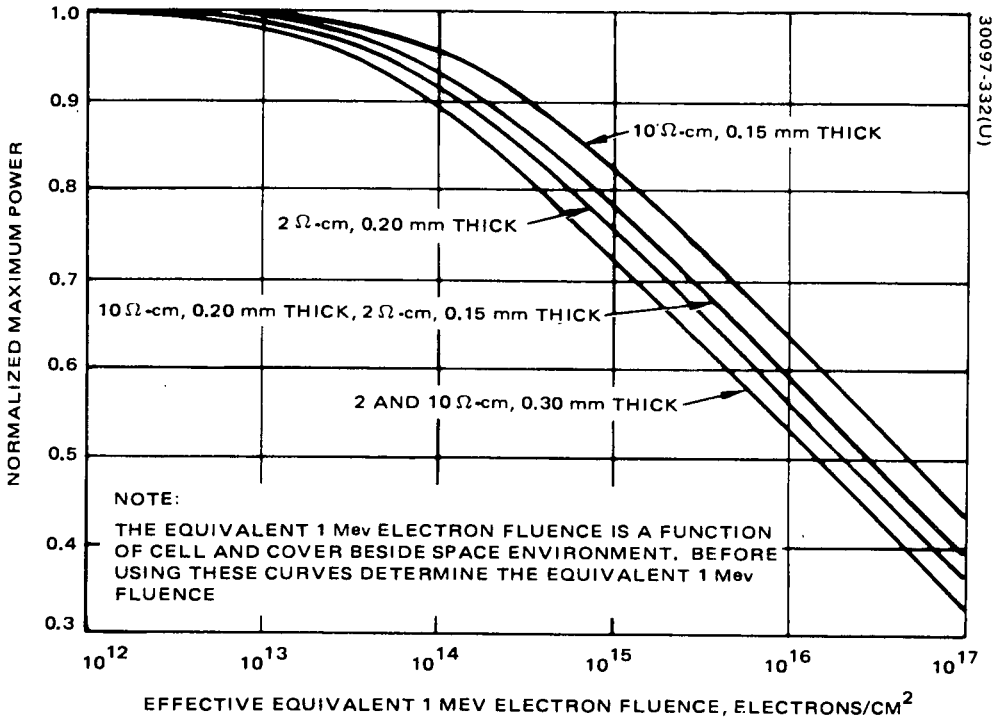

Figure 125. Normalized Maximum Power Versus Effective Equivalent 1 Mev Electron Fluence

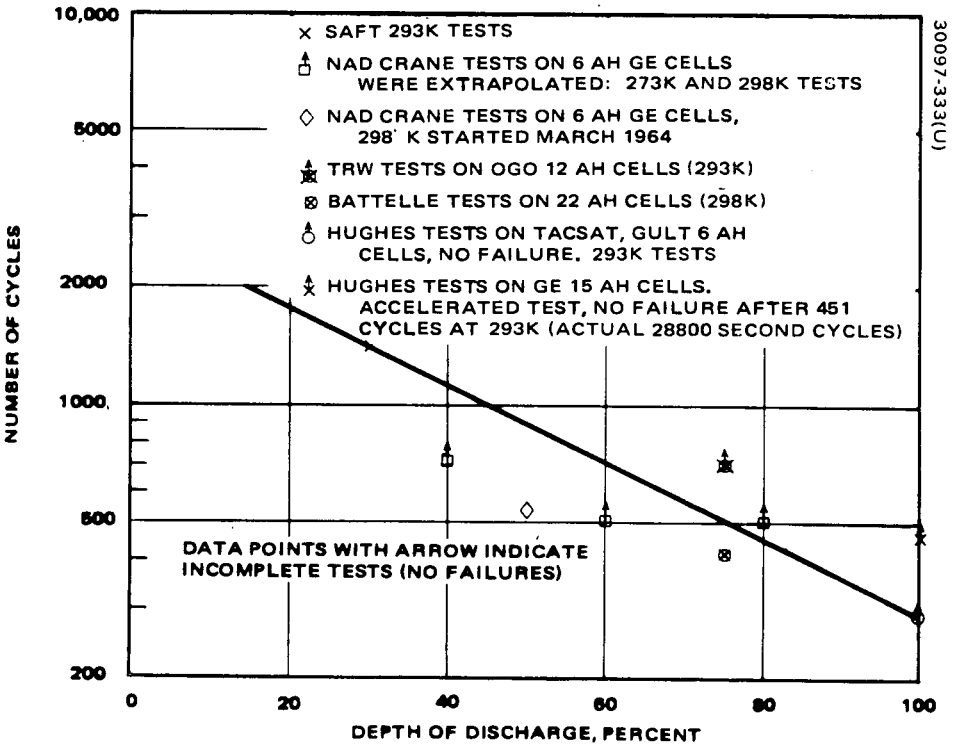

Figure 126. Battery Cycle Life in Simulated 24 Hour Synchronous Orbit

4. 3. 6. 2 Batteries

During a 5 year mission in synchronous equatorial orbit, there are 450 eclipse cycles when the spacecraft is powered by batteries. Battery design selection was based on laboratory cycle life test data, orbital experience with batteries, and on careful consideration of battery temperature, depth of discharge, charge rate, limitation of overcharge, and trickle charge after completion of charging. Two parallel connected nickel-cadmium batteries are provided that will operate at a maximum of 60 percent depth of discharge during the maximum solar eclipse when supporting a "full-up" satellite operation. Unfortunately, there is only a limited amount of laboratory test data on battery cycle life in 24 hours synchronous orbit. Figure 126 shows the cycle life test data collected from different sources. These tests were conducted under varying charge-discharge regimes, and most followed a simulated in-orbit eclipse cycling. Eclipses varied from 0 to 1. 2 hours over a 46 day period twice a year. Trickle charging was used during the noneclipse seasons. The depth of discharge in this figure indicates the maximum for each eclipse season, while the average depth of discharge is 76 percent of maximum. The points marked with an arrow indicate incomplete or continuing test. None of these batteries was reconditioned between eclipse cycles. The Battelle tests were more severe than the rest. Their failure criterion was a minimum 1. 1 volt per cell end of discharge. Accelerated tests run by Hughes at continuous 100 percent rated depth-of-discharge cycling indicate a higher cycle life capability than the average shown in this figure.

Each battery consists of 16 cells of 10 A-hr capacity and is assembled in two packs. The battery design is an improved version of the Intelsat IV battery which is space-proven.

The battery discharge voltage is stepped up by a boost discharge regulator to 25. 5 volts. Each battery can operate successfully with 14 out of 16 cells operational and two cells shorted. Since open cell failures have not been experienced in flight-qualified batteries, the design provides considerable redundancy. In the event of a single battery failure, the satellite remains fully operational in sunlight operation and will provide reduced communication capability in eclipse. The battery design data are listed in Table 44.

To maximize battery life, the battery operating temperature must be kept as low as possible. This can be achieved by proper thermal control and by preventing overcharging. The battery is designed to give the best possible thermal relief, at the lowest mass, without compromising structural integrity. Similar cell and packaging design temperatures were within 3 K of the prediction. The battery temperature in the TDRSS design will be between 273 and 298 K. Battery charging will be terminated when the temperature rises above 300 K indicating overcharge condition. The batteries will be kept on trickle charge after charging and will also be trickle-charged between eclipse seasons.

TABLE 44. BATTERIES

Type	Nickel-cadmium
Number	Two
Cells	10 A-hr
Number of cells in series	Sixteen packaged in two to eight cell packs
Maximum depth of discharge	60%
Eclipse cycles	450
Charge rate end of life	C/15 constant current
Trickle charge rate	C/60
Maximum temperature	300 K
Battery system mass	15.4 kg

Use of overtemperature control for charge termination instead of third electrode control was selected based on Hughes extensive experience with synchronous orbit battery applications. It is, however, realized that recent NAD Crane tests on GE 12 A-hr batteries in simulated synchronous orbit were using third electrode control successfully. These batteries indicated practically no degradation in 3 years of testing at 273 K and 293 K and at 60 and 80 percent maximum depth of discharges. The good performance of these batteries can also be attributed to the relatively high rate of charging, C/4, which is not practical for application. A C/15 rate in Hughes experience will give similarly good results.

The life expectancy of batteries is primarily a wear out function rather than random failures, compounded by damage due to improper in-orbit battery management. The wearout function is strongly dependent on operating temperature, and depth of discharge; this is heavily dependent on cell design, i.e., overcharge margin (excess negative capacity), precharge, presence of carbonates, loss of overcharge margin due to hydrolysis of nylon separators (accelerated by high temperatures, either ambient or due to overcharge). These characteristics can be controlled by highly detailed procurement specifications, vendor selection based on proven in-orbit performance, and laboratory life tests, electrochemical analysis before and during life tests, etc.

In-orbit battery management has two facets. The most important is battery integration such as battery thermal design, spacecraft thermal control, selection of maximum depth of discharge, charge rates, charge-termination techniques, fail-safe protection such as temperature cutoff, etc. The second is that of meticulous ground control when exercising override options on automatic battery control. The probability of successful survival of batteries for 5 years in the proposed application is largely based on the statistical record to date of the nickel-cadmium batteries used by Hughes in previous satellites. These data are also supplemented by extensive laboratory test data taken by Hughes, NAD-Crane, Battelle, SAFT, TRW, and others.

The capability of the battery design to meet mission requirements will be verified by a three-part test program: 1) development testing of cells and cell packs, 2) qualification test of flight hardware, and 3) life testing of a complete flight battery assembly. Physical, chemical, and electrochemical analyses will be performed for each section of the test program to provide a further assessment of cell performance.

4.3.6.3 Battery Control Electronics

Battery Charge and Recondition Control

The functions include: 1) automatic recharging of the batteries on exit from eclipse, 2) automatic charge termination, 3) ground control override for functions 1 and 2 on each battery separately, and 4) ground control of reconditioning discharge. The automatic electronic charge circuit will connect the batteries to the battery charge arrays of the solar panel. In the event of anomaly, it is possible to command charging for one or two batteries at a time. Solar cell strings supply a current-limited power source. When batteries are not being charged, these solar cell strings provide power to the main bus.

The batteries begin charging after emergence from an eclipse and continue charging until all batteries are fully charged. The primary method of charge cutoff is battery temperature. Four temperature set points are available for cutoff levels. The charge controller will be set to the enabled state by sensing collapse of charge string voltage.

Ground commands can be sent to override any of the charge controller functions and also to select the temperature value to be used for charge termination. Due to the pulse nature of the TT&C subsystem command outputs, the charge controller stores the command in the command buffer latches. Digital type status signals for telemetry output are obtained from these storage latches.

The battery charge circuits are essentially similar to those used on Telesat and Intelsat IV. Except here, each battery can be charged and trickle-charged from separate battery charge solar cell strings as indicated in Figure 127, a functional block diagram of the battery charge controller. The battery charge control electronics is designed initially redundant; any single component failure will not result in loss of battery for the mission.

The individual temperature inputs are derived from a constant current source into a set of thermistors, one on each battery pack, which provides a mean battery temperature. Charge is terminated when individual battery temperature exceeds the common temperature reference.

Flip-flop 14 outputs determine which batteries (1, or 2, or both) are charging. The individual batteries are cut back from full charge to trickle charge on an individual basis by the NAD gates G14 - G15. Manual charge override inputs are provided via the OR gates (G18 - G19) to allow control charging of individual batteries at the high rates, in the event of an automatic malfunction. The trickle charge command enters G22 - G23 as an OR gate signal and trickle-charges both batteries at once.

The relays K1 - K2 can be used to disconnect the individual batteries from the charge control circuitry. This prevents battery failure due to switch failure which could result in long-term high rate charging.

Battery Discharge Controllers

The battery/discharge controllers will be similar to those previously qualified for HS-318. The controller also functions to force equal battery current sharing within ± 5 percent. The circuit is of the boost choke type and uses pulse width modulation. It requires a minimum number of power transistors and results in lowest stress per power transistor and minimum input line filtering. To reduce power transistor stress and to minimize output filter size, each circuit is two phase, with forced current sharing between phases. In addition, each circuit is internally redundant; in effect, there are four parallel operating discharge controllers equally sharing the load during eclipse operation. Figure 128 is a block diagram of the discharge controller.

The battery discharge controllers maintain a regulated output voltage of 25.5 volts ± 0.5 volt. The battery voltage can vary from 21.6 to 16.1 volts during discharge. The battery controller output is also unaffected by short circuit failure of up to two battery cells.

In case of battery controller circuit failure, the redundant battery controller circuit will automatically take over the load. The redundant circuit design also protects against complete battery failure which is most unlikely. In that case, one battery must support all the spacecraft loads and only two battery controllers out of four will operate. Since the circuits are redundant, such 100 percent overload on one battery will not result in extra stresses on the discharge controller. The four discharge controllers are packaged in one assembly with adequate heat sinking to provide for emergency mode of operation.

The function of each controller is to boost the output of the battery to hold the main bus within an allowable band, with variation in battery voltage and load. This design is electrically identical to the battery controller presently used on HS-318 program, except for reduced power rating relative to HS-318. Following is a description of the controller operation in charge and discharge modes.

Upon entering the earth's shadow during orbital eclipses, the electrical power subsystem undergoes a transitional mode from total solar panel power operation to total battery power operation with no interruption of power to spacecraft loads. As the sun intensity decreases in the penumbra, the main bus being supplied by the solar panel will experience a corresponding reduction in voltage, and at a nominal set point of 25.5 volts dc, battery discharge control will start to function. The battery sources will then begin to share the load with the solar arrays. The power stage of the battery discharge control is variable K boost circuit that provides a regulated output voltage higher than the battery terminal voltage. This boosted output is feedback loop controlled to maintain the output voltage between 25 and 26 volts.

Page intentionally left blank

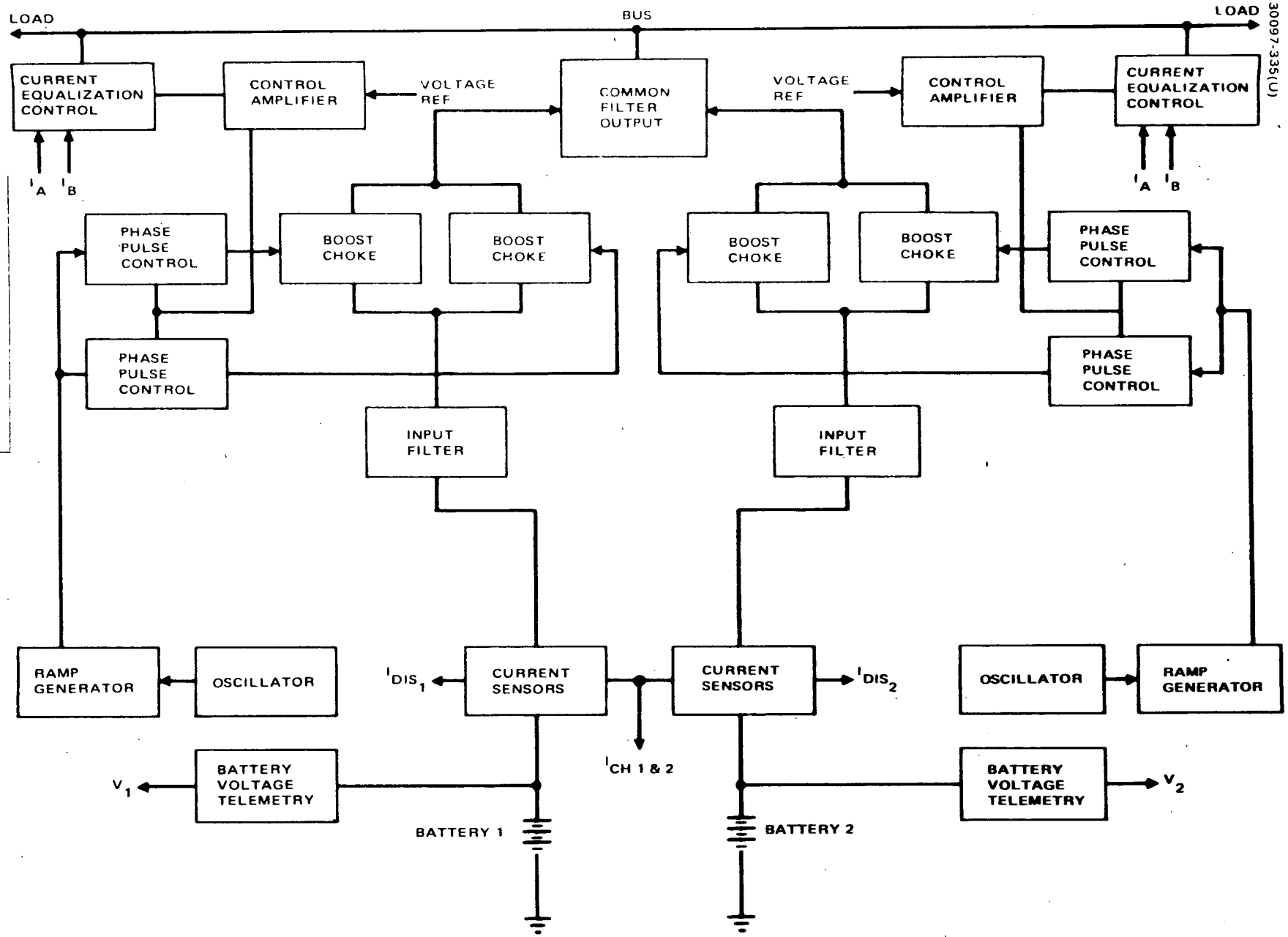

Figure 128. Battery Discharge Control Block Diagram

Thus, as the output of the solar array continues to decrease, the spacecraft batteries will continue to assume an increasingly larger portion of the load current until operation of the spacecraft is on batteries only.

As the battery terminal voltage decreases during normal discharge cycling, the voltage feedback loop continuously adjusts the K boost factor to maintain the regulated output voltage. The minimum battery control output voltage is 25 volts with two cells in a battery shorted and the battery discharged to 1.15 volts per cell.

The discharge current of each battery is sensed with a magnetic current sensor and an analog output from the sensor is provided to a current comparator circuit in each battery discharge control. This circuit acts to modify voltage control in each boost-choke stage to provide current sharing between batteries to within an allowable control rating and battery depth of discharge.

The biasing effect of the current equalizing control is designed so that the output of the battery discharge control will remain within its limits in the event of one regulator circuit failure and also will not adversely affect the performance of the three remaining batteries.

4.3.6.4 Voltage Limiters

Two types of voltage limiters will be used: a shunt tap limiter and a dissipative shunt bus limiter. Both types have been qualified for other spacecraft, i.e., tape limiter for Telesat, bus limiter for TACSAT. These limiters present low loss in series with the solar panel at EOL and full load. Additionally, they either add only a small heat load to the spacecraft when full load is on, or add a significant and desirable heat load when repeater loads are turned off.

The principal function of the tap limiter is to hold the bus voltage below 29.5 volts with full load applied, dumping surplus solar panel power at beginning of life by shunting or eliminating the current supplied by the tapped strings to the main bus. Most of the surplus power is radiated by the panel. Tap limiters also clamp the bus at 30 volts after exiting eclipse. Four tap limiters, each shunting a separate section of the array (1/8 of total array in each section) are provided. The limiters have set points separated by 0.1 volt, so that operation is incremental. A bus voltage increases, each limiter moves from open circuit to a linear control mode and finally to a short circuit.

Bus limiters place resistive loads across the bus when the bus voltage exceeds 29.5 volts. They replace some of the heat removed from the despun section during the transfer orbit, or any other time that spacecraft loads are light, to keep the temperature in the despun section above an acceptable limit and to maintain the bus voltage under 30 volts.

Tap Limiters

The function of the solar panel tap limiters is to limit the main bus voltage in the illumination period with variations in the output of the solar array caused by temperature, load, and degradation. The tap limiter group will limit the bus voltage to a value between 29 and 29.4 volts when the load is less than the array can support.

The limiter is subdivided into four units and each unit will be active over a narrow range of bus voltage. The gain of each of the limiters will be adjusted so that about 100 mV change in bus voltage will operate the power dissipating transistor output stages from cutoff to saturation. The set points for each of the units will be separated from the others by 100 mV so that only one unit is active at a time. The resultant power dissipation and operating range for each of the limiters would fit together so that individual limiter dissipation would be kept low (less than 35 watts), and the total peak dissipation would be less than 60 watts. This point is illustrated in Figure 129.

From the curves in Figure 129, it can be seen that each limiter is active over only a 100 mV bus voltage range and that this causes each regulator to go from cutoff to saturation. The amount of current carried when saturated is equal to the short circuit current of the solar array cell group that provides its input power. The power dissipation of each limiter is determined by the solar cell characteristics and by the way the cells are grouped to provide input current to the limiters.

The number of cells in series to the tap point is determined by the open circuit voltage of the cells remaining in the string after the limiter has saturated, by the saturation voltage of the limiter, and the voltage drop of the isolation diode. The open circuit voltage of the unshunted portion of the string plus the saturation voltage of the limiter and diode must be less than the desired bus voltage. This means that the tap for each limiter must be roughly at midpoint in the series string.

Upon emergence from eclipse, the tap limiters will saturate and the full bus shunt limiters may also turn on. Ground commands can be used to disable one or more tap limiters so that more bus shunt limiters will be energized and the power dissipated by the bus shunt limiters aids in warming the despun platform. As the array warms up, the bus shunt limiters turn off and control is taken wholly by the tap limiters. The total shunt current curve is a summation of the currents from each of the four units and provides a smooth transfer curve from one end of the regulation band to the other.

Bus Limiter

The bus limiter operates as a four-stage current-limited shunt regulator that, when used in conjunction with other voltage limiters, will prevent the solar panel bus voltage from exceeding 30 volts. Each voltage limiter consists of two sublimiters A and B which are adjusted to turn on at the set

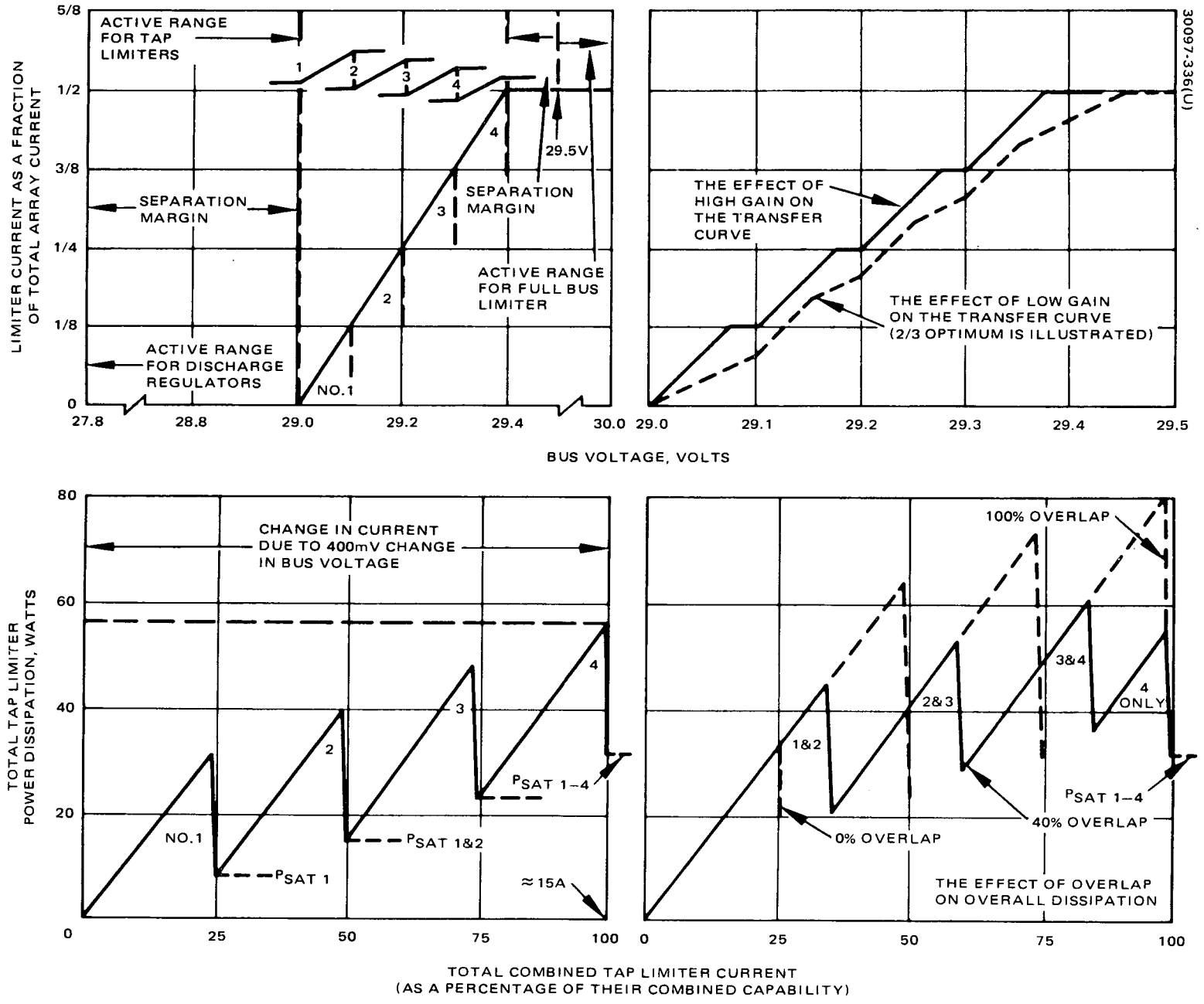

Figure 129. Tap Limiter Current and Dissipation Characteristics

points. One-half of each limiter has a turnon or set point 0.25 volt lower than the other half. Without any set point change due to commands, as the bus voltage rises, one-half of each limiter will start conducting before the other half of any limiter. This affords even distribution of heat.

Each bus limiter and its associated external load resistors dissipate a minimum of 110 watts at a bus voltage of 30 volts. Total dissipation for both bus limiters is 220 watts minimum at a primary bus voltage of 30 volts. With a primary bus voltage below 29.5 volts, the limiters are in a standby condition and dissipate a maximum of 0.58 watt.

The bus limiter will see a temperature variation at the mounting surface of 272 to 319 K during a normal orbit. A minimum mounting surface temperature of 272 K will occur in a typical eclipse orbit. Since the voltage limiter is a low dissipation device when in the standby condition, the temperature of the electronics will be very close to the mounting surface temperature. When the limiter is turned on, a maximum of 27.5 watts will be dissipated in the unit, thereby increasing the unit temperature. Heavy duty mounting webs for the high power dissipating components provide an efficient heat path to the mounting surface. The external power resistors will see a mounting surface temperature of 272 to 316 K during a normal orbit and a minimum of 255 K during a typical eclipse. Each 18 ohm power resistor will dissipate a maximum of 12.5 watts when its associated limiter is turned on.

4.3.6.5 Power Subsystem Performance

The power subsystem is designed to satisfy the power requirements listed in Table 40. Table 45 is a summary of the power system performance.

TABLE 45. POWER SUBSYSTEM PERFORMANCE – SOLAR ARRAY OUTPUT END OF LIFE

Summer solstice	364 W
23 days before equinox	397 W
Maximum bus voltage	30 V
Battery discharge turn-on voltage	25.5 V
Minimum bus voltage, battery power	24.5 V
Solar array maximum power voltage	26.5 V
Solar array temperature	300 K maximum, 183 K minimum
Battery depth of discharge maximum	60%
Number of eclipse cycles	450
Battery charging rate	C/15
Battery charge termination	Temperature signal
Battery trickle charge rate	C/60
Cell failures permitted per battery	Two
Battery discharge voltage	21.6 to 16.1 V
Battery operating temperature range	225 to 300 K
Battery discharge controller voltage	25.0 to 26.5 V
Battery charge controller operation	Automatic or ground commanded
Battery discharge controller operation	Automatic
Battery reconditioning	On ground command
Tap limiters, operating voltage	29 to 29.5 V
Bus limiters, operating voltage	29.5 to 30 V

4.3.6.6 Technology Status

The power subsystem design is based on 1973 state of the art. Any advancement in technology would result only in improved design margins.

Solar arrays will use a design similar to Intelsat IV and Telesat with solar cells mounted on a cylindrical substrate. The 0.25 mm thick 2 cm by 6.2 cm solar cells are state of the art and similar to those used on current Hughes satellite programs. The ceria-doped microsheet solar cell covers are available from Pilkington Perkin-Elmer Company and were used on European satellite programs. Both the performance and the price of these covers is expected to be better than of fused silica covers. With hardware procurement starting in 1974, it is anticipated that further improvements in solar cell technology could result in 5 to 10 percent more power.

The battery design is similar to that used on Intelsat and Telesat Programs. Selection of battery cell size and number of series connected cells is relatively flexible with a boost add-on discharge system.

Electronics in the power system are space proven, similar to that used in HS-318, Telesat and TACSAT. Components were only resized to match the solar array and battery requirements.

4.3.7 Apogee Motor

The only motor currently under development to serve as a synchronous apogee motor for a 2914 launch vehicle payload is Thiokol's TE-616, being built for the Canadian Technology Satellite. Due to concern with the CTS schedule and the lack of growth potential, preliminary designs from United Technology Center (UTC), Aerojet Solid Propellant Company (ASPC), and Hercules Incorporated (HI) were reviewed. Evaluation results are shown in Table 46. The only design offering a significant mass advantage was the Hercules motor, which was selected as the baseline. For the TDRS mission, approximately 10 kg of the spacecraft mass could be saved. The mass savings are due entirely to the higher performance of the HI propellant.

TABLE 46. CANDIDATE MOTORS

Designation	Manufacturer	Effective ISP, seconds	Mass, kilograms			Status
			Propellant	Inert	Motor	
TE-616	TCC	290.3	301	29.5	331	In development for CTS
-	Aerojet	291.0	300	33.1	333	New size based on SVM-5
-	UTC	281.0	306	33.1	339	New size based on FW-5
-	Hercules	298.1	293	27.7	321	New size based on X-259

4.3.7.1 Apogee Motor Description

The chamber is filament wound of S-901 glass fiber and a catalyzed epoxy resin system, which has been successfully used for many applications, including the X-259, BE-3, and the first and second stage Poseidon chambers. The winding will be of interspersed layers of 20 degree helical and 90 degree circumferential wraps of the resin-impregnated glass fiber. The chamber interior will be thermally protected from the propellant combustion gases during motor operation by asbestos-filled styrene-butadiene rubber (SBR/ asbestos insulation, selected because of its demonstrated high reliability and extensive use in the X-259 motor, and its compatibility with the propellant chamber system and the motor's operating conditions. The best design features of the nozzles used on three Hercules motors are combined in the proposed design. These motors have an impressive reliability record, with over 400 successful firings. The design is regarded as state-of-the-art technology incorporating standard, flight-proven materials.

The throat and inside exit diameters are 8.19 and 57.7 cm, respectively. Internal surfaces of the nozzle are fully contoured, and efficiency losses and erosion are minimized by a hyperbolic spiral entry, which achieves a uniform and predictable heat transfer film coefficient. The expansion cone is contoured to a basic Rao parabolic geometry, modified for the propellant metal content, and provides an expansion ratio of 50:1. The motor design is shown in Figure 130.

The nozzle entrance and throat region are supported with an aluminum attach flange. Tapers provide an effective pressure seal and efficient method of load transmittal. The expansion cone is a composite of graphite phenolic from the throat insert aft to an expansion ratio of 7:1, and asbestos phenolic extends through the rest of the cone. The entire nozzle is overwrapped with glass filament.

The selected propellant has been used in over 850 Hercules production motors. Its performance has been well characterized in over 65 static and 190 flight tests and has remainted consistent in motors fired after a period of 7 years. Because of its burn rate, high density, high delivered specific impulse, and excellent mechanical properties, this propellant is suitable for the apogee motor. It is a composite-modified, double-base (CMDB) formulation.

The grain configuration selected is patterned after the highly successful X-259 grain design and consists of a centerbore with nine aft-end wing slots. This configuration provides a relatively neutral thrust-time curve. It has the benefit of extensive use in the X-259 motor, wherein both the manufacturing technique is well established and the reliability is defined by test history.

The motor ignition system consists of the Pelmac 20674 electromechanical safe and arm device, used on Titan III and located at the forward end of the motor, and a pyrogen igniter mounted to the forward closure. The proposed design is an adaptation of proven design concepts and components from the Minuteman stage III M-57 motor and the X-259 motor.

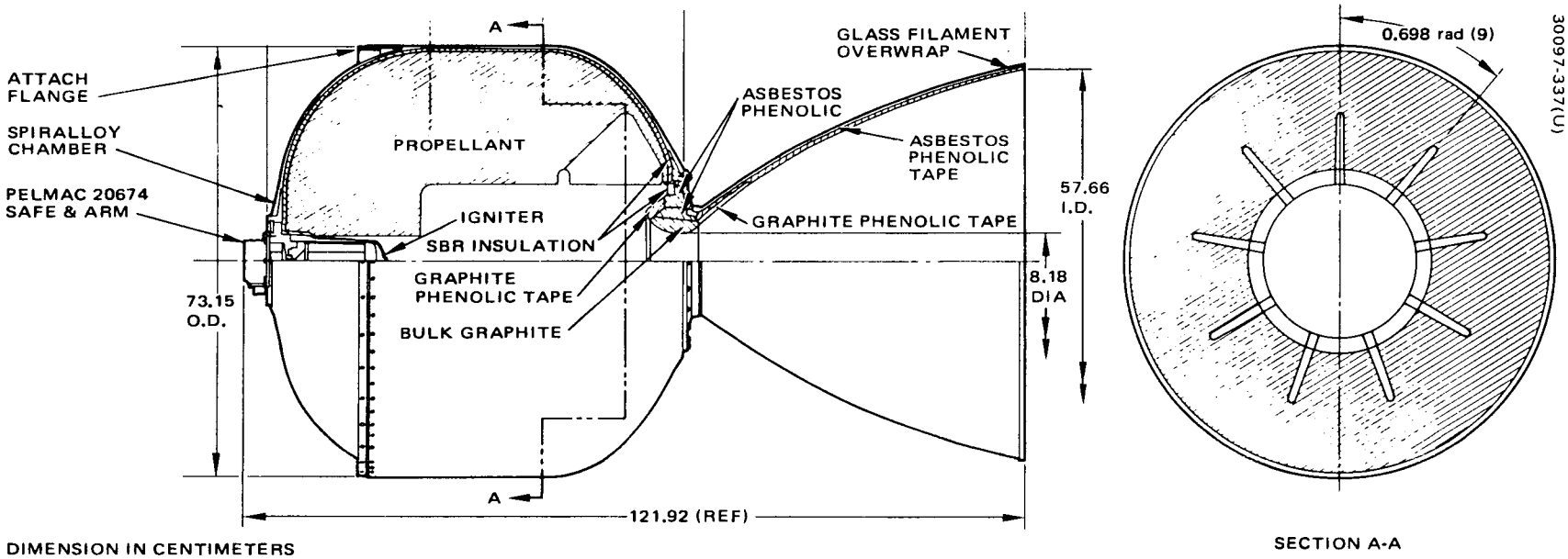

Figure 130. Hercules Apogee Motor

4.3.7.2 Performance

Table 47 is a summary of apogee motor ballistic parameters at a nominal operating temperature of 297 K. The maximum insulator-chamber bondline temperature during burning is predicted to be 367 K. The maximum temperature under all conditions is 394 K during burning and 533 K. Table 47 shows the calculated prefire mass of the motor. During firing, an estimated 2.27 kg of inert mass will be expended.

The apogee motor requirements are summarized in Table 48. The nominal velocity increment required to circularize the spacecraft orbit at synchronous altitude from the nominal transfer orbit and to remove 20.7 degrees of inclination is 1679 m/s. The variation will be held within +1.0 percent by requiring the motor manufacturer to verify predictions of total impulse within ±1 percent of all motors tested and delivered. Maximum thrust of 50 kiloNewtons and acceleration of 113 m/s^2 (11.5 g) for a 678 kg spacecraft are imposed to limit the acceleration and static loads on the spacecraft. The maximum allowable case temperature of 533 K has been established to protect the spacecraft.

The maximum allowable cg misplacement from the center of the mounting rings is set at 0.5 mm for the loaded motor and 1 mm for the burned out motor. (These values limit the static imbalance imposed by the spacecraft nutation requirement.) Dynamic imbalance limits have been

TABLE 47. APOGEE MOTOR PERFORMANCE AND MASS

Parameter	Nominal Value
Vacuum propellant specific impulse	300.0
Vacuum total impulse	861,885 N-s
Average vacuum thrust	40.7 kN
Maximum vacuum thrust	47.9 kN
Average chamber pressure	4.28 MN/m^2
Burn time	21.2 s
Propellant mass	293.2 kg
Expended energy	2.3 kg
Total motor mass	320.9 kg
Burnout mass	25.4 kg

TABLE 48. APOGEE MOTOR REQUIREMENTS

Performance	
ΔV	1679 m/s ±1% (5498 fps ±1%)
Maximum thrust	50 kN
Maximum acceleration	113 m/s^2 (11.5 g)
Maximum external case temperature	533 K
Physical Characteristics	
CG: loaded	0.5 mm
burned out	1.0 mm
Balance: loaded	0.022 $kg\text{-}m^2$
burned out	0.011 $kg\text{-}m^2$
Thrust alignment displacement	0.5 mm
angular	0.002 cm/cm
Moment of inertia	Known within ±5%
Environmental Conditions	
Operating temperatures	278 to 306 K
Storage life	3 years
Spin rate	100 rpm
Hard vacuum	10 days

established at 0.022 $kg\text{-}m^2$ for the loaded motor and 0.011 $kg\text{-}m^2$ for the burned out motor. The allowable thrust misalignment was set at 0.5 mm displacement and 0.1 degrees angular misalignment, which also limits spacecraft nutation and, in turn, velocity errors during motor operation.

The operating temperature range was established at 278 to 306 K and 272 to 311 K for qualification. The required storage life is 3 years at any temperature between 278 to 311 K. The motor must operate in any orientation while rotating at speeds up to 100 rpm and after exposure to hard vacuum for up to 10 days. The motor vibration and acceleration requirements are the same as the spacecraft requirements. These vibration levels will be applied to the apogee motor at the launch vehicle interface of the motor adapter so that the transmissibility to the apogee motor is duplicated.

4.3.7.3 Technology Status

The Hercules apogee motor design is a technology blend of the very successful X-259 and BE-3 motors which have had over 280 consecutive successes in space applications. Only flight proven design concepts and materials are used as shown in Table 49.

4.3.8 Spacecraft Structure

The TDRS is designed to be compatible with the Delta 2914 launch vehicle utilizing the standard 3731 spacecraft attach fitting assembly. The design requirement is to maintain the structural integrity of the spacecraft over the predicted environment for a minimum 5 year mission, including ground handling, launch, orbit injection, and on-orbit operations. A primary objective of the structural design is to satisfy the requirements with a minimum mass load carrying structure.

The TDRS is a relatively large spacecraft for the Delta 2914 launch vehicle, and light structural design approaches are mandatory. Design concepts used on previous spacecraft which minimize structural mass have been adapted to TDRS. Beryllium has been selected as the principal structural material with attendant mass savings of the order of 20 to 30 percent as compared to conventional aluminum and magnesium structures.

TABLE 49. MOTOR DEVELOPMENT STATUS

Component	Comment
Case	New size using X259 and BE-3 materials)S-901 glass fiber) and design
Nozzle	New size using X259 and BE-3 materials and design except for contour and expansion ratio
Propellant	Composite modified double base (CMDB) fully characterized with 65 static tests and 190 flight firings over the last 7 years 318×10^6 kg (3500 tons) processed to date
Insulation	SRB/asbestos used on X259. Excellent compatibility with CMDB.
Liner	Epoxy resin standard for case bonded CMDB grains.
Igniter	Pyrogen igniter - X259 and Minutemanstage III materials and design
Safe and arm	Pelmac 20674 used on Titan III and FW5

The Hughes Gyrostat type spacecraft design concept is used. The apogee injection motor is integrated into the central thrust tube, which also supports the cylindrical solar cell array and the despun communication equipment platform. The mating despin bearing assembly is bypassed during launch by a rigid load clamp.

The primary structure of the spacecraft is made up of three basic assemblies: spun section, despun equipment section, and antenna support mast. This division results in three assemblies of roughly the same size. Manufacturing and assembly operations proceed in parallel and the spacecraft can also be checked out and shipped more conveniently.

4.3.8.1 Spun Section

The spun section consists of a central thrust cone, four ribs connected by a thin cover sheet for shear strength, and a cylindrical solar panel substrate. The central thrust cone is an assembly of three formed conical skins and six machined rings. The formed skins are beryllium while the rings are fabricated from aluminum alloys. The lower cone has an aft ring that is machined to provide a mating surface with the launch vehicle attach fitting and a Marman type separation clamp. It also includes provisions for supporting separation switch pads and separation spring pads.

The intermediate cone section and the lower cone are joined by a ring that serves a dual purpose. It provides an attachment for the lower inboard end of the spun ribs and support end alignment for the apogee motor. A ring at the juncture of the intermediate and forward cones provides the forward support for the inboard end of the spun ribs as well as the attachment of the inner perimeter of the thin magnesium sheet mounted on the rib tops. The forward ring of the cone mates with the BAPTA housing forward flange and it is configured to accept the Marman type load clamp. Intermediate rings permit radial support for the BAPTA and the hydrazine propellant tank upper fitting. All rings are machined from aluminum alloy forgings.

The rib assembly includes four tapered beryllium ribs, intercostal ties between the tips of the ribs, and a thin magnesium cover plate that provides shear transfer in torsional loading. Four propellant tank lower fittings attach directly to each rib. In areas where equipment is mounted to the rib web, local doublers and stiffening members are provided. Support brackets for radial jets, attitude sensors, and electrical umbilicals are located on the rib intercostals. Machined fittings, mounted at the outboard end of each spun rib support the cylindrical solar panel.

The cylindrical solar panel substrate is of sandwich construction with an aluminum honeycomb core, fiberglass face sheets, and edge closures. Metal inserts are bonded into the substrate for structural attachments.

4.3.8.2 Despun Equipment Section

The despun equipment section structure is composed of a central hub, six tapered radial ribs, and an equipment shelf. The hub and ribs are fabricated from beryllium sheet; the shelf is of plate and stringer construction. The machined central hub supports 1) the BAPTA despun shaft, the load clamp and the despun shelf at its aft radial flange, 2) the antenna mast on its forward flange, and 3) the despun ribs on the cylindrical portion of the hub. The ribs are of a web and tee cup flange design, with a maximum rib depth at the central hub, and tapering in depth as they extend outboard. The aft flange supports the equipment shelf. The tee sections are constructed by bonding two angles formed from beryllium sheet back to back along the edge of the beryllium web.

4.3.8.3 Antenna Support and Mast Assembly

The mast structural assembly consists of a fixed central mast, deployable arms that are pivoted from the upper end, and platform mounted support links. The assembly is fabricated from extruded beryllium tubular elements. The cylindrical central mast has a machined fitting that mates with the despun section hub. Machined fittings provide for the support of the Ku band antennas and their two axis positioners, and the nutation damper. The AGIPA support is hinged at the top of the fixed mast. The central mast is tubular in cross section, but has a chemically milled tapered wall to provide a minimum mass design.

The Ku band and UHF antennas are tied to despun platform ribs and they are separately supported by struts. All antenna supports are connected to the central mast for launch. After lock release in orbit, all antennas are located in their respective positions by spring loaded deployment mechanism and structural links to the spacecraft.

4.3.8.4 Structural Performance Analyses

During Phase I of the TDRS study effort, a detailed mathematical model was generated for the spacecraft in its launch configuration. The present Phase II spacecraft design differs in its structural characteristics from the previous design by

1) The solar panel length shortened to 2.03 meters for the Phase II configuration (2.21 meters for Phase I design)

2) The addition of the AGIPA mass loading onto the central support mast

3) Minor decreases and/or shifts in mass property distributions due to subsystem design changes

All these changes are small with respect to the detailed modeling for the dynamic analysis, and therefore the Phase I study results are considered

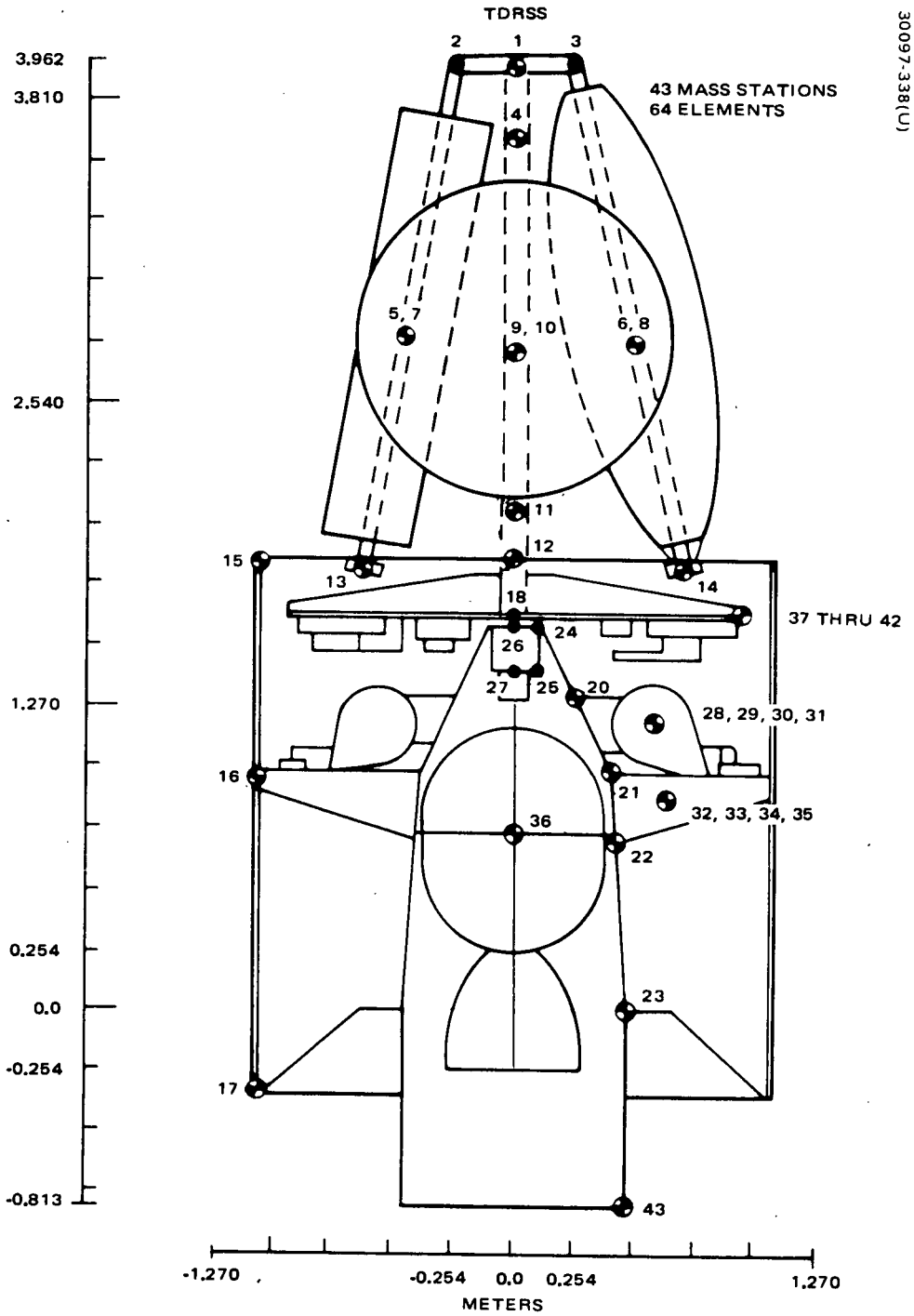

Figure 131. Mass Stations

valid. A total of 43 mass stations and 64 connecting structural elements were used to generate a representative usable model (see Figure 131). The structure is fixed at the base of the booster adapter, STA 43. STA 23 denotes the separation plane.

The structural elements were directly modeled using the Hughes computer routine MARS type one, two, three, and five elements which are beam, shell, and plate elements, respectively. The only exceptions were the antennas. For modeling purposes, equivalent stiffness type two elements were formed based on a 50 Hz lateral natural frequency for pinned end supports. Structural joints for the model are assumed to be rigid, except where antenna hinges are modeled.

Table 50 identifies natural frequencies and mode shapes up to a frequency limit of 95 Hz. Figures 132 through 135 show the first two bending mode shapes for the X and Y system axes. The mode shapes of these fundamental spacecraft frequencies are dominated by the central antenna support mast characteristics. A change in mass distribution as achieved by adding the AGIPA antenna will reduce the resonance frequencies slightly; however, the mode shapes remain essentially the same.

4.3.8.5 Preliminary Stress Analysis

A preliminary stress analysis of the primary structural elements of the spacecraft has been performed. A summary of minimum margins of safety together with the corresponding design load cases and modes of failure are presented in Table 51. The analysis was performed using three static load conditions listed in Table 52. All design loads correspond to a Delta 2914 boost vehicle using an MDAC 3731 adapter. The nonuniform lateral loading case (Case 2, Figure 136) proved to be critical for design of the mast and thrust cones. Case 4, Figure 136, which assumes a longitudinal load factor of 35 g (ultimate) resulting from longitudinal spacecraft vibration testing, was critical in sizing the spun and despun support ribs and the main stiffening rings.

A summary of the maximum shear, axial load, and bending moment for several spacecraft stations and corresponding math model stations is presented in Table 53.

Analysis of the thrust cones is summarized in Table 54. The three cones were sized for both aluminum and beryllium using the Hughes CONEA computer program which computers the minimum wall thickness and margin of safety for a given set of parameters. Beryllium conical skins result in the lighter mass structure. The antenna support mast was sized for beryllium in the interest of mass reduction. Beryllium also resulted in the lightest design for the spun and despun support ribs. The ribs are builtup sections composed of beryllium cross-rolled sheet for the webs and extruded caps.

TABLE 50. MODAL CHARACTERISTICS

Mode	Frequency, Hz	Type
1	11.2	X bending of mast
2	12.3	First despun torsion
3	13.6	Y bending of mast
4	23.1	Second X bending
5	24.4	Second Y bending
6	36.1	First despun shelf rocking (Y axis)
7	36.8	Second despun shelf rocking (X axis)
8	38.2	First solar panel torsion
9	41.1	Third despun shelf mode (X axis) antenna coupling
10	43.9	Antenna mode (X)
11	44.8	Fourth despun shelf rocking (Y axis)
12	44.9	Antenna mode (Y)
13	46.0	Fifth despun shelf plate mode (about Y axis) (antenna coupling)
14	46.1	Sixth despun shelf plate mode
15	46.4	Antenna (X)
16	46.7	Antenna (Y)
17	53.7	Antenna, despun shelf coupled
18	55.3	K_u band parabolic reflect antenna
19	56.2	Antenna, despun shelf coupled
20	59.0	Solar panel X bending
21	59.1	Solar panel Y bending
22	72.4	Antenna mode
23	85.0	Third X bending
24	89.6	Tank mode
25	90.0	Coupled X bending (fourth) and tank mode
26	90.7	Tank mode
27	91.1	Coupled X bending (fourth) tank and apogee motor
28	92.8	Tank mode
39	149	Axial of solar panel
48	223	Axial of solar panel

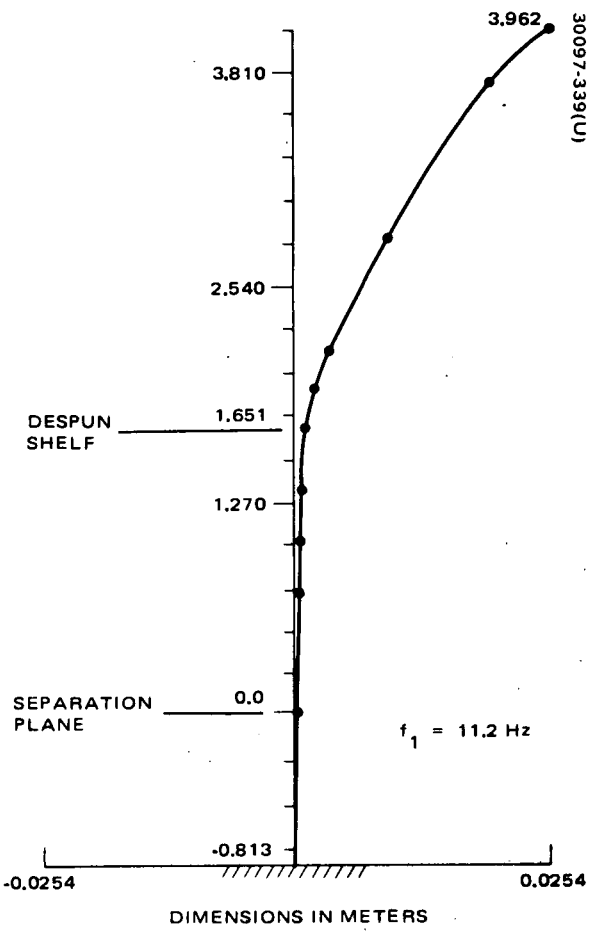

Figure 132. First X Bending of Mast

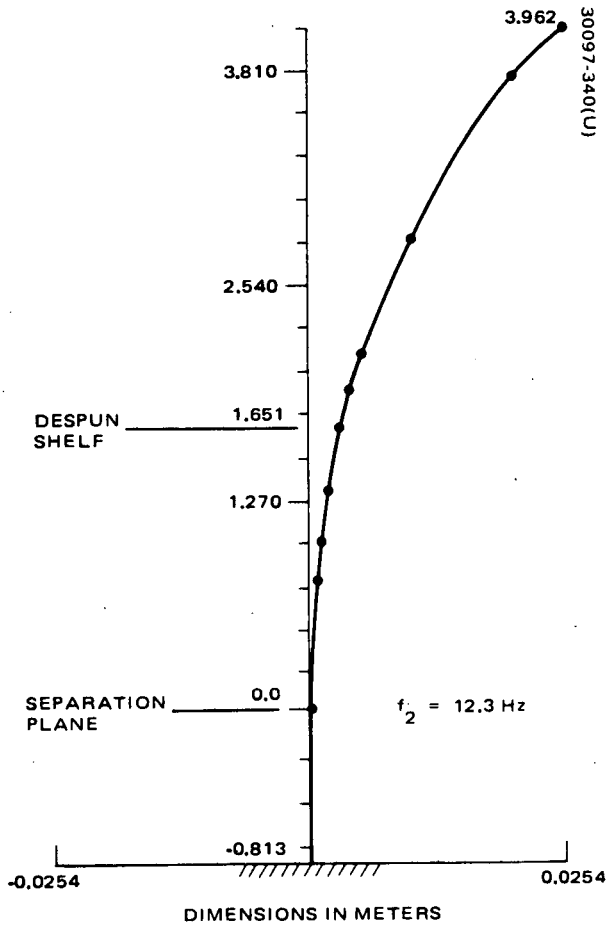

Figure 133. First Y Bending of Mast

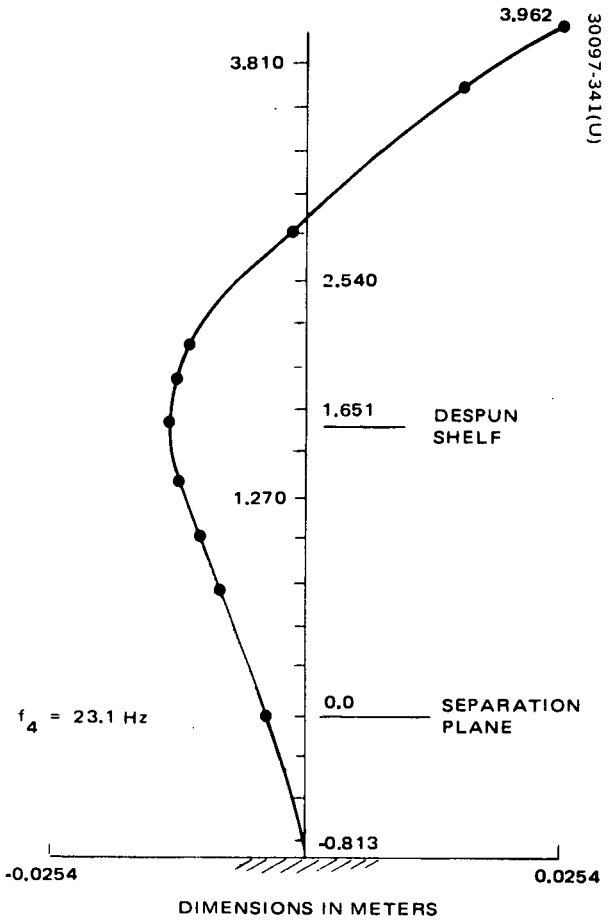

Figure 134. Second X Bending of Mast

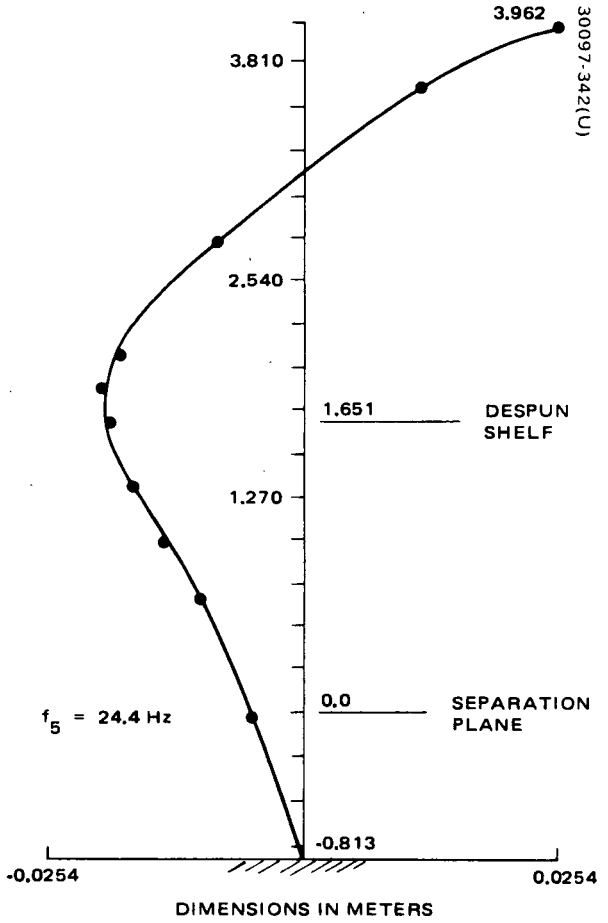

Figure 135. Second Y Bending of Mast

TABLE 51. SUMMARY OF MINIMUM MARGINS OF SAFETY

Part Name	Critical Condition	Type of Loading	Mode of Failure	Margins of Safety	
				MSy	MSu
Aft thrust cone	Nonuniform quasi-static loading	Bending plus shear plus compression	Buckling	-	0.17
Apogee motor run	Longitudinal vibration	Bending	Fracture	-	0.22
Intermediate thrust cone	Nonuniform quasi-static loading	Bending plus shear plus compression	Buckling	-	0.18
Forward ring – intermediate cone	Longitudinal vibration	Bending	Fracture	-	0.51
Aft separation ring	Nonuniform quasi-static loading	Bending plus compression	Fracture	-	0.30
Forward thrust cone	Nonuniform quasi-static loading	Bending plus shear plus compression	Buckling	-	0.16
Despun ribs	Longitudinal vibration	Compression in flange	Fracture	-	0.34
Spun ribs	Longitudinal vibration	Shear in web	Shear buckling	-	0.48
Lower mast	Nonuniform quasi-static loading	Bending	Fracture	0.14	-
Middle mast	Nonuniform quasi-static loading	Bending	Fracture	0.015	-
Upper mast	Nonuniform quasi-static loading	Bending	Fracture	0.19	-

TABLE 52. CRITICAL LOAD CASES

Spacecraft Status	Axis	Acceleration, m/s^2
Case 1	Thrust (Z)	-177
POGO event	Lateral (X, Y)	± Uniform 9.8
Case 2*	Thrust (Z)	-44, +15
Liftoff, maximum g	Lateral (X, Y)	± Nonuniform load curve
Case 3**	Thrust (Z)	-159
Third-stage motor burn	Radial	132 R (centrifugal at R meters radius)
	Lateral (X, Y)	5 uniform
Case 4	Thrust (Z)	±353
Estimated vibration test loads, maximum		

*Loads due to MECO are encompassed by the POGO and liftoff events.
**Case 3 also applies to apogee motor burn.

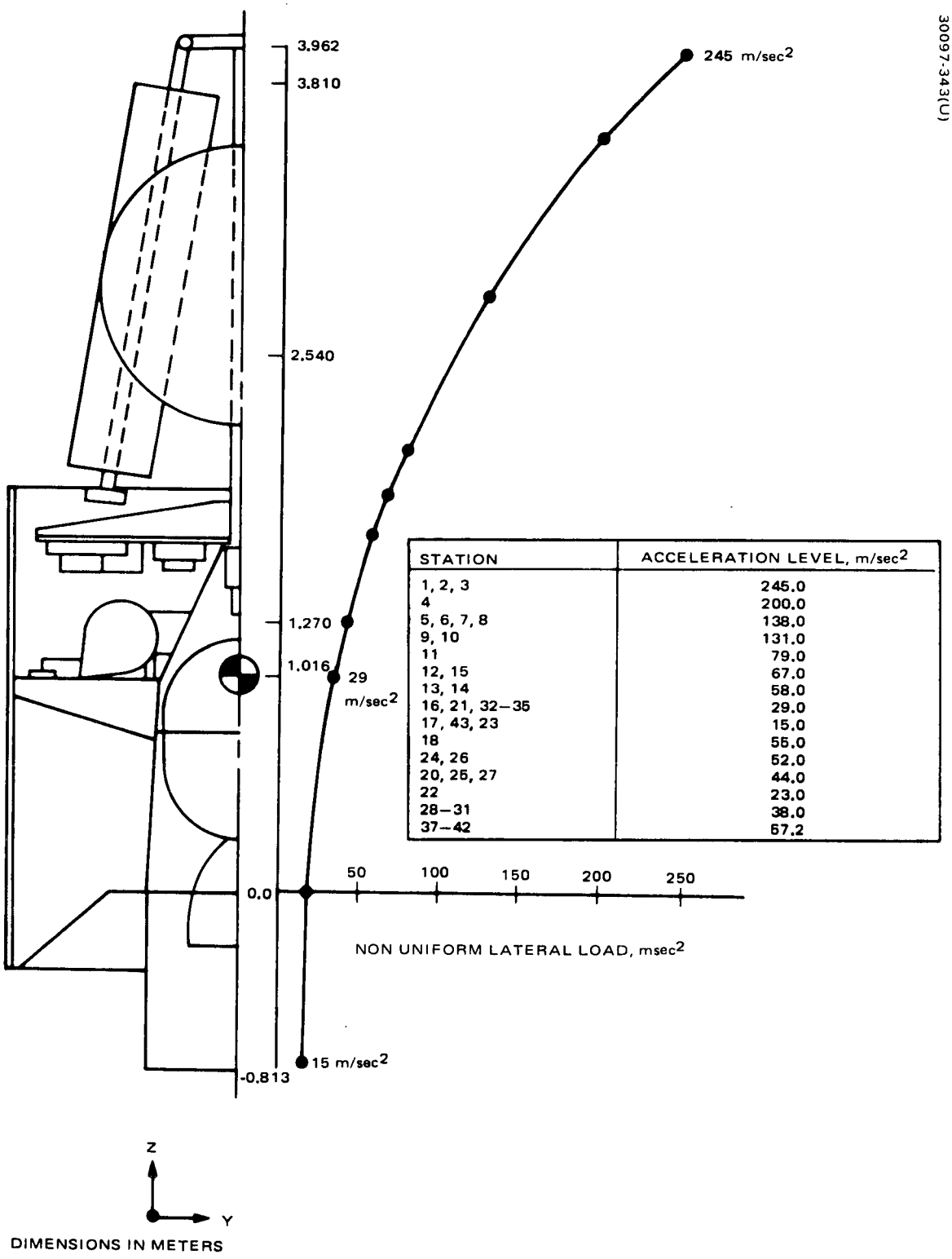

Figure 136. TDRSS Design Loads - Condition 2: Lateral Loads

TABLE 53. CRITICAL DESIGN LOADS (ULTIMATE)

Spacecraft Station	Math Model Station	Condition	Axial* Load, newtons	Shear** Load, newtons	Moment** M_y or M_x (newton-meter)
3.962	1	IIB	1,828	1,397	247
3.556	4	IIB	1,828	1,397	(190)
	4–10	IIA	2,277	5,142	4,006
	4–10	IIB	2,042	249	1,902
2.794	10	IIA	2,691	6,370	3,908
2.096	11	IIA	2,691	6,370	8,487
1.880	12	IIA	2,807	6,579	9,908
1.651	18	IIA	3,007	6,877	11,478
1.600	24	IIA	7,108	13,474	11,320
1.270	20	IIA	7,108	13,474	17,478
1.270	20	IIB	6,512	15,288	17,420
0.991	21	IIB	6,512	15,288	19,750
0.991	21	IIB	14,728	19,233	20,596
0.737	22	IIB	14,728	19,233	25,477
0.737	22	IIB	29,852	27,192	25,680
0	23	IIB	29,852	27,192	45,711

*All axial loads are in the -Z direction (aft).

**Signs have been omitted. The most critical combination of shear and bending moment is used.

TABLE 54. SUMMARY OF DESIGN LOADS FOR THRUST CONES (ULTIMATE)

		Condition I			Condition II		
Position Name	Spacecraft Station	Axial Load, newtons	Shear Load, newtons	Moment, newton-meters	Axial Load, newtons	Shear Load, newtons	Moment, newton-meters
Forward thrust	1.600	26,700		2,260	7,108 (Be:0.035)	13,470	11,320 (A1:0.066)
Intermediate cone	0.991	–	–	–	14,730 (Be:0.027)	19,230	20,600 (A1:0.050)
Aft thrust cone	0.546	120,900	13,340	6,780	29,850 (Be:0.032)	26,870	30,600 (A1:0.059)
Separation plane	0.0	–	–	–	29,850	27,190	45,720

TABLE 55. SPACECRAFT STRUCTURE COMPONENTS

Item	Type of Construction	Material
Spun platform	Four ribs with stiffened shear plates	Beryllium ribs, magnesium plate
Cylinder solar substrate	2 cm honeycomb core, two-ply facesheets	Aluminum fiberglass
Despun platform	Six ribs with stiffened equipment mounting plate	Beryllium
Antenna support mast	Thin wall tubes machined fittings	Beryllium, aluminum
Bearing clamp	Marman band with four clamp shoes	Steel, titanium

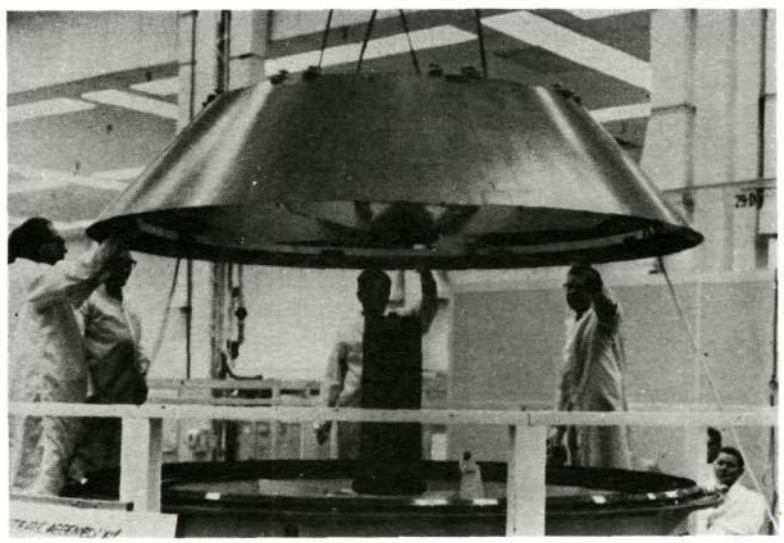

- LARGEST STRUCTURAL ELEMENT KNOWN TO EXIST MADE ENTIRELY FROM BERYLLIUM
- CARRIES ALL SPACECRAFT LOADS
- SAVES 50 lb, COMPARED TO EQUIVALENT ALUMINUM STRUCTURE
- CONSTRUCTION ID MONOCOQUE WITH ALL BONDED JOINTS
- STRUCTURE ALSO SERVES AS ELECTRICAL POWER SOURCE, WITH SUBSEQUENT ADDITION OF 1 in. HONEYCOMB SUBSTRATE TO WHICH SOLAR CELLS ARE ATTACHED

Figure 137. Beryllium Structures - Conical Assembly (Photo 4B328)

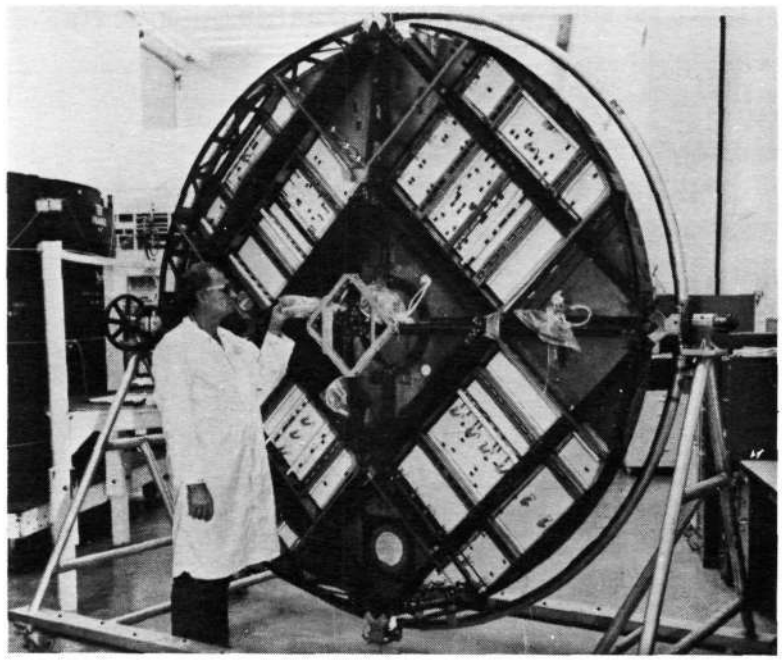

- STRUCTURE IS ALL BERYLLIUM EXCEPT FOR ALUMINUM LAUNCH LOCKS ON ENDS OF ARMS
- 80 INDIVIDUAL PIECES OF BERYLLIUM ARE USED IN PLATFORM
- CONSTRUCTION USES ALL BONDED JOINTS
- STRUCTURE WEIGHT 50 lb; WOULD WEIGH 85 TO 90 lb IF MADE FROM ALUMINUM

Figure 138. Beryllium Structures - Despun Platform (Photo A29886)

Details of the TDR spacecraft structure subsystem are illustrated in the configuration drawing shown in the system summary description. A summary for major structure components construction concepts and materials is provided in Table 55. All components are configured after previous Hughes spacecraft structure elements. The use of beryllium in primary load bearing structures has been demonstrated at Hughes in military spacecraft applications such as HS-308, HS-318, and HS-350. Examples of beryllium structural components are shown in Figures 137 and 138.

4.3.9 Thermal Control

4.3.9.1 Thermal Design Requirements

The spacecraft thermal control subsystem must provide an adequate temperature environment for all functioning subsystems for a period of at

TABLE 56. SUBSYSTEM TEMPERATURE REQUIREMENTS

Equipment	Design Range, kelvin	Eclipse Minimum, kelvin
Despun		
Transmitters, receivers, and other repeater electronics	267 to 311	261
Telemetry and command electronics	267 to 311	261
S band antenna positioner	222 to 367	222
Antenna mast and cabling	200 to 367 Mast deflection due to diametral temperature difference 0.28	200
Antennas	117 to 395	117
Spinning		
Apogee motor	278 to 306	278
Despin bearing	273 to 311	284
Despin electronics	267 to 323	261
Batteries*	273 to 300	273
Solar panel	222 to 297	172
RCS tanks	278 to 333	278
Lines	278 to 367	278
Valves	278 to 339	278

*No overcharge.

C-4

least 5 years in synchronous equatorial orbit. In particular, the design must be sufficiently flexible to accommodate significant variations in internal power dissipation that result from a combination of seasonal changes, long mission life, and optional system operating modes. The orbital design must also be compatible with survival and/or operation of all subsystems during ascent, transfer to synchronous orbit, and apogee motor burn.

Table 56 presents the subsystem temperature requirements that have been established for the study baseline. The expected extremes in system power dissipation using baseline estimates of equipment power requirements, operational modes, and solar panel electrical characteristics have been obtained from Table 40. The maximum dissipation for the spinning equipment complement will occur when the batteries are on charge at the beginning and end of the eclipse season (short eclipse times). However, the batteries will be continuously monitored to prevent overcharge, which may cause the battery to exceed the high temperature limit.

4.3.9.2 Design Description

The overall concept is one of passive thermal control, which takes advantage of both the temperature averaging that results from the uniform spin rate of the vehicle solar panel and the containment of the sun within ±30 degrees of the orbit plane. The key features of the thermal design are identified in Figure 139. As a result of the large dimensions of the spacecraft, radiation is the dominant mode of heat transfer between the major elements. The temperature of the spinning structure and low power dissipation regions are controlled by providing good radiation coupling to the solar panel in the same manner as that used for Intelsat IV. The batteries, which constitute the largest source of thermal dissipation on the spinning side, are hard-mounted to the structural ribs to provide thermal fin capability. The lines and valves of both the axial and radial thrusters are provided with molded blanket heaters that prevent any portion of the system from reaching the freezing point of hydrazine at any time during the operational life of the spacecraft. These heater elements are wrapped with low emittance aluminum tape to minimize the heater power requirements. The hydrazine tanks can be maintained above the freezing point with multilayer insulation and do not require active heating.

The bulk of the power dissipating units are grouped on a despun platform across the forward end of the solar panel, and temperature control is achieved in the same manner as used in the TACSAT design. Platform dissipation is radiated to an intermediate radiating surface provided just forward of the platform. Most of the intermediate radiating area (inboard) is despun, while the outermost rim is spinning. The high dissipating units are located near the perimeter of the despun shelf, below the spinning cover. The use of second surface aluminized teflon as the finish on the intermediate surface serves to attenuate the temperature variation of the platform with respect to solar incidence angle. Temperature sensitivity of this platform is further attenuated by radiation coupling to the stable solar panel boundary.

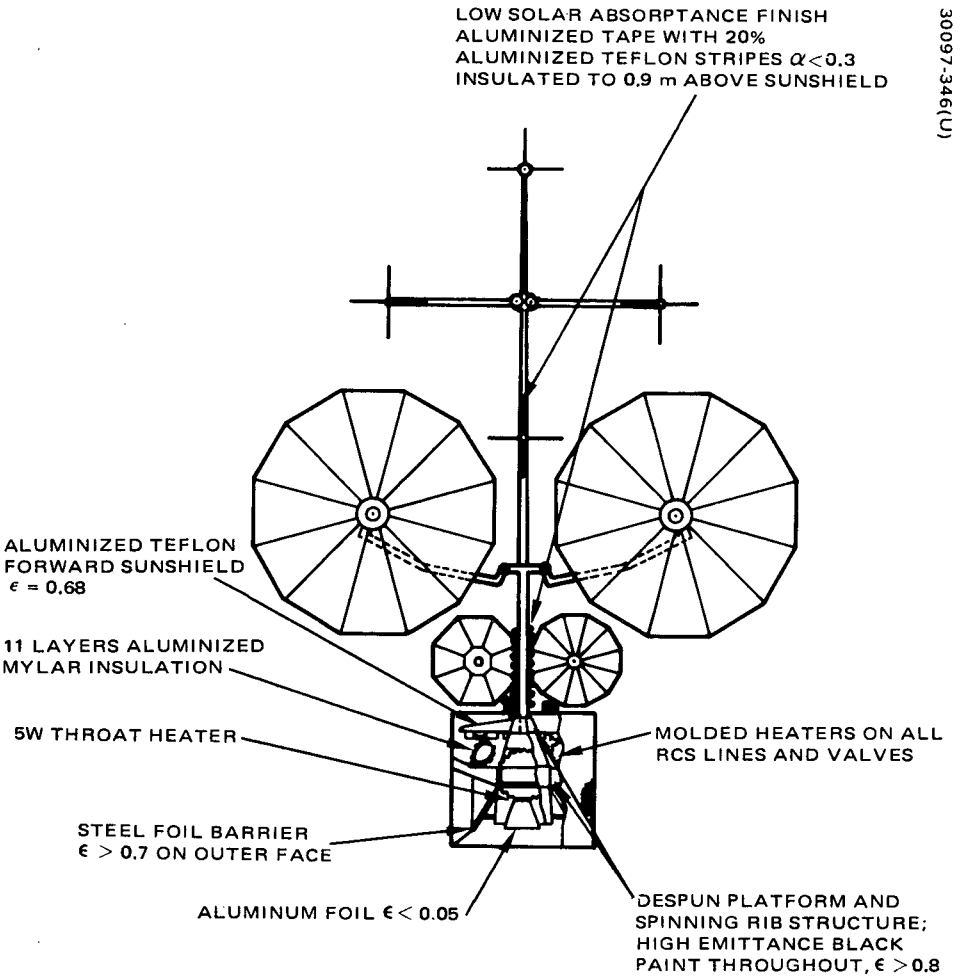

Figure 139. Spacecraft Thermal Control Configuration

The antenna mast is treated with a combination of aluminum foil and second surface aluminized teflon stripes to limit both the thermal bending of the mast and the peak temperature of the cabling that will be attached to the mast. The mast will be insulated for approximately 0.9 meter above the sunshield to provide the desired boundary conditions for the motor bearing assembly. The antenna element will have high emittance finishes only to the extent necessary to limit peak temperatures below 422 K in any critical areas; otherwise, these element finishes will be as dictated by functional rather than thermal requirements.

The apogee motor has an aluminized kapton multilayer insulation blanket to protect the spacecraft from post firing thermal soakback. Additional thermal isolation is provided around the aft end and around and over the nozzle to limit undesirable local temperatures near the nozzle throat during the transfer orbit. In addition to this isolation, an active heater on the nozzle throat is provided in the baseline to assure adequate temperature control of this critical element. The aft end of the spacecraft is closed and

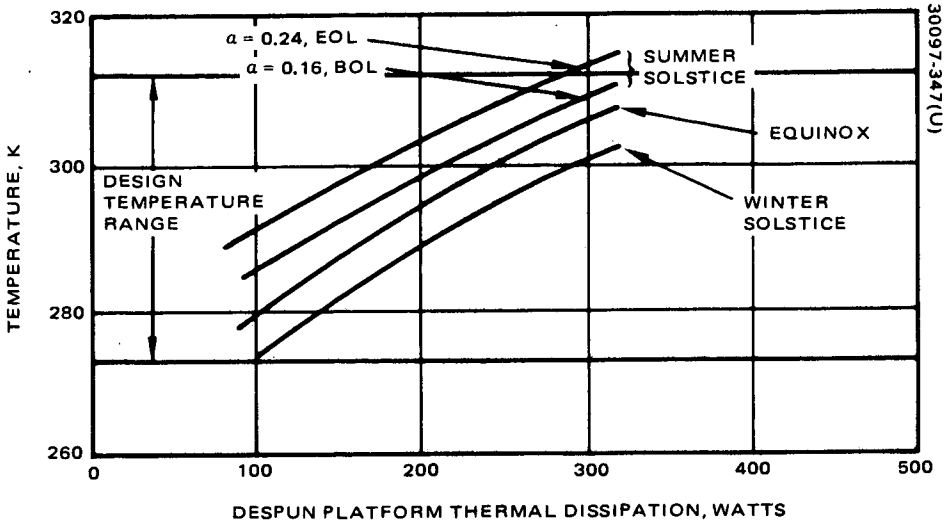

Figure 140. Despun Platform Thermal Performance

protected from apogee motor plume heating by a 51 μm thick stainless steel aft barrier. This barrier has hanovia gold on the surface that faces the spacecraft interior to minimize heat inputs to the spacecraft during apogee motor firing and to minimize heat transfer at this interface during all orbital steady state conditions.

4.3.9.3 Thermal Performance

Despun Platform

The power temperature performance characteristics of the baseline despun platform design are shown in Figure 140. The temperature performance is well within the equipment design range for the extremes in both season and operating mode. Further, the end-of-life performance of the degraded teflon sunshield appears adequate for this mission. Thus, the aluminized teflon shield used for TACSAT is the baseline preference over the more stable, but heavier and more complex, silvered quartz mirror approach used to meet the 10 year Intelsat IV requirement.

Equipment temperature drops on the order of 16.7 to 22.2 K can be expected during eclipse. This drop will result in short-term exposure of the electronic equipment to temperatures of 264 to 269 K, which satisfies the established eclipse limit of 261 K.

Motor Bearing Assembly

The motor bearing assembly (MBA) installation is shown in Figure 141. The bearing assembly used in this design is very similar to that used in the Telesat program. Full advantage has been taken of the detailed analysis and test data completed on the Telesat program. The only changes that are pertinent to the thermal performance are the addition of the slip ring assembly and the structural attachments, which resulted in some flange modification. The internal motor design and bearing configuration is thermally equivalent to that analyzed and tested on the Telesat program.

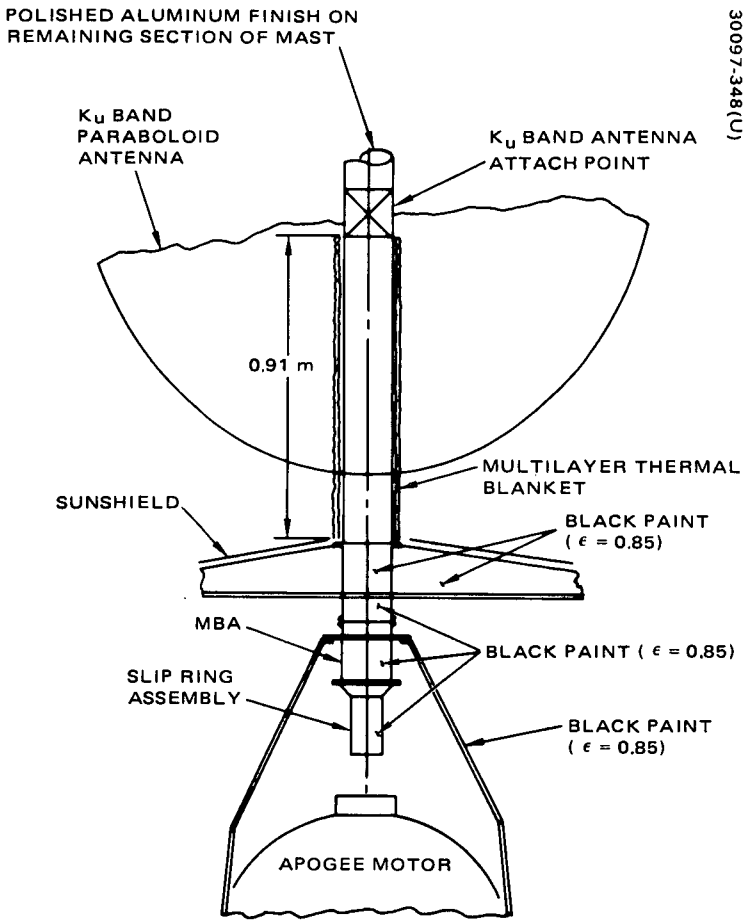

Figure 141. Motor Bearing Assembly/ Structure Thermal Interface

TABLE 57. MBA THERMAL PERFORMANCE

Node	Location	Minimum Steady-State Boundary, kelvin	Maximum Steady-State Boundary, kelvin
1	Upper inner bearing race	280	304
2	Upper outer bearing race	281	305
3	Upper despun flange	281	304.5
4	Center outer spinning housing	282	304.5
5	Lower spinning flange	280.5	304
6	Lower outer bearing race	291	308
7	Lower inner bearing race	291.5	307.5
8	Lower despun flange	291.5	307.5
9	Center despun shaft	284	306
10	Spinning cone structure	279	301
11	Slip ring assembly	291.5	307.5

Thermal analysis results are presented in Table 57. Both warm and cold boundary condition cases were analyzed to assure that the thermal coupling between the antenna mast and the MBA does not cause significant temperature changes on the MBA. It was verified that the antenna mast will not significantly affect MBA temperatures if the mast is insulated to a point approximately 0.9 meter above the sunshield. The MBA installation shown in Figure 141 provides excellent boundary conditions for the MBA, since it is coupled tightly to the despun platform, which provides a stable thermal environment. The high thermal mass of the MBA results in solar eclipse bulk temperature changes of less than 11 K. During the eclipse season, the steady-state temperature prior to eclipse will be no less than 283 K. Therefore, the bulk temperature will be greater than 273 K at the end of a 72 minute solar eclipse.

The temperature differential across the bearings is shown to be less than 2.8 K for the worst case conditions. The 3 watt dissipation in the slip ring assembly will cause that section to run about 8.3 K warmer than the motor housing; however, it will remain well below the 323 K allowable temperature for the slip ring assembly. All motor and bearing temperatures will remain within the 273 to 311 K operational design range.

Power Subsystems

The temperature characteristics of the cylindrical spinning solar array concept are well established through correlation of predicted performance with both test and flight data. The steady-state solar panel temperature for the baseline configuration will vary from a minimum of 285 K at summer solstice to a maximum of 295 K at equinox. The expected eclipse response of the panal is shown in Figure 142 and is based on the Intelsat IV substrate heat capacity and radiative properties.

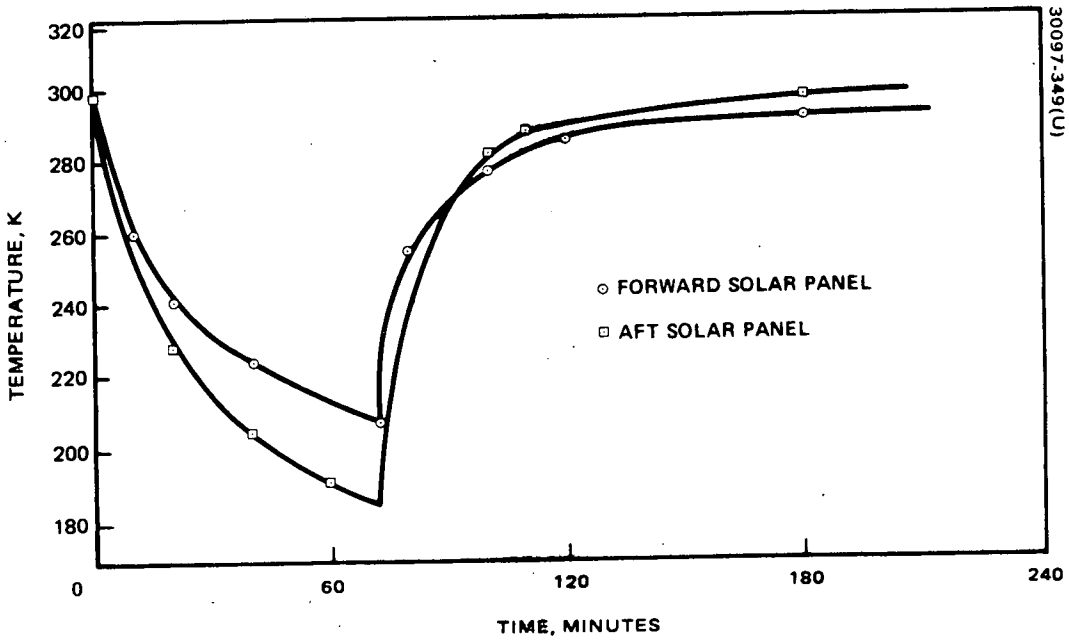

Figure 142. Solar Panel Eclipse Response

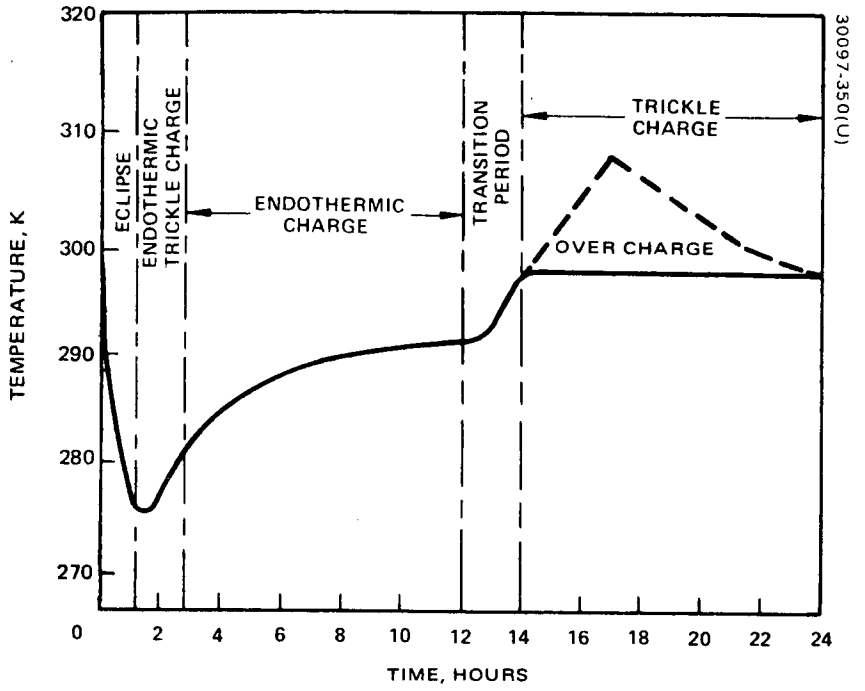

Figure 143. 24 Hour Battery Profile For Typical Rib Mounted Pack

The battery system can constitute the major thermal dissipator on the spinning side of the spacecraft. Figure 143 shows a typical orbital temperature cycle for an Intelsat IV battery pack where the charge rate is commanded by ground command. As indicated by the solid line, the battery temperature never exceeds 300 K. As shown in test data, the cooler the battery remains (ideally, but impossibly, 278 K), the longer lifetime it has. However, if the charge rate is not closely monitored and the battery is allowed to overcharge, the battery temperature will rise to 308 K as shown in the dashed line.

Reaction Control System

The heater system will require approximately 0.3 W/m of line and 0.75 W/thruster to ensure that no portion of the system reaches the freezing point of the propellant and oxidizer. The heater system is to be on continuously during the eclipse season and off for all other conditions.

Antenna/Mast Assembly

Mast deflection can be minimized either by using a low absorptance surface finish or, if high stability is required, by wrapping the mast with multilayer insulation. The key design parameters for the antenna tubular support structure are given in Figure 144. The beryllium tubes will be wrapped with a combination of aluminum tape and aluminized teflon. The aluminum tape wrapping and the aluminized teflon wrapping each have the same absorptance (α = 0.17).

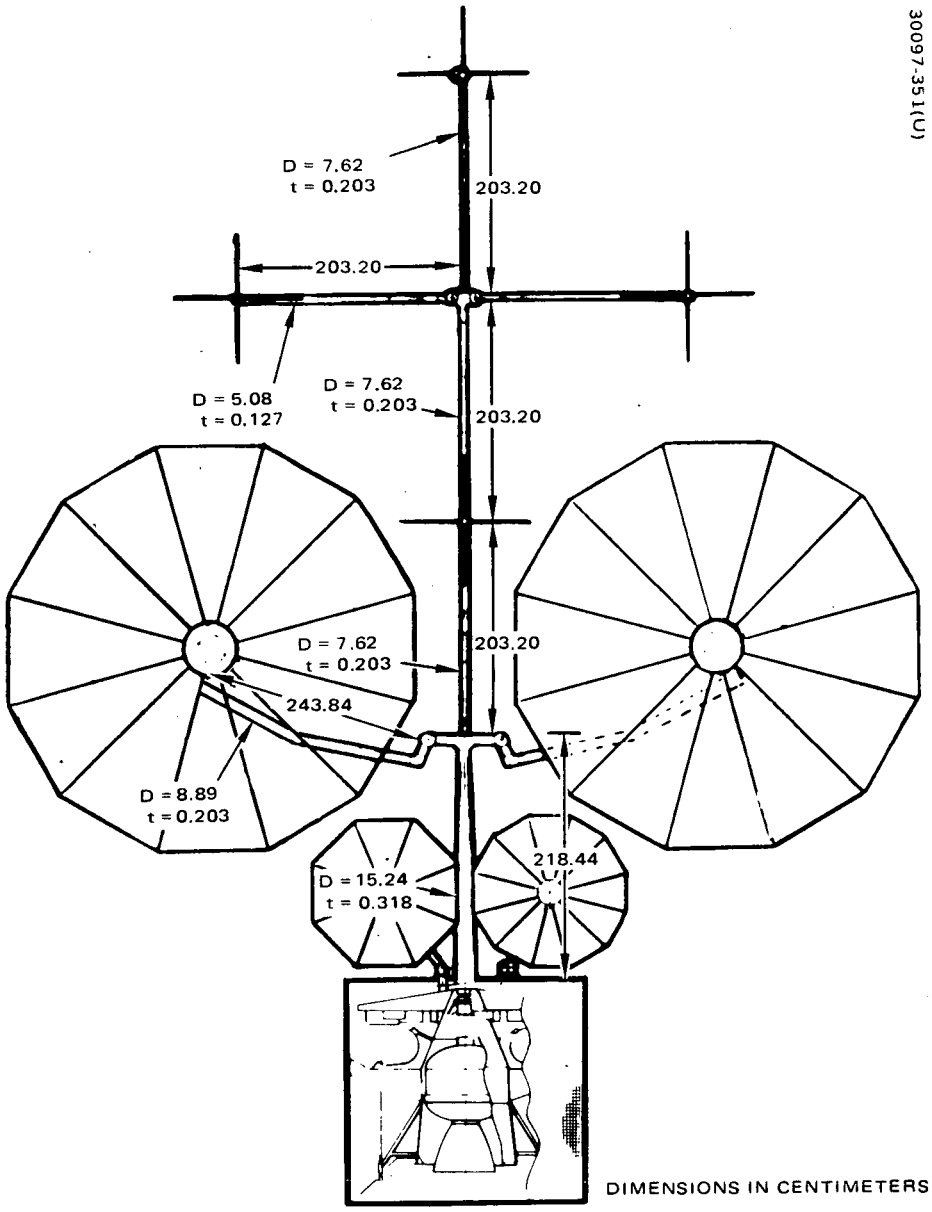

Figure 144. Configuration Model For Thermal Distortion of Beryllium Antenna Support Tubes

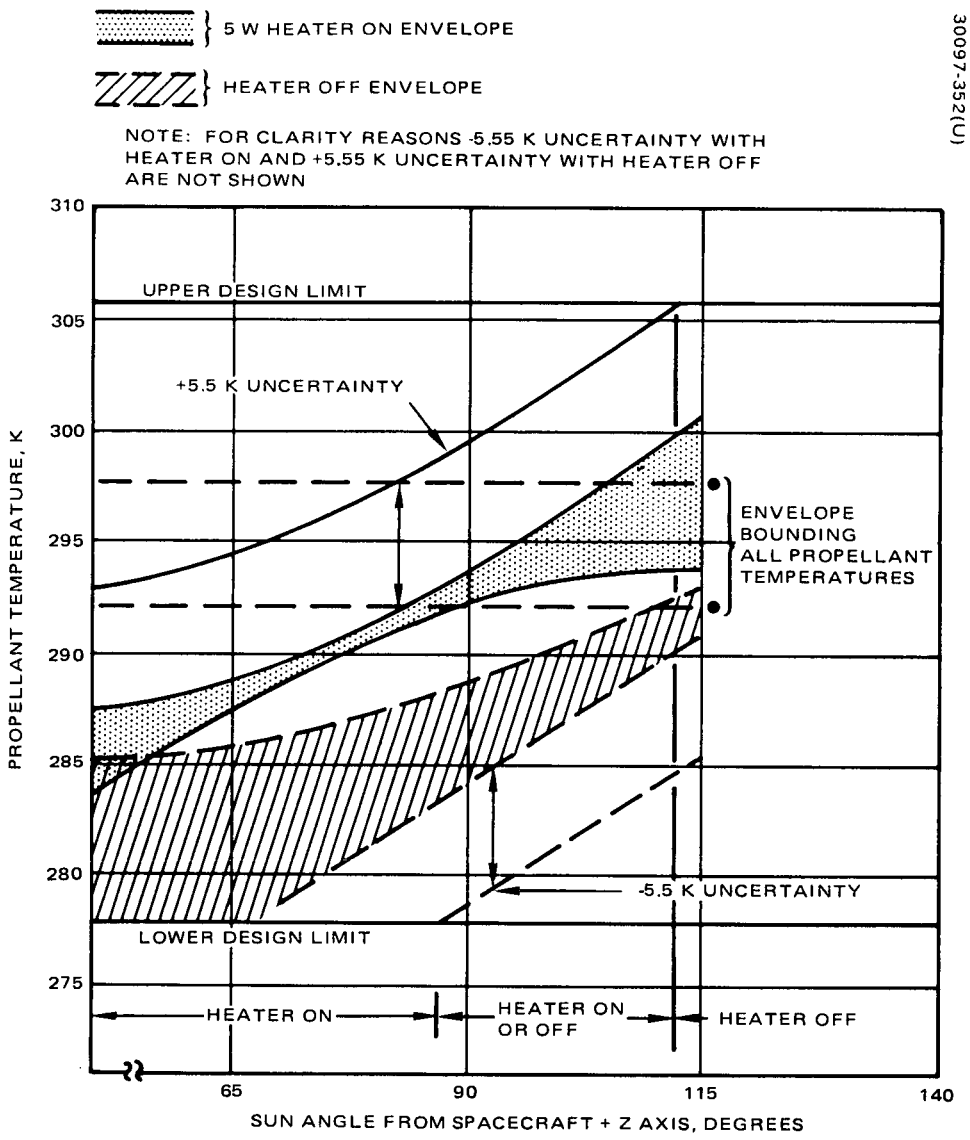

Figure 145. Apogee Motor Propellant Temperature Envelope

Apogee Motor Integration

The temperature performance of the apogee motor in the transfer orbit will be very similar to that developed for the Canadian Domestic Communication Satellite motor. Figure 145 describes the temperature performance resulting from a detailed integration analysis of the apogee motor, and shows that use of a 5 watt commandable heater at the throat can provide sufficient flexibility to meet the requirements for the full range of possible transfer orbit sun angles.

Aft Barrier Design

To maintain the required spacecraft heat balance, a low emittance aft barrier is required. However, this barrier is subjected to transient high heating rates during the apogee motor and axial attitude thruster firings and, therefore, must sustain temperatures exceeding the limits of aluminized plastic films commonly utilized for barriers. The barrier design selected for the TDRSS is a single layer of stainless steel foil, locally stiffened and thermally isolated at its attachment points. To limit its maximum temperature, the exterior surface of the foil is coated with Bo-Chem black oxide and with hanovia gold on the interior surface to provide the required thermal isolation. The design is utilized on the Telesat.

The suitability of this aft barrier design was demonstrated for the Phase I configuration. For the present baseline the exit plane of the apogee motor is closer to the aft end of the solar panel, thus providing a more benign spacecraft environment during apogee motor firing.